ELECTRONIC & OPTICAL PROCESSES IN QUANTUM DOT'S IN THE PRESENCE OF ELECTROMAGNETIC FIELDS

Thesis
Submitted to
Delhi Technological University
in partial fulfilment of the requirements for the Degree of

DOCTOR OF PHILOSOPHY
in
PHYSICS

By

SUMAN DAHIYA
(Reg. No. 2K17/Ph.D./AP/03)

Under the Supervision of

Prof. (Dr.) Rinku Sharma
Professor
Department of Applied Physics
Delhi Technological University
Bawana Road, Delhi-110042

Dr. Siddhartha Lahon
Associate Professor
Kirori Mal College
University of Delhi
Delhi-110007

DEPARTMENT OF APPLIED PHYSICS
DELHI TECHNOLOGICAL UNIVERSITY
DELHI-110 042, INDIA

DECEMBER 2023

Dedicated to
My Beloved Family

DECLARATION

This is to certify that the Ph.D. thesis entitled **"*Electronic & Optical Processes in Quantum Dot's in The Presence of Electromagnetic Fields*"** submitted to Delhi Technological University (DTU) for the award of the degree of **"Doctor of Philosophy"** in Applied Physics is a record of bonafide work carried out by me under the guidance & supervision of ***Prof. (Dr.) Rinku Sharma*** and Co-Supervision of ***Dr. Siddhartha Lahon*** at ***Atomic, Molecular and Terahertz Radiation Emission & Advance Simulation Lab***, ***Department of Applied Physics***, ***Delhi Technological University*** and has fulfilled the requirements for the submission of this thesis. The results contained in this thesis are original and have not been submitted to any other University/Institutions for the award of any degree or diploma.

Suman Dahiya
Research Scholar
(Reg. No. 2K17/Ph.D./AP/03)

Date:
Place: Delhi

Delhi Technological University

Formerly Delhi College of Engineering

(Under Delhi Act 6 of 2009, Govt. of NCT of Delhi)

Shahbad Daulatpur, Bawana Road, Delhi-110042

CERTIFICATE

This is to certify that the Ph.D. thesis entitled **"*Electronic & Optical Processes in Quantum Dot's in The Presence of Electromagnetic Fields*"** submitted to Delhi Technological University (DTU) for the award of the degree of **"Doctor of Philosophy"** in Applied Physics is a record of bonafide work carried out by me under the guidance & supervision of ***Prof. (Dr.) Rinku Sharma*** and Co-Supervision of ***Dr. Siddhartha Lahon*** at ***Atomic, Molecular and Terahertz Radiation Emission & Advance Simulation Lab, Department of Applied Physics, Delhi Technological University*** and has fulfilled the requirements for the submission of this thesis. The results contained in this thesis are original and have not been submitted to any other University/Institutions for the award of any degree or diploma.

Suman Dahiya
Research Scholar
(Reg. No. 2K17/Ph.D./AP/03)

This is to certify that the above statement made by the candidate is correct to the best of our knowledge.

Prof. (Dr.) Rinku Sharma
(Supervisor)

Dr. Siddhartha Lahon
(Co-Supervisor)

Prof. (Dr.) A. S. Rao
Head of the Department
Department of Applied Physics
Delhi Technological University
Delhi, India-110042

ACKNOWLEDGEMENTS

The journey of my research is accomplished with the valuable support of many people. It is a pleasant aspect that I have now the opportunity to express my gratitude for all of them.

At the outset, I would like to my profound sense of gratitude, indebtedness and reverence to my supervisor, ***Prof. (Dr.) Rinku Sharma****, Dean PG, Department of Applied Physics, Delhi Technological University, Delhi, and* ***Dr. Siddhartha Lahon****, Associate Professor, Department of Physics, Kirori Mal College, University of Delhi, Delhi, who nurtured my research capabilities for a successful scientific career. It has been an honor to work under excellent, enthusiastic and distinguished supervisors. Their unremitting encouragement, constant help, meticulous supervision and constructive criticism throughout the course of my study for carving another milestone in my academic journey. Their immense knowledge of the subject, analytic gaze, farsightedness and perseverance were a constant source of inspiration during the course of this thesis work.*

I feel privileged to have worked under such a great supervision. I further stand ovated to ***Prof. (Dr.) A. S. Rao****, Head, Department of Applied Physics, DTU, for their valuable help and suggestions. My heartfelt recognitions for* ***Prof. (Dr.) S.C. Sharma****, former DRC Chairman & Head Department of Applied Physics, DTU, my SRC & DRC committee members for their enduring support and appropriate propositions. I express my sincere gratitude especially to Prof. Manmohan, University of Delhi, for their timely advice and support.*

It is my pleasure to express my sincere thanks to all the faculty members of Department of Applied Physics, DTU for their continuous encouragement and help during my research work. I am also grateful technical and non-technical staff for their timely support and cooperation whenever required.

I sincerely thank my dear former and present lab-mates whose support helped in accomplishing my work. It is my pleasure to thank my juniors ***Ms. Richa*** *&* ***Ms. Priyanka*** *for their support. I would also like to thank all the other research scholars of Department of Applied Physics, Delhi Technological University, Delhi for their help and advice. I wish to acknowledge the enjoyable company and suitable help rendered by my dear friends****, Dr. Prateek Sharma, Ms. Ritika Ranga, Mr. Mukesh Kr. Sahu, Dr. Mrityunjay Kr. Singh, Dr. Ritika Khatri*** *for their help and support during this tenure.*

Finally, I thank my family for their support and motivation, every moment of my research period. With heartful gratitude and love, I express my gratefulness to my father ***Mr. Surender Dahiya****, mother* ***Mrs. Sumitra Devi*** *for their continual love and encouragement over the entire course of my life. I am thankful to my sister* ***Kusum Dahiya,*** *brother-in-law* ***Mr. Nitin Sindhu*** *&* *brother* ***Dr. Rajat*** *for the valuable suggestions, care, love and having faith in me throughout my existence. I am thankful to my extended maternal and paternal family for helping me maintain a positive attitude throughout my studies. I always thankful to all my beloved friends across the globe for sharing my happiness and sorrowI gratefully acknowledge the financial assistance provided by Delhi Technological University in the form of Junior Research Fellowship and Senior Research Fellowship during the period of my research. I extend my*

gratitude to Delhi Technological University and staff in Administration, Accounts, Store & Purchase, Library and Computer Centre for their help and services.

I thank one and all for helping me accomplish the successful realization of the thesis.

Thank you all!!!

Suman Dahiya

LIST OF PUBLICATIONS

Paper Published & Included in the Thesis

1. "***Effects of temperature and hydrostatic pressure on the optical rectification associated with the excitonic system in a semi-parabolic quantum dot***", *Suman Dahiya, Siddhartha Lahon and Rinku Sharma, Physica E: Low-dimensional Systems and Nanostructures, 118, 2020,113918.*
2. **"*Study of third harmonic generation in $In_xGa_{1-x}As$ semi-parabolic 2-D quantum dot under the influence of Rashba spin-orbit interactions (SOI): Role of magnetic field, confining potential, temperature & hydrostatic pressure",*** *Suman Dahiya, Siddhartha Lahon & Rinku Sharma Physica E: Low-dimensional Systems and Nanostructures, 147, 2023, 115620.*
3. ***"Tuning the nonlinear optical properties of a 1-D excitonic GaAs Quantum Dot system under a semi-parabolic potential with a detailed comparison with the experimental results: interplay of Hydrostatic pressure & Temperature",*** *Suman Dahiya, Siddhartha Lahon & Rinku Sharma, Nanosystems -Physics Chemistry Mathematics 15(5) (2024) 1-11.*
4. ***"Impurity Interplay on nonlinear optical properties in a 1-D $Ga_xAl_{1-x}As/GaAs/Ga_xAl_{1-x}As$ Quantum Dot's under a finite square well potential",*** *Suman Dahiya, Siddhartha Lahon & Rinku Sharma, Physica E-Low-dimensional Systems and Nanostructures (Under Review)*

Paper Published but not included in the Thesis

1. ***"The Effect of Relativistic Quantum Corrections on the Thermal Properties of Three-Dimensional Spherical Semiconductor Quantum Dot Under a Magnetic Field",*** *Suman Dahiya, Manthan Verma, Siddhartha Lahon and Rinku Sharma, Journal of Atomic, Molecular, Condensate and Nano Physics, Volume 5, Issue 1, Pages 41-53 (2018).*
2. ***"To Study the Relativistic Effect under the Magnetic Field on the Linear and Nonlinear Optical Absorption Coefficients and Refractive Index Changes in 3-D GaAs Quantum Dot",*** *Suman Dahiya, Siddhartha Lahon, Rinku Sharma and Manthan Verma, Journal of Basic and Applied Engineering Research, 5 (4), 2018, 311-315.*
3. ***"A Study of Confined Stark effect, Hydrostatic Pressure and Temperature on nonlinear optical properties in a 1-D $Ga_xAl_{1-x}As$/GaAs/ $Ga_xAl_{1-x}As$ Quantum Dot's under a finite square well potential"****, Rohit Chaurasiya, Suman Dahiya & Rinku Sharma, Nanosystems: Phys. Chem. Math., 2023, 14 (1), 44–53.*
4. ***Finite element analysis of multilayered spherical quantum dots: Effects of layer dimensions, alloy composition, and relaxation time on the linear and nonlinear optical properties,*** *A. Fakkahi, S. Dahiya, M. Jaouane, A. Ed-Dahmouny, R. Arraoui, A. Sali, Mohammad N. Murshed, H. Azmi, N. Zeiri, Physica B: Condensed Matter, 690, 2024, 416215.*

Paper Published in Conference/Workshop Proceeding

1. ***"Study of temperature and hydrostatic pressure effect on SHG associated with the excitonic system in an InN Quantum dot",*** *Suman Dahiya, Siddhartha Lahon, Rinku Sharma, Workshop on Recent Advances in Photonics (WRAP), 1-3, IEEE, 2019.*

2. **"Study of temperature and hydrostatic pressure effect on nonlinear optical properties associated with the excitonic system in an InAs quantum dot", *(Conference Presentation),*** *Suman Dahiya, Siddhartha Lahon, Rinku Sharma, Nonlinear Optics and its Applications 2020, 11358, 113581G, 2020.*

3. ***"Temperature and hydrostatic pressure effect on the optical rectification in a semi-parabolic quantum dot associated with the excitonic system",*** *Suman Dahiya, Siddhartha Lahon, Rinku Sharma, ICOL-2019: Proceedings of the International Conference on Optics and Electro-Optics, Dehradun, India, Chapter 58, 255-257, Springer Singapore, 2021.*

4. ***"Study of temperature and hydrostatic pressure effect on SHG associated with the excitonic system in an InAs Quantum dot",*** *Suman Dahiya, Siddhartha Lahon, Rinku Sharma, Proceedings of the International Conference on Atomic, Molecular, Optical & Nano Physics with Applications, 978-981-16-7690-1, 492284_1_En, (Chapter 11), 2021.*

5. ***"Effect of Pressure and Optical Intensity on linear and nonlinear optical properties of a GaAs Quantum dot for a parabolic system",*** *Rinku Sharma, Ayushi Kansal, Varnit Sharma and Suman Dahiya, ICAPIE 2021.*

6. ***"Study of Confined Stark Effect on Refractive Index and Coefficient of Absorption for a $Ga_xAl_{1-x}As/GaAs/ Ga_xAl_{1-x}As$ Finite Potential 1-D Quantum Dot",*** *Rohit Chaurasiya; Suman Dahiya; Rinku Sharma, 2022 IEEE International Conference on Nanoelectronics, Nanophotonics, Nanomaterials, Nanobioscience & Nanotechnology (5NANO), 2022, pp. 1-3.*

Awards / Recognition received

1. ***Commendable Research Award*** *received for research work in the year* ***2023*** *for publishing research articles in internationally reviewed journals at* ***7rd Research Excellence Awards*** *by Delhi Technological University on* ***5th September 2024***.
2. ***Commendable Research Award*** *received for research work in the year* ***2020*** *for publishing research articles in internationally reviewed journals at* ***4rd Research Excellence Awards*** *by Delhi Technological University on* ***15th March 2021***.
3. *Awarded with Best Poster Award for "****To Study the Relativistic Effect under the Magnetic Field on the Linear and Nonlinear Optical Absorption Coefficients and Refractive Index Changes in 3-D GaAs Quantum Dot"*** *at International Conference on Innovative Research in Applied Physical, Chemical, Mathematical Sciences, Statistics and Emerging Energy Technology for Sustainable Development" (APCMSET-2018) On 19th May 2018 at Convention Centre, Jawaharlal Nehru University, New Delhi.*
4. *Awarded with Best Poster Award for* ***"Study of temperature and hydrostatic pressure effect on SHG associated with the excitonic system in an InAs Quantum dot"*** *at International Conference on Atomic, Molecular, Optical & Nano Physics with applications (CAMNP 2019) at Delhi Technological University Delhi, India held during 18 - 20 Dec. 2019.*

ABSTRACT

Nanotechnology term signifies a novel realm of scientific exploration focused on fabricating devices that harness the extraordinary properties of materials at the nanoscale, typically ranging from 1 to 100 nanometres. Due to quantum confinement effect, semiconductor nanostructures offer a great promise by exhibiting superior optical & electronic properties as compared to that of bulk semiconductors & have diverse applications in the field of optical sensors, photo catalysts for environmental protection, flat panel displays, storage devices, laser diodes, and LED's (light emitting diodes). Semiconductor sensor and photo catalyst nanostructures are found to be of more particular importance out of all the applications due to their intricately connection with the appraisal of environmental clean-up technologies.

Nonlinear processes, including multiphoton transitions, have been explored extensively both theoretically and experimentally in atomic and molecular systems, as well as in bulk matter. However, the emergence of quantum nanostructures which includes quantum wells, quantum wires, and quantum dots, has given birth to a new class of nonlinear materials for studying multiphoton phenomena and nonlinear optical properties. These nanostructures have found applications in optoelectronic devices such as optical switching, THz multi-photon quantum well infrared photodetectors, multi-photon bioimaging, and frequency up-conversion.

Moreover, the field of semiconductor physics has witnessed a shift towards investigation of external perturbations including hydrostatic pressure, temperature, electric field & magnetic field as well as spin-dependent phenomena due to its wide

range of potential applications, including spin transistors, spin filters, and quantum computing. The study of spin-related effects in semiconductor nanostructures often involves considering the spin-orbit interaction. Understanding the spin-orbit interaction is crucial for studying its impact on nonlinear optical processes in quantum nanostructures. Theoretical investigations of various physical phenomena arising from the interaction between quantum nanostructures and strong fields, in the presence of spin-orbit interaction, have become paramount. Such studies allow us to gain insights into fundamental physics and optimize spin-based devices in nanostructures. Consequently, external parameters such as static magnetic fields, static electric fields, photon energy, hydrostatic pressure, temperature and laser intensity have also become vital aspects in exploring the linear and nonlinear properties associated with inter subband transitions in nanostructures like quantum dots and quantum wells.

In this thesis, the linear and nonlinear optical properties of quantum nanostructures mainly quantum dots & quantum well have been explored within the presence of hydrostatic pressure, temperature, electric field and magnetic field, as well as Rashba spin-orbit interaction. To observe nonlinear processes, high laser intensities are required, necessitating the use of non-perturbative methods for their study.

Chapter 1 provides a brief introduction about the nanostructures, external perturbations, linear & nonlinear properties, and multiphoton processes. A brief discussion about the desired characteristics of nanostructures i.e., Quantum well and quantum dots, as well as about the chosen material by highlighting their unique properties is given in this chapter.

The effects of external perturbations that includes hydrostatic pressure, temperature, electric field & magnetic field on the behavior of low-dimensional semiconductors are enlightened in the chapter, as these perturbations can significantly influence the optical and electronic properties of these systems. Understanding these effects is crucial for studying their behavior and potential applications. Next, the chapter discusses about the specific types of low-dimensional semiconductor structures, including quantum dots, quantum well. Each structure is defined and explained, highlighting their unique properties and characteristics.

Furthermore, the introduction section of **Chapter I** provides definitions and explanations of various optical properties and nonlinear optical properties. The behavior of materials while interacting with light, such as absorption, reflection, and transmission denotes the optical properties. Nonlinear optical properties, on the other hand, describe the response of materials to intense light, where the relationship between the input and output light is nonlinear.

Overall, **Chapter I** serves as an overview, setting the foundation for the subsequent chapters by introducing the key concepts, structures, and properties associated with low-dimensional semiconductors and their optical behavior.

In **Chapter 2**, we investigate the optical rectification coefficient of a GaAs quantum dots under the influence of radius, hydrostatic pressure & temperature for an excitonic system. A detailed discussion about the mathematics to find out the eigenvalues and eigen-energies using density matrix approach under effective mass approximation is presented in chapter 2. Our findings indicate that an increase in the radius, hydrostatic pressure & Temperature as well as excitons strongly play a role in affecting the peak

position as well as blue/red shift is observed in optical rectification coefficient. The results are presented as functions of incident photon energy for different parameter values. Our findings reveal that the hydrostatic pressure causes a red shift in the ORC (optical rectification coefficient) peaks, while the temperature shift these peaks towards the blue end of the spectrum. Furthermore, an increase in the quantum dot radius is found to induce a red shift in the peaks.

Chapter 3 of the study focuses on investigating the (THG) third harmonic generation coefficients of $In_xGa_{1-x}As$ quantum dots in the presence of confining potential, magnetic field, hydrostatic pressure & temperature with Rashba spin-orbit interaction. Density matrix procedure within the effective mass approximation have been employed to determine the energy levels and wave functions.

The study reveals that the THG coefficients depend on several factors, including the confining potential, -orbit interaction strength, magnetic field strength, Rashba spin, and photon energy. The consequences reveal that increasing the Rashba spin-orbit interaction coefficient has a strong impact on the THG peak positions. Additionally, it can be observed that the coefficient of THG is significantly enhanced by increasing/decreasing the magnetic field or confinement potential.

This feature makes them valuable for optical control in spintronics, indicating potential applications in spin photodetectors and ultra-sensitive spintronic devices.

Overall, **Chapter 3** provides a detailed investigation of the THG coefficients in $In_xGa_{1-x}As$ quantum dots under the influence of THz laser fields with Rashba spin-orbit interaction and a magnetic field. The results highlight the importance of various

parameters in controlling the spin dynamics and optical properties of quantum dots, paving the way for potential advancements in spintronics and bioimaging devices.

Chapter 4 of the study focuses on the investigation of the linear and nonlinear absorption coefficients, as well as the change in refractive index in a semi-harmonic potential spherical GaAs excitonic quantum dot (QD). The chapter begins by discussing the Hamiltonian, applied potential & density matrix formalism employed to obtain the linear and nonlinear optical properties of the quantum dots. This formalism allows for a detailed analysis of the effects of various parameters on the optical behavior of the QD.

The study analyzes the linear and nonlinear absorption coefficients, as well as the refractive index change, under the influence of external hydrostatic pressure and temperature. Additionally, the influence of the excitons is also investigated, and a comparison is made between the cases of with and without excitonic effects as well as a detailed comparison is carried out between theoretical observed results and experimental data.

The results are expressed as functions of the incident photon energy for dissimilar parameter values. The findings reveal that the application of hydrostatic pressure leads to a red shift in the absorption peaks, both for linear and third-order processes. On the other hand, temperature causes a shift of these peaks towards the blue end of the spectrum. Similar effects are observed in the dispersion regions of the refractive index change. Also, it can be noticed from the results that the results obtained using taking excitons in consideration are found to be more prominent than the case of where excitons are not taken into account.

In summary, **Chapter 4** provides a detailed analysis of the linear and nonlinear absorption coefficients, as well as the refractive index change, in a GaAs excitonic quantum dot under the influence of hydrostatic pressure and temperature. The results highlight the effects of these external parameters on the optical properties of the quantum dot and provide valuable insights into the behavior of inter subband transitions.

Chapter 5 delves into the investigation of the effect of transverse electric field, hydrostatic pressure & temperature on a quantum dot with finite square well potential. We focus on determining the nonlinear optical rectification as well as nonlinear refractive index changes for a finite well. Our findings reveal that the transverse electric field as well as temperature blue shifts the peaks of the optical rectification coefficient as well as nonlinear refractive index changes, while hydrostatic pressure shift these peaks towards the red end of the spectrum. These findings suggest the potential to control the electronic and optical properties.

In conclusion, this study is expected to stimulate both experimental and theoretical investigations, contributing significantly to the understanding of nonlinear optical properties in nanostructures particularly for quantum dots and quantum well with external perturbations such as electric field, magnetic field, hydrostatic pressure & temperature and Rashba spin-orbit interaction. By investigating the influence of external perturbations such as electric field, magnetic field, hydrostatic pressure & temperature and Rashba Spin Orbit interactions, the thesis explores the possibility of tuning the effective band gap and other material properties in the studied system. This

tunability is particularly relevant for optical applications in devices utilizing narrow-bandgap semiconductors.

The attained results are anticipated to be highly advantageous for gaining an advancement in optical applications in narrow-bandgap semiconductor devices. Furthermore, the outcomes of this research are anticipated to inspire further experimental studies in this field in the near future.

Finally, we provide a summary and concise conclusion of the work presented in the preceding chapters of the thesis, along with an outline of future aspects to be explored in this research. The references are provided in numbers within square brackets, appearing in the order in which they appear in the text, and a bibliography is presented at the end of each chapter. The equation numbers are indicated within small brackets.

CONTENTS

LIST OF FIGURES

LIST OF TABLES

CHAPTER 1
INTRODUCTION

1.1 Nanoscience and technology

In recent times, an extraordinary advancement has been observed in the field of technology giving escalation to an empowering situation of production of semiconductor structures at nano-meter size. Primarily the growing attention that has been given to the semiconductor nanostructures is mainly governed by the factor that semiconductor nanostructures are striking from both technical and methodological point of view as they are capable of offering production of non-natural potentials for electrons-hole carriers in semiconductors at a scale of comparable or smaller than the de Broglie wavelength [1-5]. As a consequence of it, quantum confinement effects become substantial as well as highly designable. In semiconductor nanostructures, many ideas that were once only theoretical models are now allowed for the investigation of their properties such that they can be realised physically. Also, quantum mechanics is another crucial element that governs the system by its application with more practical approach [6-8] as well as scholarly interest. By utilising confinement effects, new gadget concepts are made possible and given more design latitude. New device concept, which has received additional degree of freedom in design become feasible by utilizing the confinement effect. For use in nano- and optoelectronics, semiconductor nanostructures in particular have a lot of potential [9–11]. Due to the capacity to tune their energy spectrum by adjusting their size and geometry, they differ from natural atoms. These characteristics are thought to make them strong contenders for use in quantum optoelectronic devices, which can process quantum information and serve as an interface between quantum bits and quantum optics [12,13].

Quantum well, quantum wire, or quantum dot's (**Figure. 1.1** represents the Confinement of dimensions and density of states in 3D, 2D, 1D and 0D) can be manipulated the energy spectrum (the collection of discrete eigen-energies) by adjusting (i) the confinement region's size and form and (ii) the confinement potential's potency. These structures are constrained into low dimension, which causes the emergence of discrete energy levels (sub-bands), which drastically alters the absorption spectra and gives rise to numerous unique features [14-15]. The quantum dot (**Figure. 1.2** represents the band gap variation with the size of the material where the energy levels are discrete in case of quantum dots) and quantum well are the two nanostructures that are the subject of the current thesis.

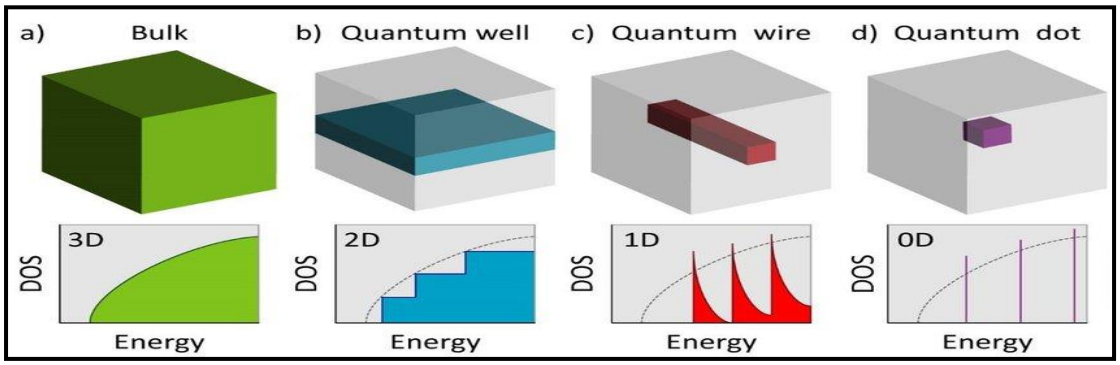

Figure 1.1: *The Confinement of dimensions and density of states in 3D, 2D, 1D and 0D [14]*

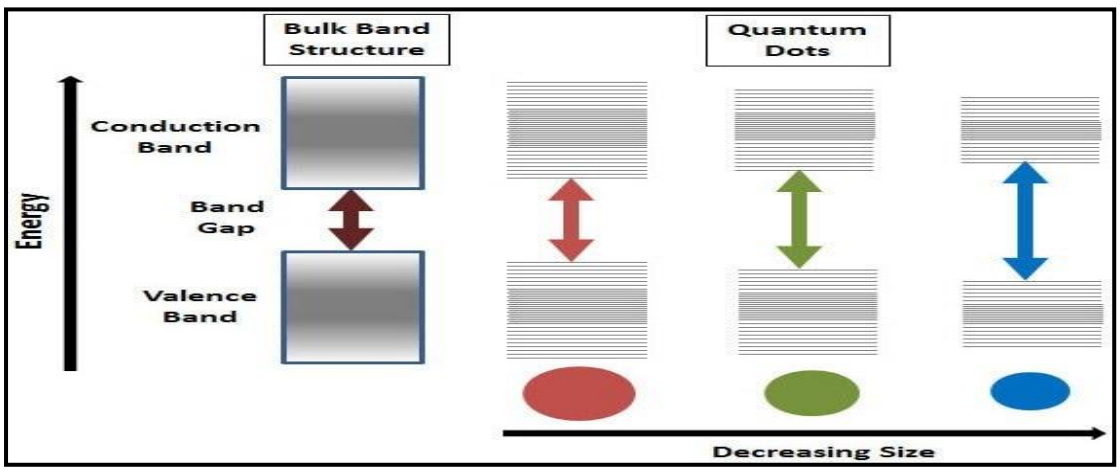

Figure 1.2: *The band gap variation with the size of the material where the energy levels are discrete in case of quantum dots [14]*

1.2 Compound semiconductors

Semiconductor materials namely small band gap insulators, can have their electronic properties modified by doping with impurities. This controllable alteration of properties allows for changes in the optical properties of the semiconductor. Such doped semiconductors are crucial for the production of devices like transistors and lasers, with various applications. Therefore, the exploration of novel semiconductor materials and the improvement in the existing ones are significant areas of study. The majority of semiconductor materials used today are crystalline inorganic solids, categorized based on the constituent atoms' periodic table groups.

Elementary semiconductors consist of single types of atoms, such as silicon (Si), germanium (Ge), and tin (Sn) from column IV, as well as selenium (Se) and tellurium (Te) from column VI of the periodic table. On the other hand, complex semiconductors are composed of two or more elements. Compound semiconductors consist of elements from different periodic table groups, often belonging to groups III-V or IIb-VIb. Examples include gallium arsenide (GaAs) from group III and group V elements, and cadmium sulfide (CdS) from group IIb and group VIb elements. The development of compound semiconductors has led to the emergence of heterostructure devices, which combine two different semiconductors and enable high-speed operation and novel device concepts [16]. Ternary alloys involve three constituent elements, while quaternary alloys involve four. The composition of ternary derivatives can be represented as $A_xB_{1-x}C$ (e.g., $Al_xGa_{1-x}As$), where elements A and B are randomly mixed in group III sublattices and element C occupies group V sublattice sites. Another composition is $AB_{1-x}C_x$ (e.g., $GaAs_{1-x}P_x$), where element A fills all group III sublattices,

and elements B and C occupy group V sublattices randomly (**Figure 1.3** illustrates the details of these semiconductor materials).

For example, LEDs (Light Emitting Diodes) are indeed made of compound semiconductors rather than elementary semiconductors. While elementary semiconductors like silicon and germanium have band gaps that result in emitted light with wavelengths in the third infrared region, making them unsuitable for LEDs, compound semiconductors are designed to emit light in the visible spectrum. The band gap of compound semiconductors can be tailored to produce light in the visible range, allowing for the creation of LEDs that emit light in various colors, including red, green, blue, and other colors. This property makes compound semiconductors ideal for applications such as lighting, displays, and optoelectronics.

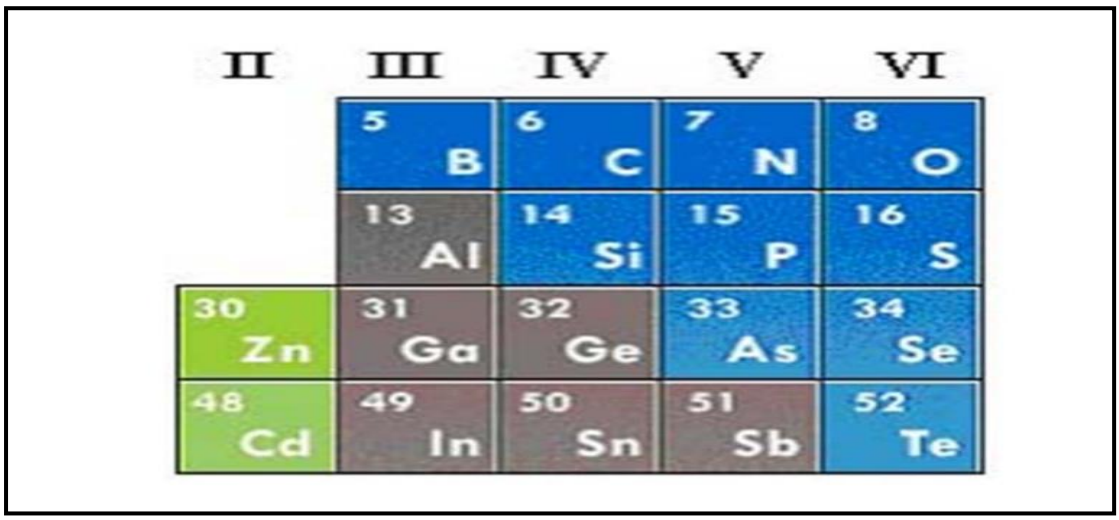

Figure 1.3: *Group II, III, IV, V and VI basic materials for semiconductor (compounds)[16]*

1.2.1 Compound III-V

III-V semiconductors are widely used in optoelectronic applications and offer potential advantages in terms of higher speed operation compared to silicon semiconductors,

particularly in areas like wireless communications. These compound semiconductors which are fashioned by atomic elements from different groups on the periodic chart are consist of crystal lattices . The composition of III-V semiconductors takes place when an element A belonging to Group III and an element B belonging to Group V combines. Each atom from Group III is bonded to four Group V atoms, and vice versa. The bonding involves electron sharing, resulting in a filled valence band with eight electrons for each atom. The nature of the bonding is mainly covalent, although there is a component of ionic bonding due to the transfer of valence charge from Group V to Group III atoms. This contrasts the elemental semiconductors having purely covalent bonds. Examples of compound semiconductors belonging to III-V group includes GaP, GaAs, GaSb, InP, InAs, and InSb [17].

1.2.2 Direct and indirect bandgap semiconductors

In the realm of semiconductor physics, semiconductor's bandgap concept is majorly categorized into two distinct types: the direct bandgap and the indirect bandgap, as depicted in **Figure 1.4** [18,19]. These two bandgap types are associated with specific k-vectors in the Brillouin zone, where the minimum energy state of conduction bands and the maximum energy state of valence bands becomes active. Direct bandgap comes into play when the k-vectors of both the bands match with each other. In such conditions, an electron can transition from the conduction band to the valence band with minimal energy change and without altering its k-value, thereby emitting the energy difference as a photon of light.

Conversely, for the cases where the k-values are different, hence referred to as an "indirect gap." This implies that a change in momentum (k) is required for a transition from the lowest point in the conduction band to the highest point in the valence band. In

indirect gap transitions, both a phonon (resulting from lattice vibration) and a photon are involved. Energy in such transitions is typically dissipated as heat into the lattice rather than being emitted as a photon.

Direct gap semiconductors exhibit unique characteristics that are advantageous for optical and electronic applications, especially in the context of interband optical transitions, such as infrared radiation detectors and emitters. GaAs-based structures, for instance, are widely utilized in the near-infrared region and are considered narrow-gap semiconductors in the mid-infrared (MIR) spectral regions. The bandgap, expressed in terms of wavelengths, holds significant importance because different applications of group III-V compound materials depend on various wavelengths in the field of optoelectronics.

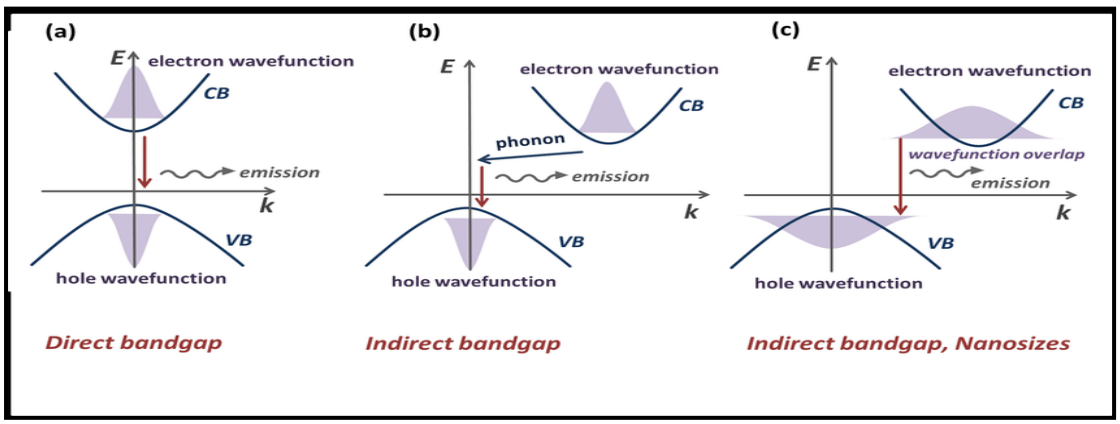

Figure 1.4: *Direct and indirect bandgap [18]*

1.2.3 Properties and applications of GaAs, InGaAs & AlGaAs

GaAs (gallium arsenide) is a semiconductor belonging to III-V group and having a direct bandgap (as shown in **Figure 1.5**) having a zinc blende crystal structure as shown in **Figure 1.6**. It is widely used in various devices such as microwave frequency integrated circuits (ICs), infrared light-emitting diodes (LEDs), laser diodes, solar cells,

and optical\windows. GaAs can be used as a substrate material for epitaxial growth of other III-V semiconductors, including $Al_xGa_{1-x}As$ and $In_xGa_{1-x}As$.

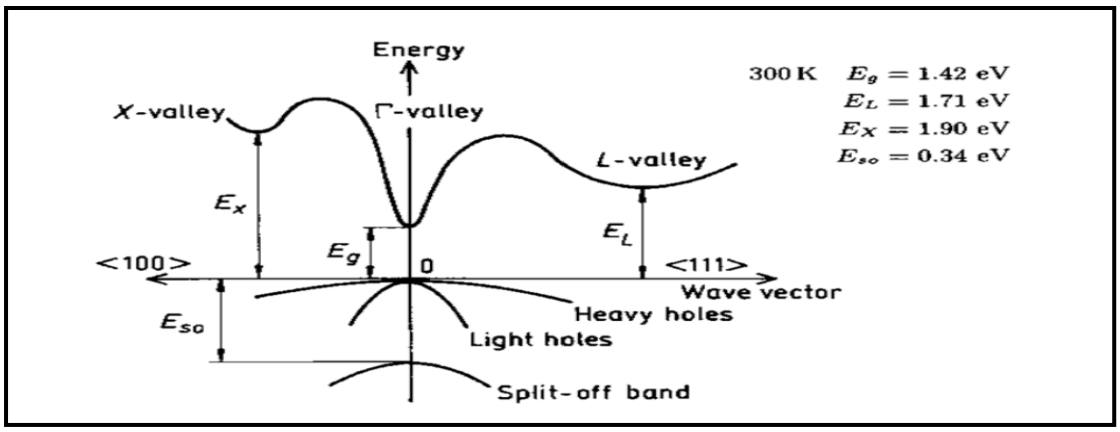

Figure 1.5: *Band structure of GaAs*

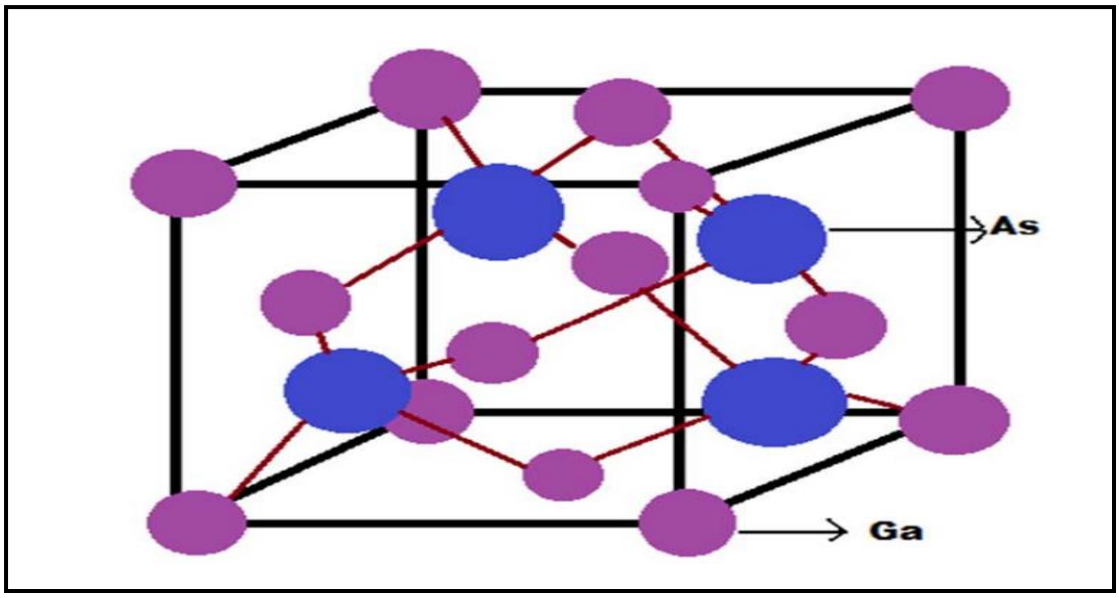

Figure 1.6: *Zinc blende crystal structure of GaAs showing tetragonally oriented bonds*

Compared to silicon, GaAs exhibits superior electronic properties. It has a higher electron mobility of 8500 cm^2/V-s at 300K, enabling GaAs transistors to operate at frequencies exceeding 250 GHz. GaAs devices are less sensitive to heat due to their wider bandgap compared to silicon junctions. Additionally, GaAs devices generally exhibit lower noise,

particularly at high frequencies, due to higher carrier mobility. GaAs finds applications in various fields, including mobile phones, satellite communications, microwave point-to-point links, and higher frequency radar systems.

The lattice constant of GaAs (5.6532 Å) is nearly identical to that of AlAs (5.6611 Å). This allows for lattice-matched growth of mixed crystal compositions, such as $Al_xGa_{1-x}As$ and $In_xGa_{1-x}As$, on GaAs substrates. This feature is advantageous as it enables the growth of ternary crystals without strain effects or the generation of dislocations.

The basic parameters of GaAs, $Al_xGa_{1-x}As$ and $In_xGa_{1-x}As$, including crystal structure, lattice constant, band gap, electron mobility, thermal conductivity, and common uses, are summarized in **Table 1.1**. It is important to note that the values for $Al_xGa_{1-x}As$ and $In_xGa_{1-x}As$ vary depending on the specific composition (x) of the alloy [20-24].

Table 1.1: *Basic Parameters of GaAs, $Al_xGa_{1-x}As$ & $In_xGa_{1-x}As$*

Basic Parameters (300 K)	**GaAs**	**$Al_xGa_{1-x}As$**	**$In_xGa_{1-x}As$**
Energy gap	1.424 eV	For x<0.45 1.424+1.247x eV x>0.45 1.9+0.125x+0.143x^2 eV	(0.36+0.63x+0.43x^2) eV (0.4105+0.6337x+0.475x^2) eV
Energy separation ($E_{\Gamma L}$) between Γ and L valleys	0.29 eV	0.29 eV	(1.37-0.63x+1.16x^2) eV
Energy separation ($E_{\Gamma X}$) between Γ and X valleys	0.48 eV	1.424+1.155x+0.37x^2 eV	(1.08-0.02x+0.65x^2) eV
Energy spin-orbital splitting	0.34 eV	0.34-0.04x eV	***
Intrinsic carrier concentration	2.1*10^6 cm^{-3}	For x=0.1 2.1*10^5 cm^{-3} x=0.3 2.1*10^3 cm^{-3} x=0.5 2.5*10^2 cm^{-3} x=0.8 4.3*10^1 cm^{-3}	4.82 *10^{15} * [(0.41-0.09x)$^{3/2}$ +(0.027+0.047x)$^{3/2}$]$^{1/2}$ x(0.025+0.043x)$^{3/4}$ [$T^{3/2}$ exp(-ν/2)(1+3.75/ν +3.28/$ν^2$ -2.46/$ν^3$)$^{1/2}$] (cm^{-3})
Intrinsic resistivity	3.3*10^8 Ω·cm	x=0.3 1*10^{12} Ω·cm x=0.5 1*10^{14} Ω·cm x=0.8 5*10^{14} Ω·cm	***
Effective conduction band density of states	4.7*10^{17} cm^{-3}	x<0.41 2.5*10^{19}*(0.063+0.083)$^{3/2}$ cm^{-3} x>0.45 2.5*10^{19} *(0.85-0.14x)$^{3/2}$ cm^{-3}	4.82 *10^{15} *(0.023+0.037x+0.003x^2)$^{3/2}$ $T^{3/2}$ (cm^{-3})
Effective valence band density of states	9.0*10^{18} cm^{-3}	2.5*1019*(0.51+0.25x)$^{3/2}$ cm^{-3}	4.82 *10^{15} * (0.41-0.1x)$^{3/2}$ $T^{3/2}$ (cm^{-3})

1.3 Quantum confinement

Quantum confinement is a unique characteristic observed in nanostructures such as quantum wells, wires, and dots & occurs when the exciton Bohr radius exceeds the physical dimensions of the system, leading to confinement effects on both the electron and hole. Consequently, the energy levels of the carriers along the confined direction become discrete, in contrast to the continuous energy distribution in bulk materials without confinement. The emergence of discrete states is a fundamental characteristic of nanomaterials. These confined systems or we can say low-dimensional systems or nanostructures, are quantum systems having charge carriers moving freely in two, one, or even zero dimensions. In nanostructured semiconductors, quasiparticles such as electrons, holes, and excitons play a significant role. The degree of confinement is determined by the effective excitonic Bohr radius, symbolized as a_B^*, which can be greater than the lattice constant a_l. Consequently, mesoscopic structures can be fashioned with dimensions comparable to or smaller than a_B^*, but still larger than a_l, where the elementary excitations experience quantum confinement. This confinement leads to finite motion along the confinement axis and infinite motion in other directions. These nanostructured systems are broadly categorized as quasi-2-D systems (e.g., single heterostructures, quantum wells, multiple quantum wells, and superlattices), quasi-1-D systems (e.g., quantum well wires), and quasi-zero-dimensional systems (e.g., quantum dots) [25,26].

1.3.1 Weak confinement

In the context of quasi-particles, the degree of confinement is determined by the magnitudes of a_B^* and the quantum confinement size, denoted as "l." There are two

distinct regimes: (i) regime of weak confinement and (ii) regime of strong confinement. The regime of weak confinement arises when the size of nanostructure confinement "l "is smaller but still a few times higher than a_B^*. Mathematically, this condition can be stated as $a_B^* << l$. In this regime, the correlation of electron and hole is exhibited, and the excitons are conceptualized as a quasiparticle moving within the nanostructure with minimal energy increase resulting from confinement. This behaviour can be described reasonably well by the infinite potential well model, assuming the single-band effective mass approximation. This model provides a reasonable explanation for the observed shift in the ground state energy of the exciton in experiments.

1.3.2 Strong confinement

The strong confinement regime occurs when the confinement effect surpasses the influence of the Coulomb potential i.e., a_B^* is comparable to l. In this regime, the electron and hole are considered as individual particles predominantly occupying their respective single-particle ground states, with minimal spatial correlation between them. The confinement effects become significantly pronounced in this regime, and the exciton in the nanostructure is strongly influenced by the boundary effects. It becomes crucial to include a finite height for the confining potential barrier to accurately describe the unique optical properties observed in small nanostructures. The ordering and spacing of discrete energy states in confined systems can be investigated by solving the Schrödinger equation for carriers using appropriate boundary conditions. Notably, the progression of states in a quantum wire differs from that in a quantum dot (or nano crystal) and also differs from a quantum well [27,28].

1.4 Effects of perturbations

In the context of the discussed study, the effects of various external perturbations on the electronic and optical properties of quantum nanostructures are explored. The following effects are mentioned:

Pressure: Electronic properties of nanostructures can be varied by changes in the electronic band structure of compounds with pressure. The pressure dependence of these properties has been interpreted by studying the pressure-induced changes in the electronic band structure. Hydrostatic pressure, which does not destroy the cubic symmetry of the crystal, has been observed to have minimal effects on the properties of the valence band [29-31].

Temperature: Changes in temperature can result in several effects in the lattice of semiconductors. The lattice can expand or contract, and the oscillations of lattice atoms around their mean positions can increase or decrease. The electron-lattice interaction is also temperature-dependent. Temperature variations can affect impurity potentials, although the ionization energy of the impurities remains relatively constant. The bandgap of compound semiconductors can change with temperature, influencing their optical properties. The specific dependence of the bandgap on temperature varies across different temperature ranges [32].

Electric field: Quantum confinement in quantum dots results in discrete energy levels. The application of an electric field can significantly influence the excitonic states in quantum dots, leading to the quantum confined Stark effect. The effect includes the contribution of strain and the built-in electric field induced by spontaneous and piezoelectric polarizations. Additionally, the combined application of electric and magnetic fields induces Stark shift and diamagnetic shift, respectively [33].

Magnetic field: Electronic orbits in atoms are associated with a magnetic moment. When atoms have multiple electronic orbits with non-parallel orientations, an external magnetic field can induce a rotating action on the individual electronic orbits. This rotation produces an induced magnetic moment, leading to a diamagnetic action. Substances composed of such molecules are referred to as diamagnetic substances [34].

Spin-orbit interactions: When an electron moves in the orbital of an atom, it experiences a magnetic field due to its own motion. This interaction between the electron's orbital motion and the magnetic field is acknowledged as spin-orbit interaction (as shown in **Figure 1.7**). In materials, the dispersion relation describes the relationship between the energy and momentum of electrons. In a simple scenario, the dispersion relation for electrons in materials is assumed to be parabolic, with a curvature determined by the effective mass. The effective mass represents the mass of the electron in the material, which can differ from its free electron mass due to interactions with the crystal lattice [35,36]. However, it has been observed that the spin-orbit interaction introduces modifications to the dispersion relation, leading to a non-parabolic behaviour in certain materials. These modifications are material-dependent and can result in a dispersion relation that deviates from the simple parabolic form. The presence of spin-orbit interactions introduces an additional coupling between the electron's spin and its orbital motion, influencing the electron's energy-momentum relationship. As a result, the dispersion relation becomes more complex and can exhibit non-parabolic features. The extent of deviation from the parabolic dispersion relation depends on the strength of the spin-orbit interaction in the specific material. This non-parabolic dispersion relation is particularly important for systems with strong spin-orbit coupling, as it affects various electronic properties and phenomena, such as energy band

structures, electronic transport, and optical properties. Understanding and characterizing the non-parabolic dispersion relation is crucial for accurately describing the behaviour of electrons in materials with significant spin-orbit interactions [37-39].

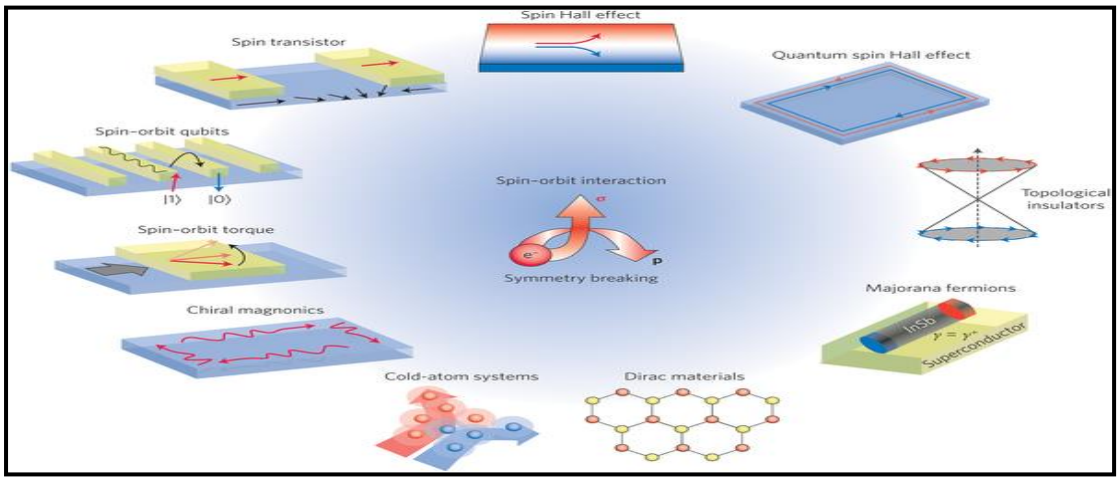

Figure 1.7: *Schematic diagram showing many realizations of spin orbit interaction [36]*

1.4.1 Rashba and Dresselhaus spin-orbit interactions

The Rashba effect, also known as the Rashba-Dresselhaus effect, refers to the momentum-dependent splitting of spin bands in two-dimensional condensed matter systems, specifically heterostructures. This splitting is a result of the combined effects of atomic spin-orbit coupling and the asymmetry of the potential in the direction perpendicular to the two-dimensional plane. The effect is named after Emmanuel Rashba, who first discovered it.

Spin-orbit interaction, which arises from the coupling between the electron's spin and its orbital motion, plays a crucial role in transitions involving a change in spin due to the Lorentz force. Rashba originally introduced this interaction to explain the absorption of radio waves in semiconductors with a wurtzite lattice structure [40].

In diamond or zinc-blende semiconductors, there exists a spin-orbit split-off band, and the bulk inversion asymmetry contributes to the spin-orbit interaction, known as the Dresselhaus term. This term alters the symmetry of the dispersion relation within a specific energy band [41].

The presence of both Dresselhaus and Rashba terms in the Hamiltonian modifies the dispersion relation of the energy bands in two-dimensional systems, resulting in spin splitting and giving rise to interesting phenomena such as spin Hall effect, spin precession, and spin manipulation. These effects have important implications for spintronics and the development of novel electronic devices.

In two-dimensional systems, there are two spin-orbit interactions that influence the dispersion within an energy band. The first contribution arises from the inversion asymmetry of the zinc-blende crystal structure in the bulk host material, leading to the Dresselhaus term (H_D) in the Hamiltonian. The second contribution, known as the Rashba term (H_R), is not related to bulk properties [42] but is present only in semiconductor heterostructures where there is a lack of inversion symmetry in the growth direction. Hence the complete Hamiltonian is given by:

$$H = H_0 + H_D + H_R \tag{1.1}$$

where H_0 is the Hamiltonian of the system without spin-orbit interactions.

The Dresselhaus spin-orbit interaction, arising from the bulk inversion asymmetry of the semiconductor material, can be described by the following expression:

$$H_D = \gamma_c \vec{k}.\vec{\sigma} \tag{1.2}$$

where γ_c represents the strength of the interaction depending on the material parameter and Pauli vector matrices is given by σ.

The Rashba spin orbit interaction between the interface of two semiconductors which is asymmetric in nature, and taking gate voltage in z-direction is given by [42]

$$H_R = \alpha_R(k_y\sigma_x - k_x\sigma_y) \tag{1.3}$$

k_x & k_y are the components of the electron wavevector in the x and y directions, respectively. σ_x & σ_y are Pauli matrices representing the electron spin components in the x and y directions.

The Dresselhaus term in the Hamiltonian modifies the dispersion relation of the conduction electrons and leads to a nontrivial spin splitting in the energy bands. This effect is particularly significant in semiconductor materials with a zinc-blende crystal structure, where the bulk inversion asymmetry plays a prominent role in the spin-orbit interaction. The Dresselhaus spin-orbit interaction is one of the contributions to the overall spin dynamics and behaviour in these materials.

1.4.2 Application of spin-orbit interaction

The inclusion of spin-orbit interactions in low-dimensional semiconductor heterostructure studies is crucial because these interactions significantly impact the electronic properties of the system. Even though spin-orbit effects may be considered small corrections to the band structure of the two-dimensional metallic state, they give rise to a wide range of novel phenomena.

Spin-orbit interactions introduce unique properties and behaviours in materials, such as spin splitting, spin precession, and spin manipulation. These effects can be harnessed to

develop innovative electronic devices known as spintronics. Unlike conventional electronic devices that rely on the manipulation of charge, spintronic devices utilize the manipulation of the electron's spin degree of freedom.

Spintronic devices offer several advantages over traditional electronic devices. They can provide increased functionality, higher processing speeds, lower power consumption, and improved data storage capabilities. By utilizing the spin degree of freedom, spintronic devices enable new possibilities for information processing and storage, as well as enhanced sensitivity in sensing and detection applications.

Incorporating spin-orbit interactions in the study and design of low-dimensional semiconductor heterostructures allows researchers to explore and exploit these spin-related phenomena. It opens up avenues for developing spin-operated electronic devices with improved performance and novel functionalities, leading to advancements in areas such as data storage, computing, communication, and sensing.

These effects highlight the importance of external perturbations, such as pressure, electric and magnetic fields, and temperature, in modulating the electronic and optical properties of quantum nanostructures. Understanding these effects is essential for tailoring the properties of these materials and optimizing their applications in optoelectronic devices.

1.5 Methods and approximations

1.5.1 The variation method

The variation method is a powerful approximate method widely used in quantum mechanics to determine approximate solutions to the Schrödinger equation. It offers a

flexible and systematic approach to obtain approximations for wavefunctions and energies of quantum systems. The central concept of the variation method is to start with a trial wavefunction that depends on a set of adjustable parameters, known as variation parameters. The trial wavefunction is chosen based on physical intuition, symmetry considerations, or by following a specific ansatz. The trial wavefunction is then used to calculate the expectation value of the Hamiltonian operator, which represents the total energy of the system. The variation parameters are adjusted systematically in order to minimize the expectation value of the Hamiltonian. This adjustment process is typically performed using numerical optimization techniques, such as gradient descent or minimization algorithms. By finding the optimal values of the variation parameters that minimize the energy, the trial wavefunction is optimized to approximate the true wavefunction of the system. The resulting trial wavefunction, obtained after minimizing the energy, serves as an approximation to the exact wavefunction of the system. The corresponding energy is an approximation to the true energy eigenvalue of the system.

The variation method is particularly useful in the situations where it is challenging to determine a good unperturbed Hamiltonian or when perturbation theory is not applicable. By allowing for flexibility in the choice of trial wavefunctions, the variation method can provide accurate approximate solutions to a wide range of quantum mechanical problems. However, in cases where a good unperturbed Hamiltonian is known, perturbation theory may offer a more efficient and straightforward approach. Overall, the variation method is a valuable tool in quantum mechanics, offering a systematic and adjustable approach to approximate wavefunctions and energies, making it a versatile and robust method for solving complex quantum mechanical problems.

Ritz theorem is the main theorem, which states that, a time-independent Hamiltonian, H, with a set of eigenvalues, E_n and eigenvectors, $|\Psi_n>$ satisfying the equation is given as:

$$H|\psi_n>=E_n|\psi_n> \tag{1.4}$$

Now, in the Hilbert space for any arbitrary ket vector $|\psi>$ and an exact ground state energy E_0, H must satisfy the ket as:

$$<H>=\frac{\langle\psi|H|\psi\rangle}{\langle\psi|\psi\rangle}\geq E_0 \tag{1.5}$$

When $|\psi> = |\psi_0>$ then the equality holds (1.6)

By expanding $|\psi>$ in the eigenstates of H we get

$$|\psi> = \sum_n C_n|\psi_n> \tag{1.7}$$

When $|C_n|^2 \geq 0$ and $E_n \geq E_0$, then we get

$$\frac{\langle\psi|H|\psi\rangle}{\langle\psi|\psi\rangle}=\geq E_0 \tag{1.8}$$

Hence, we can conclude that E_0 is a lower bound on the $<H>$, which means that we can approximate E_0 by a minimization of $<H>$ with respect to any parameters that $|\psi>$ might depend on. The lower the value of $<H>$, the closer it is to E_0. Therefore, $<H>$ can be minimized by varying ψ and take the minimum value of $<H>$ in an estimate for E_0. The variation of ψ is performed by first choosing for a suitable

functional form depending on a number of parameters say α, β, γ..... Then, minimization of the Hamiltonian is accomplished by finding values of α, β, γ..... for which the condition

$$(\frac{dH}{d\alpha})_{\alpha=\alpha_0} \tag{1.9}$$

is satisfied. Thus, α_o gives the minimum value of $< H >$ [43].

1.5.2 Density matrix approach

The density matrix is considered as a highly valuable concept in quantum mechanics, as it extends the notion of a quantum state from a simple vector in a Hilbert space to a full-fledged operator, offering a more comprehensive description of a quantum system. This generalization is particularly significant because it enables the treatment of composite systems in a natural and efficient manner, especially when focusing on specific properties of one subsystem within the larger quantum system.

In essence, the density matrix is a mathematical representation that provides a complete description of a quantum system's quantum states, as well as information about the statistical distribution of those states. It allows us to consider the probabilities of different quantum states in a system and, as a result, is highly useful in various quantum mechanical calculations.

One key advantage of the density matrix is its versatility. It can be employed to describe mixed states, which represent situations where a quantum system is not in a pure state but rather exists in a statistical mixture of multiple states. This is particularly relevant in the study of open quantum systems or systems that interact with their environment, as they tend to evolve into mixed states.

Furthermore, the density matrix is instrumental in the study of subsystems within a larger quantum system. By tracing out or partial tracing over the degrees of freedom of other subsystems, one can extract information and calculate properties of the subsystem of interest. This property makes it a powerful tool for addressing complex quantum systems, such as those encountered in quantum information theory, quantum thermodynamics, and many-body physics.

In summary, the density matrix is a fundamental and versatile tool in quantum mechanics that allows for a comprehensive description of quantum states and their statistics. Its ability to handle composite systems and focus on subsystem properties makes it an indispensable tool in various areas of quantum physics and quantum information science.

The density matrix formalism is frequently employed because it offers the ability to handle broadening of resonances caused by collisions, a phenomenon that is not readily addressed using traditional theoretical approaches based solely on wave functions.

The state vector $|\psi>$ comprises of the maximal information about a quantum system. Definition of the projector $\hat{\rho}\psi = |\psi><\psi|$ is possible due to its alignment to any state vector $|\psi>$,. Let's consider that the density matrix or density operator of the system is symbolized by the symbol $\hat{\rho}$. This operator is basically a generalization of the projector $\hat{p}\psi$. Considering only the discrete case in which the system admits a wave- function described as $\hat{\rho} = \hat{p}\psi$. Then, for a normalized $|\psi>$, $\hat{\rho}$ possesses the important properties, which follow as

$$p^2 = p,\ \hat{\rho}^2 = \hat{\rho}, \tag{1.10}$$

and

$$Tr\left(p\right)=1,\ Tr\ (\hat{\rho})=1 \tag{1.11}$$

where $Tr(\hat{o}) = \sum_{j} < b_j \mid \hat{o} \mid b_j >$ is the trace of the operator $\hat{o}$ and $\left\{b_j\right\}$ an orthonormal basis on the Hilbert space of the system. If a density operator $\hat{\rho}$ is not normalized, i.e., $Tr(\hat{\rho}) \neq 1$, but finite then it is normalized as follows:

$$p = \frac{p}{Tr(p)}, \hat{\rho} = \frac{\hat{\rho}}{Tr(\hat{\rho})} \tag{1.12}$$

If the density operator can be expressed as a single projector, then $Tr(\hat{\rho}) = 1$. Density matrices fall into two major classes: pure states $\hat{\rho}$ which satisfy the equation $\hat{\rho}^2 = \hat{\rho}$. mixtures $\hat{\rho}$ which satisfy the equation, $Tr(\hat{q}^2) < Tr(\hat{q})$. The introduction of the density operator leads to two important statistical features of quantum mechanics:

i. From the knowledge of the density operator, it is probable to compute the mean value of any observable; and.
ii. The density operator itself progresses with time, which aids to study time dependent system [44].

The Schrödinger equation for a quantum mechanical system with time evolution is denoted by a wave function ψ_k and is given as:

$$i\hbar \frac{\partial}{\partial t}\left|\psi_k\right| = H(r,t)\left|\psi_k\right| \tag{1.13}$$

Here, complete system's Hamiltonian $H(r,t)$ is given as:

$$H(r,t) = H_0(r) + H_I(r,t) \tag{1.14}$$

Where $H_I(r,t)$ represents the interaction part of the Hamiltonian and $H_0(r,t)$ represents the unperturbed part of the Hamiltonian with eigen values and eigenfunction as E_n & $|u_n\rangle$ respectively. These eigenfunctions are assumed to be orthonormal such that $\langle u_n|u_m\rangle = \delta_{nm}$ & $\sum|u_n\rangle\langle u_n| = 1$. Hence the wavefunction for the system can be written as:

$$|\psi_k\rangle = \sum_n c_n^{(k)}(t)|u_n\rangle \tag{1.15}$$

Here, the expansion coefficients are represented by $c_n^{(k)}(t)$ which is the probable amplitude of the system having a wavefunction $|u_n\rangle$. From equation (1.13) & (1.15), we have:

$$i\hbar\sum_n \frac{d}{dt}c_n^{(k)}(t)|u_n\rangle = \sum_n H(r,t)c_n^{(k)}(t)|u_n\rangle \tag{1.16}$$

By taking the inner product of the above equation with $\langle u_m|$ and applying the orthogonality condition, the equation reduces to:

$$i\hbar\frac{d}{dt}c_m^{(k)}(t) = \sum_n c_n^{(k)}(t)H_{nm} \tag{1.17}$$

Where $$H_{nm} = \langle u_m|H_0|u_n\rangle + \langle u_m|H_I|u_n\rangle \tag{1.18}$$

At a given instant of time, the solution of the equations (1.18) & (1.16) may be used to determine the wavefunction $|\psi_k\rangle$ of the system.

Also, the expectation value of any observable quantity such as Hermitian operator 'A' may be obtained at any instant to time 't' by using this wave function $|\psi_k\rangle$ and is given as:

$$\langle A\rangle = \langle \psi_k | H_0 | \psi_k \rangle \tag{1.19}$$

The expectation value of A can be determined by using (1.19) & (1.15) such that

$$\langle A\rangle = \sum_k c_n^{(k)}(t) c_m^{(k)*}(t) A_{nm} \tag{1.20}$$

If the initial & final states are known then the above two equations are very useful in determining all the physical quantities associated with the system. But for the case of electron-phonon interactions, these equations are not sufficient in determining the exact energy of the state. Hence for this particular case, we have to apply density matrix formulation such that the combination of $|\psi_1\rangle, |\psi_2\rangle, |\psi_3\rangle .....$ with $\rho = \sum_k p_k |\psi_k\rangle\langle\psi_k|$ gives:

$$p_1 + p_2 + p_3 + ... = \sum_k p_k = 1 \tag{1.21}$$

As no quantum mechanical effect is able to explain why the probability is classical in nature, hence, can't be written as square of some probability amplitude. Hence, a density operator p_k is introduced such as

$$\rho = \sum_k p_k |\psi_k\rangle\langle\psi_k| \tag{1.22}$$

such that the density matrix elements are:

$$\rho = \sum_k p_{\ k} |\psi_k\rangle\langle\psi_k| \tag{1.23}$$

Here, the ensemble average is represented by summation over 'k'. The diagonal elements ρ_{nn} of the density matrix gives the probability of the system being at the energy eigenstate and $|u_n\rangle$ & $|u_m\rangle$ energy eigenstates at coherent superposition gives the of diagonal elements. The expectation value is given as:

$$\langle A\rangle = \sum_k p_k \langle\psi_k|A|\psi_k\rangle = \sum_{nm}[\sum_k p_k c_n^{(k)}(t)c_m^{(k)*}(t)]A_{nm} \tag{1.24}$$

Which can also be written as:

$$\langle A\rangle = \sum_{nm} \rho_{nm} A_{nm} \tag{1.25}$$

Again, simplifying equation (1.25), the equation becomes:

$$\langle A\rangle = \sum_m (\rho A)_{nm} = Tr(\rho A) \tag{1.26}$$

The time derivative of (1.23) helps in obtaining the of any observable quantity associated with the system which is given as:

$$\frac{\partial\rho}{\partial t} = \sum_k [p_k \{\frac{d}{dt}|\psi_k\rangle\}\langle\psi_k| + p_k \langle\psi_k|\{\frac{d}{dt}|\psi_k\rangle\} + |\psi_k\rangle\langle\psi_k|\frac{d}{dt} p_k \tag{1.27}$$

Now use of the equation (1.23) in equation (1.27), results in:

$$\frac{\partial\rho}{\partial t} = \frac{1}{i\hbar}[H,\rho] + |\psi_k\rangle\langle\psi_k|\frac{d}{dt} p_k \tag{1.28}$$

Here, the first term on the right-hand side serves as a commutator between the Hamiltonian and the density operator. Next term represents the relaxation term. Considering the case of pure state, time derivation for the classical probability lying within quantum states tends to fade away i.e., for the case of phonon-electron interactions.

Hence the equation (1.28), when the time derivative is replaced by relaxation time becomes:

$$\dot{\rho} = \frac{1}{i\hbar}[H, \rho] - \Gamma(\rho - \rho^{(eq)}) \tag{1.29}$$

Here, the decay rate defines the relaxation of ρ which is given by Γ into the equilibrium state $\rho^{(eq)}$.

1.5.3 Effective mass approximation

The effective mass approximation involves treating bound electrons within a material as if they were free particles, but with a modified mass, denoted as "m*". This approach focuses on representing the influence of the potential through the change in mass (from the original mass, "m", to the effective mass, "m*"), rather than explicitly considering a potential energy, V. By permitting the mass of an electron to vary, we can approximate any dispersion relation using a plane wave. This modified mass is referred to as the "effective mass." Within this approximation, we treat the electron as a classical particle, and numerous intricate phenomena are encapsulated by the concept of effective mass.

The free electron relation for energy-wave vector is given by:

$$\varepsilon = \left(\frac{\hbar^2}{2m}\right)k^2 \tag{1.30}$$

The above equation is known as effective mass equation and the approximation is called as effective mass approximation. Here, ε vs k is determined by the coefficient of k^2. Curvature is determined by the reciprocal of the mass i.e., $1/m$. When subjected to an applied electric or magnetic field within a periodic lattice, an electron behaves as though it possesses an effective mass, and this leads to its acceleration relative to the lattice.

The group velocity is defined as:

$$v_g = \hbar^{-1} \frac{d\varepsilon}{dk} \tag{1.31}$$

By differentiating the above equation, we get

$$\frac{dv_g}{dt} = \hbar^{-1} \frac{d^2\varepsilon}{dkdt} = \hbar^{-1}\left(\frac{d^2\varepsilon}{dk^2}\frac{dk}{dt}\right) \tag{1.32}$$

Where $$\frac{dk}{dt} = \frac{F}{\hbar} \tag{1.33}$$

Substituting equation (1.16) in equation (1.15), it is obtained:

$$\frac{dv_g}{dt} = \left(\frac{1}{\hbar^2}\frac{d^2\varepsilon}{dk^2}\right)F \tag{1.34}$$

Hence $$F = \left(\frac{\hbar^2}{d^2\varepsilon / dk^2}\right)\frac{dv_g}{dt} \tag{1.35}$$

As from Newton's law of motion, the value of mass for an electron from equation (1.18) is equal to $\left(\frac{\hbar^2}{d^2\varepsilon / dk^2}\right)$, hence the effective mass m^* is given by:

$$\frac{1}{m^*} = \frac{1}{\hbar^2}\frac{d^2\varepsilon}{dk^2} \tag{1.36}$$

In an energy band, a single electron can exhibit either positive or negative effective mass. A positive effective mass indicates an upward curvature of the band, denoted by a positive $\frac{d^2\varepsilon}{dk^2}$. Conversely, a negative effective mass signifies a downward curvature of the band, with a negative $\frac{d^2\varepsilon}{dk^2}$ [45].

1.6 Optical properties

When a photon interacts with a III-V semiconductor, it induces changes in its optical characteristics. Therefore, studying these optical properties provides valuable information about the semiconductor. The infrared spectra of various compounds can be utilized to obtain information about their binding energy, while the absorption of free carriers serves as supportive evidence for their effective mass. In terms of optical processes, there are three distinct types. At shorter wavelengths, photons interact with valence electrons, causing their excitation into the conduction band. This phenomenon is known as interband transition. On the other hand, longer wavelengths affect the semiconductor's optical properties through the interaction between photons and free carriers. Consequently, transitions occur either within the valence band or the conduction band, which are referred to as intraband transitions. Interband transitions, specifically between the conduction and valence bands, play a crucial role in most semiconductor devices. Bipolar devices, typically involving a p-n junction, operate based on these interband transitions. The relaxation time for such transitions is typically in the nanosecond range. A new category of devices, such as quantum cascade lasers,

relies on transitions occurring between bands within the conduction or valence bands. These transitions have a much shorter relaxation time, typically in the picosecond range. In contrast, intraband devices operate on transitions within a single band and are considered unipolar. These devices exhibit faster response times compared to interband devices. In this wavelength range, the optical properties are influenced by both the lattice structure and the presence of free carriers. Additionally, there is another type of intraband transition involving the transfer of a carrier from one subband to the same subband. This transition occurs through the absorption of a photon and the emission of a phonon, ensuring momentum conservation [46].

1.6.1 Interband transitions

In indirect gap semiconductors, optical transitions at the band edge can only occur with the assistance of phonons to provide the necessary momentum. This is because the momentum conservation requirement cannot be satisfied by the electron and hole alone. However, in low-dimensional semiconductors, such as quantum dots or nanocrystals, electron and hole wave functions confinement in real space leads to enlargement of their wave functions in momentum space. As a result, radiative recombination or optical absorption can advance through direct transitions without any involvement of phonons [47]. In the case of direct no-phonon transitions, only vertical transitions are allowed, meaning the electron and hole transition directly between energy states without any change in their momentum. However, the efficiency of these no-phonon transitions is relatively low. On the other hand, in bulk silicon and germanium, interband transitions can only occur with the assistance of phonons because the conservation of total momentum is required during an optical transition. Phonon-assisted transitions, although involving phonons, remain more efficient than no-phonon transitions in a wide

range of nanocrystal sizes [48].

1.6.2 Intraband transitions

In doped semiconductors in bulk materials, the transitions primarily involve only one type of carriers, allowing for the probing of the electronic structure in either the valence band or the conduction band. In bulk materials, this scenario is often treated as a system of free electrons. Since transitions must occur vertically in momentum space (k space), direct transitions between two states with different wave vectors are not possible. Instead, electron-phonon interactions play a role in facilitating these transitions. With a continuous succession of states, the carrier's transition can be perceived as an acceleration induced by the electromagnetic field resulting from the absorption of light by the carriers [49].

In quantum wells and quantum dots, the carriers are confined, and as a result, the optical absorption becomes dependent on the polarization of the incident light. Direct transitions are not permitted, and scattering mechanisms induced by phonons come into play. In quantum wells, intraband transitions occur between bound states and the continuum of states located above the barrier potential. These transitions are commonly employed in infrared detectors [50-52].

In quantum dots, due to confinement potential in all three spatial dimensions, intraband transitions can take place for any polarization of light without the need for scattering mechanisms [53]. Consequently, atomic-like selection rules can be applied to these optical transitions.

Transitions are only allowed if there is a difference of ±1 in the quantum number “l”

between the initial and final states. Intraband transitions in nanocrystals are particularly interesting as they typically occur in the infrared spectral range and involve only one type of carrier. Moreover, these transitions strongly depend on the charge state of the quantum dot, which can be intentionally altered [54-56].

1.6.3 Optical rectification

Electro-optic rectification, also known as optical rectification, is a nonlinear optical process that involves the generation of a quasi-DC polarization in a nonlinear medium when subjected to an intense optical beam. Optical rectification is a second-order phenomenon rooted in the inverse electro-optic effect [57]. This phenomenon can be understood by considering the symmetry properties of the nonlinear medium. The polarization does not change its sign simultaneously with the driving field. Consequently, if the driving field is represented as a sinusoidal wave, an average DC polarization is produced. When an applied electric field is delivered by a femtosecond pulse-width laser, the associated spectral bandwidth is extremely wide due to the short duration of the pulses. The mixing of different frequency components leads to the generation of a polarization that emits electromagnetic waves in the terahertz region. Zinc telluride is one of the materials capable of generating radiation in the 1mm wavelength range. Additionally, optical rectification occurs in low-dimensional semiconductor systems as second harmonic generation. Optical rectification serves as a significant mechanism for the generation of terahertz lasers [58].

1.7 Nonlinear optical processes

The behavior of light in nonlinear media defines one of the fields of the optics known as Nonlinear optics, where the dielectric polarization P exhibits a nonlinear response to the

electric field E of the light. Generally, at tremendously high intensities this kind of nonlinearity is observed, where the values of electric field and interatomic electric fields are comparable, typically they are the order of 10^8 V/m. The initial demonstration of nonlinear properties in the optical region was achieved through the harmonic generation of light by Franken and colleagues [59]. Nonlinear optics encompasses a wide range of optical phenomena, including:

I. Second harmonic generation: The process entails the production of light with a frequency doubled (wavelength halved) by annihilating two photons. This annihilation event leads to the creation of a single photon carrying twice the frequency.
II. Third harmonic generation: The process involves the conversion of light into a higher frequency by tripling its frequency (reducing its wavelength to one-third) through the annihilation of three photons, resulting in the creation of a single photon with triple the frequency.
III. And many other nonlinear effects.

Nonlinear effects can be classified into two main categories: parametric and non-parametric effects. Parametric nonlinearity denotes about those interactions where quantum state of the nonlinear material remains unchanged after interaction with the optical field. Consequently, these processes occur instantaneously. Energy and momentum conservation are crucial in the optical field, making phase matching and polarization dependence significant considerations in such interactions.

When a dielectric medium is exposed to an electric field, it undergoes polarization unless the medium has a transition occurring at the frequency of the field. In such cases,

each individual molecule within the medium behaves as a dipole, possessing a dipole moment denoted by P_i. The dipole moment vector per unit volume, symbolized as P, can be expressed as follows:

$$P = \sum_I P_i \tag{1.37}$$

The summation in the equation is performed over the dipoles present within the unit volume. The alignment or orientation of the molecular dipoles in response to the external field is influenced by both the properties of the medium and the strength of the field. Therefore, the effect can be expressed as [60].

$$\vec{P}(\omega) = \varepsilon_0 \chi^{(1)} \vec{E}(\omega), \tag{1.38}$$

The symbol $\chi^{(1)}$ represents the polarizability or dielectric susceptibility of the medium. This relationship holds true for field strengths generated by conventional sources. However, the quantity $\chi^{(1)}$ is not constant but varies with frequency. It remains independent of the field strength (E) only in the sense that its magnitude is a function of the frequency. When dealing with highly intense laser radiation, the aforementioned relation becomes inadequate and needs to be generalized to a more comprehensive form given as:

$$\vec{P}(\omega) = \varepsilon_0 \left(\chi^{(1)} \vec{E}(\omega) + \chi^{(2)} \vec{E}^{\,2}(\omega) + \chi^{(3)} \vec{E}^{\,3}(\omega) + \ldots\ldots\ldots \right) \tag{1.39}$$

where $\chi^{(1)}$ is the same as χ in Eq. (1.14) the coefficients $\chi^{(2)}, \chi^{(3)}, \ldots\ldots\ldots\ldots$ define the degree of nonlinearity and are acknowledged as nonlinear optical susceptibilities of the order of second and third. The medium in which the polarization is described by a

nonlinear relation is called a nonlinear medium [61,62].

Here, $\vec{P}^{(2)} = \chi^{(2)} \vec{E}^{2}(\omega)$ defines the second order nonlinear polarization and $\vec{P}^{(3)} = \chi^{(3)} \vec{E}^{3}(\omega)$ represents the third order nonlinear polarization.

1.7.1 Second order and third order harmonics

The incident field on a medium is

$$E = E_0 \cos \omega t \tag{1.40}$$

where E_0 represents the amplitude of the field and ω defines the angular frequency.

Substitution of eq. (1.16) in eq. (1.15) leads to

$$P = \varepsilon_0 \chi^{(1)} E_0 \cos \omega t + \varepsilon_0 \chi^{(2)} E_0^2 \cos^2 \omega t + \varepsilon_0 \chi^{(3)} E_0^3 \cos^2 \omega t + ... \tag{1.41}$$

Simplification of eq. (1.17) is written as:

$$P = \frac{1}{2}\varepsilon_0 \chi^{(2)} E_0^2 + \varepsilon_0 (\chi^{(1)} + \frac{3}{4}\chi^{(3)} E_0^2) E_0 \cos \omega t + \frac{1}{2}\varepsilon_0 \chi^{(2)} E_0^2 \cos 2\omega t + \frac{1}{4}\varepsilon_0 \chi^{(3)} E_0^3 \cos^2 \omega t + ... \tag{1.42}$$

Here, the first term represents a constant term by which a dc field is being arise across the medium, having a comparatively little practical importance. External polarization is given by second term and is known as first or fundamental harmonic of polarization. The third term which is oscillating at a frequency of 2ω is named as second harmonic of polarization. The fourth term is entitled as the third harmonic of polarization and so on [63]. The nonlinear susceptibility of m^{th} order is obtained by using equation (1.42) and the density matrix as:

$$\chi^{(m)} = \frac{1}{\varepsilon_0 N_\nu E^m(t)} Tr(\rho^{(m)} er) \tag{1.43}$$

Where, ε_0 is the primitivity of free space, N_ν is the charge carrier density and Tr denotes the trace or summation over diagonal elements of matrix $\rho^{(m)} er$. Hence, we obtained [64-67]:

Optical Rectification coefficient term is given as:

$$\chi_0^{(2)} = 4\frac{N_\nu{}^3\sigma}{\varepsilon_0\hbar^2}\mu_{01}^2\delta_{01} \times \frac{\omega_{01}^2(1+\frac{T_1}{T_2}) + (\omega^2 + \frac{1}{T_2^2})(\frac{T_1}{T_2} - 1)}{[(\omega_{01}-\omega)^2 + \frac{1}{T_2^2}][(\omega_{01}+\omega)^2 + \frac{1}{T_2^2}]} \tag{1.44}$$

Second harmonic generation term is represented by the formula:

$$\chi_\omega^{(2)} = \frac{\sigma}{\varepsilon_0} \frac{M_{12}M_{23}M_{31}}{(\hbar\omega - E_{12} - i\hbar\Gamma_{21})(2\hbar\omega - E_{31} - i\hbar\Gamma_{31})} \tag{1.45}$$

Third harmonic generation term is given as:

$$\chi_{3\omega}^{(3)} = \frac{N_\nu e^4}{\hbar^3} \frac{M_{01}M_{12}M_{23}M_{30}}{(\omega - \omega_{10} + i\Gamma_o)(2\omega - \omega_{20} + i\Gamma_o)(3\omega - \omega_{30} + i\Gamma_o)} \tag{1.46}$$

Here, e is representing electronic charge, and relaxation time is represented by T_1, T_2 & Γ_o. $\omega_{ij} = (E_i - E_j)/\hbar$ shows the frequency for the transition and matrix elements are given by $M_{ij} = \left|\langle \psi_i | er | \psi_j \rangle\right|$ $(i, j = 0,1,2,3)$

1.7.2 Absorption coefficient and Refractive index change

On multiplying each and every element of equation (1.29) by $\langle u_n|$ and $|u_m\rangle$, final

equation becomes:

$$\dot{\rho_{nm}} = \frac{1}{i\hbar}[H, \rho]_{nm} - \Gamma_{nm}(\rho - \rho^{(eq)})_{nm} \tag{1.47}$$

Where $$\dot{\rho}_{nm} = \langle u_n | \dot{\rho} | u_m \rangle \tag{1.48}$$

Now using equation (1.14) and equation (1.48), the equation that arises is given as:

$$\dot{\rho}_{nm} = \frac{1}{i\hbar}[H_0, \rho]_{nm} + \frac{1}{i\hbar}[H_I, \rho]_{nm} - \Gamma_{nm}(\rho - \rho^{(eq)})_{nm} \tag{1.49}$$

Now, using the value of $H_I(r,t) = er.\varepsilon E(t)$, where ε represents the unit polarization vector and applying the eigen value equation, the equation (1.49) becomes

$$\dot{\rho}_{nm} = -i\omega_{nm}\rho nm + \frac{E(t)}{i\hbar}\sum_i (M_{ni}\rho_{im} - \rho_{ni}M_{im}) - \Gamma_{nm}(\rho - \rho^{(eq)})_{nm} \tag{1.50}$$

Here, M_{nm} represents the dipole matrix elements and transition frequency is given by ω_{nm}. When the expectation value of the matrix elements of $H_I(r,t)$ are comparable to energy spacing of eigenstates, then the solution of equation (1.50) is given as:

$$\rho = \rho^{(0)} + \lambda\rho^{(1)} + \lambda^{(2)}\rho^{(2)} + \lambda^{(3)}\rho^{(3)} + ... \tag{1.51}$$

Now, replacing H_I by λH_I using λ as a positive number smaller than 1, signifying the smallness of H_I, comparing the coefficients of λ from equation (1.51) with equations (1.49) and (1.51), the obtained equation is

$$\dot{\rho}_{nm}^{(0)} = -i\omega_{nm}\rho_{nm}^{(0)} - \Gamma_{nm}(\rho - \rho^{(eq)})_{nm} \tag{1.52}$$

And for N=0,1,2,3……

$$\dot{\rho}_{nm}^{(N+1)} = -(i\omega_{nm} + \Gamma_{nm})\rho_{nm}^{(N+1)} + \frac{E(t)}{i\hbar}\sum_{i}(M_{ni}\rho_{im}^{(N+1)} - \rho_{im}^{(N+1)}M_{im}) \tag{1.53}$$

Now, for simplification involving higher orders of density matrix elements some substitutions were made in equation (1.53). the final equation obtained is given as:

$$\rho_{nm}^{(1)}(t) = \frac{1}{i\hbar}\sum_{j}(M_{nj}\rho_{jm}^{(0)} - \rho_{jm}^{(0)}M_{jm})e^{-(i\omega_{nm}+\Gamma_{nm})t}\int_{-\infty}^{t} E(t')e^{(i\omega_{nm}+\Gamma_{nm})t'}dt' \tag{1.54}$$

Absorption coefficient: The absorption coefficient governs the penetration of light having any particular wavelength into a material before its absorption. For the material's which is thin & have low absorption coefficient, light is not absorbed properly also, it appears to be transparent to that wavelength. The absorption coefficient depends on the material as well as on the wavelength of light which is being absorbed. Semiconductor materials having a sharp edge within their absorption coefficient as the light having an energy below the band gap does not contains adequate energy to excite an electron into the conduction band from the valence band, hence, this light is not absorbed. Also, different semiconductor materials bag to have a different absorption coefficient:

- Materials having high absorption coefficients absorb a photon more readily and further excite an electron into the conduction band easily.
- The absorption coefficients of materials assist the engineers in the determination of the material to be used for their solar cell designs.

The Fourier expansion of the electric field for an electromagnetic field for an interacting

system is given as:

$$E(t) = \sum_j F(\omega_j) e^{-i\omega_j t} \tag{1.55}$$

Solving equation (1.56) and (1.55) and applying the condition for off diagonal elements as well as trace, we obtained the formula for absorption coefficient and refractive index which is given as:

$$\alpha^{(1)}(\omega) = \omega\sqrt{\mu/\varepsilon_r}\,\frac{|M_{01}|^2 N\hbar\Gamma_0}{[(E_{10}-\hbar\omega)^2+(\hbar\Gamma_0)]^2} \tag{1.56}$$

$$\alpha^{(3,\mathrm{I})}(\omega) = -2\omega\sqrt{\mu/\varepsilon_r}\,(\mathrm{I}/\varepsilon_0\eta_r c)\frac{|M_{01}|^4 N\hbar\Gamma_0}{[(E_{10}-\hbar\omega)^2+(\hbar\Gamma_0)]^2} \times\left(1-\frac{|M_{11-}M_{00}|^2}{4|M_{01}|^2}\left\{\frac{(E_{10}-\hbar\omega)^2-(\hbar\Gamma_0)^2+2E_{10}(E_{10}-\hbar\omega)}{(E_{10})^2+(\hbar\Gamma_0)^2}\right\}\right) \tag{1.57}$$

Total absorption coefficient $\alpha(\omega,\mathrm{I})$ is given as:

$$\alpha(\omega,\mathrm{I}) = \alpha^{(1)}(\omega) + \alpha^{(3)}(\omega,\mathrm{I}) \tag{1.58}$$

Refractive index: The refractive index or index of refraction denoted by n of any substance (optical medium) helps in describing the propagation of light, or any other radiation, through any medium.

Using real part of the susceptibility, refractive index changes can be determined as:

$$\frac{\Delta n(\omega)}{n_r} = \mathrm{Re}\left[\frac{\chi(\omega)}{2n_r^2}\right] \tag{1.59}$$

$$\frac{\Delta\eta^{(1)}(\omega)}{\eta_r} = \frac{1}{2\eta_r{}^2\varepsilon_0}\left|M_{01}\right|^2\left[\frac{E_{10}-\hbar\omega}{(E_{10}-\hbar\omega)^2+(\hbar\Gamma_0)^2}\right] \tag{1.60}$$

$$\frac{\Delta\eta^{(3,\mathrm{I})}(\omega,\mathrm{I})}{\eta_r} = -\frac{\mu c}{4\eta_r{}^3\varepsilon_0}\left|M_{01}\right|^2\left[\frac{N\mathrm{I}}{[(E_{10}-\hbar\omega)^2+(\hbar\Gamma_0)^2]^2}\right]$$
$$\times\left[4(E_{10}-\hbar\omega)\left|M_{01}\right|^2-\frac{\left|M_{11-}M_{00}\right|^2}{(E_{10})^2+(\hbar\Gamma_0)^2}\{(E_{10}-\hbar\omega)\times[E_{10}(E_{10}-\hbar\omega)-(\hbar\Gamma_0)^2(2E_{10}-\hbar\omega)\}\right] \tag{1.61}$$

The total refractive index change is

$$\frac{\Delta\eta(\omega,\mathrm{I})}{\eta_r} = \frac{\Delta\eta^{(1)}(\omega)}{\eta_r} + \frac{\Delta\eta^{(3,\mathrm{I})}(\omega,\mathrm{I})}{\eta_r} \tag{1.62}$$

Where $\mu_{ij} = \left|\left\langle\psi_i\left|z_{T1}\right|\psi_j\right\rangle\right|(i,j=0,1)$ are the matrix elements of the dipole moment, $\psi_i(\psi_j)$ are the Eigen functions, $\omega_{01} = \frac{E_1-E_0}{\hbar}$ is the difference between two energy levels. ω is the frequency of Electromagnetic field, Γ_0 relaxation time.

1.8 Problem statement and objectives

The principal objective of the present thesis is to explore the interaction between electrons-hole correlation and linear & non-linear optical properties in Quantum Dots (QDs) in the presence of hydrostatic pressure & temperature. Additionally, we aim to investigate how the third harmonic generation in QDs changes with variations in the Rashba SOI factor, magnetic field, hydrostatic pressure & temperature. We also investigated how optical rectification coefficient & optical absorption behaves in quantum well in the presence of electric field, hydrostatic pressure & temperature. Understanding the optical response in the presence of external perturbations in QD &

QW is not only fascinating but also holds significant potential for various applications such as quantum dot lasers, quantum information processing, photodetectors, and opto-spintronics devices [68,69].

Furthermore, our study focuses on multiphoton transitions during optical excitation, which offer unique advantages over single-photon processes [70], particularly in biological and medical applications [71]. Multiphoton excitations play a crucial role in the development of ultra-sensitive quantum wells, infrared photodetectors, and Quantum Cascade Lasers (QCL) [72]. These devices rely on intraband transitions, which have also been utilized for wavelength conversion in QCL for near-infrared signals [73].

To investigate this dynamic problem involving the interplay of different external perturbations, such as the effect of electric field, magnetic fields, hydrostatic pressure & temperature and Rashba SOI in QDs & QW, we employed the powerful effective mass approximation & Density matrix theory for enhanced accuracy. These theories established a connection between the solution of the Schrödinger equation, considering a periodic Hamiltonian, and the solution of another equation with a time-independent Hamiltonian represented by an infinite matrix known as the Density matrix. This method, which has been successfully applied to various atomic systems and nanostructures in previous studies [74-77], offers the distinct advantage of simultaneously addressing discrete and continuous states within a single system.

References

[1] R.Dingle, A.C.Gossard and W.Wiegmann, Phys. Rev. Lett.33 (1974) 827.

[2] L.L. Chang, L.Esaki and R.Tsu, Appl. Phys. Lett. 24 (1974) 593.

[3] Guoqiang, Kouta Tateno, Hideki Gotoh and Tetsuomi Sogawa, Special Feature: Front-line Materials Research, 8 (2010) 8.

[4] R Khordad, Ind. J. Phys., 87(7) (2013) 623.

[5] R Khordad and H R Rastegar Sedehi, Eur. Phys. J. Plus, 134 (2019) 133.

[6] S Sargolzaeipor, H Hassanabadi and W S Chung Eur. Phys. J. Plus 133 (2018) 11827.

[7] Xin-Jun Ma, Wei Zhang, Shuang Han, Xianglian, Pei-Fang Li, Cui-Lan Zhao, Zhao-Hua Ding, Yong Sun and Jing-Lin Xiao, Physica E: Low-dimensional Systems and Nanostructures, 144 (2022) 115387.

[8] Mikhail I.F.I., Ismail I.M.M. and El Shafee, Indian J Phys, 96 (2022) 2717.

[9] G. A. Prinz, Science 282 (1998) 1660.

[10] Supriyo Bandyopadhyay, Physics of Nanostructured Solid State Devices, Springer (2012).

[11] E. U. Rafailov, M. A. Cataluna, and W. Sibbett, Nat. Photonics 1 (2007) 395.

[12] J. Berezovsky, M. H. Mikkelsen, N. G. Stoltz, L. A. Coldren, and D. D. Awschalom, Science 320, (2008) 349.

[13] K. Hennessy, A. Badolato, M. Winger, D. Gerace, M. Atature, S. Gulde, S. Falt, E. L. Hu, and A. Imamoglu, Nature 445 (2007) 896.

[14] S. Banerjee and D. Charkavorty, J. Mater. Sci. 37 (2002) 4261.

[15] Siddhartha Lahon, P.K. Jha, and Man Mohan, J. Appl. Phys. 109 (2011) 054311.

[16] Bhattacharyya K., Debnath D. and Chatterjee A., Sci Rep 13 (2023) 5500.

[17] S. K. Tewksbury, Semiconductor Materials, (1995).

[18] Zanatta, A.R., Sci Rep 9 (2019) 11225.

[19] Sharma H. K., Sil S. and Chatterjee A., J. Magn. Magn Mater., 529 (2021) 167711.

[20] S Sargolzaeipor, H Hassanabadi and W S Chung Mod. Phys. Lett. A 34 (2019) 1950023.

[21] John Dakin, Robert G. W. Brown, Handbook of optoelectronics, Volume 1, CRC Press, (2006).

[22] S. J. Moss, and A. Ledwith, The Chemistry of the Semiconductor Industry, Springer, (1987).

[23] Bhattacharyya K., Debnath D. and Chatterjee A., J. Magn. Magn. Mater., 506 (2020) 166745.

[24] J. Tersoff, Phys. Rev. B, 30(8) (1984) 4874.

[25] A. L. Efros, Sov. Phys. Semicond., 16 (1982) 772.

[26] L. E. Brus, J. Chem. Phys., 79 (1983) 5566.

[27] A. K. Atayan, E.M. Kazaryan, A.V. Melikesetyan and H. A. Sarkisyan, The European Physical Journal, B63 (2008) 485.

[28] X. Wen-fang, Chin.Phys.Soc. 9 (2005) 139.

[29] R Khordad and H R Rastegar Sedehi, Sol. Stat. commun., 269 (2018) 118.

[30] W. Paul, D.M. Warschauer in Solids under pressure – McGraw Hill – (1963).

[31] H. Ehrenreich, J. Appl. Phys., 32 (1961) 2155.

[32] P. M. Mathews and K. Venkatesan – A Textbook of Quantum Mechanics- TMH – eigth reprint- (1984).

[33] S. L. Gupta and Kumar, Solid State Physics, seventh edition – (1989).

[34] Pallab Battacharya, Semiconductor optoelectronic devices, PHI- (1994).

[31] M.S. Dresselhaus, Optical properties of Solids- Part II.

[32] E.Rashba and Fiz. Tverd, Sov. Phys. Solid State 2 (1960)1109.

[33] G. Dresselhaus, Phys. Rev. 100 (1955) 580.

[34] M. D'yakonov and V.I. Perel. Fiz. Tverd. Tela. 60, 1954, Sov. Phys.Solid State,33 (1971)1053.

[35] S. Datta, B. Das, Appl. Phys. Lett. 56 (1990) 665.

[36] A. Manchon, H.C. Koo, J. Nitta, S.M. Frolov, R.A. Duine, Nat. Mater. 14 (2015) 871.

[37] Mikhail I.F.I., Ismail I.M.M. and El Shafee, Eur. Phys. J. Plus, 137 (2022) 610.

[38] Y.A. Bychkov, E.I. Rashba and J. Phys. C Solid State Phys. 17 (1984) 6039.

[39] A.A. Portacio, B.A. Rodriguez and P. Villamil, Phys. B, 511 (2017) 68.

[40] Rani R., Kumar V., Bhardwaj S.B. and Chand F., Indian J Phys 94 (2020) 1705.

[41] P. Saini, A. Boda, A. Chatterjee, J. Mag. Mag. Mat. 485 (2019) 407.

[42] E.I. Rashba, J. Supercond. 18 (2005) 137.

[43] M.R.Brozel and G.E. Stillman, Properties of Gallium Arsenide, IEEE (1996).

[35] Gennaro Auletta, Mauro Fortunato, Giorgio Parsi – Quantum Mechanics – Cambridge University Press – (2014).

[36] C. Hilsum and A.C. Rose Innes, Semiconducting III-V Compounds (1961).

[37] D.S. Kumar, S. Mukhopodhyay and A. Chatterjee, Phys. B, 501 (2016) 129.

[38] E. Papp and C. Micu, Superlatt. Microstruct., 48 (2010) 9.

[39] R. Shankar, Principles of Quantum Mechanics (Plenum Press), New York, (1982).

[40] G. Bastard: wave Mechanics Applied to Semiconductor Heteristructures (les editions de Physique, Paris, (1990).

[41] C. Weisbuch, B.Vanter : Quantum Semiconductor Structures, Fundamentals and Applications, Academic Press, New York (1991).

[42] E. Rosencher, B.Vinter : Optoelectronique (Massson, Paris (1998).

[43] Dieter Bimberg, Semiconductor Nanostructures Springer-Verlag Pub., 2010.

[44] Y. Safaei, S. Davatolhagh, M.M. Golshan, Superlatt. Microstruct., 64 (2013) 140.

[45] S.M. Sze, Physics of semiconductor devices, 2nd edition, Wiley Publisher, (1981).

[46] Pallab Battacharya, Semiconductor optoelectronic devices, PHI- (1994).

[47] W. Kohn, Shallow impurity states in silicon and germanium, (Solid State Physics v.5 Ed. Sietz F. Turnbull, D.) Academic, 257 (1957).

[48] L.D. Landau, Phys.Z.Sowjetunion 3 (1965) 664.

[49] H. Fröhlich, H.Pelzer, S.Zienau, Phil. Mag. 41 (1950) 221.

[50] R Khordad and H R Rastegar Sedehi, Eur. Phys. J. Plus, 134 (2019) 133.

[51] Y. Toyozawa, J.Phys.Chem.Sol. 25 (1964) 59.

[52] Vikhnin, Phys. Sol. Stat. 40 (1998) 834.

[53] G.Allan, C.Delerue, Y.M. Niquet, Phys. Rev. B 63 (2001).

[54] Cyril Hilsum and A.C. Rose Innes, Semiconductor III-V Compounds, Pergamon Press, (1961).

[55] S. Sakiroglu, B. Gisi, Y. Karaaslan, E. Kasapoglu, H. Sari, I. Sokmen, Phys. E, 81 (2016) 59.

[56] Kh. Shakouri, B. Szafran, M. Esmaeilzadeh and F.M. Peeters, Phys. Rev. B, 85 (2012) 165314.

[57] M. Akbari, G. Rezaei, R. Khardad, Superlatt. Microstruct., 101 (2017) 429.

[58] M. D'yakonov and V.I. Perel. Fiz. Tverd. Tela. 60, 1954, Sov. Phys.Solid State,33 (1971)1053.

[59] M.I. Dyakonov and V.I. Perel, Sov. Phys. JETP Lett. 13 (1971) 467.

[60] A. Vanitha, C.W. Lee, A.J. Peter, Phys. Lett. A, 375 (2010) 208.

[61] J.E. Hirsch Phys. Rev. Lett. 83 (9) (1999) 1834.

[62] N.A. Sinitsyn, J.Phys. Condens. Matter 20 (2008) 2.

[63] Y. Kato, R.C. Myers, A.C. Grossard, D.D.Awschalom, Science 306 (1910) 5703.

[64] S. Benner and H. Haug, Phys. Rev. B 47 (1993) 15750.

[65] M. J. Karimi and G. Rezaei, J. Appl. Phys. 111 (2012) 064313.

[66] Siddhartha Lahon, P.K. Jha, and Man Mohan, Physica E 43 (2010) 211.

[67] Mehmet Sahin, J. Appl. Phys. 106 (2009) 063710.

[68] L.M. Burileanu, and A. Radu, Optics Communications 284 (2011) 2050.

[69] Tairong Chen, and Wenfang Xie, Solid State Communications 152 (2012) 314.

[70] M.E. Mora-Ramos, C.A. Duque, E. Kasapoglu, H. Sari, I. Sökmen, Journal of Luminescence 132 (2012) 901.

[71] H. Yildirim, M. Tomak, Phys. Stat. Sol. B 243 (2006) 4057.

[72] R. Khordad, B. Mirhosseini, Optics Communications 285 (2012) 1233.

[73] Anchala, S. P. Purohit, and K. C. Mathur, J. Appl. Phys. 112 (2012) 94306.

[74] M. Kirak and Y. Altinok, Eur. Phys. J. B 85 (2012) 344.

[75] Zhi-Hai Zhang, Kang-Xian Guo, Bin Chen, Rui-Zhen Wang, Min-Wu Kang, Superlatt. Microstruct. 46 (2009) 672.

[76] A. Voskoboynikov, C.P. Lee, O. Tretyak, Phys. E 10, 107 (2001).

[77] N.N. Lebedev, Special Functions and Their Applications (Prentice Hall Inc., London, 1965).

CHAPTER 2

MANIPULATING OPTICAL RECTIFICATION CO-EFFICIENT WITH EXTERNAL PARAMETERS*

2.1 Introduction

In the past two decades, there have been speedy developments in the field of nanoscience and nanotechnology. Hence the detailed study of all the aspects of the low-dimensional semiconductor nanostructures becomes imperative. These nanostructures, namely, quantum dots (QDs), quantum wires and quantum wells exhibit unique electronic and optical properties, contrasting to macroscopic structures [1-4]. Because of these standalone properties, scientists have shown great interest in nanostructures, as they offer a wide area of research to understand them as well as the associated physics [5-7]. Charge carriers in various nanostructures are confined to one, two, and three dimensions in accordance with their structural dimensions. Out of these three classes, the class of zero-dimensional structures, also called as QDs, in which charge carriers are constrained in all the 3-dimensions, is the most extensively studied class of semiconductor structures. This quantum constriction of charge carriers leads to the peculiar changes such as discrete energy levels generation, increase in the density of states at some specific energies and the counterintuitive alteration in the optical absorption spectrum [8-12]. Also, the effect of confinement on the optical and electronic properties strengthens as we move from quantum wells to QDs. A 1D-quantum dot is a nanostructure that can be considered as a small part of a 1D QW bordered by a two-wall potential. In 1D QW, the charge carriers are free to move along

* *(Part of this work has been published in **Physica E: Low-dimensional Systems and Nanostructures, 118 (2020), 113918**)*

the wire whereas in 1D QD, the charge carriers are restricted from moving along the length [13-15].

Linear and nonlinear optical [16-18] properties such as the nonlinear ORC, optical absorption coefficient, and alteration in the refractive index have wide potential applications in optoelectronic and photonic devices such as photo-detectors, far-infrared laser amplifiers, and high-speed electro-optical modulators. Amongst all the nonlinear optical properties, the second-order nonlinear optical property has a vital role to play due to its simplest and the lowermost order nonlinear effect, as well as magnitude, being greater than all the other nonlinearities. Second-harmonic generation (SHG) and ORC are produced due to second-order nonlinear optical interaction of two incident fields with optical media. Xie and Bass et al. in 1962 performed initial work on OR [19, 20] whereas Franken et al. reported the very first experimental observation of SHG [21]. The discovery of SHG leads to the beginning of the field of nonlinear optics [22]. As all the incident beams at frequency ω are transformed to frequency 2ω, the role of SHG becomes more efficient [23]. Baskoutas et al. studied the effect of exciton in OR for the case of semi-parabolic QDs for excitons in semi-parabolic potential [24]. Duque et al. also have investigated the combined effects of hydrostatic pressure, temperature, intense laser field, magnetic field, and applied electric field in the excitonic system [25-29].

Many researchers have studied the interaction effect for the 2^{nd} order nonlinear properties in 1-D semi-parabolic QDs [30-33]. By applying the method of analytical approximation, it is shown that the SHG and OR coefficients are affected by the effect of excitons. With the application of temperature and external hydrostatic pressure, band

structure and the semiconductor materials properties can be enhanced, which can be further used in the designing and preparation of a new generation of efficient semiconductor devices like heterostructure lasers, QLEDs, white light sources, etc.

However, only a handful of works are available in the literature which has investigated the effect of excitons to study the nonlinearities of the QDs, quantum wells, or quantum wires. Further, not many studies are performed in this regard while taking the effect of pressure and temperature into consideration. Here we have considered the factors of hydrostatic pressure and temperature into consideration and investigated the ORC in an excitonic semi-parabolic QD. We obtained many interesting results wherein we have shown how external hydrostatic pressure, temperature and excitonic pairing interplay to shift the ORC peaks. We also observe how these parameters change the strength of the ORC peaks. In this chapter, a brief introduction is given in Section 1. In Section 2, exciton states are obtained by using the Eigenfunction and Eigen-energies. The numerical results for GaAs semi-parabolic QDs are presented in Section 3. Hence, the study of nonlinearities in QD's by considering only the electron state is not appropriate. Finally, Section 4 draws the conclusions.

2.2 Theory and Model

In the framework of effective mass approximation, for a pair of electron-hole in 1D QDs, Hamiltonian with semi-parabolic confining potential is given by [13, 34]:

$$H_e = \frac{p_h^2}{2m_h^*} + \frac{p_e^2}{2m_e^*} + V(z_e) + V(z_h) - \frac{e^2}{\varepsilon |z_e - z_h|} \tag{2.1}$$

where (z_e , z_h > 0).

Where m_h^* and m_e^* respectively represents an effective mass of hole and electron. The background dielectric constant is given by ε, and the semi-parabolic potential is given by $V(z_l)$ which is written as:

$$V(z_l) = \begin{cases} \frac{1}{2} m_i^* \omega_0^2 z_l^2, & z_l \geq 0, \\ \infty, & z_l \leq 0 \qquad (l = e, h) \end{cases} \tag{2.2}$$

The effective pressure and temperature variation are associated with the variation of hole and electron effective masses as [35-37]:

$$m_e^*(P,T) = m_o[1 + \frac{7510}{E_g(P,T) + 341} + \frac{15020}{E_g(P,T)}]^{-1} \tag{2.3}$$

With $$E_g(P,T) = [1519 - \frac{0.5405T^2}{T + 204} + 10.7P] \tag{2.4}$$

And $$m_h^*(P,T) = (0.09 - 0.20 \times 10^{-3} P - 3.55 \times 10^{-5} T) m_0 \tag{2.5}$$

Here E_g is in meV, P is in "kbar" and T is in "Kelvin."

The Hamiltonian is segmented into two terms considering, the relative motion and center of mass, respectively [37,38]:

$$H_e = H_r + H_c \tag{2.6}$$

Where $$H_r = \frac{p^2}{2\mu} + \frac{1}{2}\mu\omega_0^2 z_r^2 - \frac{e^2}{\varepsilon(P,T)|z_r|}, \tag{2.7}$$

And $$H_c = \frac{P^2}{2M_T} + \frac{1}{2} M_T \omega_0^2 Z_T^2 \tag{2.8}$$

And for

$$\text{T<200K, } \varepsilon(P,T) = 12.74e^{(9.4\times10^{-5})(T-75.6)+1.73\times10^{-3}P} \tag{2.9}$$

And the coordinate of the centre of mass is given by:

$$Z_T = \frac{m_h^* z_h + m_e^* z_e}{M_T} \tag{2.10}$$

Here, the complete mass is given by $M_T = m_h^* + m_e^*$; the relative coordinate is $z_r = z_e - z_h$, momentum operator is $p = \frac{\hbar}{i}\nabla$, and the reduced mass $\mu_r = m_h^* m_e^* / M_T$.

The exciton wave function and energy levels are obtained as

$$\psi_f(z_h, z_e) = \varphi(z_r)\phi(Z_T), \tag{2.11}$$

$$E_T = E_{z_r} + E_{Z_T} \tag{2.12}$$

The term representing the centre of mass part can be considered as the problem for 1D semi-parabolic oscillator where Hamiltonian is given by H_c and Eigen functions & Eigen energies are determined to be [39,40]:

$$\phi_k(Z_T) = N_k \exp(-\frac{1}{2}\alpha^2 Z_T^{\,2}) H_{2k+1}(\alpha Z_T) \tag{2.13}$$

And $$E_k = (2k + \frac{3}{2})\hbar\omega_{0,}\ k = (0,1,2.....), \tag{2.14}$$

Where 'H' is the Hermite Polynomial,

$$\alpha = \sqrt{M_T \omega(P)/\hbar} \tag{2.15}$$

$$N_k = [\frac{1}{\alpha}\sqrt{\pi}2^{2k}(2k+1)!]^{-1/2} \tag{2.16}$$

With $$\omega(P) = \omega_0 / [1 - 2P(1.16\times10^{-3} - 7.4\times10^{-4})] \tag{2.17}$$

We analytically obtained the eigenvalues & wave function of the relative motion part in the strong and weak confinement regime. For the strong regime, H_r reduces to:

$$H_{rs} = \frac{p^2}{2\mu} + \frac{1}{2}\mu\omega_0^2 z_r^2 \tag{2.18}$$

Neglecting the coulomb term as per the strong confinement regime, $\varphi(z_r)$ is determined as:

$$\varphi(z_r) = N_n \exp[-\frac{1}{2}\beta^2 z_r{}^2]H_{2n+1}(\beta z_r), \tag{2.19}$$

And $$E_y = (2n + \frac{3}{2})\hbar\omega_0 \ (y = 0,1,2,....), \tag{2.20}$$

Where,

$$N_m = [\frac{1}{\beta}\sqrt{\pi}2^{2m}(2m+1)!]^{-1/2} \tag{2.21}$$

$$\beta = \sqrt{\mu\omega(P)/\hbar} \tag{2.22}$$

Neglecting the confinement term in the weak confinement regime, H_r reduces to:

$$H_{rw} = \frac{p^2}{2\mu} - \frac{e^2}{\varepsilon(P,T)|z_r|} \tag{2.23}$$

And considering the relative-motion part as 1D hydrogenic type problem, $\varphi(z_r)$ is determined as:

$$\varphi(z_r) = C_x z_r \exp[-\frac{\gamma z_r}{x+1}]F[-z_r, 2, \frac{2\gamma z_r}{x+1}], \tag{2.24}$$

Where $\gamma = \frac{\mu e^2}{\varepsilon \hbar^2}$, F is the confluent Hypergeometric function, and C_x is the normalization constant.

And $$E_x = E_n = -\frac{\mu e^4}{2(n+1)^2 \varepsilon^2 \hbar^2} \tag{2.25}$$

Where $(n = 0,1,2,...)$

The nonlinear ORC for our 2-level system in 1D semi-parabolic QD is arrived at by applying a density matrix approach wherein perturbation expansions are used. It is given as [14, 33-35]:

$$\chi_0^{(2)} = 4\frac{e^3 \sigma_s}{\varepsilon_0 \hbar^2} \mu_{01}^2 \delta_{01} \times \frac{\omega_{01}^2(1+\frac{T_1}{T_2}) + (\omega^2 + \frac{1}{T_2^2})(\frac{T_1}{T_2} - 1)}{[(\omega_{01} - \omega)^2 + \frac{1}{T_2^2}][(\omega_{01} + \omega)^2 + \frac{1}{T_2^2}]} \tag{2.26}$$

When $\omega \sim \omega_{01}$ there is a peak value of $\chi_0^{(2)}$

$$\chi_{0,\max}^{(2)} = \frac{2e^3 T_1 T_2 \sigma_s}{\varepsilon_0 \hbar^2} \mu_{01}^2 \delta_{01}, \tag{2.27}$$

Where $\mu_{ij} = \left|\langle \psi_i | z_r | \psi_j \rangle\right| (i, j = 0,1)$ are the matrix elements of the dipole moment, $\psi_i(\psi_j)$ are the Eigen functions, $\delta_{01} = \left|\langle \psi_1 | z_r | \psi_1 \rangle - \langle \psi_0 | z_r | \psi_0 \rangle\right|$, $\omega_{01} = \frac{E_1 - E_0}{\hbar}$, and ω is the frequency

of the incident electromagnetic field, σ_s is the electron density in the QDs, T_2 is the transverse relaxation time, and T_1 is the longitudinal relaxation time.

For the regime of strong confinement, by considering relative coordinate electronic state, and energy levels, electronic wave functions are defined as

$$\phi_k = N_k \exp[-\frac{1}{2}\alpha^2 z_r{}^2] H_{2k+1}(\alpha z_r) \tag{2.28}$$

$$E_k = (2k+\frac{3}{2})\hbar\omega_0 \text{, with } (k = 0,1,2.....), \tag{2.29}$$

Where $$N_k = [\frac{1}{\alpha}\sqrt{\pi}2^{2k}(2k+1)!]^{-1/2} \tag{2.30}$$

Then the dipole matrix elements are obtained as

$$\mu_{01} = \left|\left\langle \phi_0(z_r)\middle| z_r \middle|\phi_1(z_r)\right\rangle\right| = \frac{4N_0N_1}{\alpha^2} = \frac{2}{\sqrt{6\pi}\alpha} \tag{2.31}$$

$$\mu_{00} = \left|\left\langle \phi_0(z_r)\middle| z_r \middle|\phi_0(z_r)\right\rangle\right| = \frac{2N_0^2}{\alpha^2} = \frac{2}{\sqrt{\pi}\alpha} \tag{2.32}$$

$$\mu_{11} = \left|\left\langle \phi_1(z_r)\middle| z_r \middle|\phi_1(z_r)\right\rangle\right| = \frac{72N_1^2}{\alpha^2} = \frac{3}{\sqrt{\pi}\alpha} \tag{2.33}$$

Finally, from Eq. (2.21) to Eq. (2.29), the maximum ORC is

$$\chi^{(2)}_{0,\max}(\omega) = \frac{8\sqrt{2}\hbar e^3 T_1 T_2 \sigma_s}{3\varepsilon_0 (m_e^* \pi\hbar\omega)^{3/2}} \tag{2.34}$$

2.3 Results and Discussion

We have considered the GaAs semiconductor material constants for our numerical results where T_1= 1ps and T_2= 0.2 ps, and we used the numerical parameters such as m_e^* =0.067 m_0, m_h^* =0.09 m_0 (m_0 is the mass of a free electron), $\sigma_s = 5\times10^{24}$ m^{-3}, ε =12.53 [14].

In figure 2.1 (a) & (b), we present the maximum ORC $\chi^{(2)}_{0,\max}(\omega)$ as a function of ω_0, the semi-parabolic confinement frequency. In both the figures 2.1(a) & 2.1(b), the maximum ORC is enhanced when the excitonic effects are taken into consideration. Both the factors of pressure & temperature affect $\chi^{(2)}_{0,\max}(\omega)$ through the alterations in effective mass & dipole matrix elements. Single electron state having energy levels and wave functions are given by Eq. (2.6) and Eq. (2.7), respectively, while for considering the case of without excitonic effect, the mass of the electron m_e^* instead of the total mass M_T has been taken into consideration. From figure 2.1(a) & (b), we can observe that the maximum ORC $\chi^{(2)}_{0,\max}(\omega)$ obtained is stronger when Excitonic effect is taken into account as compared to when no such effect is considered — this stretching due to the towering of the dipole matrix elements $\mu_{01}^2\delta_{01}$. Due to the EE, the charge distribution in the QD is distributed in a manner that the opposite polarity charge carriers are separated by a distance $(z_e - z_h)$. This gives rise to stronger dipole matrix elements which in turn leads to enhance nonlinear effects. The same is manifested in the higher values of maximum ORC in case off EE as compared to WEE.

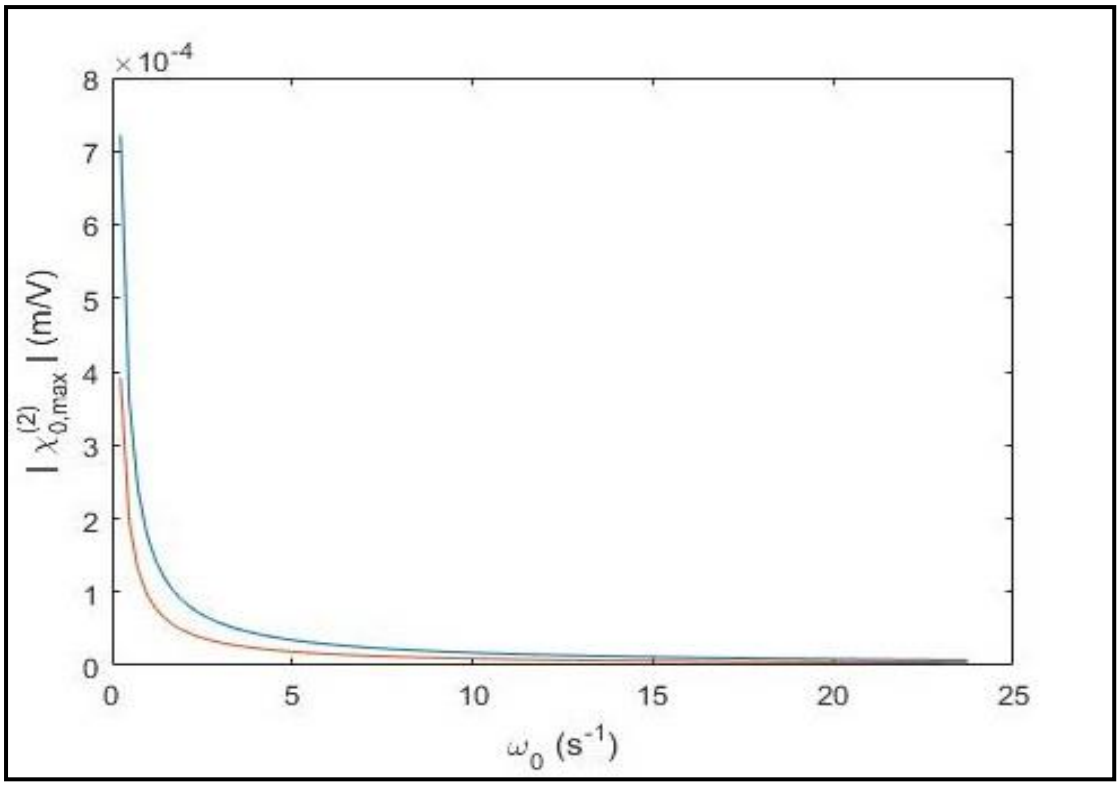

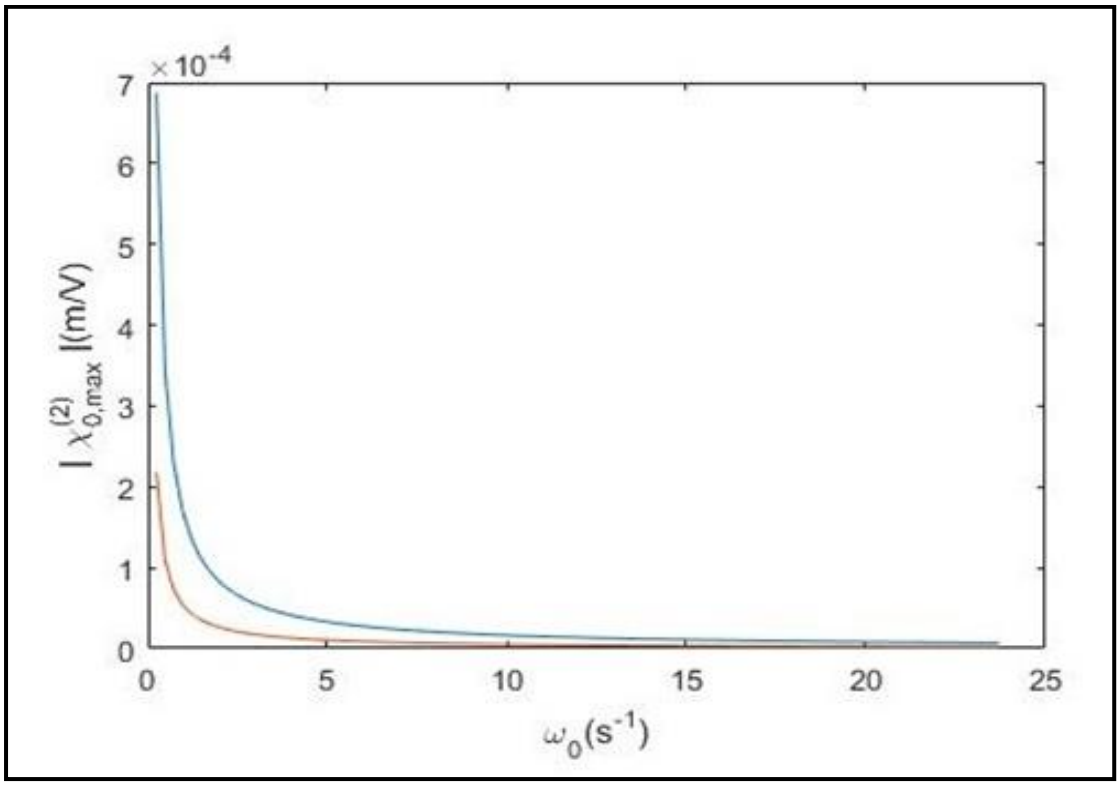

Figure 2.1: *Maximum ORC as a function of frequency for (a) for EE &WEE for R= 10nm, P=150kbar and T=50K (b) for EE & WEE for R= 10nm, P=50kbar and T=150K*

In figure (2.2), we present the results of the inclusion of excitonic effect on the second harmonic generation peaks when the temperature is varied from 50K to 100K. It is found that the excitonic effect blue shifts the optical rectification peaks for both the temperatures. When the nanostructure is kept at 50K temperature, the optical rectification peak blue shifts from 155meV to 275meV as the excitonic effects are included. At the same time, the peak height diminishes to a slightly lower value of $3.4*10^{-4}$ m/V from $4.3*10^{-4}$ m/V. Similar effects are seen in the case when the ambient temperature is maintained at 100K. In this scenario, the peak position shifts from 160meV to 290meV as the excitonic effect comes into play. We also observe that as the temperature is increased, the peak heights value decreases. In both the cases of EE as well as WEE the ambient temperature plays an important role in shifting the peaks and reducing the peak height by affecting the energy band gap. The blue shift of the peaks occurring due excitonic effects is attributed to enhancement of the energy values of subsequent eigenstates because of the attractive interaction between the electron and hole.

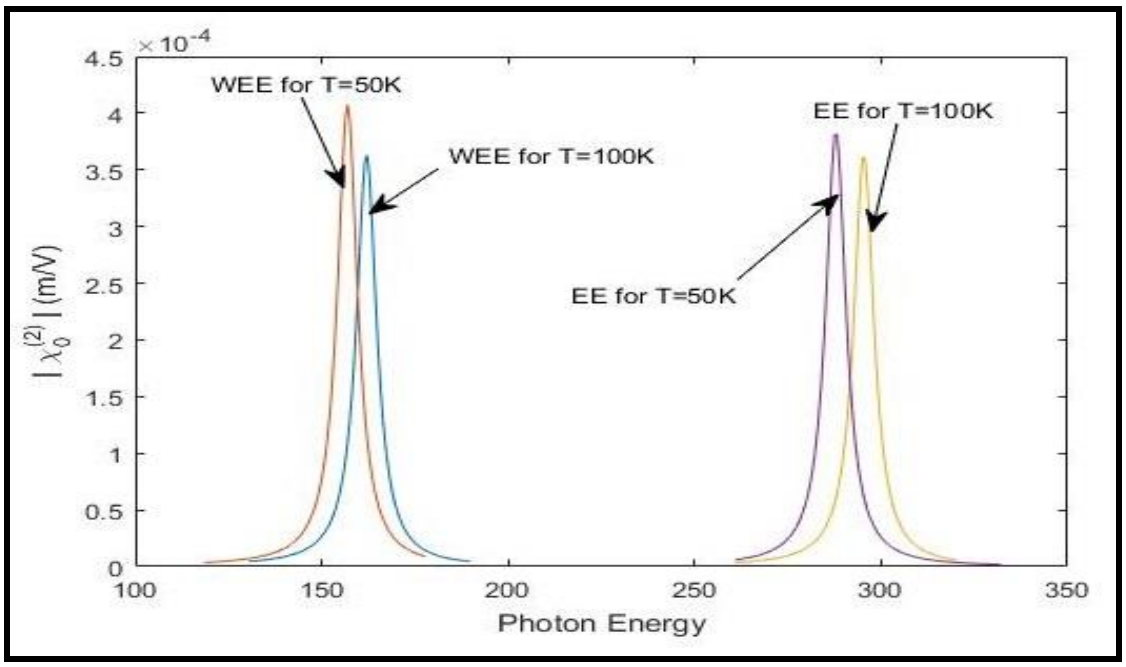

Figure 2.2: *ORC as a function of incident photon energy for T=50K &100K keeping R&P constant at R=10nm and P=50kbar.*

Figure 2.3 shows the variation of optical rectification by the nanostructure for two values of radii of the semi-parabolic QD at P=50kbar & T=50K. It can be observed that the peaks are blue shifted when the radius of the QD is reduced to 10nm from 15nm. This blue shift is the result of increase in the difference between subsequent energy states due to stronger confinement when radius is decreased. The consideration of excitonic effect for both the radii takes the peak position to higher values, viz. from 60meV to 100meV where R=15nm & from 140meV to 255meV for R=10nm. The peak height is reduced when the radius is lowered to 10nm from 15nm. This occurs due to the diminishing of the dipole matrix element as the radiusis decreased. Further, the inclusion of EE enhances the optical rectification peaks by enhancing the matrix element.

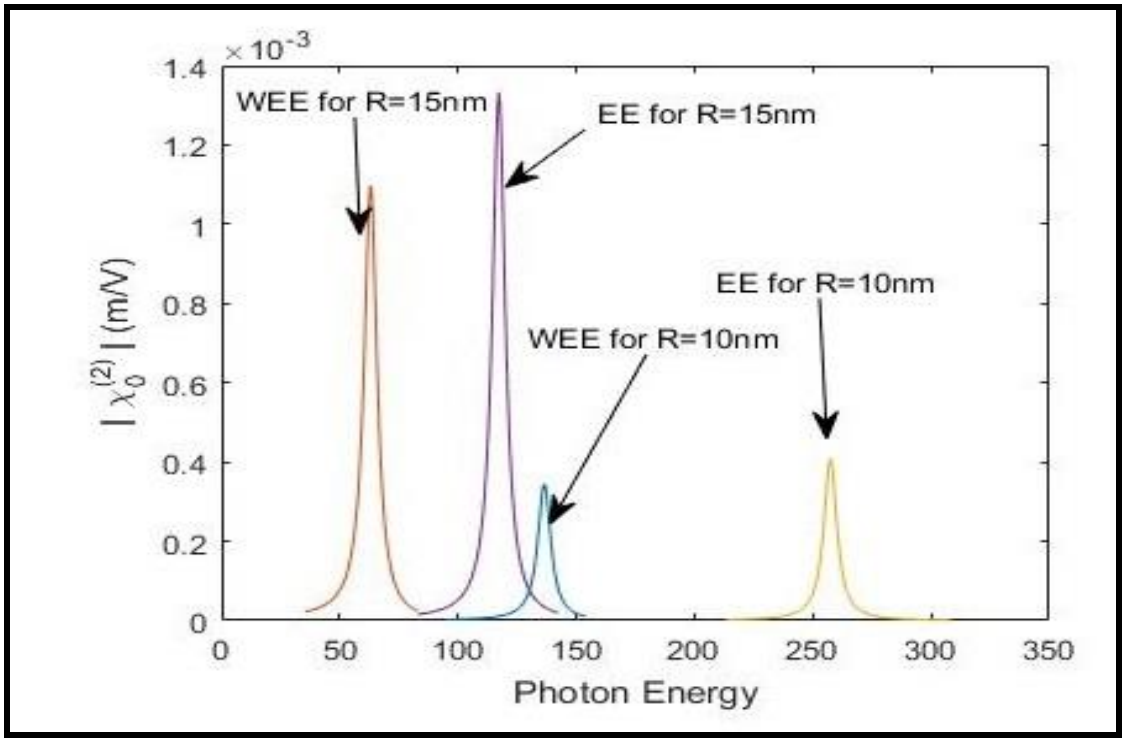

Figure 2.3: *ORC as a function of photon energy for R=10nm &15nm keeping P&T constant at P=50kbar and T=50K*

In figure 2.4, we present the changes in the peaks due to changing hydrostatic pressure while keeping the temperature fixed at 50K & radius at 10nm. We observe that the increase in hydrostatic pressure drags the optical rectification peaks to lower energy state. For the case, including the excitonic effects, the redshift with an increase in pressure from 50kbar to 100kbar is of 10meV, i.e., from 290meV to 280meV whereas for the same change in pressure the shifting in the optical rectification peaks is of 15meV, i.e., from 135meV to 130meV when the excitonic effects are ruled out. The dependence of effective mass of the charge carrier's interplays with the change in $\omega(P)$ when pressure is changed to bring in these shifting in optical rectification peaks.

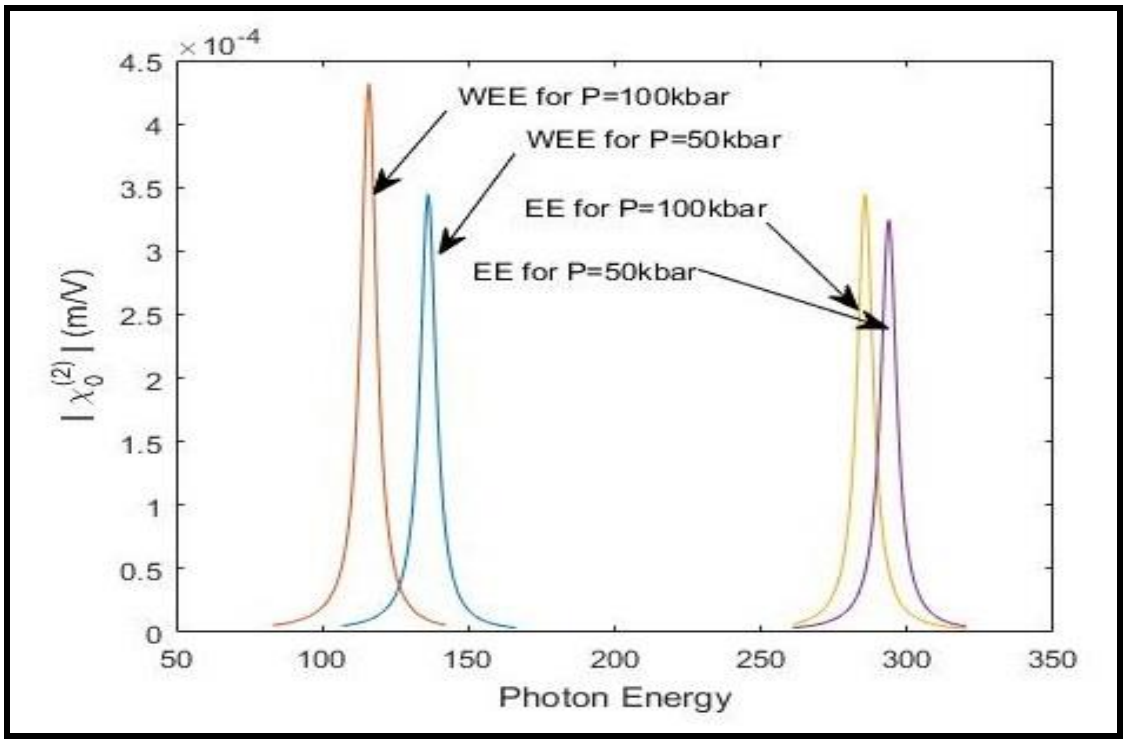

Figure 2.4: *ORC as a function of photon energy for P=50kbar&100kbar keeping R&T constant at R=10nm and T=50K*

2.4 Conclusions

The combined effects of correlation between the electron-hole pair, temperature, and hydrostatic pressure on the optical rectification in as semi-parabolic GaAs QDs is studied using the formalism of density matrix and the effective mass approximation. The results were calculated in the strong confinement regime. The obtained results show that the ORC is considerably magnified when exciton states in the QDs are taken into consideration. We found that the ORC peak positions are affected by both temperature & pressure where the blue shift and red shift are induced when temperature & hydrostatic pressure are changed. Moreover, the OR strength is also found to be strongly affected by radius, temperature & pressure. It is observed that the interplay of the variation of effective mass and $\omega(P)$ induces varied alteration of the ORC of the QD for the case of exciton effect and without it. The variation of temperature & pressure can thus use as external parameters to control the OR from QD.

References

[1] Y. Y. Lin and J. Singh, J. Appl. Phys. 92, 6205 (2002).

[2] S. T. Perez-Merchancano, R. Franco, and J. Silva-Valencia, Microelectron J. 39, 383 (2008).

[3] 1G. Almogy and A. Yariv, J. Nonlinear Opt. Phys. Mater. 4, 401 (1995).

[4] E. Rosencher and B. Vinter, Optoelectronics (Cambridge University Press, Cambridge, 2003).

[5] Caposso F, Mohammed K, and Cho A Y 1986 IEEE J. Quantum Electron. 22 1853.

[6] Miller D A B 1991 Int. J. High-Speed Electron. Syst. 1 19.

[7] Schneider H, Fuchs F, Dischler B, Ralston J D and Koidl P 1991 Appl. Phys. Lett. 58 2234.

[8] D. K. Ferry and S. M. Goodnick, Transport in Nanostructures (Cambridge University Press, Cambridge, 1997).

[9] H. A. Sarkisyan, Mod. Phys. Lett. B 18, 443 (2004).

[10] S.N. Saravanamoorthy, A. John Peter, C.W. Lee, Chem. Phys. 483, 1 (2017).

[11] A. Bera, M. Ghosh, Physica B 515, 18 (2017).

[12] C.Y. Chen, D.S. Sun, Acta Photon. Sin. 30, 104 (2001).

[13] Yu Y-B, Zhu S-N, Guo K-X, Phys Lett A, 175, 335, 2005.

[14] A. Braggio, M. Grifoni, M. Sassetti, F. Napoli, Europhys. Lett. 50 (2000) 236.

[15] F.D.M. Haldane, J. Phys. C 14 (1981) 2585.

[16] W. Xie, Chem. Phys. 423, 30 (2013).

[17] Zang C-J, Guo K-X, and Lu Z-E, Physica E, 36, 92, 2007.

[18] Y.-Y. Zhang, G.R. Yao, J. Appl. Phys. 110 (2011) 093104.

[19] W. Xie, "The nonlinear optical rectification of a confined excitonin a quantum dot," Journal of Luminescence, vol. 131, no. 5, pp.943–946, 2011.

[20] M. Bass, P. A. Franken, J. F. Ward, and G. Weinreich, "Optical rectification," Physical Review Letters, vol. 9, no. 11, pp. 446–448,1962.

[21] P. A. Franken, A. E. Hill, C. W. Peters, and G. Weinreich, "Generation of optical harmonics," Physical Review Letters, vol.7, no. 4, pp. 118–119, 1961.

[22] R.W. Boyd, Nonlinear Optics, Elsevier, 3rd edition, 2008.

[23] S. L. Chuang, S. Schmitt-Rink, B. I. Greene, P. N. Saeta, andA. F. J. Levi, "Optical rectification at semiconductor surfaces, "Physical Review Letters, vol. 68, no. 1, pp. 102–105, 1992.

[24] S. Baskoutas, E. Paspalakis, and A. F. Terzis, "Effects of excitons in nonlinear optical rectification in semi parabolic quantum dots," Physical Review B, vol. 74, no. 15, Article ID 153306, 2006.

[25] Duque CM, Mora-Ramos ME, Duque CA, Physica E, 43, 1002, 2011.

[26] Karabulut İ, M.E. Mora-Ramos, and Duque A Carlos, Journal of Luminescence 131, 1502 1509, (2011).

[27] Zapata Alejandro, Acosta E Ruben, Mora-Ramos Miguel, and Duque A Carlos, Nanoscale Research Letters 7:508, 1-9 (2012).

[28] M.E. Mora-Ramos, M.G. Barseghyan, C.A. Duque, Physica E 43, 338-344 (2010).

[29] C.M. Duque, M.E. Mora-Ramos, C.A. Duque, Superlattices and Microstructures 49, 264-268 (2011).

[30] Sauvage S, Boucaud P, Brunhes T, Glotin F, Prazeres R, Ortega J-M, Gérard JM: Phys Rev B,63, 113312, (2001).

[31] Baskoutas S, Paspalakis E, Terzis AF, Phys Rev B,74,153306, 2006.

[32] Zhang C-J, Guo K-X, Lu Z-E, Phys E, 36, 92, 2007.

[33] Karabulut İ, Şafak H, Tomak M, J Phys D: Appl Phys, 41, 155104, 2008.

[34] Karabulut İ and Şafak H, Physica B, 82, 368, 2005.

[35] C. M. Duque, M. E. Mora-Ramos, C. A. Duque, J Nanopart Res 13:6103–6112, 2011.

[36] Sheetal Antil, Manoj Kumar, Siddhartha Lahon, Sajjan Dahiya, Anil Ohlan, Rajesh Punia, A.S. Maan, Physica B: Condensed Matter 552 (2019) 202–208.

[37] Sheetal Antil, Manoj Kumar, Siddhartha Lahon, A.S. Maan, Optik - International Journal for Light and Electron Optics 176 (2019) 278–286.

[38] N. Raigoza, A.L. Morales, A. Montes, N. Porras-Montenegro, C. A. Duque, Phys. Rev. B, 69 (2004), p. 045323.

[39] Rosencher E, Phys Rev B, 44,11315,1991.

[40] Boyd R: Nonlinear Optics. 3 edition. New York: Elsevier; 2008.

CHAPTER 3

THIRD HARMONICS IN A QD WITH RASHBA SPIN ORBIT INTERACTIONS AS CONTROL FACTOR*

3.1 Introduction

As quantum confinement has become apparent in all spatial directions, ultra-small semiconductor heterostructures have gained the immense focus of researchers around the world. These heterostructures such as quantum heterostructure including quantum dot, quantum wire, etc. have many unique potential applications due to the confinement as the movement of charge carrier is restricted and hence leads to the development of a set of discrete energy levels where the carriers may exist. There are many microfabrication techniques including MBE, lithography, vapor deposition technique, etc. to fabricate these quantum heterostructures of different shapes and sizes. Explicitly, optical properties such as linear and nonlinear optical properties & susceptibilities have more scientific interest as they offer massive efficacy in understanding numerous semiconductor optoelectronic devices such as quantum LED's, solar cells, quantum dot lasers, single-electron transistors & quantum computing computers, etc. [1-7].

The role of externally applied fields, SOI (spin orbit interactions), temperature & hydrostatic pressure, etc. is very significant in altering the properties of the quantum heterostructures as any prominent change in the property can result in momentous changes in the working of the nano-scale device [8-11]. This dependence has often been used to externally alter the properties of these nano-scale devices to the operator's own will and thus has been one of the most widely researched areas in recent times. On

* *(Part of this work has been published in **Physica E: Low-dimensional Systems and Nanostructures, 147 (2023), 115620**)*

application of a perpendicular magnetic field to the plane of QD (quantum dot), energy levels are supplied with a supplementary structure as well as interacting electrons confined in QD results in correlation effect. Many different techniques have been utilized to study the electronic, optical and thermodynamic properties. Many authors have theoretically solved the 2-electron QD Hamiltonian with an enclosure of the effect of the magnetic field for obtaining the respective eigen energies and eigenstates of the QD-system [12-20] but to our sincere belief, the effect of external factors & SOI with doping is relatively a less discovered area.

Second and third-order nonlinear optical interaction of 2- incident fields with optical media results in the generation of SHG (second harmonic generation) & THG (third harmonic generation) and ORC (optical rectification coefficient). Xie and Bass et al., in 1962 performed initial work on OR [21], whereas Franken et al. were the first to report the experimental observation of SHG [22,23]. Baskoutas et al. investigated the impact of exciton in optical susceptibility for a semi-parabolic Quantum dot for a semi-parabolic potential [24] whereas F. Ungan et al. focused on the impact of the Electric field on TAC (total absorption coefficient) and RIC (refractive index coefficient) of an asymmetric Quantum dot [25]. Xuechao Li et al. [26], focused on the outcome of the Magnetic field on TAC of an asymmetric Quantum dot and studied the distinctions including the parameters such as radius and magnetic field intensity.

Many important factors including temperature, hydrostatic pressure, applied electric and magnetic fields and intense laser fields have a significant effect on the linear and nonlinear optical properties of QD's. On the application of these external field factors, the band structure, and the optical nonlinearity of the QD system is controlled and

altered. Hence, concluding that the geometry of systems, as well as external perturbations, are equally contributing significantly influencing the nonlinear optical properties of semiconductor structures. Unidimensional quantum dots have been studied immensely in recent times, but studies on the 2D semi-parabolic quantum dot with doping focusing on the dependence of its properties on external factors are scarce. In this study, we explored the variation of optical properties, such as THG on applied hydrostatic pressure, temperature, magnetic field, Rashba spin for $In_xGa_{1-x}As$ Quantum dot in the presence of SOI. The first section contains a crisp introduction of the topic, whereas the theory and the formulas have been mentioned in the second section. The third section consists of the obtained results and the graphs and is followed by the fourth section which contains well-drawn solutions.

3.2 Theoretical model

This section describes the detailed theory of 1-electron QD consisting of two parts given as equation (3.1) for QD Hamiltonian & equation (3.2) for exact diagonalization method for the $In_xGa_{1-x}As$ QD.

Considering a 2-D $In_xGa_{1-x}As$ QD with a semi-parabolic confining potential as given in equation (3.3), with a vertical magnetic field given as $\vec{B} = B\hat{k}$ having a symmetric gauge as: $A = B(-y, x, 0)/2$, the Hamiltonian for a one-electron system within effective mass taking spin into account is given as [27-31]:

$$H_{ST} = H_{ws} + H_{so}^{R} + \frac{1}{2} g^{*} \mu_B B\sigma \tag{3.1}$$

Where

$$H_{ws} = \frac{1}{2m^{*}(P,T)} [P - \frac{e}{c} A(r)]^{\vec{2}} + V_r \tag{3.2}$$

And the potential is given as

$$V_r = \frac{1}{2} m^*(P,T)\omega_0^2(x^2 + y^2) \tag{3.3}$$

In eq. (3.1), g^* represents the effective Lande factor for the semiconductor and electron spin z projection is given by $\frac{1}{2}\sigma$ having $\sigma = \pm$. Here up spin and down spin is represented by $\sigma = +1$ and $\sigma = -1$ respectively. SOI term H_{SO} contains two parts (i) Dresselhaus SOI term, H_{SO}^D (ii) Rashba SOI term, H_{SO}^R. As H_{SO}^R dominates over H_{SO}^D for the narrow gap, hence, neglecting H_{SO}^D, we have H_{SO}^R as:

$$H_{SO}^R = \frac{\alpha}{\hbar}[\vec{\sigma} \times (\vec{p} - \frac{e}{c}\vec{A}]_z \tag{3.4}$$

The term $\frac{\alpha}{\hbar}[\vec{\sigma} \times (\vec{p} - \frac{e}{c}\vec{A}]_z$ represents the spin-orbit coupling due to the inhomogeneous potential confining the electrons to the 2D plane and possible external gate voltages applied on the top of the dot. The strength of this coupling is determined by these parameters with a variation in magnitude when external gate voltages are applied. Here, the Rashba coupling coefficient is given by α and is controllable by varying the applied gate voltage in z direction, spinors and canonical momentum are represented by σ_x & σ_y and p_x & p_y respectively.

In effect. mass approx., total Hamiltonian H_{ST} for the combination of H_{ws} and H_{SO}^R is given as:

$$H_{ST} = \frac{p^2}{2m^*} + \frac{e}{m^*} A.p + \frac{e^2 A^2}{2m^*} + V_r + \frac{1}{2} g^* \mu_B B\sigma + \frac{\alpha}{\hbar}[\vec{\sigma} \times (\vec{p} - \frac{e}{c}\vec{A}]_z \quad (3.5a)$$

$$H_{ST} = \frac{p^2}{2m^*} + \frac{e}{m^*} A.p + \frac{e^2 A^2}{2m^*} + V_r + \frac{1}{2} g^* \mu_B B\sigma + \frac{\alpha}{\hbar}[\sigma \times p]_z + \frac{e\alpha}{\hbar}[\sigma \times A]_z \quad (3.5b)$$

Here:

m^* = represents effect. mass of charge carrier.

$\hbar\omega_o$ = confining potential strength corresponding to the size of the QD.

The temperature and hydrostatic dependent Effect. mass of the electron for *GaAs* is given as [32]:

$$m_e^*(P,T) = m_o[1 + \frac{7510}{E_g(P,T) + 341} + \frac{15020}{E_g(P,T)}]^{-1} \quad (3.6a)$$

with

$$E_g(P,T) = [1519 - \frac{0.5405T^2}{T + 204} + 10.7P] \quad (3.6b)$$

Here Temperature and hydrostatic pressure-dependent energy gap for *GaAs*, E_g is in meV, P is in "kbar" and T is in "Kelvin." The pressure-dependent oscillator frequency is expressed as

$$\omega(P) = \omega_0 / [1 - 2P(1.16 \times 10^{-3} - 7.4 \times 10^{-4})] \quad (3.6c)$$

Eigenfunction of Hamiltonian in eq (3.1) is represented by Fock-Darwin states $|n,l\rangle$ and is given as:

$$\psi_{nl\sigma}(r) = \frac{1}{\sqrt{2\Pi}} R_{nl}(r) e^{in\phi} \chi_\sigma \quad (3.7a)$$

with

$$R_{nl\sigma}(r) = \sqrt{\frac{2}{c_l}}\sqrt{\frac{(2n+1)!}{(2n+1+|l|)!}}\exp(\frac{-r^2}{2a^2}) + (\frac{r^2}{a^2})^{|l|/2} L_{2n+1}^{|l|}(\frac{r^2}{a^2})\chi_\sigma \quad (3.7b)$$

Where $a = (\frac{\hbar}{m^*\Omega})^{1/2}$, $\Omega^2 = \omega_o^2 + \frac{\omega_c^2}{4}$, χ_σ = spinor function and $\omega_c = \frac{eB}{m^*}$ (cyclotron frequency).

Eigen energies for eq. (3.1) is given as:

$E_{nl} = (2n+|l|+3/2)\hbar\Omega + \frac{\hbar}{2}l\omega_c + \sigma(\frac{1}{2}g^*\mu_B B + l\alpha m^*\omega_o^2)$, where $m = 0,1,2,3.....$,

$l = 0,\pm1,\pm2.....$ and $\Omega_\sigma^2 = \omega_o^2 + \frac{\omega_c^2}{4} + \frac{\sigma l\alpha m^*\omega_o^2\omega_c}{\hbar}$ (3.8)

Also, Ω_σ is influenced by Rashba SOI, resulting in an upsurge in the up-spin energy gap with diminution in spin-down energy. SOI also affects the energy term in such a way that at B=0 energy term becomes independent of the magnetic field and helps in uplifting spin degeneracy states.

An analytic expression for THG related to an optical inter-subband transition can be obtained using the density matrix formalism and an iterative procedure [33–35]. The wavefunction $\psi_{nl}(r)$ of the quantum dot with Rashba can be expanded in terms of an orthogonal and complete set of eigenvectors of H_0. The expansion takes the form [36] & hence, the Schrödinger equation $H\psi = E\psi$ becomes:

$$(E_{n,l,\sigma}^0 - E)C_{n,l}^\sigma + \sum_{n,l,\sigma'\neq\sigma}(H_R)_{nn'll'}^{\sigma,\sigma'}C_{n'll'}^{\sigma'} = 0 \quad (3.9a)$$

with

$$\psi_{nl\sigma} = \sum_{nl\sigma} C_{nl}^{\sigma} \phi_{nl\sigma} \tag{3.9b}$$

The matrix elements are given by:

$$(H_R)_{nn'll'}^{\sigma,\sigma'} = \left\langle \phi_{n,l}^{\sigma} \left| H_R \right| \phi_{n',l'}^{\sigma'} \right\rangle = a\delta_{l',l+1} \Sigma (C_n^{'\uparrow} C_n^{\uparrow} \sqrt{n+l+1} - C_{n-1}^{'\uparrow} C_n^{\uparrow} \sqrt{n} + C_n^{'\downarrow} C_n^{\downarrow} \sqrt{n+l+2} - C_{n-1}^{'\downarrow} C_n^{\downarrow} \sqrt{n}) \tag{3.10}$$

The polarized electromagnetic field for an exciting system with frequency ω is given as:

$$E(t) = Ee^{i\omega t} + E^* e^{-i\omega t} \tag{3.11}$$

Also, relationship between the electronic polarization P(t) & polarized electromagnetic field are expressed by:

$$P(t) = \varepsilon_o \chi(\omega) E e^{-i\omega t} + \varepsilon_o \chi(-\omega) E^* e^{-i\omega t} = \frac{1}{V} Tr(\rho M) \tag{3.12}$$

where ρ is density matrix for one-electron and V is the volume of the system, ε_0 represents permittivity of free space, and the symbol Tr (trace) denotes the summation over the diagonal elements of the matrix.

The electronic polarization of the quantum dot can be expressed as:

$$P(t) = P^{(1)}(t) + P^{(2)}(t) + P^{(2)}(t) + ... \tag{3.13}$$

$$P(t) = \varepsilon_0 \chi_{\omega}^{(1)}(t) + \varepsilon_0 \chi_{2\omega}^{(2)} E(t) + \varepsilon_0 \chi_{3\omega}^{(3)} E(t) + ... \tag{3.14}$$

Where $\chi_{\omega}^{(1)}, \chi_{2\omega}^{(2)}$ and $\chi_{3\omega}^{(3)}$ are representing the susceptibilities such as linear, SHG and THG, respectively. THG relation is given as [17, 37-40]:

$$\chi_{3\omega}^{(3)} = \frac{n_o e^4}{\hbar^3} \frac{M_{01} M_{12} M_{23} M_{30}}{(\omega - \omega_{10} + i\Gamma_o)(2\omega - \omega_{20} + i\Gamma_o)(3\omega - \omega_{30} + i\Gamma_o)} \tag{3.13}$$

Here, the system's electron density is given as n_o, e is representing electronic charge, and relaxation time is represented by Γ_o. $\omega_{ij} = (E_i - E_j)/\hbar$ shows the frequency for the transition and matrix elements are given by $M_{ij} = \left|\left\langle \psi_i \left| er \right| \psi_j \right\rangle\right|$ $(i, j = 0,1,2,3)$ such as $M_{01} = \left|\left\langle \psi_{nl\sigma} \left| er \right| \psi_{n'l'\sigma'} \right\rangle\right| where\, 0 = nl\sigma \quad and\, 1 = n'l'\sigma'$.

3.3 Results and discussion

In this section, the simultaneous effect of the magnetic field, Hydrostatic Pressure, Temperature, confining potential in the presence of SOI on THZ in $In_xGa_{1-x}As$ semi-parabolic 2-D quantum dot is calculated. For this purpose, the physical parameters that have been used are given as follows: Γ_o =.66ps and $m_e^* = 0.041m_0$, where mass of a free electron m_0. σ_s is taken as $5 \times 10^{22}\ m^{-3}$, $\varepsilon_r = 12.53$, and g=-15 [41,42].

Considering a QD system in semi parabolic potential having (0 0 –1) as ground state and (1 –1 –1) and (1 1 –1) as excited states having degenerate intermediate states, when both the magnetic field and spin are zero. This degeneracy can be wrecked by applying a magnetic field 'B' and introducing an "α", and; hence, by using these two parameters some manipulation in the energy can be done. Figure 3.1. represents a Schematic conduction band energy level diagram (n l –1) for $In_xGa_{1-x}As$ semi-parabolic quantum dot having four possible routes.

For THG, four possible routes having (0 0 –1) (nlσ) as ground state and their corresponding transition energies with potential confinement at $\hbar\omega$ = 10 meV, Rashba factor α = 10 meV nm, Pressure 10 kbar, temperature= 10 K and magnetic field B = 1 T is given in figure 3.1. Figure 3.2. represents four individual possible paths for transition

for the THG coefficients vs incident photon energy with confining potential keeping at $\omega = 10$ meV, fixing the Rashba SOI parameter at $\alpha = 10$ meV nm, Hydrostatic Pressure at 10 kbar, Temperature at 10 K and applying an external magnetic field, B = 1 T to the QD. As it can be observed from figure 3.2. that one, two, three-photon resonances are occurring at different photon energies due to the intermediate ladder states. Alteration in peaks as well as in peak heights can also be observed for different transition energies in each dissimilar path. According to the observation, two-photon resonance peaks are found to be stouter than one & three-photon resonance peaks as peak height corresponding to the strength of the dipole matrix element also increases with a significant increase in the coupling.

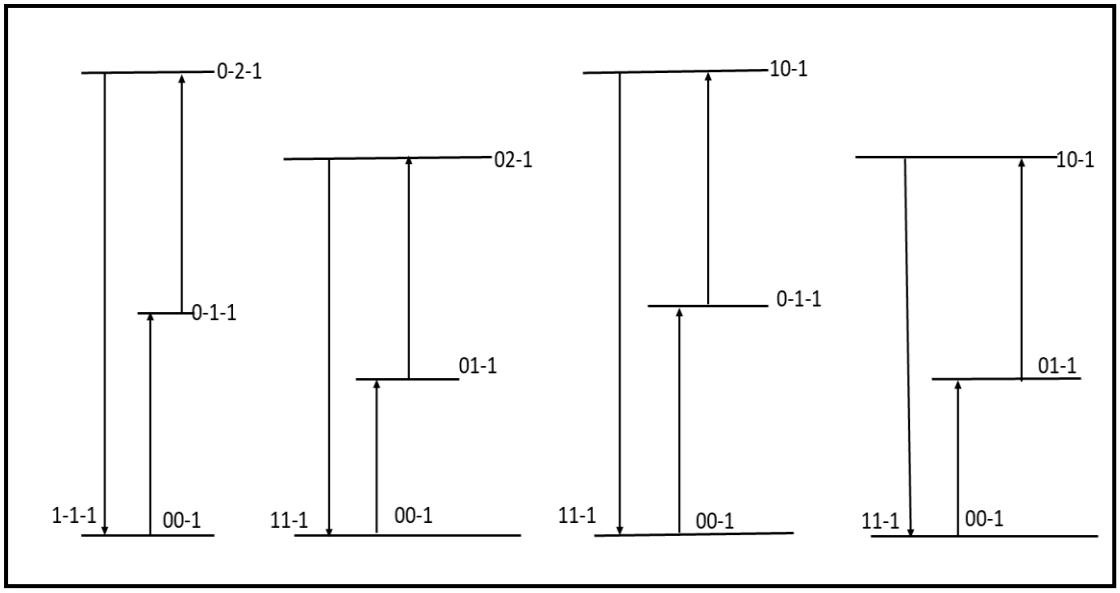

Figure 3.1: *Schematic conduction band energy level diagram (n l - σ) for $In_xGa_{1-x}As$ quantum dot having four possible routes*

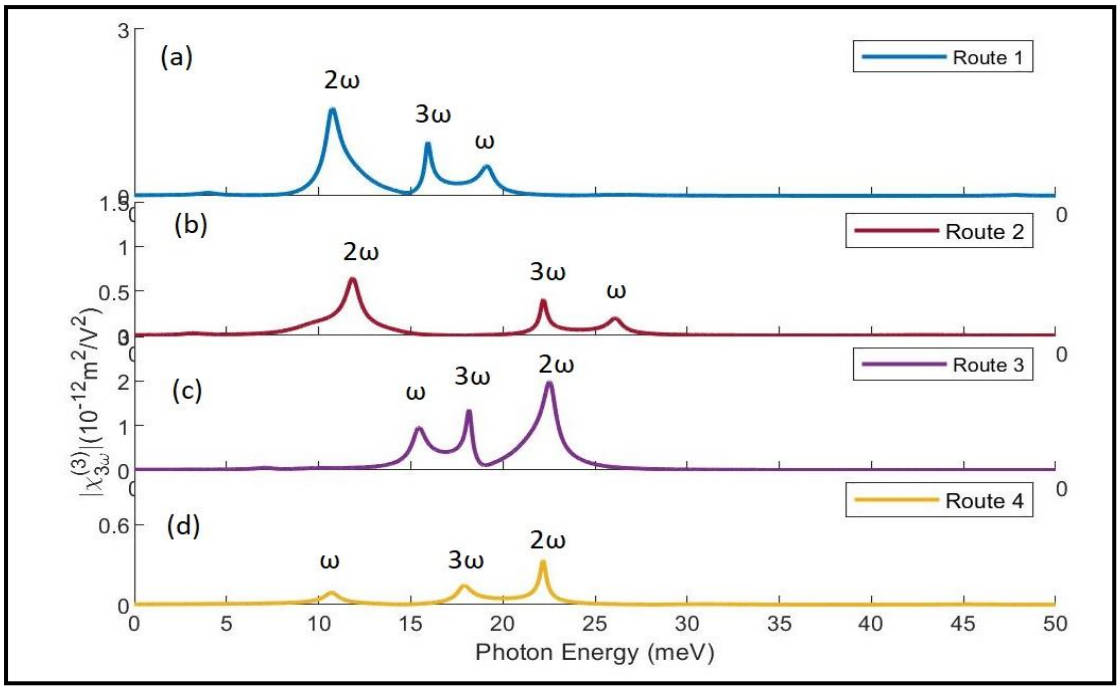

Figure 3.2: *Coefficient of THG vs photon energy for four possible routes (a) 1st route; (b) 2nd route; (c) 3rd route; (d) 4th route having ħ ω = 10 meV, α = 10 meV nm, P=10 kbar, T=10 K and B = 1 T.*

The magnetic field is having a significant effect in shifting the peaks as well as changing the magnitude of the peaks which is evident in fig. 3.3 where THG coefficient vs incident photon energy has been plotted for four different values of the magnetic field. As the energy levels are getting affected by the magnetic field hence in figures 3.3a–3.3d, a 2-way shifting of different positions of resonance can be observed. Here, the cyclotron frequency term supports dropping the energy level as well as (-) l whereas the Zeeman term helps in boosting the energy. As B is independent of the sign of l i.e., whether l is + or -, it will always help in enhancing Ωσ. Same can be observed from the expression of eigen energy given in equation 3.8. Further, it is also observed from the figure that for 1st two paths, the three-photon resonance is having some significance on the right side of the highest peak while for the 3rd and 4th path, peaks are enhancing but three-photon resonances are not having much significant value due to involvement of –l

states in the resonance position which are independent of three photons resonances and hence shifting towards the lower energy side, whereas the involvement of +l states in the resonance positions helps in shifting the excited states to a state of higher photon energy.

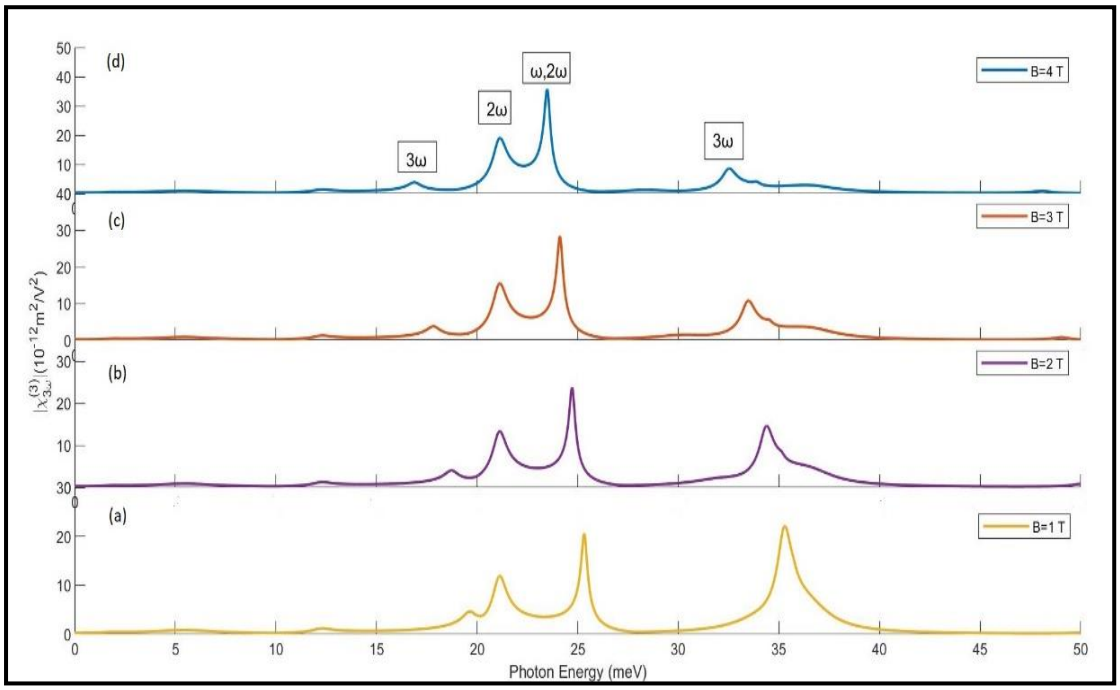

Figure 3.3: *Coefficient of THG vs incident photon energy at diverse Magnetic field values keeping α = 10 meV nm, P=10 kbar, T=10 K and confining potential ħ ω = 10 meV.*

In fig. 3.4, THG Coefficient and photon energy for dissimilar values of the QD confinement potential (a) ħ ω = 10 meV, (b) ħ ω = 15 meV, (c) ħ ω = 20 meV , (d) ħ ω = 25 meV keeping B= 1T, P=10 kbar, T=10 K and α = 10 meV nm are plotted. From this figure it is concluded that both the blue/redshifts are observed for the resonant peaks of the THG i.e., some resonant peaks are moving toward lower photon energies exhibiting redshift and some are moving toward higher photon energies displaying blue shift with an increase in the confining potential. Due to the quantum confinement effect, an increased confinement potential roots towards the lesser radius of charge carriers in a

QD. Due to weak confinement, the energy separation between the states tends to decrease and hence, exhibits a blue shift in the peaks. It is also observed that the peaks are having unequal spacing with a difference in the number of photon resonance as they are belonging to different energy levels.

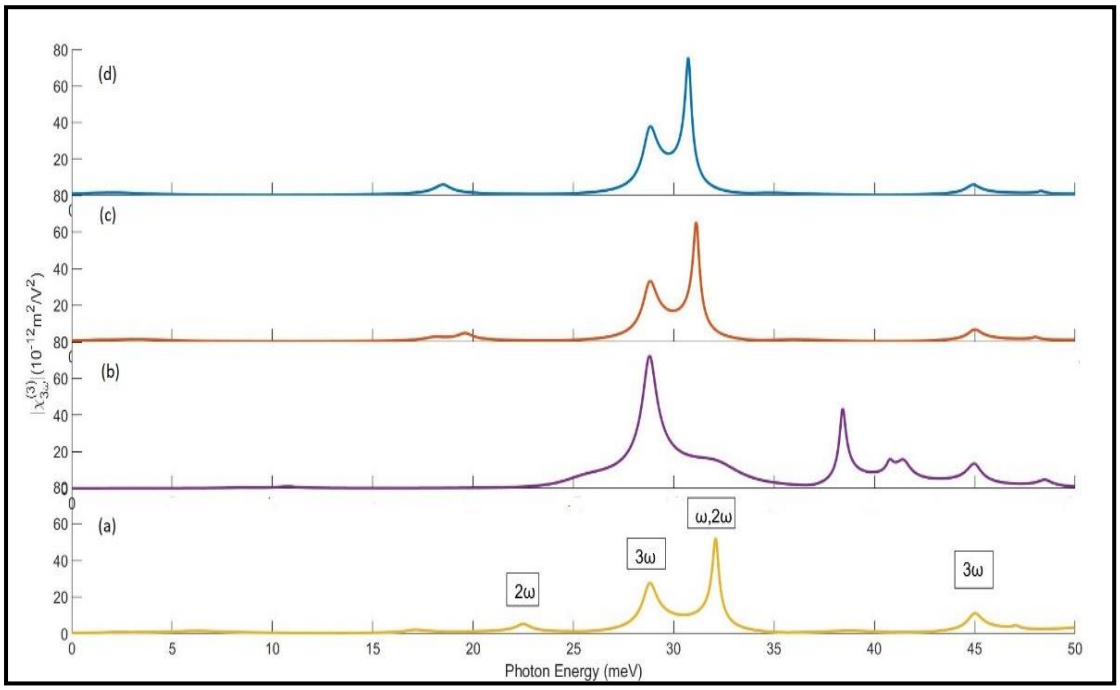

Figure 3.4: *Coefficient of THG vs incident photon energy for the diverse value of confining potential keeping B= 1T, P=10 kbar, T=10 K and α = 10 meV nm.*

Figure 3.5 represents a plot between THG coefficient and incident photon energy for different values of α at a confining potential of ω = 10 meV and B = 1 T, where α is increasing at a step of 5 meV nm. With an increase in α from a value of 10 meV nm to 25 meV nm, a slight redshift can be observed in one and two-photon resonance peaks, whereas a shifting towards the higher energy end can be observed in three-photon resonance positions resulting in a blue shift. As α is playing a two-way role while handling the values of energy levels hence red/blue shifts are observed. Further, a decrease in peak height can also be observed with an increase in the value of the Rashba parameter.

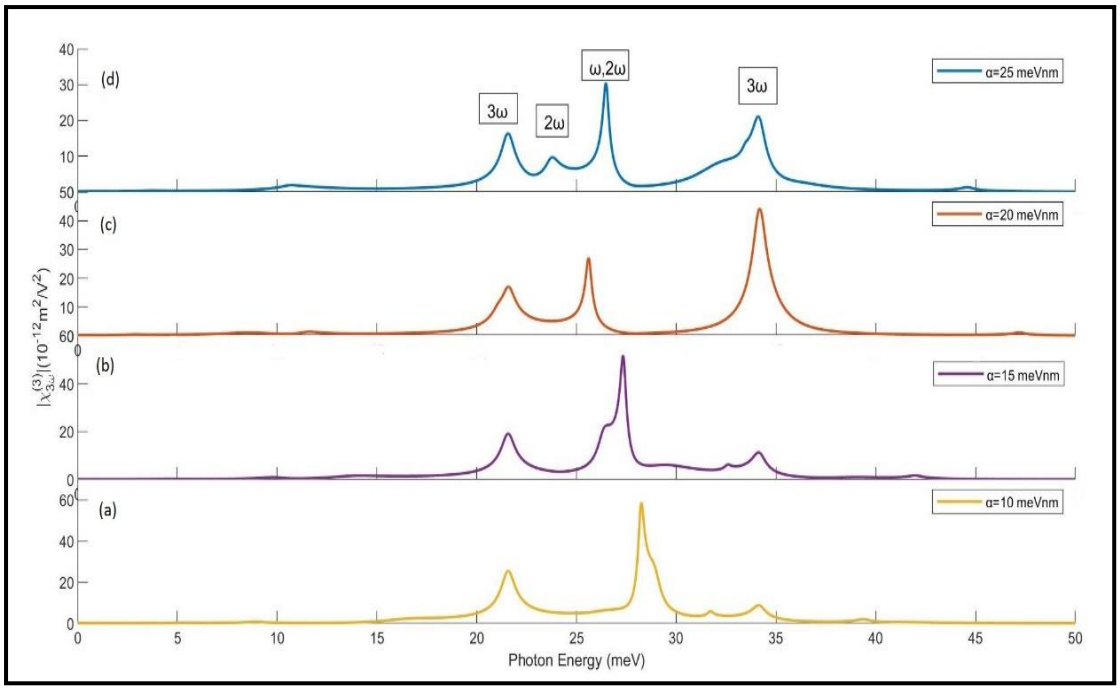

Figure 3.5: *Coefficient of THG vs incident photon energy for the diverse value of Rashba SOI coupling factor keeping confining potential $\hbar\omega$ = 10 meV, P=10 kbar, T=10 K and B = 1 T.*

Figure 3.6(a) is showing the coefficient of THG vs incident photon energy for four diverse values of pressure fixing confining potential $\hbar\omega$ = 10 meV, T=10 K, α = 10 meV nm and B = 1 T. With an increase in Hydrostatic Pressure, the magnitude of THG resonant peaks increases with a slight decrease in peak height as the peaks are shifting towards lower energy. It is observed that the change in the magnitude of the THG resonant peaks is directly correlated to the dipole matrix element term $M_{01}M_{12}M_{23}M_{30}$ in the numerator as well as to the energy interval ω_{10}, ω_{20} and ω_{30} in the denominator. Additionally, as dipole matrix elements are decreasing with an increase in pressure hence the red shift in resonant peaks is observed with an increase in hydrostatic pressure, as shown in fig. 3.6(b). This is explained by the fact that the quantum confinement becomes weak with the decrease in the energy interval with a rise in hydrostatic pressure.

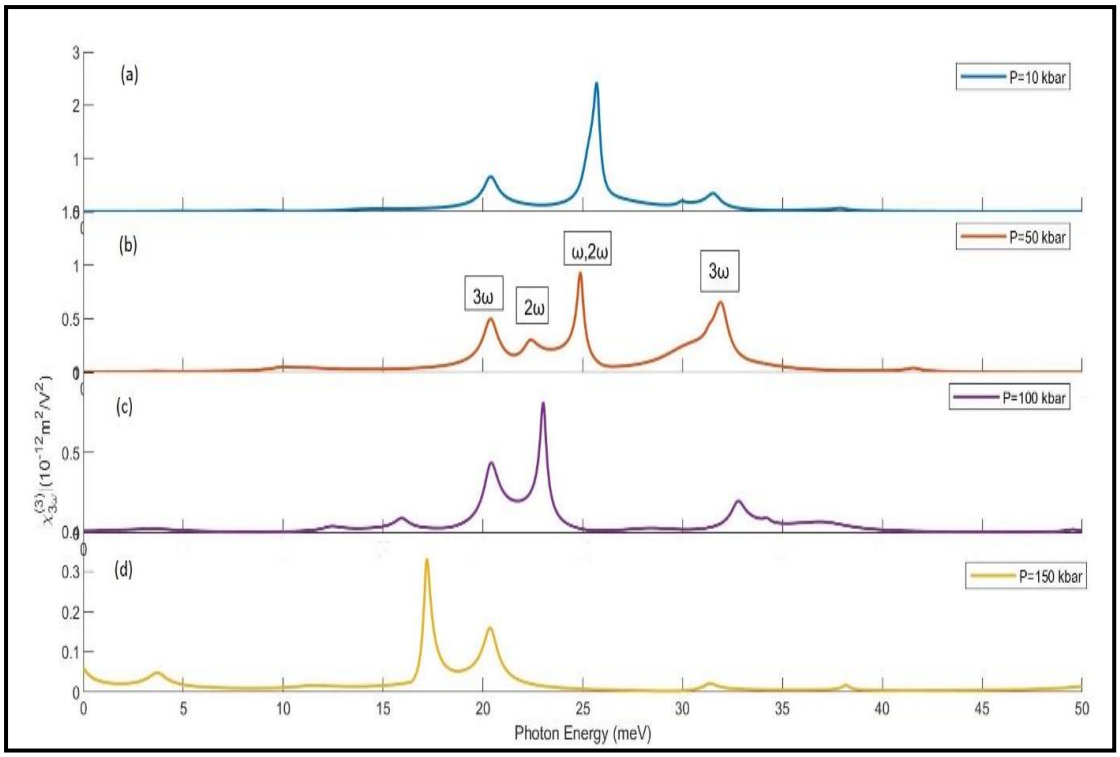

Figure 3.6(a):*Coefficient of THG vs incident photon energy for diverse value of pressure fixing confining potential* $\hbar\omega = 10$ *meV, T=10 K,* $\alpha = 10$ *meV nm and B = 1 T.*

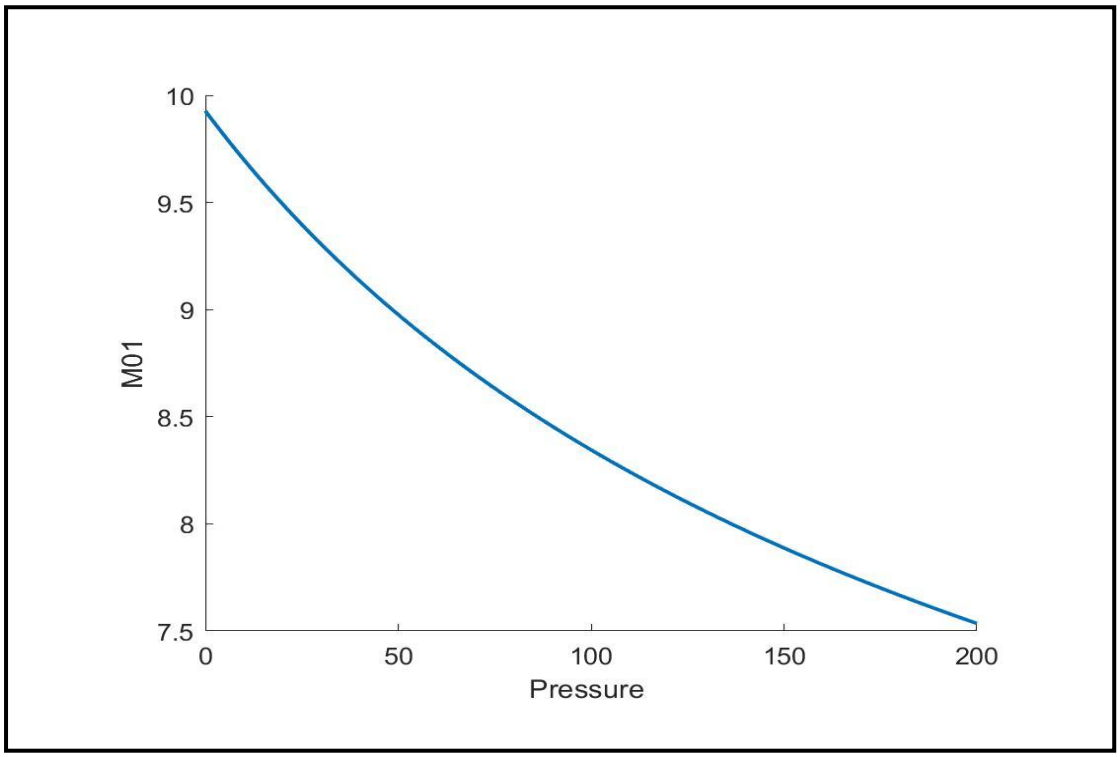

Figure 3.6(b): *Variation of dipole matrix element* M_{01} *vs Pressure*

Figure 3.7(a). is showing a plot of THG and incident photon energy for four diverse values of temperature fixing confining potential $\hbar\omega$ = 10 meV, P=10 kbar, α = 10 meV nm and B = 1 T. Blueshift can be observed with an increase in the temperature as the resonant peaks are moving towards higher energy region with a significant increase in the peak height. As one can see from fig. 3.7(b) that the dipole matrix element M_{01} gets enhanced with increase in temperature, consequently the peak height corresponding to (ω, 2ω) gets enhance along with its blueshift. The dipole matrix element M_{01}'s value increases with temperature as the effective radius changes with an increment in temperature. However, the peak corresponding to 3ω at higher energy gets suppressed at higher temperature. This can be attributed to the fact that as temperature increases, the sharp resonances get fuzzy due to the thermal energy of the electrons.

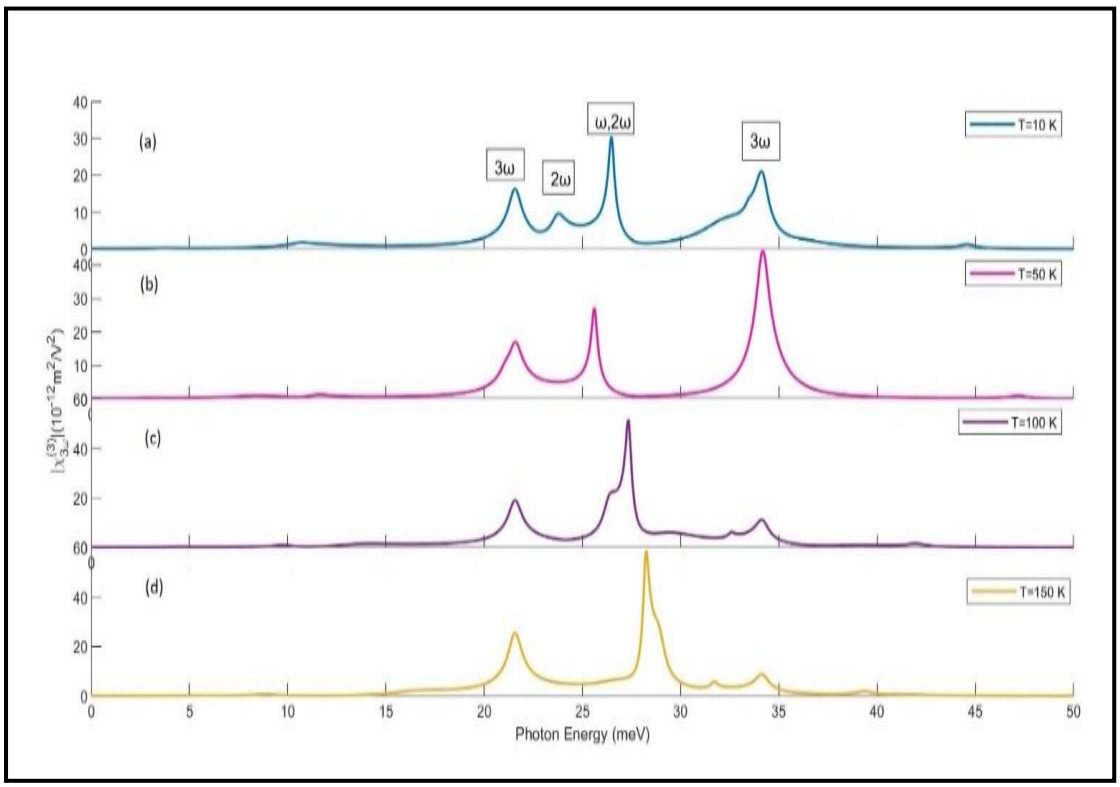

Figure 3.7(a): *Coefficient of THG vs incident photon energy for diverse value of Temperature fixing confining potential $\hbar\omega$ = 10 meV, P=10 kbar, α = 10 meV nm and B = 1 T.*

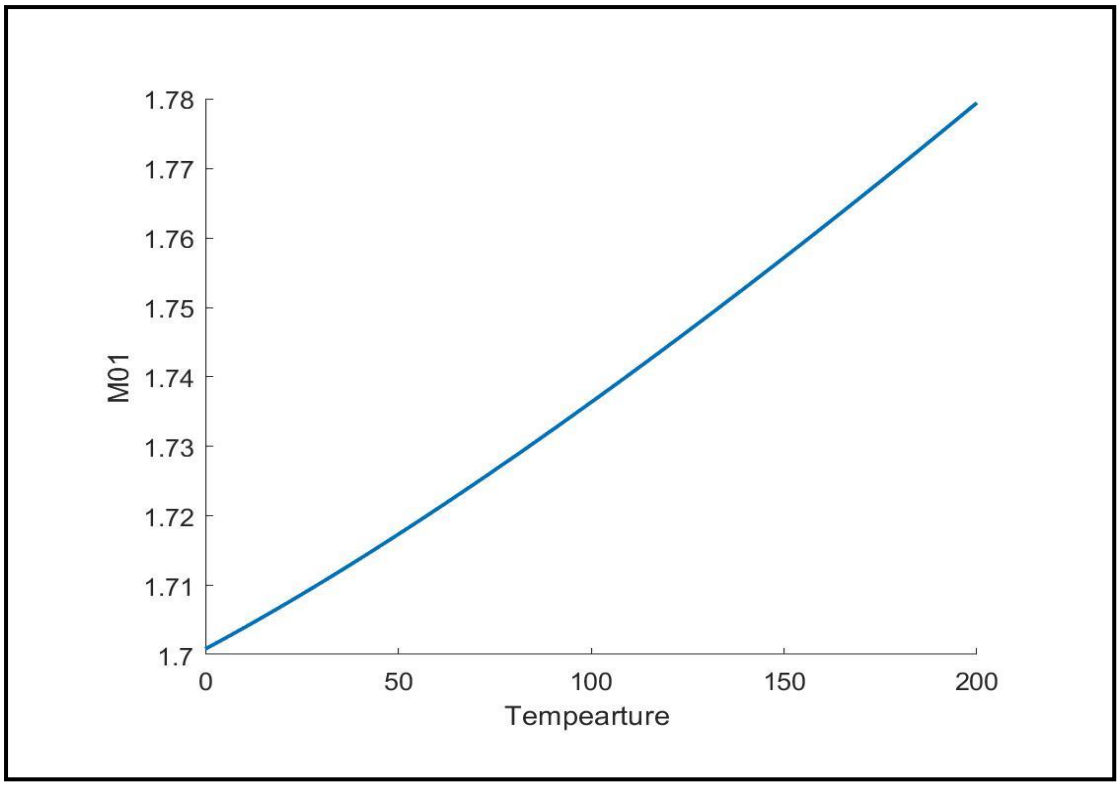

Figure 3.7(b): *Variation of dipole matrix element M01 vs Temperature*

3.4 Conclusions

A detailed investigation for the THG coefficients for an $In_xGa_{1-x}As$ QD in THz laser field with Rashba SOI with the impact of the magnetic field in the vertical direction is carried out in the present study. To carry out the detailed investigation, energy levels with respective wave functions within the effect. mass approx. is being determined using the variational technique. The variation of THG coefficients vs incident photon energy is explored for various external parameters such as temperature, hydrostatic pressure, confining potential, the magnetic field in the presence of Rashba SOI strength. Results are signifying that with an upsurge in the Rashba SOI coefficient, a strong effect on the THG peak positions is observed. It can also be observed that the two-photon resonance peaks are stronger than three-photon resonance peaks due to an

increase in the coupling of levels as the peak height corresponds to the strength of the dipole matrix element. The outcomes are displaying that for the detailed engineering of optical devices based on the QD's, consideration of SOI is a must and optical properties of the optoelectronic devices are controllable using the tunable strength parameter.

References

[1] S.J. Liang & W. Xie, Eur. Phys. J. B, 81, (2011), 79.

[2] H. Hartmann &R. Schuck, Int. J. Quant. Chem.,18, (1980), 125.

[3] I. Zutic, J. Fabian & S. Das Sarma, Rev. Mod. Phys., 76, (2004), 323.

[4] J. Jayabalan, M.P. Singh & K.C. Rustagi, Phys. Rev. B, 68, (2003), 075319.

[5] R. Khordad, Opt. Quant. Electron., 46, (2014), 283.

[6] R. Khordad & H. Bahramiyan, Pramana J. Phys., 88, (2017), 50.

[7] S.A. Wolf, et al., Science, 294, (2001), 148

[8] W. Xie & S. Liang, Physica B, 406, (2011), 4657.

[9] R. Khordad, S.K. Khaneghah & M. Masoumi, Superlatt. Microstruct.,47, (2010), 538.

[10] R. Khordad, Superlatt. Microstruct., 47, (2010), 422.

[11] G. Rezaei & S.S, Superlatt. Microstruct., 53, (2013), 99.

[12] B. Gil, P. Lefebvre & P. Boring, Phys. Rev. B, 44, (1991), 1942.

[13] R. Khordad, J. Lumin., 134, (2013), 201.

[14] R. Khordad, Int. J. Mod. Phys. B, 3, (2017), 1750055.

[15] S. Liang, W. Xie, X. Li, et al., Superlatt. Microstruct., 49, (2011), 623.

[16] P. Lefebvre, B. Gil & H. Mathieu, Phys. Rev. B, 35, (1987), 5630.

[17] R. Khordad, Opt. Commun., 391, (2017), 121.

[18] Karabulut İ & Şafak H, Physica B, 82, (2005), 368.

[19] C. M. Duque, M. E. Mora-Ramos & C. A. Duque, J Nano part Res., 13, (2011), 6103.

[20] S. Baskoutas, E. Paspalakis & A.F. Terzis, Phys. Rev. B 74, (2006), 153306.

[21] W. Xie, J. Lumin., 131, (5), (2011), 943.

[22] M. Bass, P.A. Franken, J.F. Ward & G. Weinreich, Phys. Rev. Lett., 9, (11), (1962), 446.

[23] P.A. Franken, A.E. Hill, C.W. Peters & G. Weinreich, Phys. Rev. Lett., 7, (4), (1961), 118.

[24] S. Baskoutas, E. Paspalakis, & A.F. Terzis, Phys. Rev. B, 74, (2006), 15.

[25] F. Ungan, M.K. Bahar, J.C. Martinez-Orozcoc & M.E. Mora-Ramos, Photonics and Nanostructures - Fundamentals and Applications, 41, (2020), 100833.

[26] Xuechao Li & Chaojin Zhang, Superlattices and Microstructures, 60, (2013) 40.

[27] Manoj Kumar, Sukirti Gumber, Siddhartha Lahon, Pradip Kumar Jha & Man Mohan, Eur. Phys. J. B, 87, (2014), 71.

[28] L. Jacak, P. Hawrylak, A. Wojs, Quantum Dots (Springer, Berlin, 1997).

[29] R. Khordad & B. Vaseghi, Chinese Journal of Physics, 59, (2019),473.

[30] R. Khordad & H. Bahramiyan, Commun. Theor. Phys., 62, (2014), 283.

[31] Khoshbakht, Y., Khordad, R. & Rastegar Sedehi, J Low Temp Phys, 202, (2021), 59.

[32] S. Dahiya, S. Lahon & R. Sharma, Physica E, 118, (2020), 113918.

[33] R. Khordad, Opt. Quant. Electron, 46, (2014), 283.

[34] S. Dahiya, M. Verma, S. Lahon & R. Sharma, Journal of Atomic, Molecular, Condensed Matter and Nano Physics, 5(1), (2018), 41–53.

[35] R.F. Kopf, M.H. Herman, Lamont Schnoes, M. Perley, A.P. Livescu & G. Ohring, J. Appl. Phys. 71, (1992), 5004–5011.

[36] R. Chaurasiya, S. Dahiya and R. Sharma, 2022 IEEE International Conference on Nanoelectronics, Nanophotonics, Nanomaterials, Nanobioscience & Nanotechnology (5NANO), 2022, 1-3.

[37] Zhi-Hai Zhang, Kang-Xian Guo, Bin Chen, Rui-Zhen Wang & Min-Wu Kang, Superlatt. Microstruct. 46, (2009), 672.

[38] L. Zhang & H.J. Xie, Phys. E, 22, (2004), 791.

[39] G.H. Wang, Phys. Rev. B, 72, (2005), 155329.

[40] Shuai Shao, Kang Xian Guo, Zhi Hai Zhang, Ning Li & Chao Pen, Solid State Communications, 151, (2011), 589.

[41] Junsaku Nitta, Tatsushi Akazaki, Hideaki Takayanagi & Takatomo Enoki, Phys. Rev. Lett., 78, (1997), 1335.

[42] M. Solaimani, L. Lavaei & S. M. A. Aleomraninejad, Journal of the Optical Society of America B, 9, 34, (2017), 1989.

CHAPTER 4

TUNING NONLINEAR OPTICAL PROPERTIES OF A 1-D QD WITH EXTERNAL FACTORS*

4.1 Introduction

The semiconductor nanomaterials such as Quantum dots (QD), quantum wires and quantum wells have many applications in the generation of optoelectronic devices such as lasers, infrared and THz photodetectors, solar cells, biological imaging devices, photovoltaics, LEDs, etc., owing to their enchanting physical properties due to the quantum confinement effects in all spatial directions [1-5]. Out of all these nanostructures, quantum dots of various shapes, sizes and strong confinement of electron & holes have been given special attention as they possess interesting physics in terms of the unique electronic & optical properties. Quasi-zero-dimensional quantum dots can be considered as Nano crystalline structures that can provide limitless utility in the realization of many semiconductors' optoelectronic devices such as quantum dot solar cells, spintronics and ultrafast quantum computers. Accordingly, unprecedented attention has been given to the semiconductor nanomaterials in the last few decades [6-13].

The parabolic and semi parabolic confinement potential can allow various resonances, due to the constant spacing of the discrete energy levels which accounts for the enormous enhancement of the nonlinear optical susceptibilities, optical transitions within the valence and conduction band, and absorption properties [14-17]. Furthermore, the parabolic and semi parabolic potential confinement is more relevant when the zero-dimensional quantum dots are fabricated by using an etching process, ion implantation or electrostatic gates. We have found considerable investigations on the

* *(Part of this work has been published in **Nanosystems -Physics Chemistry Mathematics 15 (5) (2024) 1**)*

nonlinear optical and electronic properties such as Refractive Index (RI), Absorption Coefficient (AC) and Rectification Coefficient (RC) with photon energy and external factors such as temperature, hydrostatic pressure and dot size [18-20]. For photons having energies equal to that of inter-subband transition energies, host material finds a significant change in dielectric constant, thereby inducing changes in the nonlinear excitonic optical properties [21-24].

Numerous investigations and interesting studies are done on the nonlinear optical properties of nanostructures especially Quantum dots under the influence of external factors such as electric field, magnetic field etc. [21-26]. Many authors studied the effect of excitons in one dimensional semi parabolic quantum dots [27-30]. Duque et al. studied the effect of external factors such as electric field, magnetic field, hydrostatic pressure, laser field and temperature on nonlinear properties in excitonic system [31-34]. Bejan et al. demonstrated the effect of electric field on the optical properties of a semi parabolic quantum dot in an excitonic system [35]. Kumar et al. further investigated the effect of hydrostatic pressure, temperature & spin on the optical & electronic properties of nanostructures [36-37]. To summarize, the interesting results of the ramifications of external factors such as hydrostatic pressure, temperature, electric field and magnetic field on the nanostructures bring out plethora of novel and exciting physical properties.

The main objective of the present work is to investigate the effect of external factors such as temperature and hydrostatic pressure on the RI and AC of excitonic system in 1-D semi parabolic quantum dot. An excitonic system is a bound electron-hole pair with more closely matched effective masses that is formed by the electrostatic interaction between the electron and hole. Theoretically, this system can be related to the hydrogenic system and it possess discrete energies. A 1-D QD is principally a nanostructure which can be

assumed as a small portion of a 1-D QW which is bordered by a two-wall potential. The charge carriers are free to move along the wire in 1-D QW, whereas they are restricted to move along the spatial length in 1-D QD [27, 38-40]. The core study undertaken in this research chapter focuses on a one-dimensional semi parabolic quantum dot, which is strongly confined in the x & y direction and electrons & holes are confined by a semi parabolic potential along the z direction. We know that the hydrostatic pressure & temperature can alter the nonlinear properties such as the refractive index & absorption coefficient for excitonic effects (EE) as well as without excitonic effect (WEE). In order to keep the study concise and in line with the experimentally available results, we have restricted our studies to the two extreme limits of a temperature range 10K-100K where it is observed that the sharpest absorption peaks or transmittance dips are observed at low temperatures in the mentioned range or even lower than that. Furthermore, it is observed that as temperature increases above 100K, the value of the thermal excitation energy of the charge carriers, namely kT/2, attains significant values.

In this work, we reported the effect of temperature and hydrostatic pressure on the optical rectification associated with the excitonic system in a semi-parabolic quantum dot [38]. It is highlighted that most available literature reports are primarily based on the nonlinear optical properties due to impurities or due to different shape of quantum structures. To our sincere understanding, there are no studies available where the hydrostatic pressure & temperature effects on the nonlinear optical properties of excitonic system in one dimensional semi parabolic quantum dots have been studied and explained. The present chapter is structured as follows: In the next section, theoretical analytical framework is presented to calculate the Eigen energies, Eigen functions & optical properties for the excitonic system. In the Results & Discussion section, we have presented our numerical results and discussion. In the last section of conclusion, we have summarized our results.

4.2 Theory and Model

A theoretical model of the system taken is presented in Model 1. Here, the gate voltage in the model is used to control Rashba SOI where the effects of SOI are studied. In our case, we have kept the gate voltage to be Zero. The x-direction is kept to be very small i.e., about 2nm so that the charge carriers behave as a 2-D charge carrier gas. The y-length of the wire is in μm range, so the charge carrier exhibit e^{-ky} wave function. The Z-directions breadth is determined by the potential strength and in our case the effective z-length turns out to be 5nm. Now, moving towards the mathematical calculations related to the system.

Hamiltonian for a 1-D excitonic QD having semi-parabolic confining potential within the framework of effective mass approximation can be written as [25, 27, 28, and 38]:

$$H_{e1} = \frac{p_h^2}{2m_h^*(P,T)} + \frac{p_e^2}{2m_e^*(P,T)} + V(z_e) + V(z_h) - \frac{e^2}{\varepsilon |z_e - z_h|} \tag{4.1}$$

Where $(z_e, z_h > 0)$

Here m_h^* and m_e^* represents effective mass of hole and electron respectively, ε represents the background dielectric constant and last term represents the electrostatic Coulomb interaction term between electron and hole. The semi-parabolic confinement potential $V(z_k)$ is written as:

$$V(z_k) = \begin{cases} \frac{1}{2} m_i^* \omega_0^2 z_k^2, & z_k \geq 0, \\ \infty, & z_k \leq 0 \qquad (k = e, h) \end{cases} \tag{4.2}$$

The Temperature and hydrostatic pressure dependent Effective mass of the electron for $GaAs$ is given as [38,40,41]:

$$m_e^*(P,T) = m_o[1+\frac{7510}{E_g(P,T)+341}+\frac{15020}{E_g(P,T)}]^{-1} \quad (4.3a)$$

$$m_h^*(P,T) = (0.09-0.20\times10^{-3}P-3.55\times10^{-5}T)m_0 \quad (4.3b)$$

with

$$E_g(P,T) = [1519-\frac{0.5405T^2}{T+204}+10.7P] \quad (4.4)$$

Here Temperature and hydrostatic pressure dependent energy gap $GaAs$, E_g is in meV, P is in "kbar" and T is in "Kelvin." The pressure dependent oscillator frequency is expressed as:

$$\omega(P) = \omega_0 / [1-2P(1.16\times10^{-3}-7.4\times10^{-4})] \quad (4.5)$$

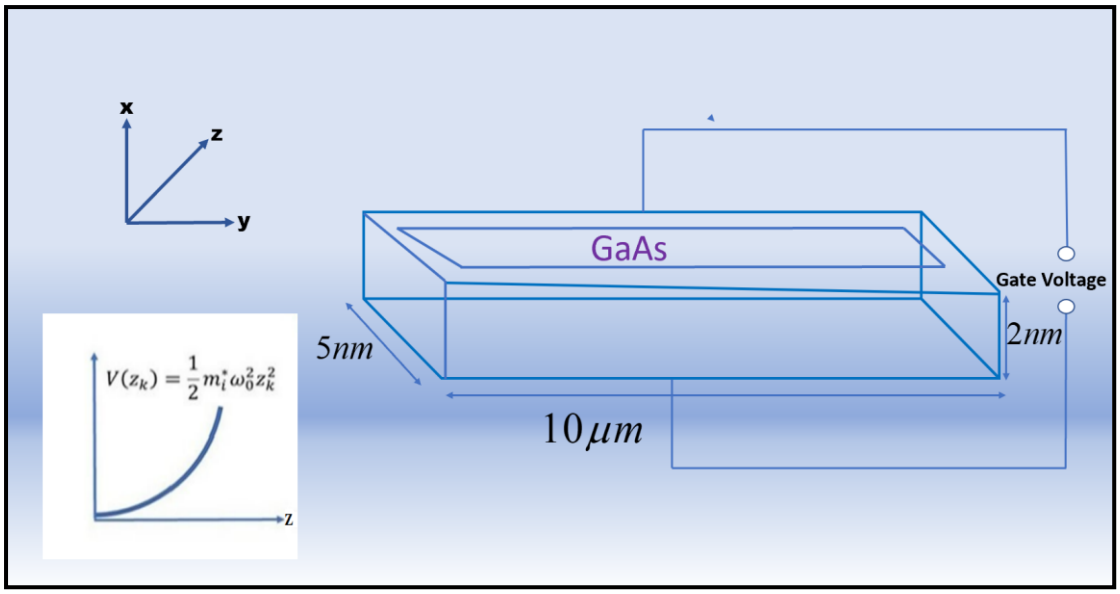

Figure 4.1: *Schematic diagram of an GaAs Quantum Dot*

The Hamiltonian is segmented into two terms taking the relative motion and center of mass into consideration and is given by:

$$H_{e1} = H_{r1} + H_{c1} \tag{4.6}$$

$$H_{r1} = \frac{p^2}{2\mu} + \frac{1}{2}\mu\omega_0^2 z_{r1}^2 - \frac{e^2}{\varepsilon(P,T)\left|z_{r1}\right|} \tag{4.7}$$

and $$H_{c1} = \frac{P^2}{2M_{T1}} + \frac{1}{2}M_{T1}\omega_0^2 Z_{T1}^2 \tag{4.8}$$

for $T < 200,$ the dielectric constant of GaAs is [38- 40]

$$\varepsilon(P,T) = 12.74e^{(9.4\times10^{-5})(T-75.6)+1.73\times10^{-3}P} \tag{4.9}$$

The coordinate of the centre of mass are written as:

$$Z_{T1} = \frac{m_h^*(P,T)z_h + m_e^*(P,T)z_e}{M_{T1}(P,T)} \tag{4.10}$$

Here, total mass is $M_{T1}(P,T) = m_h^*(P,T) + m_e^*(P,T)$; the relative coordinate is $z_{r1} = z_e - z_h$, momentum operator is $p_{Z_{T1}} = \frac{\hbar}{i}\nabla_{Z_{T1}}$, and the reduced mass is

$$\mu_{r1}(P,T) = m_h^*(P,T)m_e^*(P,T) / M_{T1}(P,T) \tag{4.11}$$

The excitonic wave function and energy levels are written as

$$\psi_{f1}(z_h, z_e) = \varphi(z_{T1})\phi(Z_{T1}) \tag{4.12}$$

$$E_{T1} = E_{z_{T1}} + E_{Z_{r1}} \tag{4.13}$$

The term signifying the center of mass part is considered as the problem for 1D semi-parabolic oscillator where the Hamiltonian is H_{c1} and Eigen function & Eigen energies are [38]:

$$\phi_{k1}(Z_{T1}) = N_{k1}\exp(-\frac{1}{2}\alpha^2 {Z_{T1}}^2)H_{2k1+1}(\alpha Z_{T1}) \tag{4.14}$$

$$E_{k1} = (2k1+\frac{3}{2})\hbar\omega_{0,} \qquad (k1 = 0,1,2,....), \tag{4.15}$$

Where H_{2k1+1} is the Hermite Polynomial

$$N_{k1} = [\frac{1}{\alpha}\sqrt{\pi}2^{2k1}(2k1+1)!]^{-1/2} \tag{4.16}$$

$$\alpha = \sqrt{M_{T1}\omega(P)/\hbar} \tag{4.17}$$

We analytically obtained the eigenvalues & wave function of the relative motion part in the strong and weak confinement regime. For the strong regime, H_{r1} reduces to:

$$H_{r1s} = \frac{p^2}{2\mu} + \frac{1}{2}\mu\omega_0^2 z_{r1}^2 \tag{4.18}$$

Neglecting the coulomb term as per the strong confinement regime, $\varphi(z_{r1})$ is determined as:

$$\varphi(z_{r1}) = N_n \exp[-\frac{1}{2}\beta^2 {z_{r1}}^2]H_{2n+1}(\beta z_{r1}), \tag{4.19}$$

$$E_{y1} = (2n+\frac{3}{2})\hbar\omega_0 \qquad (y1 = 0,1,2,....), \tag{4.20}$$

$$N_n = [\frac{1}{\beta}\sqrt{\pi}2^{2n1}(2n+1)!]^{-1/2} \tag{4.21}$$

$$\beta = \sqrt{\mu\omega(P)/\hbar} \tag{4.22}$$

Our quantum dot interacts with electromagnetic field E(t) having a frequency ω, such that [41- 45]:

$$E(t) = Ee^{i\omega t} + E^* e^{-i\omega t} \tag{4.23}$$

Upon such interactions, the time evolution equation for the matrix elements of one-electron density operator, ρ, is given by:

$$\frac{\partial \rho}{\partial t} = \frac{1}{i\hbar}[H_0 - qxE(t), \rho] - \Gamma(\rho - \rho^{(0)}) \tag{4.24}$$

where H_0 represents the Hamiltonian of this system in the absence of the electromagnetic field $E(t)$, and electronic charge is given by q, unperturbed density matrix operator is $\rho^{(0)}$, and Γ is the phenomenological operator responsible for the damping due to the electron-phonon interaction, collisions among electrons, etc. It is assumed that Γ is a diagonal matrix and its elements are equal to the inverse of relaxation time Γ_0.

For solving Eq. (4.19), standard iterative method is being used and hence ρ has been expanded as $\rho(t) = \sum_n \rho^{(n)}(t)$. Now, using this expansion in Eq. (4.19), density matrix elements can be obtained as shown below:

$$\frac{\partial \rho_{ij}^{(n+1)}}{\partial t} = \frac{1}{i\hbar}[H_0, \rho^{(n+1)}]_{ij} - \Gamma_{ij}\rho_{ij}^{(n+1)} - \frac{1}{i\hbar}[qx, \rho^{(n)}]_{ij} E(t) \tag{4.25}$$

As the density matrix ρ has been obtained hence, the electronic polarization $P_e(t)$ and susceptibility $\chi(t)$ can be calculated as:

$$P_e(t) = \varepsilon_o \chi(\omega) E e^{-i\omega t} + \varepsilon_o \chi(-\omega) E^* e^{-i\omega t} = \frac{1}{V} Tr(\rho M) \tag{4.26}$$

where ρ is density matrix for one-electron and V is the volume of the system, ε_0 represents permittivity of free space, and the symbol Tr (trace) denotes the summation over the diagonal elements of the matrix.

Now, using real part of the susceptibility, refractive index changes can be determined as:

$$\frac{\Delta n(\omega)}{n_r} = \mathrm{Re}[\frac{\chi(\omega)}{2n_r^2}] \tag{4.27}$$

Within a two-level system approach, the linear and third order nonlinear optical absorption coefficient are obtained from the imaginary part of the susceptibility [25, 30, 41-47] as:

$$\alpha^{(1)}(\omega) = \omega\sqrt{\mu/\varepsilon_r}\,\frac{|M_{01}|^2 N\hbar\Gamma_0}{[(E_{10}-\hbar\omega)^2+(\hbar\Gamma_0)]^2} \tag{4.28}$$

$$\alpha^{(3,\mathrm{I})}(\omega) = -2\omega\sqrt{\mu/\varepsilon_r}\,(\mathrm{I}/\varepsilon_0\eta_r c)\frac{|M_{01}|^4 N\hbar\Gamma_0}{[(E_{10}-\hbar\omega)^2+(\hbar\Gamma_0)]^2} \times\left(1-\frac{|M_{11-}M_{00}|^2}{4|M_{01}|^2}\left\{\frac{(E_{10}-\hbar\omega)^2-(\hbar\Gamma_0)^2+2E_{10}(E_{10}-\hbar\omega)}{(E_{10})^2+(\hbar\Gamma_0)^2}\right\}\right) \tag{4.29}$$

Total absorption coefficient $\alpha(\omega,\mathrm{I})$ is given as:

$$\alpha(\omega,\mathrm{I}) = \alpha^{(1)}(\omega)+\alpha^{(3)}(\omega,\mathrm{I}) \tag{4.30}$$

The linear and nonlinear changes in the refractive index are written as [25, 30, 42-50]:

$$\frac{\Delta\eta^{(1)}(\omega)}{\eta_r} = \frac{1}{2\eta_r{}^2\varepsilon_0}|M_{01}|^2\left[\frac{E_{10}-\hbar\omega}{(E_{10}-\hbar\omega)^2+(\hbar\Gamma_0)^2}\right] \tag{4.31}$$

$$\frac{\Delta\eta^{(3,\mathrm{I})}(\omega,\mathrm{I})}{\eta_r} = -\frac{\mu c}{4\eta_r{}^3\varepsilon_0}|M_{01}|^2\left[\frac{N\mathrm{I}}{[(E_{10}-\hbar\omega)^2+(\hbar\Gamma_0)^2]^2}\right] \times\left[4(E_{10}-\hbar\omega)|M_{01}|^2-\frac{|M_{11-}M_{00}|^2}{(E_{10})^2+(\hbar\Gamma_0)^2}\{(E_{10}-\hbar\omega)\times[E_{10}(E_{10}-\hbar\omega)-(\hbar\Gamma_0)^2(2E_{10}-\hbar\omega)]\}\right] \tag{4.32}$$

The total refractive index change is:

$$\frac{\Delta\eta(\omega,\mathrm{I})}{\eta_r}=\frac{\Delta\eta^{(1)}(\omega)}{\eta_r}+\frac{\Delta\eta^{(3,\mathrm{I})}(\omega,\mathrm{I})}{\eta_r} \tag{4.33}$$

Where $\mu_{ij}=\left|\left\langle\psi_i\left|z_{T1}\right|\psi_j\right\rangle\right|(i,j=0,1)$ are the matrix elements of the dipole moment, $\psi_i(\psi_j)$ are the Eigen functions, $\omega_{01}=\frac{E_1-E_0}{\hbar}$ is the difference between two energy levels. ω is the frequency of Electromagnetic field, Γ_0 relaxation time.

4.3 Results and Discussion

We have considered the GaAs semiconductor material constants for our numerical results. We used the numerical parameters such as [38, 40-44] $m_e^*=0.067\,m_0$, $m_h^*=0.09\,m_o$ (m_O is the mass of a free electron), $N=3\times10^{22}\,m^{-3}$, $\Gamma_0=0.2\,ps^{-1}$, $\varepsilon=12.53$, $\mathrm{I}=2000MW/m^2$.

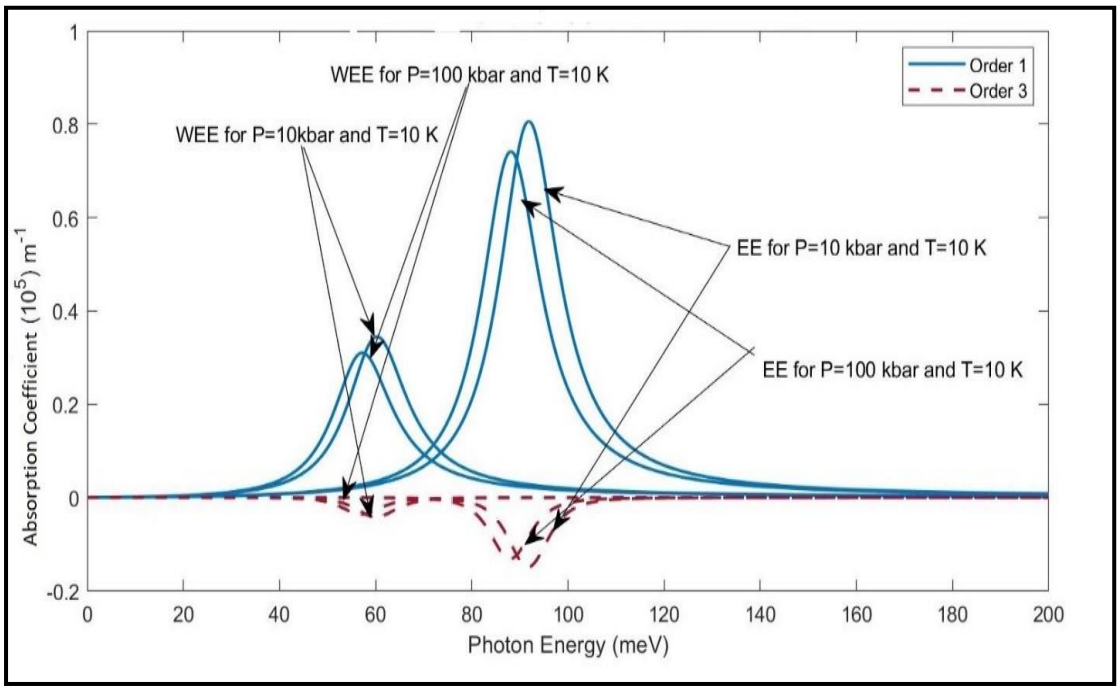

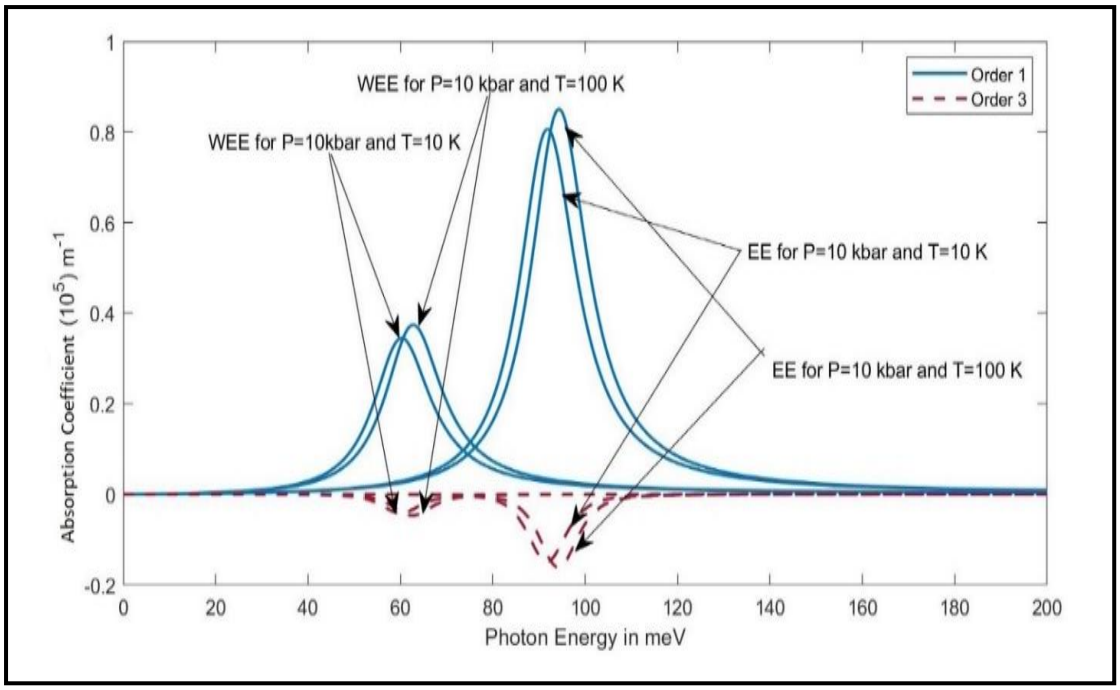

Figure 4.2 (a, b): *Represents the linear and nonlinear absorption coefficients with and without considering excitonic (EE & WEE) effects for T=10 K & 100 K and P=10 kbar & P=100 kbar and I = 2000MWm^{-2}.*

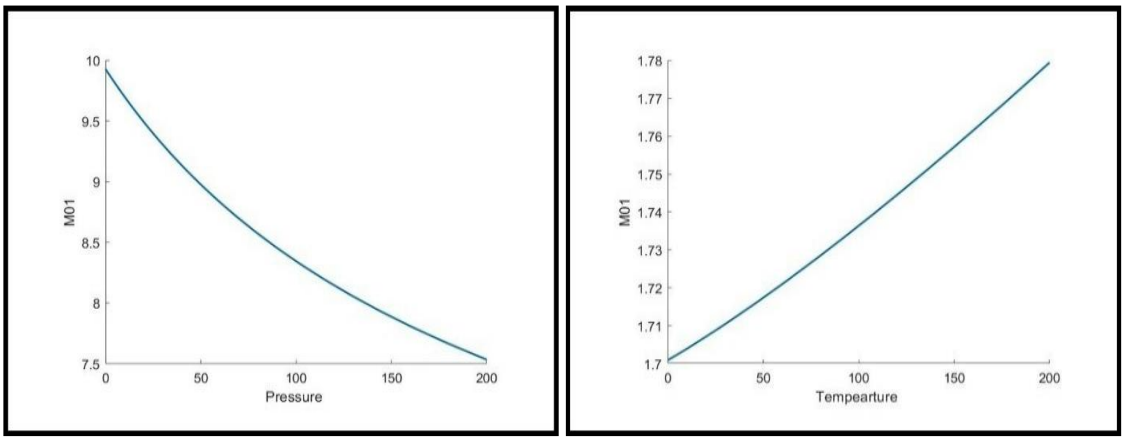

Figure 4.2(c, d): *Represents behavior of matrix element with pressure and temperature.*

To understand the effect of change in hydrostatic pressure and temperature on the Linear Absorption Coefficient (LAC) and third order (Nonlinear) Absorption coefficient (NAC), we present the same in figure 4.2 (a) & (b). Here we also have shown the effects of inclusion of Excitonic Effects (EE) on the LAC & NAC. One can observe that for the cases where [4.2 (a) & 4.2 (b)] the EE is not included, the NAC & LAC peaks occurred at

photon energies much lower than the cases of inclusion of EE in the study. This is attributed to the energy associated with the excitonic interactions between the electron & holes. Moreover, the peak heights, for both LAC & Total Absorption Coefficient (TAC), increased when excitonic effects are taken into account. This is a consequence of enhancement of the dipole moment due to the positive-negative charge separation of the electron-hole pair, which otherwise is not there in the case of Without Excitonic Effects (WEE). In figure 4.2 (a), shift from 60.28meV to 56.70meV when pressure is increased from 10kbar to 100kbar in case of WEE. Whereas for identical change in pressure, the LAC and NAC peaks are shifted from 91.78meV to 88.58meV for the case of EE. This shifting is accompanied by decrease in absorption LAC peak height from $0.35x10^5m^{-1}$ to $0.32x10^5m^{-1}$ in case of WEE and from $0.80\ x10^5m^{-1}$ to $0.72\ x10^5m^{-1}$ for the EE case. Similar effects are also observed for the NAC. The LAC & NAC shifts towards the lower energy end of the spectrum as the pressure increases. This shifting is accompanied by a diminishing absorption peak height for both EE &WEE case. These effects are due to the counter affecting action of pressure on the confinement potential and energy band gap. The pressure increases the confinement strength but it also strongly alters the energy band gap. For GaAs, in the pressure range of 10kbar to 100bar, these two opposing effects results in a net red shift of the peaks as the pressure increases. Whereas, in figure 4.2 (b), one can see that the absorption peaks, LAC & NAC, moves from 60.28meV to 62.40meV and peak heights of LAC increases from $0.35x10^5m^{-1}$ to $0.39x10^5m^{-1}$ and NAC changes from $-0.062\ x10^5m^{-1}$ to $-0.066\ x10^5m^{-1}$ when temperature is increased from 10K to 100K, keeping P=10kbar. For the case of EE, the blue shift in peaks happen from 91.7meV to 94.39meV and the LAC peak heights changes from $0.80\ x10^5m^{-1}$ to $0.85\ x10^5m^{-1}$ and the NAC peak enhances from $-0.13\ x10^5m^{-1}$ to $-0.17\ x10^5m^{-1}$ as the temperature is increased from 10K to 100K. These effects, similar in nature for both EE & WEE, results from the

interplay complex second term of eqn. (5) & the direct dependence of m^* on the temperature. Physically, the change in the entropy of the charge carriers induces a change in the energy of the states. In figure 4.3 (a, b), we present the TAC as a function of incoming photon energy. Here, we observe similar effects of change in pressure & temperature on the TAC peaks as in the case of LAC & NAC. However, in TAC, the effects of LAC dominate the NAC for the light intensity of 2000 MW / m^2. Furthermore, owing to the diametrically opposed behavior of the first and the third-order nonlinear ACs, a decrease in the total ACs is observed due to reduction in the effective mass of the electron with the intensification of the temperature. A close relationship between the peak values of the total ACs, the transition dipole element and the difference between energy levels E_{10} can be disclosed from the figure. Total ACs is influenced in opposite by the dipole matrix element $|M_{10}|^2$ to that of the energy difference E_{10}. Hence, a blue shift is observed as a result of increase in temperature and red shift is observed when pressure is increased. This is happening due to increase/decrease in transition energy E_{10} on a significant increase in temperature/pressure. Upon increasing temperature/pressure, a drop/enhancement in the electron effective mass with an expansion/compression of the transition energy is observed due to dependency of the electron-photon interaction on the temperature/pressure. Hence, the blue/red shift is observed. Same can be observed from fig. 4.2 (c, d) that how matrix elements are getting varied with pressure and temperature.

To compare our results in fig. 4.2 (b), we plotted the total absorption coefficient and compared with experimental data (Lourenc et al. 2007, Gurmessa et al. 2015) [51, 52] at T ≅ 10 K & 100 K. As it can be observed from the graph that a similar pattern is observed in both the experimental results as well as theoretical results but deviation can be observed in the theoretical prediction from the experimental data (Lourenc et al.

2007, Gurmessa et al. 2015). At T=10 K, the quantitative value is similar to the experimental value but this is not same for the T=100 K. Although, it can be observed from both experimental values as well as theoretical values that a blue shift is happening in the absorption coefficient on increasing the temperature. For example, for temperature between 0-20K and 40-100K peaks are shifting towards higher energy values for both the cases i.e., theoretical and experimental. But as there was not significant difference between the peaks ranging from 21-90K, hence, only values for 20K and 100K have been presented in the theoretical graphs. Several points can be thought of as a cause for this deviation in the quantitative value. Some of these points are: (i) electronic transitions are not perfectly exact for the two-level system, (ii) several parameters such as dot size, intensity, σ, υ are temperature dependent but are here considered as temperature independent, (iii) calculations have been performed theoretically using numerical methods and these methods have some limitations, (iv) approximation have been taken into account for solving the equations (23-27).

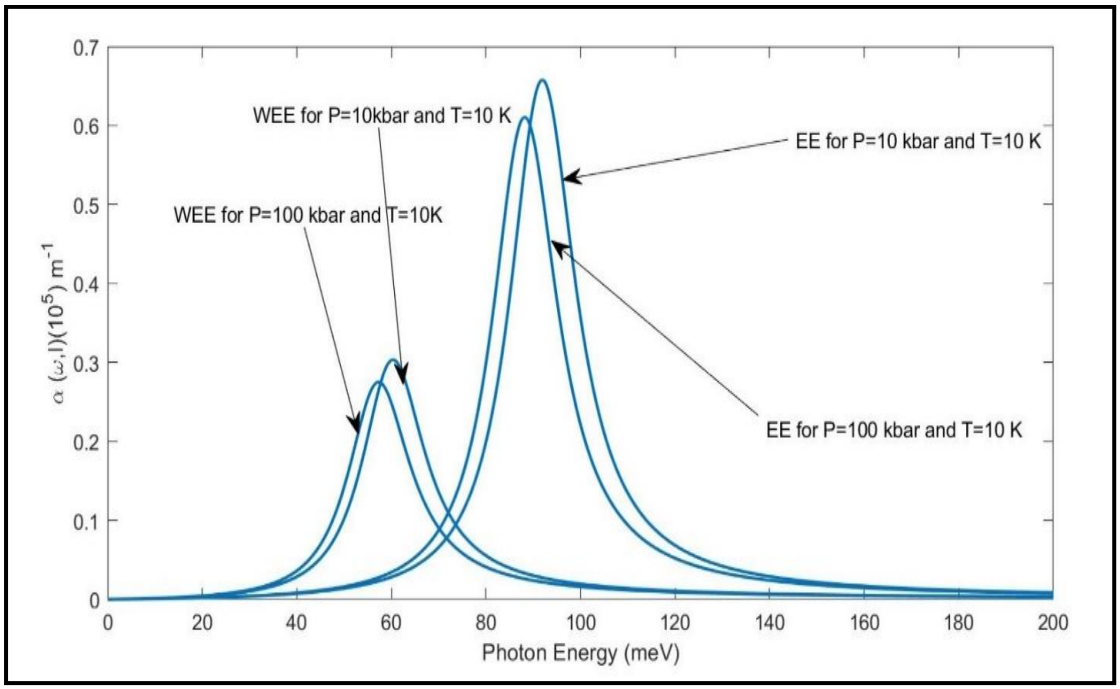

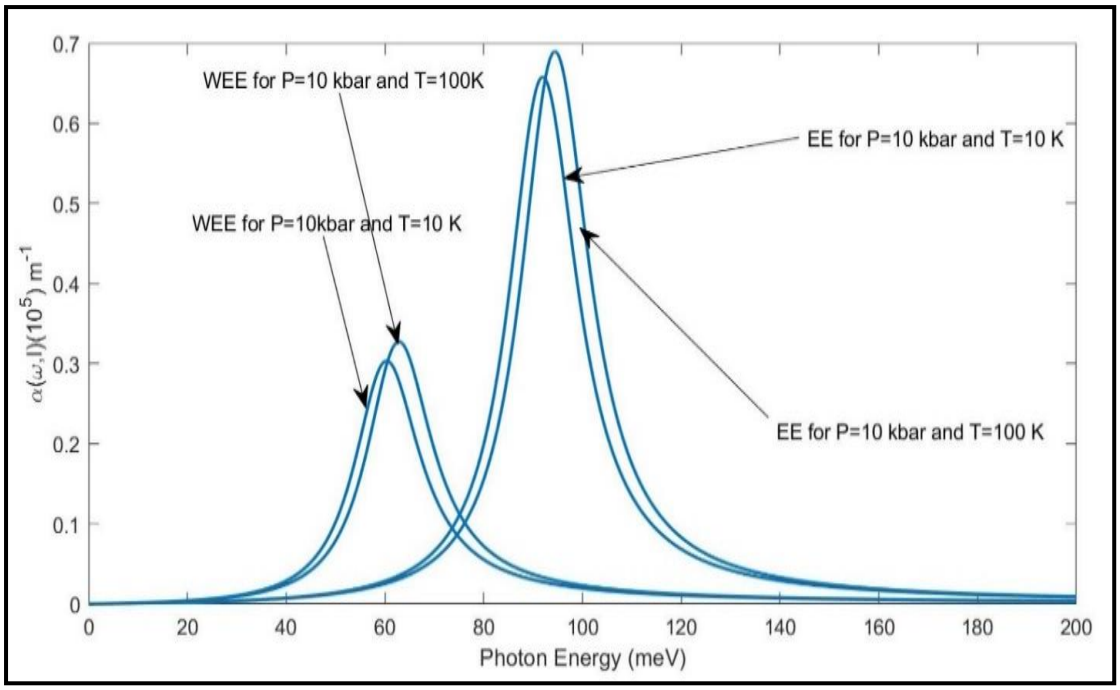

Figure 4.3 (a,b): *Represents total absorption coefficients with and without considering excitonic (EE & WEE) effects for T=10 K & 100 K and P=10 kbar & P=100 kbar and I = 2000MWm^{-2}*

As the interacting light changes the physical nature of the quantum dot material, it, therefore induces drastic changes in the refractive index of the QDs near the resonance energy. The same can be observed from the dispersion curves presented in fig. 4.4 (a, b) & fig. 4.4 (c, d). In fig. 4.4 (a), for WEE and hydrostatic pressure of 10kbar, the dispersion curve of Linear Refractive Index change (LRI) rises to a maximum value 0.062 at photon energy 60.28meV and crosses over to the negative polarity region to reach -0.063 at photon energy 74.40meV. When the pressure is increased to 100kbar, this dispersion area of red shifts to 56.70meV (maxima of 0.059) and 64.86meV (minima of -0.059). Further in fig. 4.4 (a), for pressure of 10kbar, when EE is taken into account the area of polarity change of the LRI shifts to higher photon energy, viz. reaches maximum at photon energy 91.7meV (maxima of 0.088) and crosses over to the negative values to reach the minimum value at 106.33meV (minima of -0.088). Again, for EE case, when

pressure is increased to 100kbar, the dispersion area red shifts to 88.58meV (maxima 0.085) and 103.48 meV (minima -0.086). Similar effects are observed (fig. 4.4 (b)) for Nonlinear Refractive Index change (NRI) at the identical photon energies as in the case of LRI. However, in case of NRI, the polarity of the refractive index change first reaches a negative valued minima and then crosses over to a positive valued maximum. Opposite nature of shifting of the dispersion is observed when the temperature is changed from 10K to 100K keeping P=10kbar [fig 4.4 (c, d)]. In figure 4.4 (c), it is obtained that the maximum value of the LRI (minimum value of NRI in figure 4.4 (d)) occurs at photon energy 60.28meV (maxima of 0.062) when the temperature is kept at 10K for the case of WEE. When the temperature is increased to100K, in case of WEE, the maximum value of the LRI (minimum of NRI, figure 4.4 (d)) shifts to a higher photon energy value of 62.40meV. Whereas for the case of EE, the LRI (and NRI) maximum value (minima for NRI) shifts from 91.7meV to 94.39meV when temperature is increased to 100K from 10K. These two-opposite natures of influences on the RI change of hydrostatic pressure & temperature are attributed to the fact that the increase in pressure strengthens the confinement whereas the temperature acts the other way.

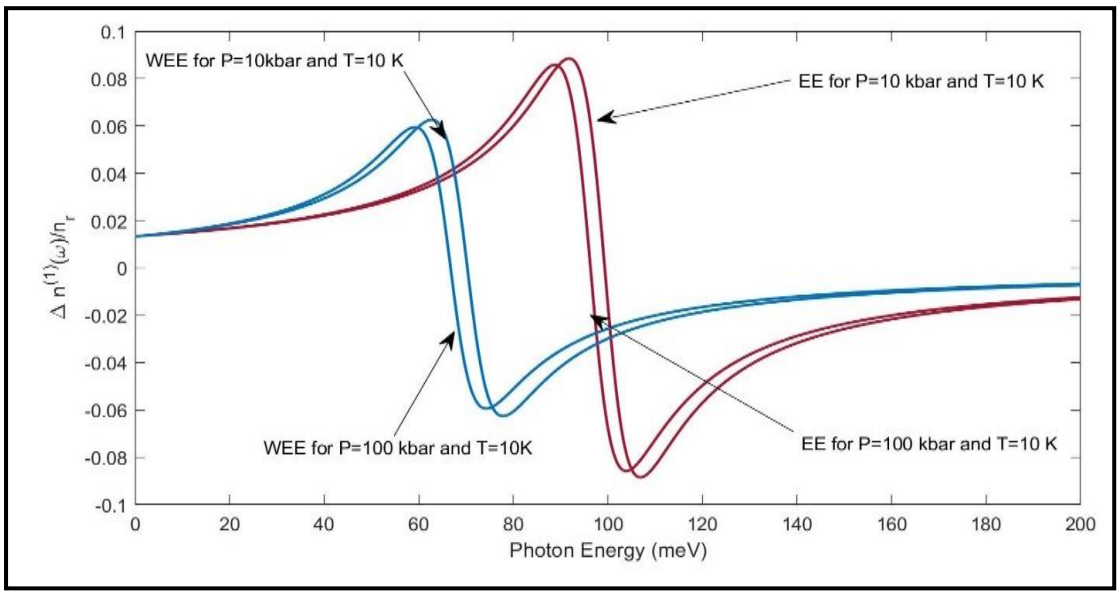

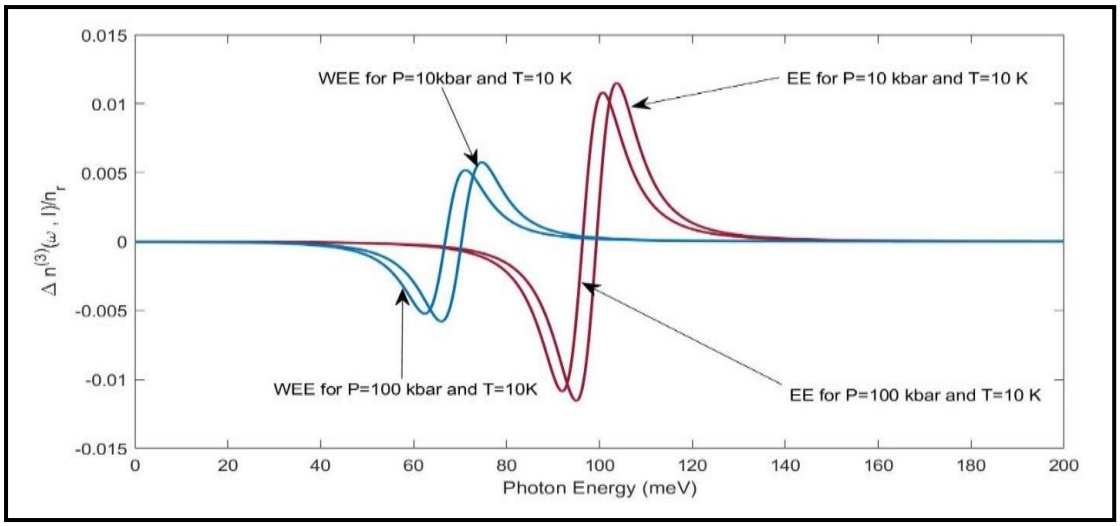

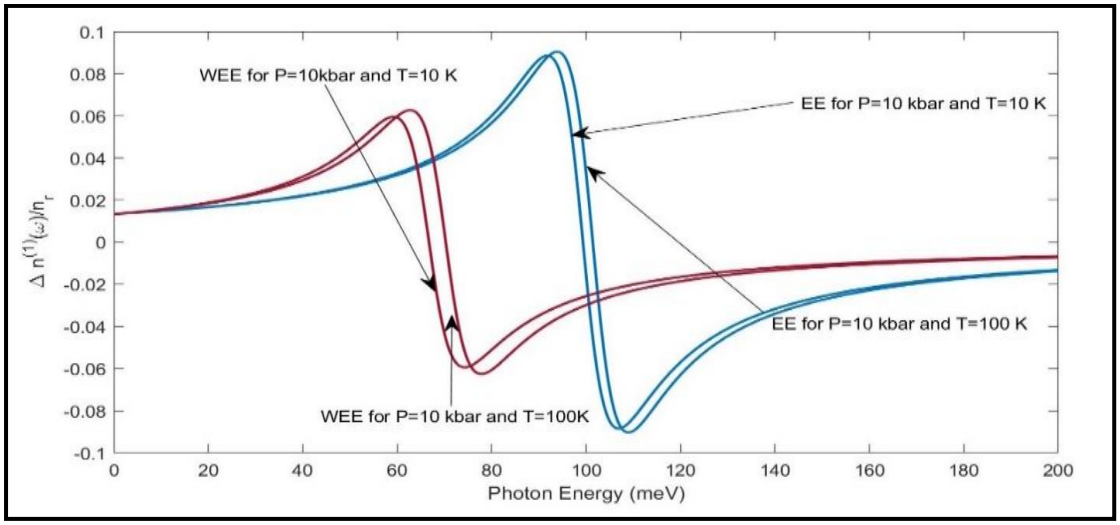

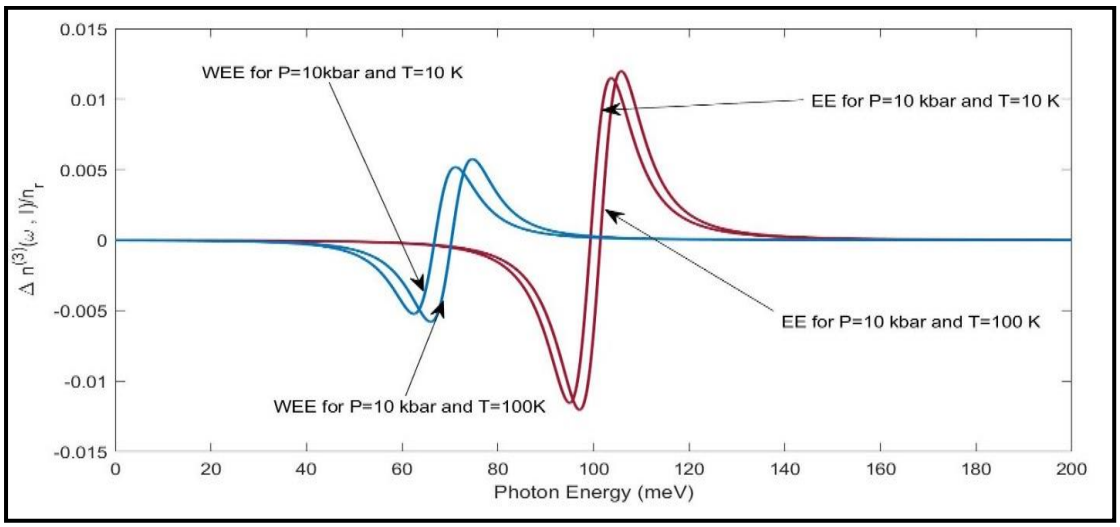

Figure 4.4 (a,b,c,d): *Represents the linear and nonlinear refractive index for with and without considering excitonic (EE & WEE) effects for T=10 K & 100 K and P=10 kbar & P=100 kbar and I = 2000MWm−2*

In figure 4.5 (a, b), the total refractive index change is presented at two values of applied hydrostatic pressure (4.5a) keeping T=10 K and in (4.5b), the temperature is varied from 10 K to 100 K keeping P=10 kbar.

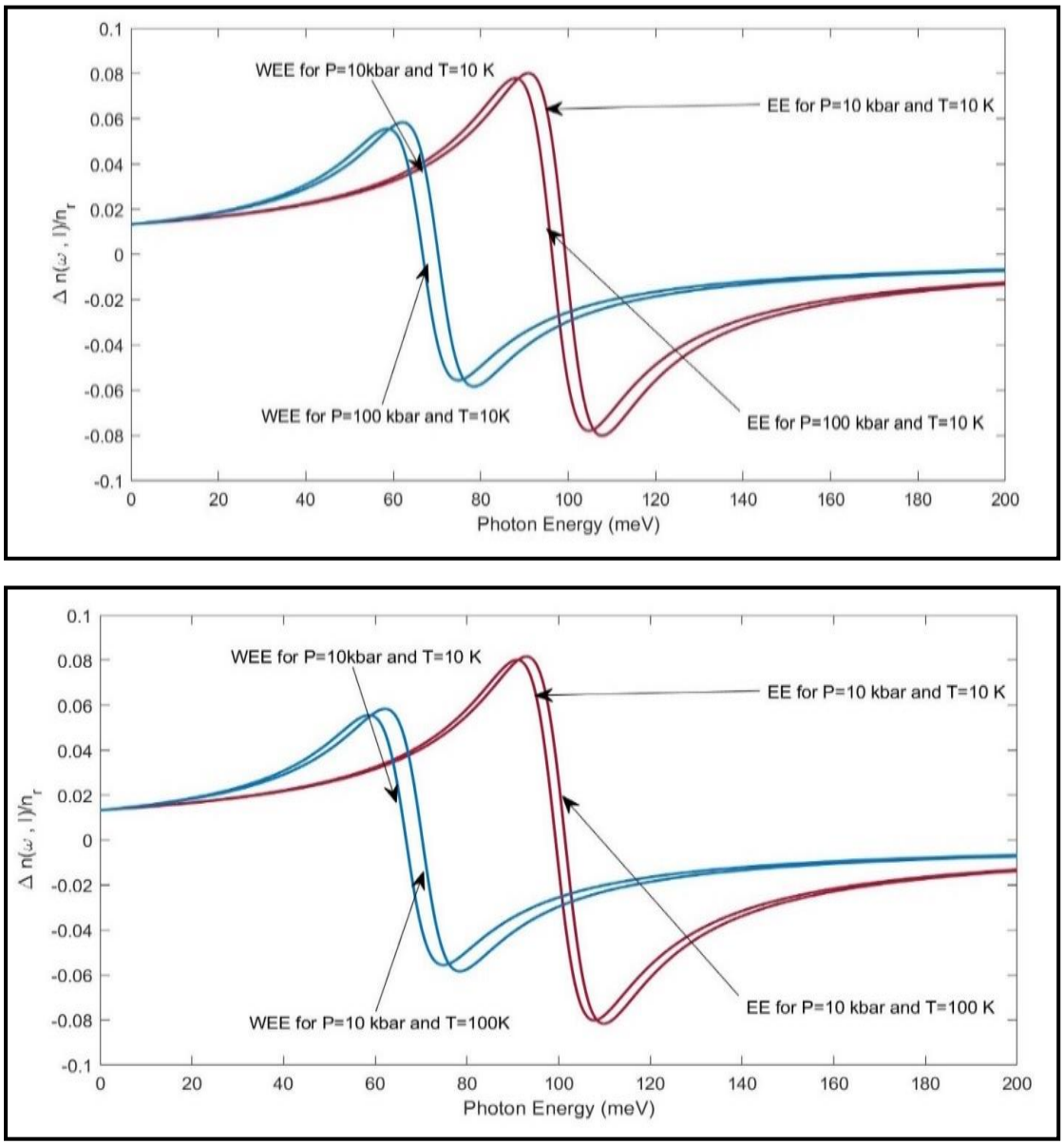

Figure 4.5 (a,b): *Represents the total refractive index for with and without considering excitonic (EE & WEE) effects for T=10 K & 100 K and P=10 kbar & P=100 kbar and I = 2000MWm^{-2}*

It can be observed that the magnitude of the change in refractive index with variation in hydrostatic pressure & temperature are different on the two scenarios, i.e., one with the

excitonic effect and the other without excitonic effects. This is the consequence of the fact that in case of WEE, the properties are determined by the effective mass of the electron whereas in case of EE, the properties are manifested from the reduced mass of the electron-hole pair. This is one of the major factors for variation in the optical properties in between EE & WEE, in addition to the fact of opposite polarity charges being involved in the case of EE.

4.4 Conclusions

We have reported the linear & nonlinear optical properties, viz. absorption coefficient & refractive index of a GaAs semi parabolic QD by employing the compact density matrix formalism. We have demonstrated that the absorption coefficient peaks and refractive index dispersion variation is blue shifted with the inclusion of excitonic effects. The increase in the pressure alters the optical properties of the QD by controlling the effective mass of electron, energy band gap and the dielectric constant. This intricate counter-balancing act results in a red shift in the nonlinear optical properties' resonance position when the applied hydrostatic pressure is incremented, while augmenting the ambient temperature results in blue shifts of the LAC, NAC & TAC and refractive index change. Further, it is observed that the enhancing the pressure lowers the peak height of the absorption coefficient & refractive index dispersions curves. This is due to the diminishing of dipole moments of the QD by the reinforcing the confinement by hydrostatic pressure which results in shrinking of the orbital wave functions. To our best knowledge no such research work illustrating the effects of Hydrostatic Pressure and Temperature on the RI & AC (Linear & third order) of GaAs QD for a semi-parabolic system (excitonic as well as non-excitonic cases) has been

carried out earlier. According to our consideration, the obtained results can have important practical applications in fabricating optoelectronic devices and hence have a sound share in progressive product technology. The shifting of absorption peaks can specially be used in devices where optical switches can be turned on and off depending on absorption of incident radiation. Hydrostatic pressure and temperature can act as external parameters. Further, the same property may also be used to detect changes in temperature and pressure by observing the refractive index change and absorption of photons at particular wavelength. Analysis of the experimental results (Lourenc et al. 2007, Gurmessa et al. 2015) and comparing with the theoretical results obtained, some disagreement is observed in the absorption coefficients. This variation with the experimental results is explained in previous section.

References

[1] T. Jamieson, R. Bakhshi, D. Petrova, R. Pocock, M. Imani & A.M. Seifalian, Biological applications of quantum dots. Biomaterials 28, 4717–4732 (2007).

[2] Salata, O. Applications of nanoparticles in biology and medicine. J Nanobiotechnol 2, 3 (2004).

[3] D. Mocatta, G. Cohen, J. Schattner, O. Millo, E. Rabani & U. Banin, Heavily doped semiconductor nanocrystal quantum dots. Science. 2011 Apr 1;332 (6025), 77-81.

[4] P.M. Koenraad & M.E. Flatté, Single dopants in semiconductors, Nat. Mater. 10, 91–100 (2011).

[5] A.E.; El-Yadri, M.; Feddi, E.M. Adjustment of Terahertz Properties Assigned to the First Lowest Transition of (D+, X) Excitonic Complex in a Single Spherical Quantum Dot Using Temperature and Pressure. Appl. Sci. 2021, 11, 5969.

[6] Schneider H, Fuchs F, Dischler B, Ralston J D and Koidl P, Intersubband absorption and infrared photodetection at 3.5 and 4.2 μm in GaAs quantum wells, Appl. Phys. Lett. 58, 1991, 2234.

[7] D. K. Ferry and S. M. Goodnick, Transport in Nanostructures (Cambridge University Press, Cambridge, 1997).

[8] H. A. Sarkisyan, Direct Optical Absorption in Cylindrical Quantum Dot, Mod. Phys. Lett. B 18, 443 (2004).

[9] S.N. Saravanamoorthy, A. John Peter & C.W. Lee, Optical peak gain in a PbSe/CdSe core-shell quantum dot in the presence of magnetic field for mid-infrared laser applications, Chem. Phys. 483, 1 (2017).

[10] A. Bera & M. Ghosh, Dipole moment and polarizability of impurity doped quantum dots driven by noise: Influence of hydrostatic pressure and temperature, Physica B 515, 18 (2017).

[11] R.D. Schaller, and V.I. Klimov, High Efficiency Carrier Multiplication in PbSe Nanocrystals: Implications for Solar Energy Conversion, Phys. Rev. Lett. 92, 186601 (2004).

[12] W.U. Huynh, J.J. Dittmer, and A.P. Alivisatos, Hybrid nanorod-polymer solar cells, Science 295, 2425 (2002).

[13] X. Zhong, R. Xie, Y. Basche, T. Zhang, and W. Knoll, High-Quality Violet- to Red-Emitting ZnSe/CdSe Core/Shell Nanocrystals, Chem. Mater. 17, 4038 (2005).

[14] F. Ungan, J.C. Mart´ınez-Orozco, R.L. Restrepo, M.E. Mora-Ramos, E. Kasapoglu & C.A. Duque, Nonlinear optical rectification and second-harmonic generation in a semi-parabolic quantum well under intense laser field: Effects of electric and magnetic fields, Superlattice Microstruct. 81, 26 (2015).

[15] M.J. Karimi & G. Rezaei, Effects of external electric and magnetic fields on the linear and nonlinear intersubband optical properties of finite semi-parabolic quantum dots, Physica B 406, 4423 (2011).

[16] J. Fl´orez & A. Camacho, Excitonic effects on the second-order nonlinear optical properties of semi-spherical quantum dots, Nanoscale Res. Lett. 6, 268 (2011).

[17] M. Cristea, Comparative study of the exciton states in CdSe/ZnS core-shell quantum dots under applied electric fields with and without permanent electric dipole moment, Eur. Phys. J. Plus 131, 86 (2016).

[18] Chaurasiya R., Dahiya S., Sharma R. A study of confined Stark effect, hydrostatic pressure and temperature on nonlinear optical properties in 1D $Ga_xAl_{1-x}As/GaAs/Ga_xAl_{1-x}As$ quantum dots under a finite square well potential. Nanosystems: Phys. Chem. Math., 2023, 14 (1), 44–53.

[19] N. Eseanu, Simultaneous effects of laser field and hydrostatic pressure on the intersubband transitions in square and parabolic quantum wells, Phys. Lett. A 374, 1278 (2010).

[20] G. Rezaei, M.J. Karimi & A. Keshavarz, Excitonic effects on the nonlinear intersubband optical properties of a semi-parabolic one-dimensional quantum dot, Physica E 43, 475 (2010).

[21] J.-H Yuan, Y. Zhang, H. Mo, N. Chen & Z.-H. Zhang, Electric field effect on the second-order nonlinear optical properties in semiparabolic quantum wells, Physica E 77, 102 (2016).

[22] I. Karabulut, H. Safak & M. Tomak, Nonlinear optical rectification in asymmetrical semiparabolic quantum wells, Solid State Commun. 135, 735 (2005).

[23] J.E. Bautista, M.L. Lyra & R.P.A. Lima, Screening effect on the exciton mediated nonlinear optical susceptibility of semiconductor quantum dots, Photon. Nanostruct. 11, 8 (2013).

[24] E. Paspalakis, J. Boviatsis & S. Baskoutas, Effects of probe field intensity in nonlinear optical processes in asymmetric semiconductor quantum dots, J. Appl. Phys. 114, 153107 (2013).

[25] I. Karabulut, H. Safak & M. Tomak, Excitonic effects on the nonlinear optical properties of small quantum dots, J. Phys. D: Appl. Phys. 41, 155104 (2008).

[26] H.M. Baghramyan, M.G. Barseghyan, A.A. Kirakosyan, R.L. Restrepo, and C.A. Duque, Linear and nonlinear optical absorption coefficients in GaAs/Ga1−xAlxAs concentric double quantum rings: Effects of hydrostatic pressure and aluminum concentration, J. Lumin. 134, 594–599 (2013).

[27] Yu Y-B, Zhu S-N & Guo K-X, Exciton effects on the nonlinear optical rectification in one-dimensional quantum dots., Phys Lett A, 175, 335, (2005).

[28] Karabulut İ and Şafak H, Nonlinear optical rectification in semiparabolic quantum wells with an applied electric field, Physica B, 82, 368, (2005).

[29] C. M. Duque, M. E. Mora-Ramos & C. A. Duque, Simultaneous effects of electron-hole correlation, hydrostatic pressure, and temperature on the third harmonic generation in parabolic GaAs quantum dots, J Nanopart Res 13:6103–6112,2011.

[30] S. Baskoutas, E. Paspalakis &A.F. Terzis, Effects of excitons in nonlinear optical rectification in semiparabolic quantum dots, Phys. Rev. B 74, 153306 (2006).

[31] C A Duque, N Porras-Montenegro, Z Barticevic, M Pacheco and L E Oliveira, Effects of applied magnetic fields and hydrostatic pressure on the optical transitions in self-assembled InAs/GaAs quantum dots, J. Phys.: Condens. Matter 18 (2006) 1877–1884.

[32] C.M. Duque, A.L. Morales, M.E. Mora-Ramos, C.A. Duque, Optical nonlinearities associated to applied electric fields in parabolic two-dimensional quantum rings, Journal of Luminescence, 143, 2013, 81-88.

[33] VN Mughnetsyan, A Kh Manaselyan, MG Barseghyan & AA Kirakosyan, Simultaneous effects of hydrostatic pressure and spin–orbit coupling on linear and nonlinear intraband optical absorption coefficients in a GaAs quantum ring, J. Lumin., 134, 24-27 (2013).

[34] C.M. Duque, M.E. Mora-Ramos & C.A. Duque, Hydrostatic pressure and electric field effects and nonlinear optical rectification of confined excitons in spherical quantum dots, Superlattices and Microstructures 49, 264-268 (2011).

[35] D. Bejan, Exciton effects on the nonlinear optical properties of semiparabolic quantum dot under electric field, Eur. Phys. J. Plus, 132, 102 (2017).

[36] S. Antil, M. Kumar, S. Lahon, S. Dahiya, A. Ohlan, R. Punia and A.S. Maan, Influence of hydrostatic pressure and spin orbit interaction on optical properties in quantum wire, Physica B: Condensed Matter 552 (2019) 202–208.

[37] S. Antil, M. Kumar, S. Lahon and A.S. Maan, Pressure dependent optical properties of quantum dot with spin orbit interaction and magnetic field, Optik - International Journal for Light and Electron Optics 176 (2019) 278–286.

[38] S. Dahiya, S. Lahon & R. Sharma, Effects of temperature and hydrostatic pressure on the optical rectification associated with the excitonic system in a semi-parabolic quantum dot, Physica E 118 113918 (2020)

[39] A. Braggio, M. Grifoni, M. Sassetti & F. Napoli, Plasmon and charge quantization effects in a double-barrier quantum wire, Europhys. Lett. 50 (2000) 236.

[40] S. Unlu, I. Karabulut & H. Safak, Linear and nonlinear intersubband optical absorption coefficients and refractive index changes in a quantum box with finite confining potential, Physica E 33 (2006) 319.

[41] Melodie Fickenscher, Teng Shi, Howard E. Jackson, Leigh M. Smith, Jan M. Yarrison-Rice, Changlin Zheng, Peter Miller, Joanne Etheridge, Bryan M. Wong, Qiang Gao, Shriniwas Deshpande, Hark Hoe Tan, and Chennupati Jagadish, Optical, Structural, and Numerical Investigations of GaAs/AlGaAs Core–Multishell Nanowire Quantum Well Tubes, Nano Letters 2013 13 (3), 1016-1022.

[42] N. Raigoza, A.L. Morales, A. Montes, N. Porras-Montenegro & C.A. Duque, Optical nonlinearities associated to applied electric fields in parabolic two-dimensional quantum rings, Phys. Rev. B 69 (2004) 045323.

[43] H. O. Oyoko, N. Parras-Montenegro, S. Y. Lopez, and C. A. Duque, Comparative study of the hydrostatic pressure and temperature effects on the impurity-related optical properties in single and double GaAs– $Al_xGa_{1-x}As$ quantum wells, Phys. Status Solidi C **4**, 298 (2007).

[44] E. Herbert Li, Material parameters of InGaAsP and InAlGaAs systems for use in quantum well structures at low and room temperatures, Physica E 5 (2000) 215.

[45] F.D.M. Haldane, 'Luttinger liquid theory' of one-dimensional quantum fluids. I. Properties of the Luttinger model and their extension to the general 1D interacting spinless Fermi gas, J. Phys. C 14 (1981) 2585.

[46] R. Shankar, Principles of Quantum Mechanics (Plenum Press), New York, (1982)

[47] Aishah AL-Naghmaish, Hassen Dakhlaoui, Taher Ghrib, Effects of magnetic, electric, and intense laser fields on the optical properties of AlGaAs/GaAs quantum wells for terahertz photodetectors, Physica B: Condensed Matter, Volume 635, 2022, 413838.

[48] Suman Dahiya, Siddhartha Lahon, Rinku Sharma, Study of third harmonic generation in $In_xGa_{1-x}As$ semi-parabolic 2-D quantum dot under the influence of Rashba spin-orbit interactions (SOI): Role of magnetic field, confining potential, temperature & hydrostatic pressure, Physica E: Low-dimensional Systems and Nanostructures, Volume 147, 2023, 115620.

[49] Kuhn, K.J., Lyengar, G.U., Yee, Free carrier induced changes in the absorption and refractive index for interurban optical transitions in $Al_xGa_{1-x}As$/ $GaAs/Al_xGa_{1-x}As$ quantum wells**,** J. Appl. Phys. 70, 5010 (1991)

[50] Kopf, R.F., Herman, M.H., Lamont Schnoes, M., Perley, A.P., Livescu, G., Ohring, Band offset determination in analog graded parabolic and triangular quantum wells of GaAs/AlGaAs and GaInAs/AlInAs, J. Appl. Phys. 71, 5004–5011 (1992).

[51] Alemu Gurmessa, Getnet Melese, Lingamaneni Veerayya Choudary and Sisay Shewamare, Photoluminescence from GaAs nanostructures**,** International Journal of Physical Sciences, 2015, 10(3), 106-111.

[52] S. A. Lourenc, I. F. L. Dias1, J. L. Duarte, E. Laureto, V. M. Aquino, and J. C. Harmand, Temperature-Dependent Photoluminescence Spectra of GaAsSb/AlGaAs and GaAsSbN/GaAs Single Quantum Wells under Different Excitation Intensities, Brazilian Journal of Physics, 2007, 37, 4, 1212-1217.

CHAPTER 5

OPTICAL BEHAVIOR OF A FINITE WELL QD IN VARIED ELECTRIC FIELD, HYDROSTATIC PRESSURE & TEMPERATURE*

5.1 Introduction

The broad range of applications of nano-scale semiconductors has piqued the interest of scientists from various fields. It has applications in quantum computing, photonic computing, photovoltaics, biomedicine, and other fields. At nanoscales, the potential barrier can be used to confine electrons and holes inside the potential well. These quantum systems are classified into three types based on the degree of confinement. When an electron is confined in all three dimensions, it is referred to as a quantum dot. When electrons are confined in two dimensions, they form quantum wires, and when they are confined in only one dimension, they form quantum layers (quantum wells in one dimension). All of these systems cause interesting changes in the nonlinear optical properties. The quantum confined Stark effect is a well-known phenomenon that occurs when an electric field is added to a potential well. This phenomenon has piqued researchers to investigate the effect [1–4]. Two distinct characters of behavior have been revealed. The electric field first induces bending and tilting of the material energy band structure. This has a direct impact on lowering electron energy, resulting in a red shift. The electric field also causes excitons to polarize. The electron and hole are pushed back, reducing the Coulomb force of attraction and increasing the energy of the electron-hole pair. As a result, the demand for non-linear crystals is increasing [5]. The study of optical behavior in the presence of the electric field provides insight into the crystal controllability. This has prompted a slew of researchers to

* *(Part of this work has been published in **Nanosystems -Physics Chemistry Mathematics 14 (2023) 43**)*

investigate these properties, as well as the impact of the electric field [6, 7]. There were numerous studies that showed the effect of field strength, temperature, and pressure on non-linear properties such as Optical Rectification Coefficient (ORC), Absorption Coefficient (AC), and change in Refractive Index (RI) in quantum dot systems including parabolic and semi-parabolic potentials [8, 9]. Observing these changes is crucial because these external factors can be used to tune and control nanoscale devices with quantum dots. The second harmonic generation was first reported experimentally by [10]. Since then, there were a plethora of simulation studies on these properties including different structures [5, 11, 12], and different potentials such as parabolic [14], semi-parabolic [13]. To the best of our knowledge, the work done on the study of non-linear optical properties, particularly for finite square well potential was not sufficient. The effect of an external electric field, pressure and temperature on optical rectification coefficient (ORC), Absorption coefficient (AC) and Refractive Index (RI) are discussed in 1D. The band gaps of semiconductor materials can also be determined by the material's composition. The energy band of ternary semiconductors, for example, is determined by the composition of one of the elements in the compound. $Al_xGa_{1-x}N$ is one of the well-established materials used for UV light emitters and detectors [15] because of its wide band gap, which may span a wide range of wavelengths in this region. These material's band structures are also affected by temperature and pressure. These variables have a significant impact on the fundamental properties of these materials including the optoelectronic properties. Many semiconductor devices, such as QLEDs, Lasers, and white light sources, can benefit from the application of these external influences, which can improve the band structures of the material and, hence, boost efficiency [8]. The study starts with an overview of the methods used to run the simulations and compute the nonlinear features, as well as the

state's wave functions and energy values. This section is followed by the problem's theoretical formulation. Following that, we present the findings and discuss them in the next section.

5.2 Theory and Method

This work considers the quantum dot system of $Ga_xAl_{1-x}As/GaAs$. A 3D quantum well is created by sandwiching a nano cube of GaAs in a sea of $Ga_xAl_{1-x}As/GaAs$. It is formed as a result of GaAs having a lower barrier potential than the surrounding material, which in our case is $Ga_xAl_{1-x}As$. When an external electric field is applied to a quantum dot system, the electron's energy tends to decrease. As a result, the allowed frequency of the light absorption or emission decreases. Correspondingly, drastic changes in nonlinear optical properties such as coefficient of absorptions and refractive index occur. Figure 5.1 (b) depicts the effect of the external electric field [16], $E = -eFx$. The potential level tilts by a slope of $-eF$ in its application, where e is the charge of the electron.

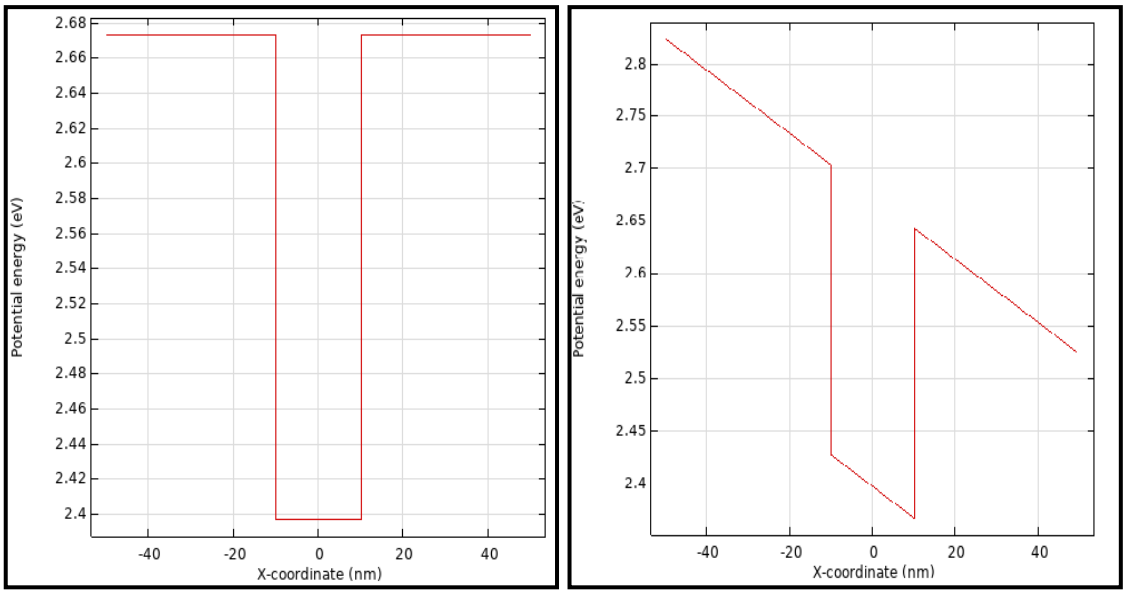

Figure 5.1: *(a) Potential well of the system with the effect of a linearly varying external electric field: no electric field is applied; (b) the application of the electric field*

5.2.1 Schrodinger equation for the system

Equation (5.1) gives the Schrodinger equation for the same system (considering only one dimension) in the presence of external electric field F for a single electron.

$$-\frac{\hbar^2}{2m_e^*}\frac{\partial^2\psi}{\partial x^2}+(V_0-eFx)\psi=E\psi \tag{5.1}$$

Where,

$$V_0=\begin{cases}V_{GaAs}, & -10nm\le x\le 10nm;\\ V_{Ga_xAl_{1-x}As}, & elsewhere.\end{cases} \tag{5.2}$$

The effective mass of the electron is denoted by m_e^*. The pressure and temperature dependent effective electron mass has been calculated using the temperature and pressure dependent relation [17] for the GaAs region. It is expressed as:

$$m_e^*(P,T)=m_o[1+\frac{7510}{E_g(P,T)+341}+\frac{15020}{E_g(P,T)}]^{-1} \tag{5.3}$$

The mass of the electron was calculated using eq. (5.4) for the region outside GaAs, which is the region of $Ga_xAl_{1-x}As$. The expression is a function of the fraction of Gallium mass in the semiconductor and the electron rest mass me [18]. For our investigation, the value of x has been set to zero.

$$m_e^*=(0.067+0.083(1-x))m_e \tag{5.4}$$

Similarly, the energy band gap for GaAs & $Ga_xAl_{1-x}As$ was calculated using the pressure and temperature dependence relation [19] given in eq. (5.5).

$$E_g(P,T) = [1519 - \frac{0.5405T^2}{T+204} + 0.01261P + 3.77\times10^{-5}P^2] \quad (5.5a)$$

& $$E_g = (1.426 + 1.247(1-x))eV \quad (5.5b)$$

Equation (5.1) is a special differential equation and its solution comes in the form of Airy functions [20]. The detailed derivation for the analytical solution of eq. 5.1 can be found in [21]. The final form of the solution is expressed in eq. (5.6):

$$V_0 = \begin{cases} A_1 A_i(x) + A_2 B_i(x), & -10nm \le x \le 10nm; \\ B_1 A_i(x) + B_2 B_i(x), & x \le -10nm. \\ C_1 A_i(x) + C_2 B_i(x), & -10nm \le x. \end{cases} \quad (5.6)$$

$A_i(x) \,\&\, B_i(x)$ are the coefficients of the Airy functions. These coefficients are in integral form and henceforth, it becomes difficult to calculate exact solution and other parameter associated in the study. Due to this reason, numerical simulation was used to perform calculations.

5.2.2 Non-linear optical properties

The study takes into account non-linear properties such as change in refractive index and optical rectification coefficient. This study addresses these properties by utilizing a two-level system. The non-linear susceptibility is directly related to the coefficient of change in refractive index and optical rectification coefficient. Consider eq. (5.7) for the effective susceptibility with linear and non-linear terms.

$$\chi_{eff} = \chi^{(1)}E + \chi^{(2)}E^2 + \chi^{(3)}E^3 \quad (5.7)$$

$\chi^{(1)}, \chi^{(2)}$ & $\chi^{(3)}$ are linear, the second order, and the third order susceptibility terms that depend on the frequency of the falling radiation. $\chi^{(2)}$ is made up of two terms: the optical rectification $\chi_0^{(2)}$ and the second harmonic generation $\chi_\omega^{(2)}$

$$\chi_0^{(2)} = 4\frac{e^3\sigma_s}{\varepsilon_0\hbar^2}\mu_{01}^2\delta_{01}\times\frac{\omega_{01}^2(1+\frac{T_1}{T_2})+(\omega^2+\frac{1}{T_2^2})(\frac{T_1}{T_2}-1)}{[(\omega_{01}-\omega)^2+\frac{1}{T_2^2}][(\omega_{01}+\omega)^2+\frac{1}{T_2^2}]} \tag{5.8}$$

$$\chi_\omega^{(2)} = \frac{\sigma}{\varepsilon_0}\frac{M_{12}M_{23}M_{31}}{(\hbar\omega-E_{12}-i\hbar\Gamma_{21})(2\hbar\omega-E_{31}-i\hbar\Gamma_{31})} \tag{5.9}$$

Equations (5.8) and (5.9) were derived by using the density matrix approach [22]. M_{ij} is the dipole transition element. It can be calculated by using the following expression: $M_{fi} = -e\left\langle\psi_f\left|x\right|\psi_i\right\rangle$ where, ψ_i & ψ_j are the initial and the final state wavefunction of the electron. The E_{ij} terms are the transition energy between ith to jth state. Finally, σ, T_1, T_2 & Γ are the electron charge density and relaxation time, respectively.

The change in RI can be given as the sum of linear and non-linear parts as shown in eq. (5.10). The linear part is given by eq. (5.11) and the non-linear term is expressed as eq. (5.12):

$$\frac{\Delta\eta(\omega,\mathrm{I})}{\eta_r} = \frac{\Delta\eta^{(1)}(\omega)}{\eta_r} + \frac{\Delta\eta^{(3,\mathrm{I})}(\omega,\mathrm{I})}{\eta_r} \tag{5.10}$$

$$\frac{\Delta\eta^{(1)}(\omega)}{\eta_r} = \frac{1}{2{\eta_r}^2\varepsilon_0}\left|M_{01}\right|^2\left[\frac{E_{10}-\hbar\omega}{(E_{10}-\hbar\omega)^2+(\hbar\Gamma_0)^2}\right] \tag{5.11}$$

$$\frac{\Delta\eta^{(3,\mathrm{I})}(\omega,\mathrm{I})}{\eta_r} = -\frac{\mu c}{4\eta_r{}^3\varepsilon_0}\left|M_{01}\right|^2\left[\frac{N\mathrm{I}}{[(E_{10}-\hbar\omega)^2+(\hbar\Gamma_0)^2]^2}\right]$$
$$\times\left[4(E_{10}-\hbar\omega)\left|M_{01}\right|^2-\frac{\left|M_{11-}M_{00}\right|^2}{(E_{10})^2+(\hbar\Gamma_0)^2}\{(E_{10}-\hbar\omega)\times[E_{10}(E_{10}-\hbar\omega)-(\hbar\Gamma_0)^2(2E_{10}-\hbar\omega)\}\right] \quad (5.12)$$

5.3 Method

To solve the Schrodinger equation in 1D, we used the finite elements method with the help of COMSOL Multiphysics. In the regions of different materials and at the boundary, suitable conditions such as mass approximation and zero probability conditions were used. The wavefunction and the eigenenergy values for eq. (5.1) are shown in fig. 5.2. The thickness of the GaAs is set at 20 nm, with values ranging from 10 to −10 nm. Using the finite element method, the numerical values of the wavefunctions were used to calculate the transition dipole matrix element. MATLAB simulation software was used to perform this calculation.

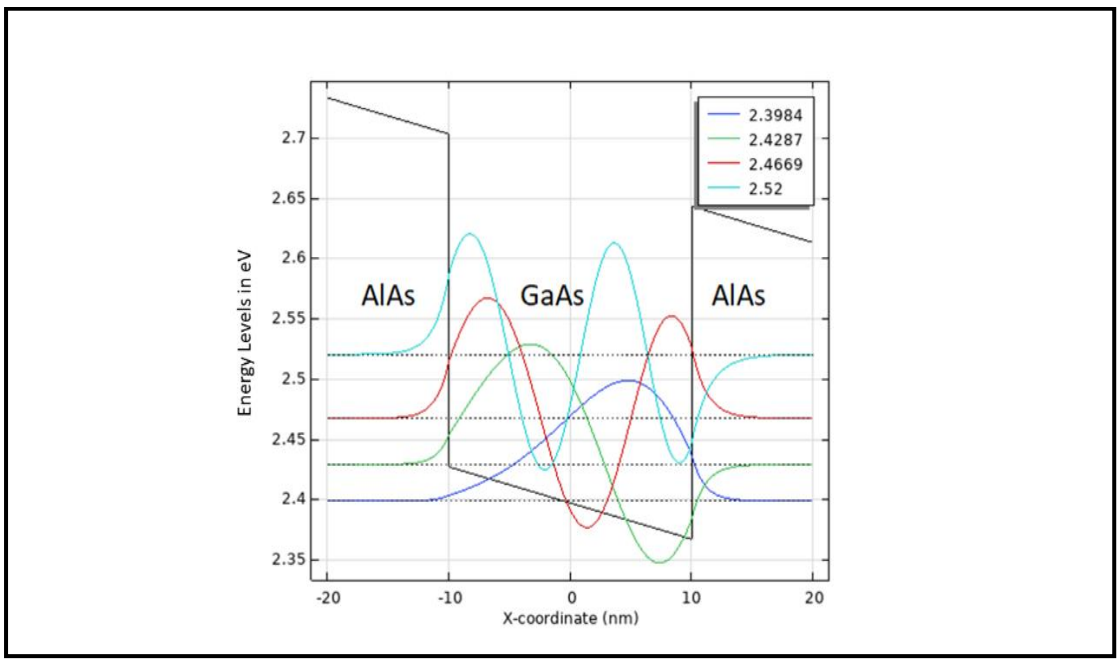

Figure 5.2: *Wavefunction of electron till 4th level. Here the y-axis shows the energy levels of the wave function*

5.4 Results and Discussion

This section presents the results of the simulations for varying electric fields, hydrostatic pressure and temperature at a fixed interval of 5k V/cm. **Table 5.1**, displays the list of fixed parameters as well as the values used to run the simulation. The values for relaxation time are as follows: $\Gamma_{31} = \Gamma_{21}/2$. The transition dipole matrix elements were calculated using the numerical wavefunctions obtained from the simulation. The matrix is important because all of the simulation results are related to its elements.

Table 5.1: *Table for parameters and values*

Parameters	Values
Electron Charge Density (σ)	$2.8\times10^{-22}m^{-3}$
Incident Intensity (I)	$4\times10^{6}Wm^{-2}$
Relative Refractive Index ((η_r)	3.2
Relaxation Time (Γ_{21})	$0.5ps^{-1}$

Optical Rectification Coefficient (ORC), with the variation of the electric field in the interval of 25 kV/cm keeping temperature and pressure constant at 50 K and 100 kbar, respectively, for the system under consideration, is depicted in fig. 5.3(a). Figure 5.3(b) demonstrates energy eigenvalues for different values of the external electric field F. It can be observed from the figure that while increasing the electric field strength, magnitude of ORC decreases and a shifting towards higher frequencies exhibiting a blue shift is observed. As we can observe from fig. 5.3(b) the increasing electric field strength leads to the increase of the energy eigenvalue, hence, an increase in the electric field leads to a increase of the difference between energy levels leading to the blue shift.

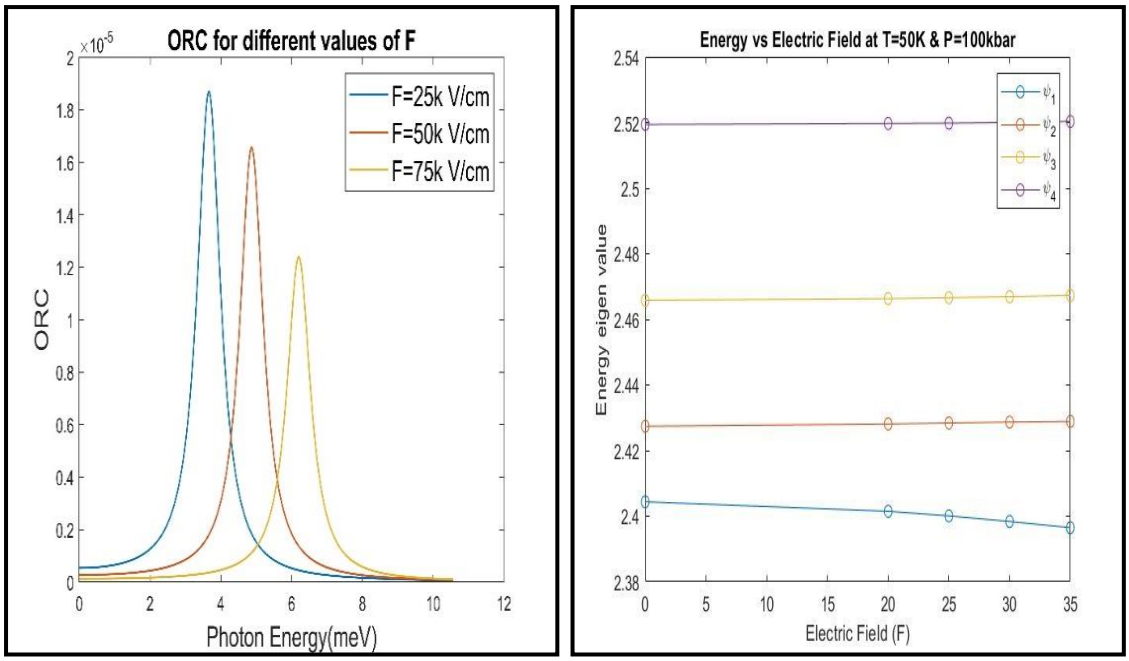

Figure 5.3: *(a) ORC for different values of electric field strength keeping temperature and hydrostatic pressure constant. (b) Energy eigenvalue vs electric field strength*

Figure 5.4.(a) shows a plot of ORC vs temperature at three diverse values fixing P = 50 kbar, electric field strength = 25 kV/cm. A blue shift is observed with an increase in the temperature as the resonant peaks move towards higher energy domain with a significant decrease in the peak height. As the transition energy goes to increase with the increase in temperature, the blue shift happens. Also, with an increase in temperature, a decrease in the effective radius of the quantum dot is observed due to an enhancement in the effective electron mass as well an increase in energy interval is observed with an increase in the temperature.

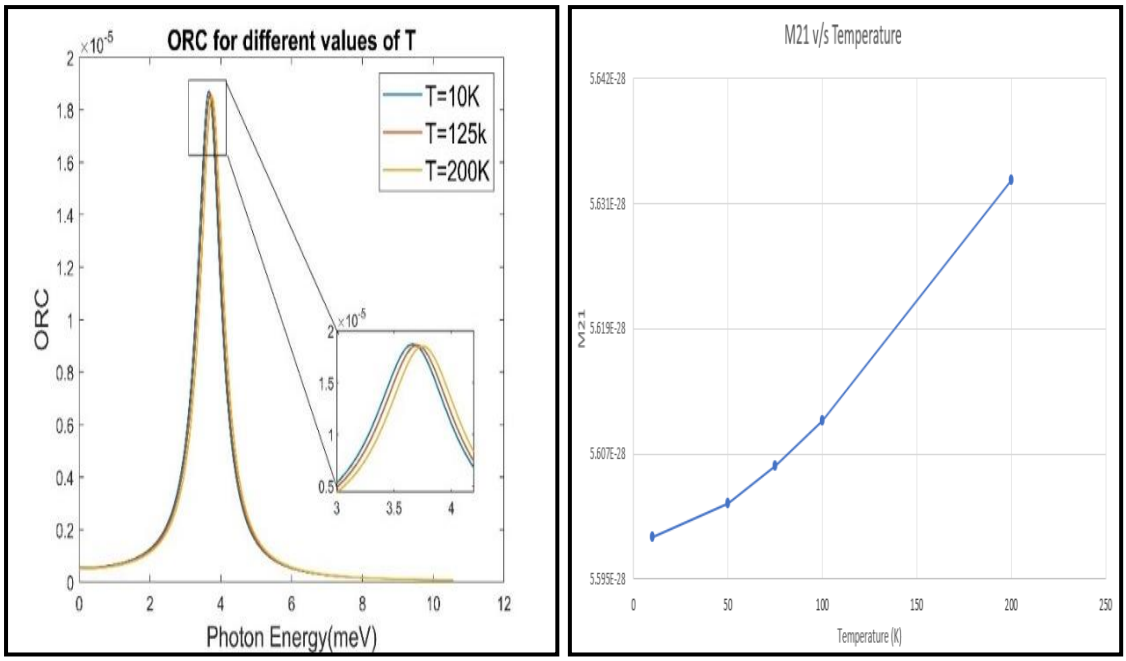

Figure 5.4: *(a) ORC for diverse values of temperature keeping the strength of the field and hydrostatic pressure constant. (b) matrix element vs temperature*

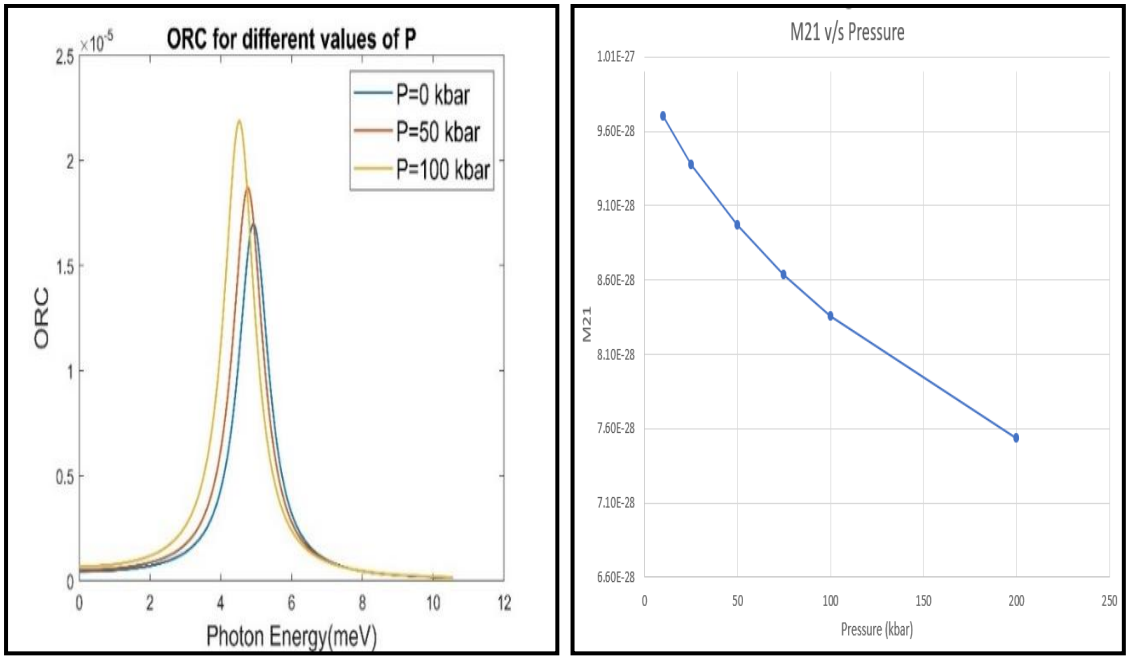

Figure 5.5: *(a) ORC for various values of hydrostatic pressure while maintaining constant electric field and temperature. (b) dipole transition M21 vs pressure*

Figure 5.5.(a) shows a plot of ORC vs pressure at three different values fixing T = 50 K, the electric field strength equals to 25 kV/cm. It is observed that with an increase in the

hydrostatic pressure the red shift is observed with the movement of resonant peaks towards higher energy domain with a substantial increase in the peak heights. This is due to the weakness of the quantum confinement with the decrease in the energy interval with a rise in hydrostatic pressure.

In fig. 5.6.(a), the refractive index for various values of the field strength keeping the temperature and the pressure constant was plotted. The 1st order linear refractive index, as well as the total refractive index, show the same behavior with an increase in the electric field, as seen in the figs. 5.6.(a) & 5.6.(b), while the 3rd order non-linear term has no effect on the total refractive index due to its minimal contribution. It is observed that the magnitude of peaks is decreasing with an increase in the electric field while going towards a high energy state resulting in the blue shift.

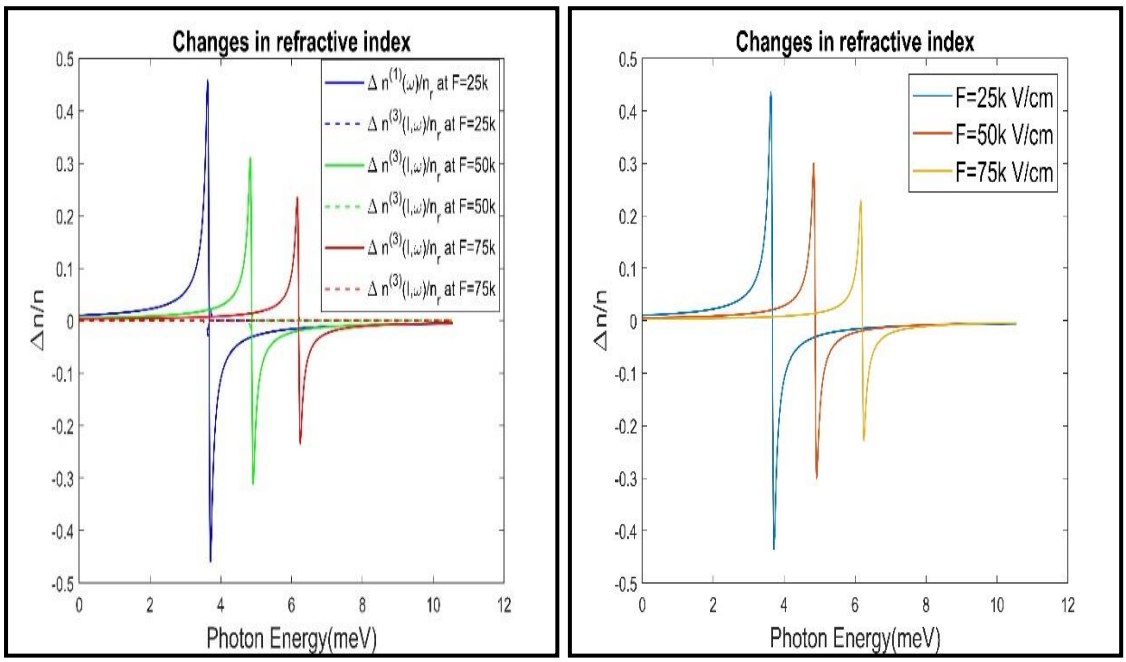

Figure 5.6: *(a) 1st and 3rd order refractive index for various values of electric field keeping temperature and pressure constant. (b) Total refractive index for various values of strength of the electric field keeping Temperature and Hydrostatic Pressure constant*

In Fig. 5.7.(a), the refractive index for various values of the temperature keeping the strength of the field & the hydrostatic pressure as constant, is plotted. It can be observed from fig. 5.7.(b) that the 1st order linear refractive index, as well as the total refractive index displays a quite similar behavior as we increase temperature but there is no noticeable change can be observed in the 3rd order non-linear term. Hence, here contribution from 1st order linear term and the total refractive index changes is taken into account due to neglecting the low contribution from the 3rd order non-linear term. A blue shift can be observed from the graphs as the peaks are moving towards a higher energy region with a significant increase in the peak height.

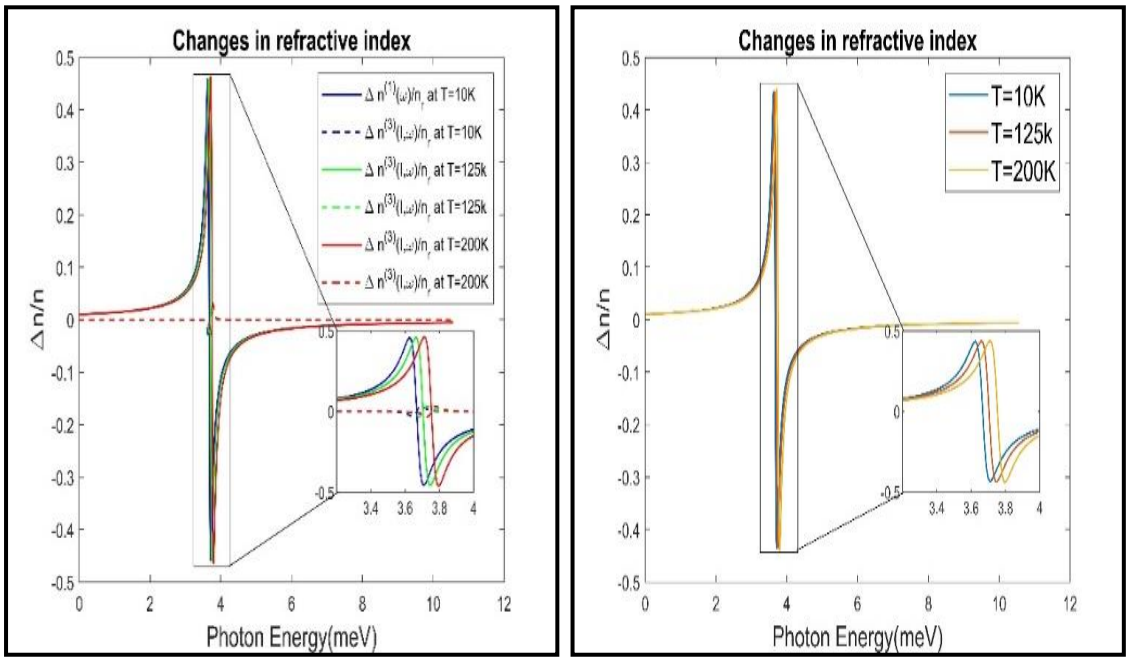

Figure 5.7: *(a) The 1st and the 3rd order refractive index for various temperature while maintaining the electric field and the hydrostatic pressure constant (b) The total refractive index at various temperature while the strength of the field and the hydrostatic pressure are held constant*

In fig. 5.8.(a), the refractive index was plotted for various values of the hydrostatic pressure while maintaining the field strength and the hydrostatic pressure as a constant. For figs. 5.8.(a, b) results are quite similar in behavior for both of the 1st order linear

refractive index as well as the total refractive index with a significant increase in the hydrostatic pressure without showing any alteration in the 3rd order non-linear term. Hence, we observe that the 1st order linear refractive index and the total refractive index are similar in magnitude as well as they exhibit the red shift with an increase in the magnitude of the peak's intensity.

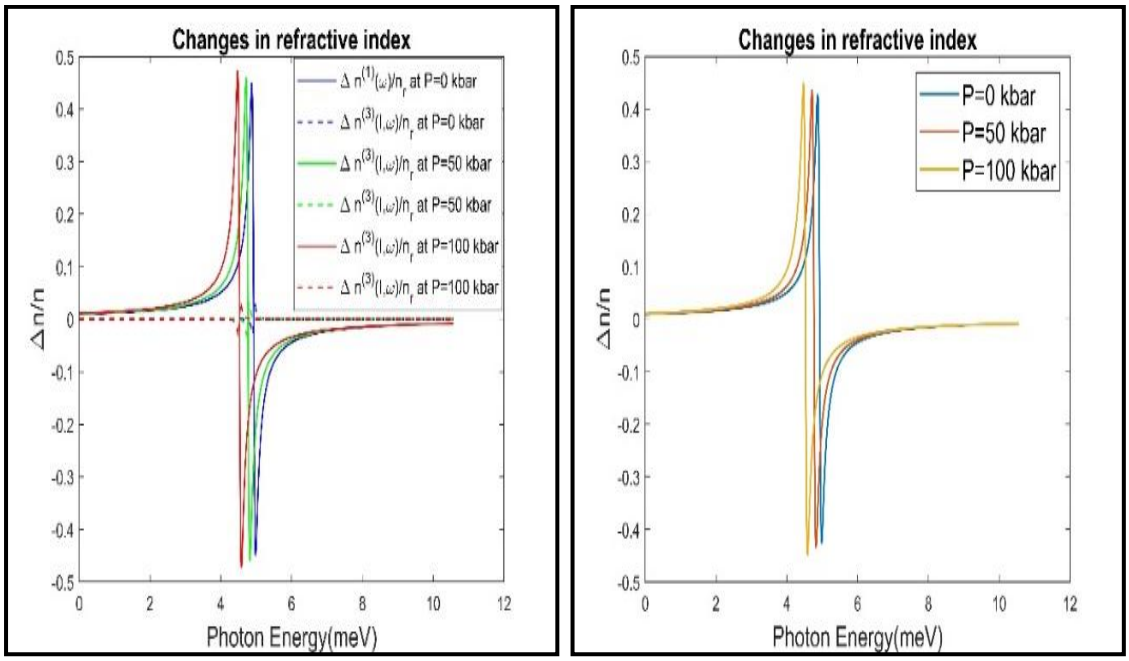

Figure 5.8: *(a) The 1st and the 3rd order refractive index for various hydrostatic pressure strengths while maintaining the electric field and the temperature constant (b) Total refractive index for various Hydrostatic pressure strengths while keeping the electric field and temperature constant*

5.5 Conclusions

In the present chapter, we reported the variation of optical properties such as optical rectification coefficient and refractive index (first order linear & third order nonlinear) as a function of the external applied electric field, hydrostatic pressure and temperature. The results display that increasing the field strength causes a red shift in all of the studied optical properties as well as a surge can be noticed in the peak's intensity with

an increase in the electric field. Furthermore, the simulation outcomes display that the rise in temperature causes a blue shift in the studied optical properties while a redshift can be observed while increasing the hydrostatic pressure. As a result, the hydrostatic pressure **P**, temperature **T**, and applied electric field **E** all are observe to have a significant impact on the system's optical response.

References

[1] Aderras L., et al. Stark-shift of impurity fundamental state in a lens shaped quantum dot. Physica E: Low-dimensional Systems and Nanostructures, 2017, 89, P. 119–123.

[2] Temkin H., et al. GexSi1−x strained-layer heterostructure bipolar transistors. Applied Physics Letters, 1988, 52 (13), P. 1089–1091.

[3] Luryi S., Kastalsky A., Bean J.C. New infrared detector on a silicon chip. IEEE Transactions on Electron Devices, 1984, 31 (9), P. 1135–1139.

[4] Rhee S.S., et al. Resonant tunneling through a Si/GexSi1−x/Si heterostructure on a GeSi buffer layer. Applied Physics Letters, 1988, 53 (3), P. 204–206.

[5] Mohamed Kria Varsha, et al. Quantum Confined Stark Effect on the Linear and Non-linear Optical Properties of SiGe/Si Semi Oblate and Prolate Quantum Dots Grown in Si Wetting Layer. Nanomaterials, 2021, 11 (6).

[6] Mourad Baira, et al. Intersubband optical nonlinearity of GeSn quantum dots under vertical electric field. Micromachines, 2019, 10 (4), 243.

[7] Dvoyan K.G., Kazaryan E.M. Impurity states in a weakly prolate (oblate) ellipsoidal microcrystal placed in a magnetic field. Physica Status Solidi B, 2001, 228 (3), P. 695–703.

[8] Suman Dahiya, Siddhartha Lahon, Rinku Sharma. Effects of temperature and hydrostatic pressure on the optical rectification associated with the excitonic system in a semi-parabolic quantum dot. Physica E: Low-dimensional Systems and Nanostructures, 2020, 118, 113918.

[9] Amal Abu Alia, Mohammad K. Elsaid, Ayham Shaer. Magnetic properties of GaAs parabolic quantum dot in the presence of donor impurity under the influence of external tilted electric and magnetic fields. J. of Taibah University for Science, 2019, 13 (1), P. 687–695.

[10] Franken P.A., et al. Generation of optical harmonics. Physical Review Letters, 1961, 7 (4), 118.

[11] Keyin Li, Kangxian Guo, Litao Liang. Effect of the shape of quantum dots on the refractive index changes. Physica B: Condensed Matter, 2016, 502, P. 146–150.

[12] Khaledi-Nasab A., et al. Optical rectification and second harmonic generation on quasi-realistic InAs/GaAs quantum dots: with attention to wetting layer effect. Int. Scholarly Research Notices, 2013 (2013).

[13] Jin-Feng You, et al. The effect of temperature, hydrostatic pressure and magnetic field on the nonlinear optical properties of AlGaAs/GaAs semiparabolic quantum well. Int. J. of Modern Physics B, 2019, 33 (27), 1950325.

[14] Yuan Lihua, et al. Effect of a magnetic field on the energy levels of donor impurities in the ZnO parabolic quantum well. J. of Semiconductors, 2011, 32 (8), 082001.

[15] Gil B. Group III nitride semiconductor compounds: physics and applications. Clarendon Press, 1998.

[16] Empedocles S.A., Bawendi M.G. Quantum-confined Stark effect in single CdSe nanocrystallite quantum dots. Science, 1997, 278 (5346), P. 2114– 2117.

[17] Zaiping Zeng, et al. Competition effects of electric and magnetic fields on impurity binding energy in a disc-shaped quantum dot in the presence of pressure and temperature. Science of Advanced Materials, 2014, 6 (3), P. 586–591.

[18] Harrison P., Valavanis A. Quantum wells, wires and dots: theoretical and computational physics of semiconductor nanostructures. John Wiley and Sons, 2016.

[19] Aghoutane N., et al., Refractive index changes and optical absorption involving 1s1p excitonic transitions in quantum dot under pressure and temperature effects. Applied Physics A, 2019, 125 (1).

[20] Vallee O., Soares M. Airy functions and applications to physics. World Scientific Publishing Company, Singapore, 2010.

[21] Ghatak A.K., Goyal I.C., Gallawa R.L. Mean lifetime calculations of quantum well structures: a rigorous analysis. IEEE J. of Quantum Electronics, 1990, 26 (2), P. 305–310.

[22] Boyd R.W. Nonlinear optics. Academic press, NY, 2020.

[23] Rezaei G., Karimi M.J., Keshavarz A. Excitonic effects on the nonlinear intersub-band optical properties of a semi-parabolic one-dimensional quantum dot. Physica E: Low-dimensional Systems and Nanostructures 43 (1) (2010), pp. 475–481.

CHAPTER 6
SUMMARY AND SCOPE OF FUTURE WORK

6.1 Summary & Important findings of the research work

Now a days, quantum nanostructures, such as quantum wells, quantum wires, and quantum dots, have emerged as a new class of nonlinear materials for studying multi-photon phenomenon as well as nonlinear optical properties, and possess some unique potential applications in optoelectronic devices including optical switches, THz multi-photon quantum well infrared photodetectors, multi-photon bioimaging, and frequency up conversion, among others [1-5]. Moreover, there has been a shift in semiconductor physics towards exploring effect of external factors such as hydrostatic pressure, temperature, electric field, magnetic field as well as spin-dependent phenomena [6-12] as they offer vast potential applications in spin transistors, spin filters, and quantum computing. The study of spin-related effects in semiconductor nanostructures typically involves considering spin-orbit interaction. Understanding effect of such external factors is crucial for investigating its impact on nonlinear optical processes in quantum nanostructures [13-18].

This thesis focuses on studying the linear and nonlinear optical properties of quantum nanostructures in the presence of external factors such as hydrostatic pressure, temperature, electric and magnetic fields, as well as considering the Rashba spin-orbit interaction [19-24]. Nonlinear processes require high laser intensities, necessitating the use of non-perturbative methods for their study.

The principal objective of the present thesis is to explore the interaction between electrons-hole correlation and linear & non-linear optical properties in Quantum Dots

(QDs) in the presence of hydrostatic pressure & temperature. Additionally, we aim to investigate how the third harmonic generation in QDs changes with variations in the Rashba SOI factor, magnetic field, hydrostatic pressure & temperature. We also investigated the behavior of the optical rectification coefficient & optical absorption coefficient in quantum well in the presence of electric field, hydrostatic pressure & temperature. Understanding the optical response in the presence of external perturbations in QD & QW is not only fascinating but also holds significant potential for various applications such as quantum dot lasers, quantum information processing, photodetectors, and opto-spintronics devices [25-26].

To investigate this dynamic problem involving the interplay of different external perturbations, such as the effect of electric field, magnetic fields, hydrostatic pressure & temperature and Rashba SOI in QDs & QW, we employed the powerful effective mass approximation & Density matrix theory for enhanced accuracy. These theories established a connection between the solution of the Schrödinger equation, considering a periodic Hamiltonian, and the solution of another equation with a time-independent Hamiltonian represented by an infinite matrix known as the Density matrix. This method, which has been successfully applied to various atomic systems and nanostructures in previous studies [26-36], offers the distinct advantage of simultaneously addressing discrete and continuous states within a single system.

Chapter 1 provides a brief introduction to nanostructures, spin-orbit interaction, linear & nonlinear properties, external perturbations and multiphoton processes. QW (quantum well) and QD (quantum dots) nanostructures along with their respective characteristics & unique properties, as well as a brief discussion about the material

taken and highlights of their exceptional properties are briefly described in chapter 1. Rashba spin-orbit interaction and other external factors such as electric field, magnetic field, hydrostatic pressure, temperature is also discoursed in this chapter.

Firstly, the chapter discusses specific types of low-dimensional semiconductor structures, including quantum dots, quantum well. Each structure is defined and explained, highlighting their unique properties and characteristics. Then the chapter discusses about the compound semiconductor explicitly about III-V semiconductors. Properties and applications of GaAs, InGaAs & AlGaAs are also discussed in this chapter.

The effects of external perturbations such as hydrostatic pressure, temperature, electric field, magnetic field & Rashba SOI on the behavior of low-dimensional semiconductors are also explained in the chapter. External perturbations can significantly impact the optical and electronic properties of these systems. Hence, understanding of these effects becomes crucial for studying the behavior of the system and their potential applications.

The chapter then delves into the methods and approximations that have been used to solve the Hamiltonian as well to find out the eigenvalues & eigen energies of the system, which describes the behavior of particles in these systems. These approximations play a vital role in streamlining the complex calculations involved in studying the low-dimensional systems.

Furthermore, the introduction section of Chapter I provides definitions and explanations of various optical properties and nonlinear optical properties. Optical properties refer to the behavior of materials when interacting with light, such as absorption, reflection, and transmission. Nonlinear optical properties, on the other hand, describe the response of

materials to intense light, where the relationship between the input and output light is nonlinear.

Overall, **Chapter I** serves as an overview, setting the foundation for the subsequent chapters by introducing the key concepts, structures, and properties associated with low-dimensional semiconductors and their optical behavior.

In **Chapter 2**, we investigate the optical rectification coefficient of a GaAs quantum dots under the influence of radius, hydrostatic pressure & temperature for an excitonic system. A detailed discussion about the mathematics to find out the eigenvalues and eigen-energies using density matrix approach under effective mass approximation is presented in chapter 2. Our findings indicate that an increase in the radius, hydrostatic pressure & Temperature as well as excitons strongly play role in affecting the peak position as well as blue/red shift is observed in optical rectification coefficient. The results are presented as functions of incident photon energy for different parameter values. Our findings reveal that the hydrostatic pressure causes a red shift in the ORC (optical rectification coefficient) peaks, while the temperature shift these peaks towards the blue end of the spectrum. Furthermore, an increase in the quantum dot radius is found to induce a red shift in the peaks.

Chapter 3 of the study focuses on investigating the THG (third harmonic generation) coefficients of $In_xGa_{1-x}As$ quantum dots in the presence of THz laser fields with Rashba spin-orbit interaction, under the influence of a magnetic field. The authors employ the variational procedure within the effective mass approximation to determine the energy levels and wave functions.

The study discloses that the third harmonic generation coefficients depend on several factors, such as confining potential, magnetic field strength, Rashba SOI strength, and photon energy. The results demonstrate that increase in Rashba spin-orbit interaction coefficient has a strong influence in shifting the peak positions of THZ. Additionally, it is also observed that the THZ coefficient is significantly enhanced by increasing/ decreasing the magnetic field or the confinement potential.

The authors emphasize that by adjusting the Rashba spin-orbit coupling factor and THz laser parameters, the average spin flip transition probability and multiphoton spin flip transitions can be enhanced. This feature makes them valuable for optical control in spintronics, indicating potential applications in spin photodetectors and ultra-sensitive spintronic devices.

The study also uncovers interesting features such as dynamic Stark shift, power broadening, and hole burning on the breaking of excited level degeneracy as the electric and magnetic field strengths vary. The enhancement and power broadening observed in excited state probabilities due to increased external fields are directly linked to the emission spectra of quantum dots. These findings suggest potential applications in future bioimaging devices, utilizing the emission spectra of quantum dots.

Overall, **Chapter 3** provides a detailed investigation of the third harmonic generation coefficients in $In_xGa_{1-x}As$ quantum dots under the influence of THz laser fields with Rashba spin-orbit interaction and a magnetic field. The results highlight the importance of various parameters in controlling the spin dynamics and optical properties of quantum dots, paving the way for potential advancements in spintronics and bioimaging devices.

Chapter 4 of the study emphases on the investigation of the linear and nonlinear absorption coefficients, as well as the change in refractive index associated with inter subband transitions in a semi-harmonic potential spherical excitonic GaAs quantum dot (QD). Additionally, a detailed comparison for obtained theoretical results with experimental data have been done in this chapter.

The density matrix formalism employed to obtain the linear and nonlinear optical properties of the quantum dots is discussed in the beginning of the chapter. This formalism allows for a detailed analysis of the effects of various parameters on the optical behaviour of the QD.

The study investigates the linear and nonlinear absorption coefficients, as well as the refractive index change, under the influence of external hydrostatic pressure and temperature. Additionally, the influence of the excitons is also investigated, and a comparison is made between cases with and without excitonic effects. A detailed comparison between theoretical and experimental absorption coefficient is also discussed in this chapter.

The results are presented as functions of the incident photon energy for different temperature & hydrostatic pressure values. The findings disclose that an increase in hydrostatic pressure leads to a red shift in the absorption peaks, both for linear and third-order processes. On the other hand, temperature causes a shift of these peaks towards the blue end of the spectrum. Similar effects are observed in the dispersion regions of the refractive index change.

In summary, **Chapter 4** provides a detailed analysis of the linear and nonlinear absorption coefficients, as well as the refractive index change, in a GaAs excitonic

quantum dot under the influence of hydrostatic pressure and temperature. The results highlight the effects of these external parameters on the optical properties of the quantum dot and provide valuable insights into the behaviour of inter subband transitions.

Chapter 5 delves into the investigation of the effect of transverse electric field, hydrostatic pressure & temperature on a quantum well with finite square well potential. We focus on determining the nonlinear optical rectification as well as nonlinear refractive index changes for a finite well. Our findings reveal that the transverse electric field as well as temperature blue shifts the peaks of the optical rectification coefficient as well as nonlinear refractive index changes, while hydrostatic pressure shift these peaks towards the red end of the spectrum. These findings suggest the potential to control the electronic and optical properties.

In conclusion, this study is expected to stimulate both experimental and theoretical investigations, contributing significantly to the understanding of nonlinear optical properties in nanostructures with spin-orbit interaction. By investigating the influence of factors such as electric field, magnetic field, hydrostatic pressure & temperature and Rashba Spin Orbit interactions, the thesis explores the possibility of tuning the effective band gap and other material properties in the studied system. This tunability is particularly relevant for optical applications in devices utilizing narrow-bandgap semiconductors.

The obtained results are expected to be highly beneficial for advancing optical applications in narrow-bandgap semiconductor devices. Furthermore, the outcomes of this research are anticipated to inspire further experimental studies in this field in the near future.

6.2 Future scope of the work

- Study of Effect of impurity with hydrostatic pressure, temperature and electric field on the optical properties of Quantum Dot with SOI.
- Study of Effect of impurity with hydrostatic pressure, temperature and magnetic field on the optical properties of Quantum Dot with SOI.
- Electric field, Hydrostatic pressure, Temperature & impurity effect on SHG and linear and non-linear optical properties in 1-D QD under infinite square well potential.
- Impurity, Electric field, Hydrostatic pressure & Temperature effect on THG in 1-D QD under infinite square well potential.

References

[1] G. A. Prinz, Science, 282 (1998) 1660.

[2] Supriyo Bandyopadhyay, Physics of Nanostructured Solid State Devices, Springer (2012).

[3] E. U. Rafailov, M. A. Cataluna, and W. Sibbett, Nat. Photonics, 1 (2007) 395.

[4] J. Berezovsky, M. H. Mikkelsen, N. G. Stoltz, L. A. Coldren, and D. D. Awschalom, Science, 320 (2008) 349.

[5] K. Hennessy, A. Badolato, M. Winger, D. Gerace, M. Atature, S. Gulde, S. Falt, E. L. Hu, and A. Imamoglu, Nature, 445 (2007) 896.

[6] E. I. Rashba, Sov. Phys. Solid State, 2 (1960) 1109.

[7] Yu. A. Bychkov and E. I. Rashba, JETP Lett., 39 (1984) 78.

[8] J. Knobbe and Th. Schapers, Phys. Rev. B, 71 (2005) 35311.

[9] Jaroslav Fabian, Alex Matos-Abiague, Christian Ertler, Peter Stano, Igor Zutic, Acta Physica Slovaca, 57 (2007) 565.

[10] J. H. Jiang, M. Q. Weng, and M. W. Wu, J. Appl. Phys., 100 (2006) 063709.

[11] W. H. Kuan, C. S. Tang, and W. Xu, J. Appl. Phys., 95 (2004) 6368.

[12] Takaaki Koga, Junsaku Nitta, and Hideaki Takayanagi, Phys. Rev. Lett., 88 (2002) 126601.

[13] R. Khordad, Opt. Quant. Electron., 46 (2014) 283.

[14] R. Khordad, H. Bahramiyan, Pramana - J. Phys., 88 (2017) 50.

[15] S. Banerjee and D. Charkavorty, J. Mater. Sci., 37 (2002) 4261.

[16] Siddhartha Lahon, P.K. Jha, and Man Mohan, J. Appl. Phys., 109 (2011) 054311.

[17] P P. Saini, A. Boda, A. Chatterjee, J. Mag. Mag. Mat., 485 (2019) 407.

[18] Elcivan dos Santos, H.O. Frota and Angsula Ghosh, Solid State Communications, 323 (2021) 11416.

[19] I Rani, R., Kumar, V., Bhardwaj and S.B. et al., Indian J Phys, 94 (2020) 1705.

[20] Mikhail I.F.I., Ismail I.M.M. & El Shafee M.M., Eur. Phys. J. Plus, 137 (2022) 610.

[21] A. Manchon, H.C. Koo, J. Nitta, S.M. Frolov, R.A. Duine, Nat. Mater., 14 (2015) 871.

[22] S. Datta, B. Das, Appl. Phys. Lett., 56 (1990) 665.

[23] S Sargolzaeipor, H Hassanabadi and W S Chung, Mod. Phys. Lett. A, 34 (2019) 1950023.

[24] G. Dresselhaus, Phys. Rev., 100 (1955) 580.

[25] Gülveren, B., J. Korean Phys. Soc., 73 (2018) 1612.

[26] J. Fabian, A. Matos-Abiague, C. Ertler, P. Stano, I. Zutic, Acta Phys. Slovaca, 57 (2007) 566.

[27] J.H. Jiang, M.Q. Weng, M.W. Wu, J. Appl. Phys. 100 (2006) 063709.

[28] W.H. Kuan, C.S. Tang, W. Xu, J. Appl. Phys. 95 (2004) 6368.

[29] M. Kumar, S. Lahon, P. Kumar Jha, M. Mohan, Phys. Status Solidi B 250 (2013) 1585.

[30] Huguet A., Wrześniewski K. and Weymann I., Sci Rep 13 (2023) 17279.

[31] M.E. Mora-Ramos, C.A. Duque, E. Kasapoglu, H. Sari, I. Sökmen, Journal of Luminescence 132 (2012) 901.

[32] Bhattacharyya, K., Debnath, D. and Chatterjee A., Sci Rep 13 (2023) 5500.

[33] R. Khordad, B. Mirhosseini, Optics Communications, 285 (2012) 1233.

[34] İbrahim Karabulut and Sotirios Baskoutas, J. Appl. Phys., 103 (2008) 073512.

[35] Xin-Jun Ma, Wei Zhang, Shuang Han, Xianglian, Pei-Fang Li, Cui-Lan Zhao, Zhao-Hua Ding, Yong Sun, Jing-Lin Xiao, Physica E: Low-dimensional Systems and Nanostructures, 144 (2022) 115387.

[36] Mikhail I.F.I., Ismail I.M.M. and El Shafee, Indian J Phys, 96 (2022) 2717.

REPRINTS OF THE PUBLISHED PAPERS

Physica E 118 (2020) 113918

Contents lists available at ScienceDirect

Physica E: Low-dimensional Systems and Nanostructures

journal homepage: http://www.elsevier.com/locate/physe

Effects of temperature and hydrostatic pressure on the optical rectification associated with the excitonic system in a semi-parabolic quantum dot

Suman Dahiya [a], Siddhartha Lahon [b,*], Rinku Sharma [a]

[a] Department of Applied Physics, Delhi Technological University, Delhi, 110042, India
[b] Physics Department, Kirori Mal College, University of Delhi, Delhi, 110007, India

A B S T R A C T

The optical rectification for a GaAs quantum dot with an excitonic system is investigated for the various applied hydrostatic pressure, ambient temperature, and different effective size. The dependence of Optical Rectification Coefficient (ORC) on the temperature, radius and hydrostatic pressure in the strong confinement regime for both excitonic as well as without excitonic effects has been studied. This work demonstrates the intricate dependence of ORC on electron-hole pair localization, temperature change, alteration in radius and variation in hydrostatic pressure.

1. Introduction

In the past two decades, there have been speedy developments in the field of nanoscience and nanotechnology. Hence the detailed study of all the aspects of the low-dimensional semiconductor nanostructures becomes imperative. These nanostructures, namely, quantum dots (QDs), quantum wires and quantum wells exhibit unique electronic and optical properties, contrasting to macroscopic structures [1–4]. Because of these standalone properties, scientists have shown great interest in nanostructures, as they offer a wide area of research to understand them as well as the associated physics [5–7]. Charge carriers in various nanostructures are confined to one, two, and three dimensions in accordance with their structural dimensions. Out of these three classes, the class of zero-dimensional structures, also called as QDs, in which charge carriers are constrained in all the 3-dimensions, is the most extensively studied class of semiconductor structures. This quantum constriction of charge carriers leads to the peculiar changes such as discrete energy levels generation, increase in the density of states at some specific energies and the counter intuitive alteration in the optical absorption spectrum [8–12]. Also, the effect of confinement on the optical and electronic properties strengthens as we move from quantum wells to QDs. A 1D-quantum dot is a nanostructure that can be considered as a small part of a 1D QW bordered by a two-wall potential. In 1D QW, the charge carriers are free to move along the wire whereas in 1D QD, the charge carriers are restricted from moving along the length [13–15].

Linear and nonlinear optical [16–18] properties such as the nonlinear ORC, optical absorption coefficient, and alteration in the refractive index have wide potential applications in optoelectronic and photonic devices such as photo-detectors, far-infrared laser amplifiers, and high-speed electro-optical modulators. Amongst all the nonlinear optical properties, the second-order nonlinear optical property has a vital role to play due to its simplest and the lowermost order nonlinear effect, as well as magnitude, being greater than all the other nonlinearities. Second-harmonic generation (SHG) and ORC are produced due to second-order nonlinear optical interaction of two incident fields with optical media. Xie and Bass et al., in 1962 performed initial work on OR [19,20] whereas Franken et al. reported the very first experimental observation of SHG [21]. The discovery of SHG leads to the beginning of the field of nonlinear optics [22]. As all the incident beams at frequency ω are transformed to frequency 2ω, the role of SHG becomes more efficient [23]. Baskoutas et al. studied the effect of exciton in OR for the case of semi-parabolic QDs for excitons in semi-parabolic potential [24]. Duque et al. also have investigated the combined effects of hydrostatic pressure, temperature, intense laser field, magnetic field, and applied electric field in the excitonic system [25–29].

Many researchers have studied the interaction effect for the 2nd order nonlinear properties in 1-D semi-parabolic QDs [30–33]. By applying the method of analytical approximation, it is shown that the SHG and OR coefficients are affected by the effect of excitons. With the application of temperature and external hydrostatic pressure, band structure and the semiconductor materials properties can be enhanced, which can be further used in the designing and preparation of a new generation of efficient semiconductor devices like heterostructure lasers, QLEDs, white light sources, etc.

However, only a handful of works are available in the literature which has investigated the effect of excitons to study the nonlinearities

* Corresponding author.
E-mail address: sid.lahon@gmail.com (S. Lahon).

https://doi.org/10.1016/j.physe.2019.113918
Received 30 August 2019; Received in revised form 23 November 2019; Accepted 20 December 2019
Available online 23 December 2019
1386-9477/

of the QDs, quantum wells, or quantum wires. Further, not many studies are performed in this regard while taking the effect of pressure and temperature into consideration. Here we have considered the factors of hydrostatic pressure and temperature into consideration and investigated the ORC in an excitonic semi-parabolic QD. We obtained many interesting results wherein we have shown how external hydrostatic pressure, temperature and excitonic pairing interplay to shift the ORC peaks. We also observe how these parameters change the strength of the ORC peaks. In this paper, a brief introduction is given in Section 1. In Section 2, exciton states are obtained by using the Eigenfunction and Eigen-energies. The numerical results for GaAs semi-parabolic QDs are presented in Section 3. Hence, the study of nonlinearities in QD's by considering only the electron state is not appropriate. Finally, Section 4 draws the conclusions.

2. Theory and model

In the framework of effective mass approximation, for a pair of electron-hole in 1D QDs, Hamiltonian with semi-parabolic confining potential is given by Refs. [13,34]:

$$H_e = \frac{p_h^2}{2m_h^*} + \frac{p_e^2}{2m_e^*} + V(z_e) + V(z_h) - \frac{e^2}{\varepsilon|z_e - z_h|} \tag{1}$$

where (z_e, $z_h > 0$).

Where m_h^* and m_e^* respectively represents an effective mass of hole and electron. The background dielectric constant is given by ε, and the semi-parabolic potential is given by $V(z_l)$ which is written as:

$$V(z_l) = \begin{cases} \frac{1}{2} m_i^* \omega_0^2 z_l^2, \ z_l \geq 0, \\ \infty, \ z_l \leq 0 \ (l = e, h) \end{cases} \tag{2}$$

The effective pressure and temperature variation are associated with the variation of hole and electron effective masses as [35–37]:

$$m_e^*(P,T) = m_o \left[1 + \frac{7510}{E_g(P,T) + 341} + \frac{15020}{E_g(P,T)}\right]^{-1} \tag{3}$$

$$\text{With } E_g(P,T) = \left[1519 - \frac{0.5405T^2}{T + 204} + 10.7P\right] \tag{4}$$

$$\text{And } m_h^*(P,T) = \left(0.09 - 0.20 \times 10^{-3} P - 3.55 \times 10^{-5} T\right) m_0 \tag{5}$$

Here E_g is in meV, P is in "kbar" and T is in "Kelvin."

The Hamiltonian is segmented into two terms considering, the relative motion and center of mass, respectively [37,38]:

$$H_e = H_r + H_c \tag{6}$$

$$\text{Where } H_r = \frac{p^2}{2\mu} + \frac{1}{2}\mu\omega_0^2 z_r^2 - \frac{e^2}{\varepsilon(P,T)|z_r|}, \tag{7}$$

$$\text{And } H_c = \frac{P^2}{2M_T} + \frac{1}{2} M_T \omega_0^2 Z_T^2 \tag{8}$$

$$\text{And for T} < 200\text{K}, \ \varepsilon(P,T) = 12.74 e^{\left(9.4\times10^{-5}\right)(T-75.6)+1.73\times10^{-3}P} \tag{9}$$

And the coordinate of the centre of mass is given by:

$$Z_T = \frac{m_h^* z_h + m_e^* z_e}{M_T} \tag{10}$$

Here, the complete mass is given by $M_T = m_h^* + m_e^*$; the relative coordinate is $z_r = z_e - z_h$, momentum operator is $p = \frac{\hbar}{i}\nabla$, and the reduced mass $\mu_r = m_h^* m_e^* / M_T$.

The exciton wave function and energy levels are obtained as

$$\psi_f(z_h, z_e) = \varphi(z_r)\phi(Z_T), \tag{11}$$

$$E_T = E_{z_r} + E_{Z_T} \tag{12}$$

The term representing the centre of mass part can be considered as the problem for 1D semi-parabolic oscillator where Hamiltonian is given by H_c and Eigen functions & Eigen energies are determined to be [39, 40]:

$$\phi_k(Z_T) = N_k \exp\left(-\frac{1}{2}\alpha^2 {Z_T}^2\right) H_{2k+1}(\alpha Z_T) \tag{13}$$

$$\text{And } E_k = \left(2k + \frac{3}{2}\right)\hbar\omega_0, \ k = (0, 1, 2.....), \tag{14}$$

where 'H' is the Hermite Polynomial,

$$\alpha = \sqrt{M_T \omega(P)/\hbar} \tag{15}$$

$$N_k = \left[\frac{1}{\alpha}\sqrt{\pi} 2^{2k} (2k+1)!\right]^{-1/2} \tag{16}$$

$$\text{With } \omega(P) = \omega_0 \big/ \left[1 - 2P\left(1.16 \times 10^{-3} - 7.4 \times 10^{-4}\right)\right] \tag{17}$$

We analytically obtained the eigenvalues & wave function of the relative motion part in the strong and weak confinement regime. For the strong regime, H_r reduces to:

$$H_{rs} = \frac{p^2}{2\mu} + \frac{1}{2}\mu\omega_0^2 z_r^2 \tag{18}$$

Neglecting the coulomb term as per the strong confinement regime, $\varphi(z_r)$ is determined as:

$$\varphi(z_r) = N_n \exp\left[-\frac{1}{2}\beta^2 {z_r}^2\right] H_{2n+1}(\beta z_r), \tag{19}$$

$$\text{And } E_y = \left(2n + \frac{3}{2}\right)\hbar\omega_0 \ (y = 0, 1, 2, ...), \tag{20}$$

where

$$N_m = \left[\frac{1}{\beta}\sqrt{\pi} 2^{2m} (2m+1)!\right]^{-1/2} \tag{21}$$

$$\beta = \sqrt{\mu\omega(P)/\hbar} \tag{22}$$

Neglecting the confinement term in the weak confinement regime, H_r reduces to:

$$H_{rw} = \frac{p^2}{2\mu} - \frac{e^2}{\varepsilon(P,T)|z_r|} \tag{23}$$

And considering the relative-motion part as 1D hydrogenic type problem, $\varphi(z_r)$ is determined as:

$$\varphi(z_r) = C_x z_r \exp\left[-\frac{\gamma z_r}{x+1}\right] F\left[-z_r, 2, \frac{2\gamma z_r}{x+1}\right], \tag{24}$$

where $\gamma = \frac{\mu e^2}{\varepsilon\hbar^2}$, F is the confluent Hypergeometric function, and C_x is the normalization constant.

$$\text{And } E_x = E_n = -\frac{\mu e^4}{2(n+1)^2 \varepsilon^2 \hbar^2} \tag{25}$$

where.$(n = 0, 1, 2, ...)$

The nonlinear ORC for our 2-level system in 1D semi-parabolic QD is arrived at by applying a density matrix approach wherein perturbation expansions are used. It is given as [14,33–35]:

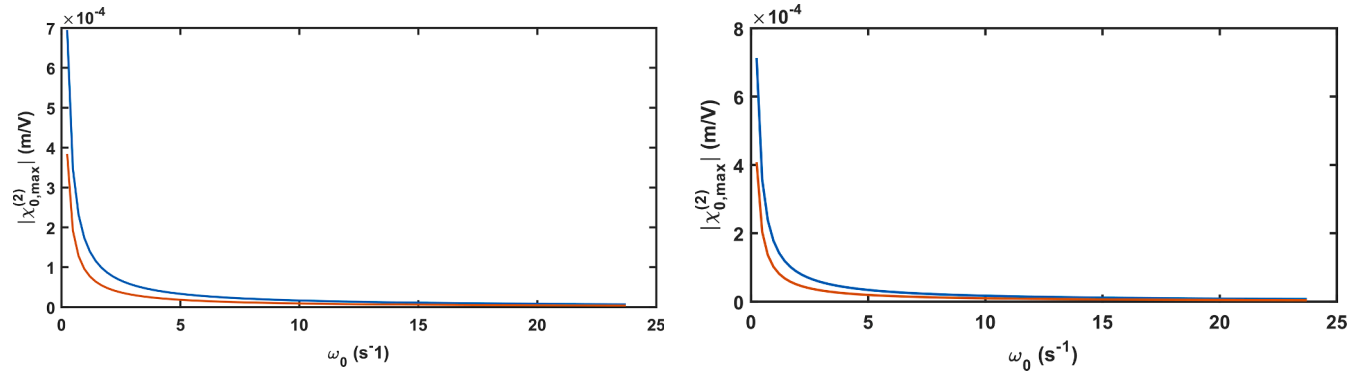

Fig. 1. Maximum ORC as a function of frequency for (a) for EE & WEE for R = 10 nm, P = 150 kbar and T = 50 K (b) for EE & WEE for R = 10 nm, P = 50 kbar and T = 150 K

$$\chi_0^{(2)} = 4\frac{e^3\sigma_s}{\varepsilon_0\hbar^2}\mu_{01}^2\delta_{01} \times \frac{\omega_{01}^2\left(1+\frac{T_1}{T_2}\right)+\left(\omega^2+\frac{1}{T_2^2}\right)\left(\frac{T_1}{T_2}-1\right)}{\left[\left(\omega_{01}-\omega\right)^2+\frac{1}{T_2^2}\right]\left[\left(\omega_{01}+\omega\right)^2+\frac{1}{T_2^2}\right]} \tag{26}$$

when $\omega \tilde{} \omega_{01}$ there is a peak value of $\chi_0^{(2)}$

$$\chi_{0,\max}^{(2)} = \frac{2e^3T_1T_2\sigma_s}{\varepsilon_0\hbar^2}\mu_{01}^2\delta_{01}, \tag{27}$$

where $\mu_{ij} = |\langle\psi_i|z_r|\psi_j\rangle|(i,j=0,1)$ are the matrix elements of the dipole moment, $\psi_i(\psi_j)$ are the Eigen functions $\delta_{01} = |\langle\psi_1|z_r|\psi_1\rangle - \langle\psi_0|z_r|\psi_0\rangle|$ $\omega_{01} = \frac{E_1-E_0}{\hbar}$, and ω is the frequency of the incident electromagnetic field, σ_s is the electron density in the QDs, T_2 is the transverse relaxation time, and T_1 is the longitudinal relaxation time.

For the regime of strong confinement, by considering relative coordinate electronic state, and energy levels, electronic wave functions are defined as

$$\phi_k = N_k \exp\left[-\frac{1}{2}\alpha^2 z_r{}^2\right] H_{2k+1}(\alpha z_r) \tag{28}$$

$$E_k = \left(2k+\frac{3}{2}\right)\hbar\omega_0, \text{ with } (k=0,1,2.....), \tag{29}$$

where

$$N_k = \left[\frac{1}{\alpha}\sqrt{\pi}2^{2k}(2k+1)!\right]^{-1/2} \tag{30}$$

Then the dipolematrix elements are obtained as

$$\mu_{01} = |\langle\phi_0(z_r)|z_r|\phi_1(z_r)\rangle| = \frac{4N_0N_1}{\alpha^2} = \frac{2}{\sqrt{6\pi}\alpha} \tag{31}$$

$$\mu_{00} = |\langle\phi_0(z_r)|z_r|\phi_0(z_r)\rangle| = \frac{2N_0^2}{\alpha^2} = \frac{2}{\sqrt{\pi}\alpha} \tag{32}$$

$$\mu_{11} = |\langle\phi_1(z_r)|z_r|\phi_1(z_r)\rangle| = \frac{72N_1^2}{\alpha^2} = \frac{3}{\sqrt{\pi}\alpha} \tag{33}$$

Finally, from Eq. (21) to Eq. (29), the maximum ORC is

$$\chi_{0,\max}^{(2)}(\omega) = \frac{8\sqrt{2}\hbar e^3T_1T_2\sigma_s}{3\varepsilon_0\left(m_e^*\pi\hbar\omega\right)^{3/2}} \tag{34}$$

3. Results and discussions

We have considered the GaAs semiconductor material constants for our numerical results where $T_1 = 1$ps and $T_2 = 0.2$ ps, and we used the numerical parameters such as $m_e^* = 0.067\ m_0$, $m_h^* = 0.09\ m_0$ ($m_0$is the mass of a free electron), $\sigma_s = 5\times10^{24}\text{m}^{-3}$, $\varepsilon = 12.53$ [14].

In Fig. 1(a) and (b), we present the maximum ORC $\chi_{0,\max}^{(2)}(\omega)$ as a function of ω_0, the semi-parabolic confinement frequency. In both Fig. 1 (a) & (b), the maximum ORC is enhanced when the excitonic effects are

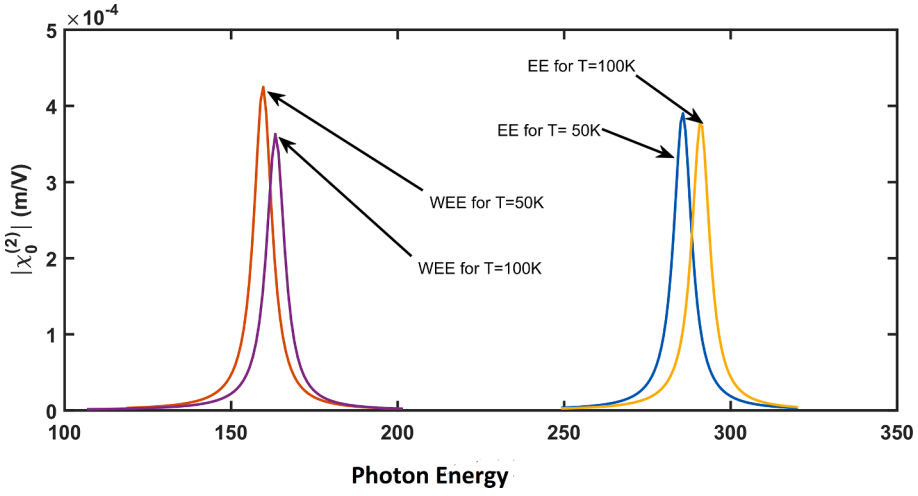

Fig. 2. ORC as a function of incident photon energy for T = 50 K &100 K keeping R & P constant at R = 10 nm and P = 50 kbar.

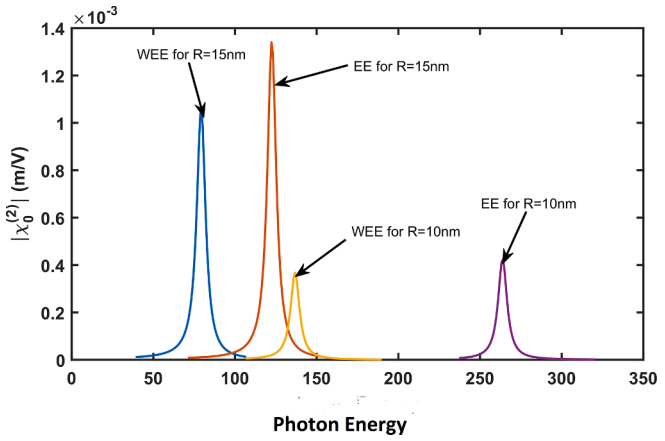

Fig. 3. ORC as a function of photon energy for R = 10 nm & 15 nm keeping P & T constant at P = 50 kbar and T = 50 K

taken into consideration. Both the factors of pressure & temperature affect $\chi^{(2)}_{0,\max}(\omega)$ through the alterations in effective mass & dipole matrix elements. Single electron state having energy levels and wave functions are given by Eq. (6) and Eq. (7), respectively, while for considering the case of without excitonic effect, the mass of the electron m^*_e instead of the total mass M_T has been taken into consideration. From Fig. 1(a) and (b), we can observe that the maximum ORC $\chi^{(2)}_{0,\max}(\omega)$ obtained is stronger when Excitonic effect is taken into account as compared to when no such effect is considered — this stretching due to the towering of the dipole matrix elements $\mu^2_{01}\delta_{01}$. Due to the EE, the charge distribution in the QD is distributed in a manner that the opposite polarity charge carriers are separated by a distance $(z_e - z_h)$. This gives rise to stronger dipole matrix elements which in turn leads to enhance nonlinear effects. The same is manifested in the higher values of maximum ORC in case off EE as compared to WEE.

In Fig. 2, we present the results of the inclusion of excitonic effect on the second harmonic generation peaks when the temperature is varied from 50 K to 100 K. It is found that the excitonic effect blue shifts the optical rectification peaks for both the temperatures. When the nanostructure is kept at 50 K temperature, the optical rectification peak blue shifts from 155 meV to 275 meV as the excitonic effects are included. At the same time, the peak height diminishes to a slightly lower value of $3.4*10^{-4}$ m/V from $4.3*10^{-4}$ m/V. Similar effects are seen in the case when the ambient temperature is maintained at 100 K. In this scenario, the peak position shifts from 160 meV to 290 meV as the excitonic effect comes into play. We also observe that as the temperature is increased, the peak heights value decreases. In both the cases of EE as well as WEE the ambient temperature plays an important role in shifting the peaks and reducing the peak height by affecting the energy band gap. The blue shift of the peaks occurring due excitonic effects is attributed to enhancement of the energy values of subsequent eigenstates because of the attractive interaction between the electron and hole.

Fig. 3 shows the variation of optical rectification by the nanostructure for two values of radii of the semi-parabolic QD at P = 50 kbar & T = 50 K. It can be observed that the peaks are blue shifted when the radius of the QD is reduced to 10 nm from 15 nm. This blue shift is the result of increase in the difference between subsequent energy states due to stronger confinement when radius is decreased. The consideration of excitonic effect for both the radii takes the peak position to higher values, viz. from 60 meV to 100 meV where R = 15 nm & from 140 meV to 255 meV for R = 10 nm. The peak height is reduced when the radius is lowered to 10 nm from 15 nm. This occurs due to the diminishing of the dipole matrix element as the radius is decreased. Further, the inclusion of EE enhances the optical rectification peaks by enhancing the matrix element.

In Fig. 4, we present the changes in the peaks due to changing hydrostatic pressure while keeping the temperature fixed at 50 K & radius at 10 nm. We observe that the increase in hydrostatic pressure drags the optical rectification peaks to lower energy state. For the case, including the excitonic effects, the red shift with an increase in pressure from 50 kbar to 100 kbar is of 10 meV, i.e., from 290 meV to 280 meV whereas for the same change in pressure the shifting in the optical rectification peaks is of 15 meV, i.e., from 135 meV to 130 meV when the excitonic effects are ruled out. The dependence of effective mass of the charge carriers interplays with the change in $\omega(P)$ when pressure is changed to bring in these shifting in optical rectification peaks.

4. Conclusion

The combined effects of correlation between the electron-hole pair, temperature, and hydrostatic pressure on the optical rectification in as semi-parabolic GaAs QDs are studied using the formalism of density matrix and the effective mass approximation. The results were calculated in the strong confinement regime. The obtained results show that the ORC is considerably magnified when exciton states in the QDs are taken into consideration. We found that the ORC peak positions are affected by both temperature & pressure where the blue shift and red shift are induced when temperature & hydrostatic pressure are changed. Moreover, the OR strength is also found to be strongly affected by radius,

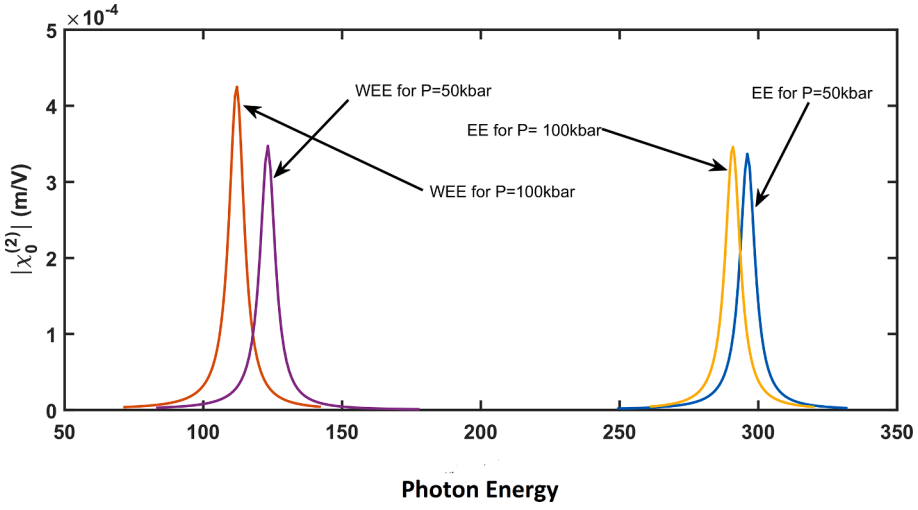

Fig. 4. ORC as a function of photon energy for P = 50 kbar & 100 kbar keeping R & T constant at R = 10 nm and T = 50 K

temperature & pressure. It is observed that the interplay of the variation of effective mass and $\omega(P)$ induces varied alteration of the ORC of the QD for the case of exciton effect and without it. The variation of temperature & pressure can thus use as external parameters to control the OR from QD.

Acknowledgments

One of the author (SD) would like to thank DELHI TECHNOLOGICAL UNIVERSITY for the financial support. We would also like to thank Prof. Man Mohan, University of Delhi for the invaluable discussions.

References

[1] Y.Y. Lin, J. Singh, J. Appl. Phys. 92 (2002) 6205.
[2] S.T. Perez-Merchancano, R. Franco, J. Silva-Valencia, Microelectron. J. 39 (2008) 383.
[3] 1G. Almogy, A. Yariv, J. Nonlinear Opt. Phys. Mater. 4 (1995) 401.
[4] E. Rosencher, B. Vinter, Optoelectronics, Cambridge University Press, Cambridge, 2003.
[5] F. Capasso, K. Mohammed, A.Y. Cho, IEEE J. Quantum Electron. 22 (1986) 1853.
[6] D.A.B. Miller, Int. J. High Speed Electron. Syst. 1 (1991) 19.
[7] H. Schneider, F. Fuchs, B. Dischler, J.D. Ralston, P. Koidl, Appl. Phys. Lett. vol. 58 (1991) 2234.
[8] D.K. Ferry, S.M. Goodnick, Transport in Nanostructures, Cambridge University Press, Cambridge, 1997.
[9] H.A. Sarkisyan, Mod. Phys. Lett. B 18 (2004) 443.
[10] S.N. Saravanamoorthy, A. John Peter, C.W. Lee, Chem. Phys. 483 (2017) 1.
[11] A. Bera, M. Ghosh, Physica B 515 (2017) 18.
[12] C.Y. Chen, D.S. Sun, Acta Photonica Sin. 30 (2001) 104.
[13] Y.-B. Yu, S.-N. Zhu, K.-X. Guo, Phys. Lett. A 175 (2005) 335.
[14] A. Braggio, M. Grifoni, M. Sassetti, F. Napoli, Europhys. Lett. 50 (2000) 236.
[15] F.D.M. Haldane, J. Phys. C 14 (1981) 2585.
[16] W. Xie, Chem. Phys. 423 (2013) 30.
[17] C.-J. Zang, K.-X. Guo, Z.-E. Lu, Physica E 36 (2007) 92.
[18] Y.-Y. Zhang, G.R. Yao, J. Appl. Phys. 110 (2011), 093104.
[19] W. Xie, The nonlinear optical rectification of a confined exciton in a quantum dot, J. Lumin. 131 (5) (2011) 943–946.
[20] M. Bass, P.A. Franken, J.F. Ward, G. Weinreich, Optical rectification, Phys. Rev. Lett. 9 (11) (1962) 446–448.
[21] P.A. Franken, A.E. Hill, C.W. Peters, G. Weinreich, Generation of optical harmonics, Phys. Rev. Lett. 7 (4) (1961) 118–119.
[22] R.W. Boyd, Nonlinear Optics, third ed., Elsevier, 2008.
[23] S.L. Chuang, S. Schmitt-Rink, B.I. Greene, P.N. Saeta, A.F.J. Levi, Optical rectification at semiconductor surfaces, Phys. Rev. Lett. 68 (1) (1992) 102–105.
[24] S. Baskoutas, E. Paspalakis, A.F. Terzis, Effects of excitons in nonlinear optical rectification in semi parabolic quantum dots, Phys. Rev. B 74 (15) (2006). Article ID 153306.
[25] C.M. Duque, M.E. Mora-Ramos, C.A. Duque, Physica E 43 (2011) 1002.
[26] İ. Karabulut, M.E. Mora-Ramos, Duque A. Carlos, J. Lumin. 131 (2011) 1502–1509.
[27] Alejandro Zapata, E Ruben Acosta, Miguel Mora-Ramos, Duque A. Carlos, Nanoscale Res. Lett. 7 (508) (2012) 1–9.
[28] M.E. Mora-Ramos, M.G. Barseghyan, C.A. Duque, Physica E 43 (2010) 338–344.
[29] C.M. Duque, M.E. Mora-Ramos, C.A. Duque, Superlattice Microstruct. 49 (2011) 264–268.
[30] S. Sauvage, P. Boucaud, T. Brunhes, F. Glotin, R. Prazeres, J.-M. Ortega, J. M. Gérard, Phys. Rev. B 63 (2001) 113312.
[31] S. Baskoutas, E. Paspalakis, A.F. Terzis, Phys. Rev. B 74 (2006) 153306.
[32] C.-J. Zhang, K.-X. Guo, Z.-E. Lu, Phys. E 36 (2007) 92.
[33] İ. Karabulut, H. Şafak, M. Tomak, J. Phys. D Appl. Phys. 41 (2008) 155104.
[34] İ. Karabulut, H. Şafak, Physica B 82 (2005) 368.
[35] C.M. Duque, M.E. Mora-Ramos, C.A. Duque, J. Nanoparticle Res. 13 (2011) 6103–6112.
[36] Sheetal Antil, Manoj Kumar, Siddhartha Lahon, Sajjan Dahiya, Anil Ohlan, A. S. Rajesh Punia, Maan, Phys. B: Condens. Mat. 552 (2019) 202–208.
[37] Sheetal Antil, Manoj Kumar, Siddhartha Lahon, A.S. Maan, Optik – Int. J. Light Electr. Opt. 176 (2019) 278–286.
[38] N. Raigoza, A.L. Morales, A. Montes, N. Porras-Montenegro, C.A. Duque, Phys. Rev. B 69 (2004), 045323.
[39] E. Rosencher, Phys. Rev. B 44 (1991) 11315.
[40] R. Boyd, Nonlinear Optics, 3 edition, Elsevier, New York, 2008.

Physica E 147 (2023) 115620

Contents lists available at ScienceDirect

Physica E: Low-dimensional Systems and Nanostructures

journal homepage: www.elsevier.com/locate/physe

Study of third harmonic generation in $In_xGa_{1-x}As$ semi-parabolic 2-D quantum dot under the influence of Rashba spin-orbit interactions (SOI): Role of magnetic field, confining potential, temperature & hydrostatic pressure

Suman Dahiya [a], Siddhartha Lahon [b,*], Rinku Sharma [a,**]

[a] Department of Applied Physics, Delhi Technological University, Delhi, 110042, India
[b] Physics Department, KMC, University of Delhi, Delhi, 110007, India

ARTICLE INFO

Handling editor: J. Nitta

Keywords:
Quantum dot
Spin-orbit interaction
Magnetic field
Third harmonic generation
Temperature

ABSTRACT

In the present case, nonlinear optical susceptibility for $In_xGa_{1-x}As$ 2-D semi-parabolic Quantum Dot with the key prominence given to the magnetic field, Hydrostatic pressure, confining potential and Temperature on THG in the presence of Rashba SOI is investigated. The main expression of THG is attained using a formalism of compact density matrix. Our results are showing that rise/diminution in the Rashba SOI coefficient strongly affects the THG peaks. Also, a blue/redshift is observed with an increase/decrease in external factors such as Hydrostatic Pressure, magnetic field, Temperature, confining potential & Rashba SOI with a corresponding increase/decrease in peak height. According to the observation, two-photon resonance peaks are found to be stouter than one & three-photon resonance peaks as with a significant increase in the coupling, the strength of the dipole matrix element also increases in correspondence to the peak height. The conclusions are demonstrating that for the comprehensive engineering of optical devices based on the QDs, SOI must be taken into consideration, and hence by tuning the strength parameter, the optical properties of the optoelectronic devices can be controlled.

1. Introduction

As quantum confinement has become apparent in all spatial directions, ultra-small semiconductor heterostructures have gained the immense focus of researchers around the world. These heterostructures such as quantum heterostructure including quantum dot, quantum wire, etc. Have many unique potential applications due to the confinement as the movement of charge carrier is restricted and hence leads to the development of a set of discrete energy levels where the carriers may exist. There are many microfabrication techniques including MBE, lithography, vapor deposition technique, etc. to fabricate these quantum heterostructures of different shapes and sizes. Explicitly, optical properties such as linear and nonlinear optical properties & susceptibilities have more scientific interest as they offer massive efficacy in understanding numerous semiconductor optoelectronic devices such as quantum LED's, solar cells, quantum dot lasers, single-electron transistors & quantum computing computers, etc. [1–7].

The role of externally applied fields, SOI, temperature & hydrostatic pressure, etc. is very significant in altering the properties of the quantum heterostructures as any prominent change in the property can result in momentous changes in the working of the nano-scale device [8–11]. This dependence has often been used to externally alter the properties of these nano-scale devices to the operator's own will and thus has been one of the most widely researched areas in recent times. On application of a perpendicular magnetic field to the plane of QD, energy levels are supplied with a supplementary structure as well as interacting electrons confined in QD results in correlation effect. The study of the electronic, optical and thermodynamic properties has been done by many different techniques. Theoretically, the 2-electron QD Hamiltonian with the inclusion of the effect of the magnetic field has been solved by many authors for obtaining the respective eigen energies and eigenstates of the QD-system [12–20] but to our sincere belief, the effect of external factors & SOI with doping is relatively a less discovered area.

Second and third-order nonlinear optical interaction of 2- incident

* Corresponding author.
** Corresponding author.
E-mail addresses: dahiyasuman90@gmail.com (S. Dahiya), sid.lahon@gmail.com (S. Lahon), rinkusharma@dtu.ac.in (R. Sharma).

https://doi.org/10.1016/j.physe.2022.115620
Received 20 September 2022; Received in revised form 14 November 2022; Accepted 16 December 2022
Available online 21 December 2022

fields with optical media results in the generation of SHG & THG and ORC. Xie and Bass et al., in 1962 performed initial work on OR [21], whereas Franken et al. were the first to report the experimental observation of SHG [22,23]. Baskoutas et al. investigated the impact of exciton in optical susceptibility for a semi-parabolic Quantum dot for a semi-parabolic potential [24] whereas F. Ungan et al. focused on the impact of the Electric field on TAC and RICC of an asymmetric Quantum dot [25]. Xuechao Li et al. [26], focused on the outcome of the Magnetic field on TAC of an asymmetric Quantum dot and studied the variations with parameters such as radius and magnetic field intensity.

Many important factors such that such as temperature, hydrostatic pressure, applied electric and magnetic fields and intense laser fields have a significant effect on the linear and nonlinearoptical properties of Q D's. On the application of these external field factors, the band structure, and the optical nonlinearity of the QD system is controlled and altered. Hence, concluding that the geometry of systems, as well as external perturbations, are equally contributing significantlyinfluencing the nonlinear optical properties of semiconductor structures. Unidimensional quantum dots have been studied immensely in recent times, but studies on the 2D semi-parabolic quantum dot with doping focusing on the dependence of its properties on external factors are scarce. In this study, we explored the variation of optical properties, such as THG on applied hydrostatic pressure, temperature, magnetic field, Rashba spin for $In_xGa_{1-x}As$ Quantum dot in the presence of SOI. The first section contains a crisp introduction of the topic, whereas the theory and the formulas have been mentioned in the second section. The third section consists of the obtained results and the graphs and is followed by the fourth section which contains well-drawn solutions.

1.1. Theoretical model

This section describes the detailed theory of 1-electron QD consisting of two parts given as (1) QD Hamiltonian (2) exact diagonalization method for the $In_xGa_{1-x}As$ QD.

Considering a 2-D $In_xGa_{1-x}As/In_yAl_{1-y}As$ QD (see Fig. 1) with a semi-parabolic confining potential as given in equation (3), with a vertical magnetic field given as $\overrightarrow{B} = B\hat{k}$ having a symmetric gauge as:$A = B(-y,x,0)/2$, the Hamiltonian for a one-electron system within effective mass taking spin into account is given as [27–31]:

$$H_{ST} = H_{ws} + H_{so}^{R} + \frac{1}{2}g^{*}\mu_B B\sigma \tag{1}$$

where

$$H_{ws} = \frac{1}{2m^{*}(P,T)}\left[P - \frac{e}{c}A(r)\right]^{\overrightarrow{2}} + V_r \tag{2}$$

And the potential is given as

$$V_r = \frac{1}{2}m^{*}(P,T)\omega_0^2\left(x^2+y^2\right) \tag{3}$$

In eq. (1), g^{*} represents the effective Lande factor for the semiconductor and electron spin z projection is given by $\frac{1}{2}\sigma$ having $\sigma = \pm$. Here up spin and down spin is represented by $\sigma = +1$ and $\sigma = -1$ respectively. SOI termH_{SO} contains two parts (i) Dresselhaus SOI term, H_{SO}^{D} (ii) Rashba SOI term, H_{SO}^{R}. As H_{SO}^{R} dominates overH_{SO}^{D} for the narrow gap, hence, neglectingH_{SO}^{D}, we have H_{SO}^{R} as:

$$H_{SO}^{R} = \frac{\alpha}{\hbar}\left[\overrightarrow{\sigma} \times \left(\overrightarrow{p} - \frac{e}{c}\overrightarrow{A}\right]_z\right. \tag{4}$$

The term $\frac{\alpha}{\hbar}\left[\overrightarrow{\sigma} \times \left(\overrightarrow{p} - \frac{e}{c}\overrightarrow{A}\right]_z\right.$ represents the spin-orbit coupling due to the inhomogeneous potential confining the electrons to the 2D plane and possible external gate voltages applied on the top of the dot. The strength of this coupling is determined by these parameters with a variation in magnitude when external gate voltages are applied. Here, the Rashba coupling coefficient is given byα and is controllable by varying the applied gate voltage in z direction, spinors and canonical momentum are represented byσ_x& σ_y and p_x& p_y respectively.

In effect. mass approx., total Hamiltonian H_{ST} for the combination of H_{ws} andH_{SO}^{R} is given as:

$$H_{ST} = \frac{p^2}{2m^{*}} + \frac{e}{m^{*}}A.p + \frac{e^2A^2}{2m^{*}} + V_r + \frac{1}{2}g^{*}\mu_B B\sigma + \frac{\alpha}{\hbar}\left[\overrightarrow{\sigma} \times \left(\overrightarrow{p} - \frac{e}{c}\overrightarrow{A}\right]_z\right. \tag{5a}$$

$$H_{ST} = \frac{p^2}{2m^{*}} + \frac{e}{m^{*}}A.p + \frac{e^2A^2}{2m^{*}} + V_r + \frac{1}{2}g^{*}\mu_B B\sigma + \frac{\alpha}{\hbar}[\sigma \times p]_z + \frac{e\alpha}{\hbar}[\sigma \times A]_z \tag{5b}$$

Here:

m^{*} = represents effect. mass of charge carrier.

$\hbar\omega_o$ = confining potential strength corresponding to the size of the QD.

The Temperature and hydrostatic dependent Effect. mass of the electron for GaAs is given as [32]:

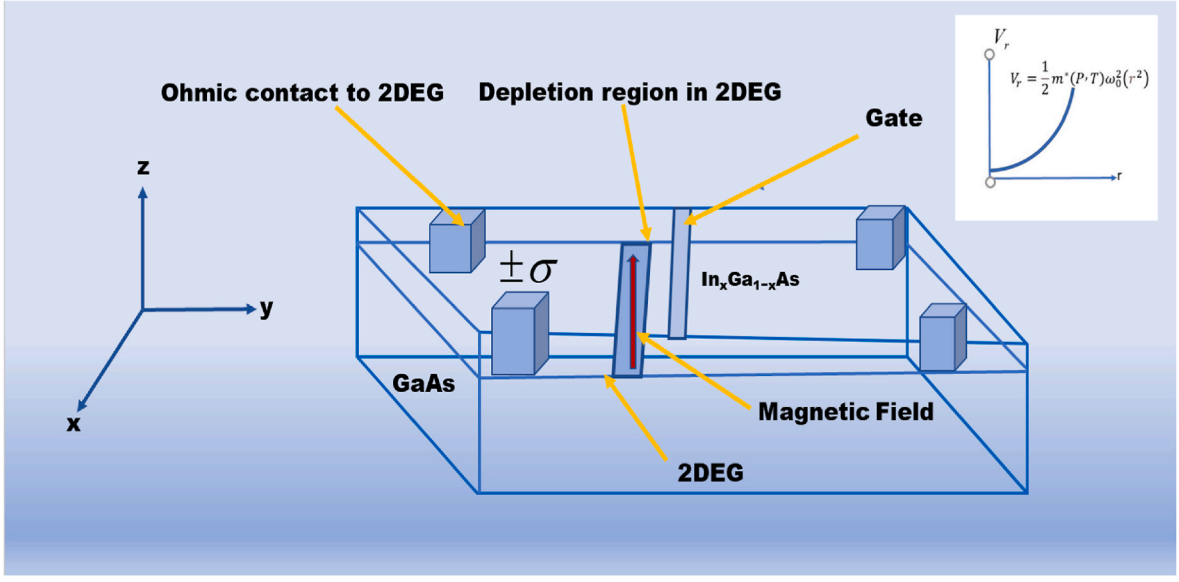

Fig. 1. Schematic diagram of an $In_xGa_{1-x}As$ Quantum Dot.

$$m_e^*(P,T) = m_o\left[1 + \frac{7510}{E_g(P,T)+341} + \frac{15020}{E_g(P,T)}\right]^{-1} \tag{6a}$$

$$With\ E_g(P,T) = \left[1519 - \frac{0.5405T^2}{T+204} + 10.7P\right] \tag{6b}$$

Here Temperature and hydrostatic pressure-dependent energy gap for G*a*As, E_g is in meV, P is in "kbar" and T is in "Kelvin." The pressure-dependent oscillator frequency is expressed as

$$\omega(P) = \omega_0 \,/\, \left[1 - 2P\left(1.16\times10^{-3} - 7.4\times10^{-4}\right)\right] \tag{6c}$$

Eigenfunction of Hamiltonian in eq (1) is represented by Fock-Darwin states $|n,l\rangle$ and is given as:

$$\psi_{nl\sigma}(r) = \frac{1}{\sqrt{2\Pi}} R_{nl}(r) e^{in\varphi}\chi_\sigma \tag{7a}$$

with

$$R_{nl\sigma}(r) = \sqrt{\frac{2}{c_l}}\sqrt{\frac{(2n+1)!}{(2n+1+|l|)!}}\exp\left(\frac{-r^2}{2a^2}\right) + \left(\frac{r^2}{a^2}\right)^{|l|/2} L_{2n+1}^{|l|}\left(\frac{r^2}{a^2}\right)\chi_\sigma \tag{7b}$$

Where $a = \left(\frac{\hbar}{m^*\Omega}\right)^{1/2}$, $\Omega^2 = \omega_o^2 + \frac{\omega_c^2}{4}$, χ_σ = spinor function and $\omega_c = \frac{eB}{m^*}$ (cyclotron frequency).

Eigen energies for eq. (1) is given as: $E_{nl} = (2n + |l| + 3/2)\hbar\Omega + \frac{\hbar}{2}l\omega_c + \sigma\left(\frac{1}{2}g^*\mu_B B + l\alpha m^*\omega_o^2\right)$, where

$$m = 0, 1, 2, 3\ldots\ldots, l = 0, \pm1, \pm2\ldots\ldots \text{ and } \Omega_\sigma^2 = \omega_o^2 + \frac{\omega_c^2}{4} + \frac{\sigma l\alpha m^*\omega_o^2\omega_c}{\hbar} \tag{8}$$

Also, Ω_σ is influenced by Rashba SOI, resulting in an upsurge in the up-spin energy gap with diminution in spin-down energy. SOI also affects the energy term in such a way that at B = 0 energy term becomes independent of the magnetic field and helps in uplifting spin degeneracy states.

An analytic expression for THG related to an optical inter-subband transition can be obtained using the density matrix formalism and an iterative procedure [33–35].

The wavefunction $\psi_{nl}(r)$ of the quantum dot with Rashba can be expanded in terms of an orthogonal and complete set of eigenvectors of H_0. Theexpansion takes the form [36]:

Hence the Schrödinger equation $H\psi = E\psi$ becomes:

$$\left(E_{n,l,\sigma}^0 - E\right)C_{n,l}^\sigma + \sum_{n,l,\sigma'\neq\sigma}(H_R)_{nn'll'}^{\sigma,\sigma'} C_{n'll'}^{\sigma'} = 0 \tag{9a}$$

$$\text{With } \psi_{nl\sigma} = \sum_{nl\sigma} C_{nl}^\sigma \varphi_{nl\sigma} \tag{9b}$$

The matrix elements are given by:

$$(H_R)_{nn'll'}^{\sigma,\sigma'} = \langle\varphi_{n,l}^\sigma|H_R|\varphi_{n',l'}^{\sigma'}\rangle = a\delta_{l',l+1}\sum\left(C_n'^{\uparrow}C_n^{\uparrow}\sqrt{n+l+1} - C_{n-1}'^{\uparrow}C_n^{\uparrow}\sqrt{n} + C_n'^{\downarrow}C_n^{\downarrow}\sqrt{n+l+2} - C_{n-1}'^{\downarrow}C_n^{\downarrow}\sqrt{n}\right) \tag{10}$$

The polarized electromagnetic field for an exciting system with frequency ω is given as:

$$E(t) = Ee^{i\omega t} + E^* e^{-i\omega t} \tag{11}$$

Also, relationship between the electronic polarization P(t) & polarized electromagnetic field are expressed by:

$$P(t) = \varepsilon_o\chi(\omega)Ee^{-i\omega t} + \varepsilon_o\chi(-\omega)E*e^{-i\omega t} = \frac{1}{V}Tr(\rho M) \tag{12}$$

Where $\chi_\omega^{(1)}, \chi_{2\omega}^{(2)}, \chi_o^{(2)}$, and $\chi_{3\omega}^{(3)}$ are representing the susceptibilities such as linear, SHG, OR and THG, respectively. THG relation is given as [17, 37–40]:

$$\chi_{3\omega}^{(3)} = \frac{n_o e^4}{\hbar^3}\frac{M_{01}M_{12}M_{23}M_{30}}{(\omega-\omega_{10}+i\Gamma_o)(2\omega-\omega_{20}+i\Gamma_o)(3\omega-\omega_{30}+i\Gamma_o)} \tag{13}$$

Here, the system's electron density is given as n_o, e is representing electronic charge, and relaxation time is represented by Γ_o. $\omega_{ij} = (E_i - E_j)/\hbar$ shows the frequency for the transition and matrix elements are given by$M_{ij} = |\langle\psi_i|er|\psi_j\rangle|(i,j = 0,1,2,3)$ such as $M_{01} = |\langle\psi_{nl\sigma}|er|\psi_{n'l'\sigma'}\rangle|where\, 0 = nl\sigma \quad and\, 1 = n'l'\sigma'$.

2. Result and discussion

In this section, the simultaneous effect of the magnetic field, Hydrostatic Pressure, Temperature, confining potential in the presence of SOI on THZ in $In_xGa_{1-x}As$ semi-parabolic 2-D quantum dot is calculated. For this purpose, the physical parameters that have been used are given as follows: $\Gamma_o = 0.66$ps and $m_e^* = 0.041m_0$, where mass of a free electron m_0. σ_s is taken as $5\times10^{22}\ m^{-3}$, $\varepsilon_r = 12.53$, and g = −15 [41,42].

Considering a QD system in semi parabolic potential having (0 0–1) as ground state and (1 –1 –1) and (1 1–1) as excited states having degenerate intermediate states, when both the magnetic field and spin are zero. This degeneracy can be wrecked by applying a magnetic field 'B' and introducing an "α", and; hence, by using these two parameters some manipulation in the energy can be done. Fig. 2 represents a Schematic conduction band energy level diagram (n l −1) for InAlAs/InGaAs semi-parabolic quantum dot having four possible routes.

For THG, four possible routes having (0 0–1) (nlσ) as ground state and their corresponding transition energies with potential confinement at ħ ω = 10 meV, Rashba factor α = 10 meV nm, Pressure 10 kbar, temperature = 10 K and magnetic field B = 1 T is given in Fig. 2. Fig. 3 represents four individual possible paths for transition for the THG coefficients vs incident photon energy with confining potential keeping at ω = 10 meV, fixing the Rashba SOI parameter at α = 10 meV nm, Hydrostatic Pressure at 10 kbar, Temperature at 10 K and applying an external magnetic field, B = 1 T to the QD. As it can be observed from Fig. 3 that one, two, three-photon resonances are occurring at different photon energies due to the intermediate ladder states. Alteration in peaks as well as in peak heights can also be observed for different transition energies in each dissimilar path. According to the observation, two-photon resonance peaks are found to be stouter than one & three-photon resonance peaks as peak height corresponding to the strength of the dipole matrix element also increases with a significant increase in the coupling.

The magnetic field is having a significant effect in shifting the peaks as well as changing the magnitude of the peaks which is evident in Fig. 4 where THG coefficient vs incident photon energy has been plotted for four different values of the magnetic field. As the energy levels are getting affected by the magnetic field hence in Fig. 4a–d, a 2-way shifting of different positions of resonance can be observed. Here, the cyclotron frequency term supports dropping the energy level as well as (−) l whereas the Zeeman term helps in boosting the energy. As B is independent of the sign of l i.e., whether l is + or -, it will always help in enhancing Ωσ. Same can be observed from the expression of eigen energy given in equation (8). Further, it is also observed from the figure that for 1st two paths, the three-photon resonance is having some

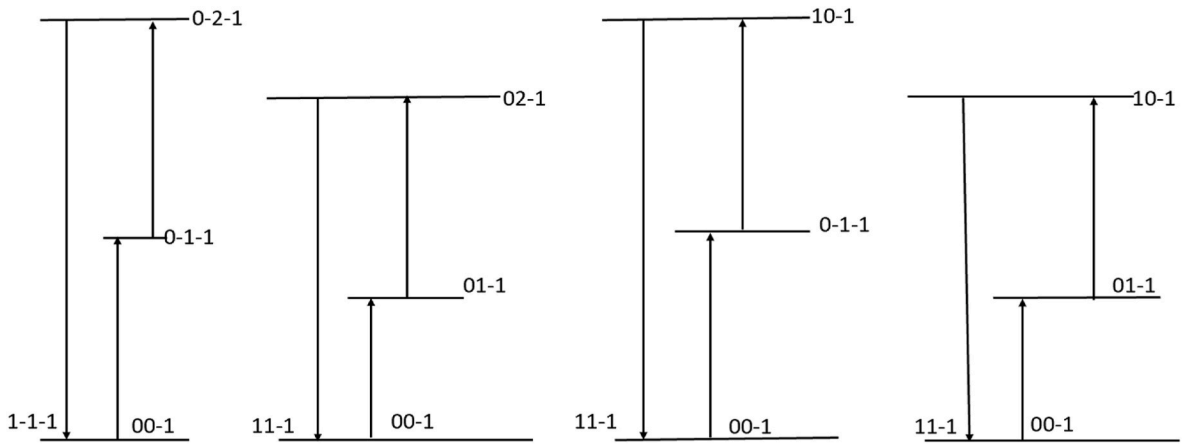

Fig. 2. Schematic conduction band energy level diagram (n l -σ) **for InAlAs/InGaAs quantum dot having four possible routes.**

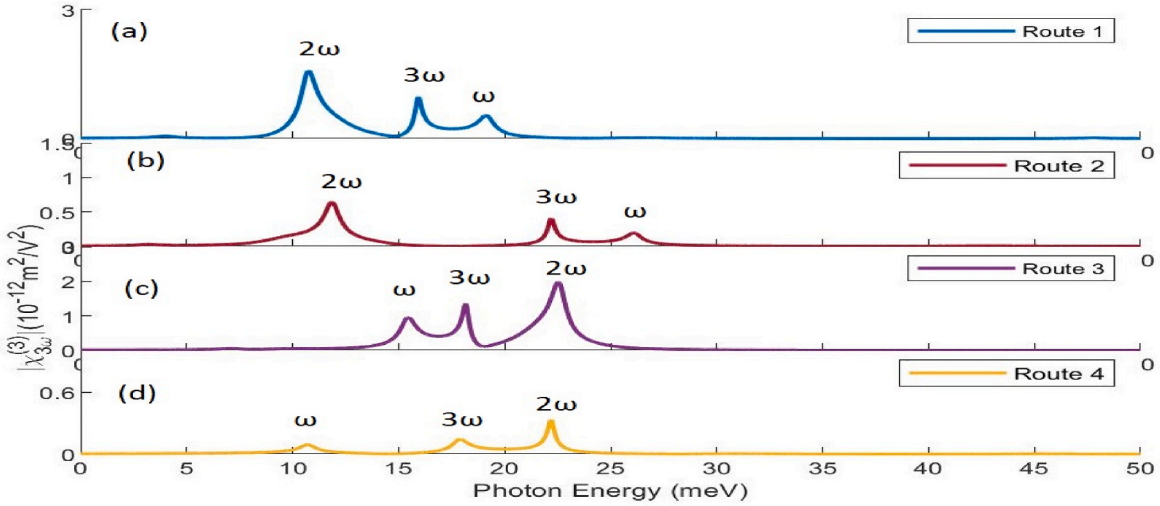

Fig. 3. Coefficient of THG vs photon energy for four possible routes (a) 1st route; (b) 2nd route; (c) 3rd route; (d) 4th route having $\hbar\,\omega = 10$ **meV,** $\alpha = 10$ **meV nm,** $P = 10$ **kbar,** $T = 10$ **K and** $B = 1$ **T.**

significance on the right side of the highest peak while for the 3rd and 4th path, peaks are enhancing but three-photon resonances are not having much significant value due to involvement of –l states in the resonance position which are independent of three photons resonances and hence shifting towards the lower energy side, whereas the involvement of +l states in the resonance positions helps in shifting the excited states to a state of higher photon energy.

In Fig. 5, THG Coefficient and photon energy for dissimilar values of the QD confinement potential (a) $\hbar\,\omega = 10$ meV, (b) $\hbar\,\omega = 15$ meV, (c) $\hbar\,\omega = 20$ meV, (d) $\hbar\,\omega = 25$ meV keeping $B = 1$T, $P = 10$ kbar, $T = 10$ K and $\alpha = 10$ meV nm are plotted. From this figure it is concluded that both the blue/redshifts are observed for the resonant peaks of the THG i.e., some resonant peaks are moving toward lower photon energies exhibiting redshift and some are moving toward higher photon energies displaying blue shift with an increase in the confining potential. Due to the quantum confinement effect, an increased confinement potential roots towards the lesser radius of charge carriers in a QD. Due to weak confinement, the energy separation between the states tends to decrease and hence, exhibits a blue shift in the peaks. It is also observed that the peaks are having unequal spacing with a difference in the number of photon resonance as they are belonging to different energy levels.

Fig. 6 represents a plot between THG coefficient and incident photon energy for different values of α at a confining potential of $\omega = 10$ meV and $B = 1$ T, where α is increasing at a step of 5 meV nm. With an increase in α from a value of 10 meV nm to 25 meV nm, a slight redshift can be observed in one and two-photon resonance peaks, whereas a shifting towards the higher energy end can be observed in three-photon resonance positions resulting in a blue shift. As α is playing a two-way role while handling the values of energy levels hence red/blue shifts are observed. Further, a decrease in peak height can also be observed with an increase in the value of the Rashba parameter.

Fig. 7(a) is showing the coefficient of THG vs incident photon energy for four diverse values of pressure fixing confining potential $\hbar\,\omega = 10$ meV, $T = 10$ K, $\alpha = 10$ meV nm and $B = 1$ T. With an increase in Hydrostatic Pressure, the magnitude of THG resonant peaks increases with a slight decrease in peak height as the peaks are shifting towards lower energy. It is observed that the change in the magnitude of the THG resonant peaks is directly correlated to the dipole matrix element term $M_{01}M_{12}M_{23}M_{30}$ in the numerator as well as to the energy interval ω_{10}, ω_{20} and ω_{30} in the denominator. Additionally, as dipole matrix elements are decreasing with an increase in pressure hence the red shift in resonant peaks is observed with an increase in hydrostatic pressure, as shown in Fig. 7(b). This is explained by the fact that the quantum confinement becomes weak with the decrease in the energy interval with a rise in hydrostatic pressure.

Fig. 8(a) is showing a plot of THG and incident photon energy for four diverse values of temperature fixing confining potential $\hbar\,\omega = 10$ meV, $P = 10$ kbar, $\alpha = 10$ meV nm and $B = 1$ T. Blueshift can be observed

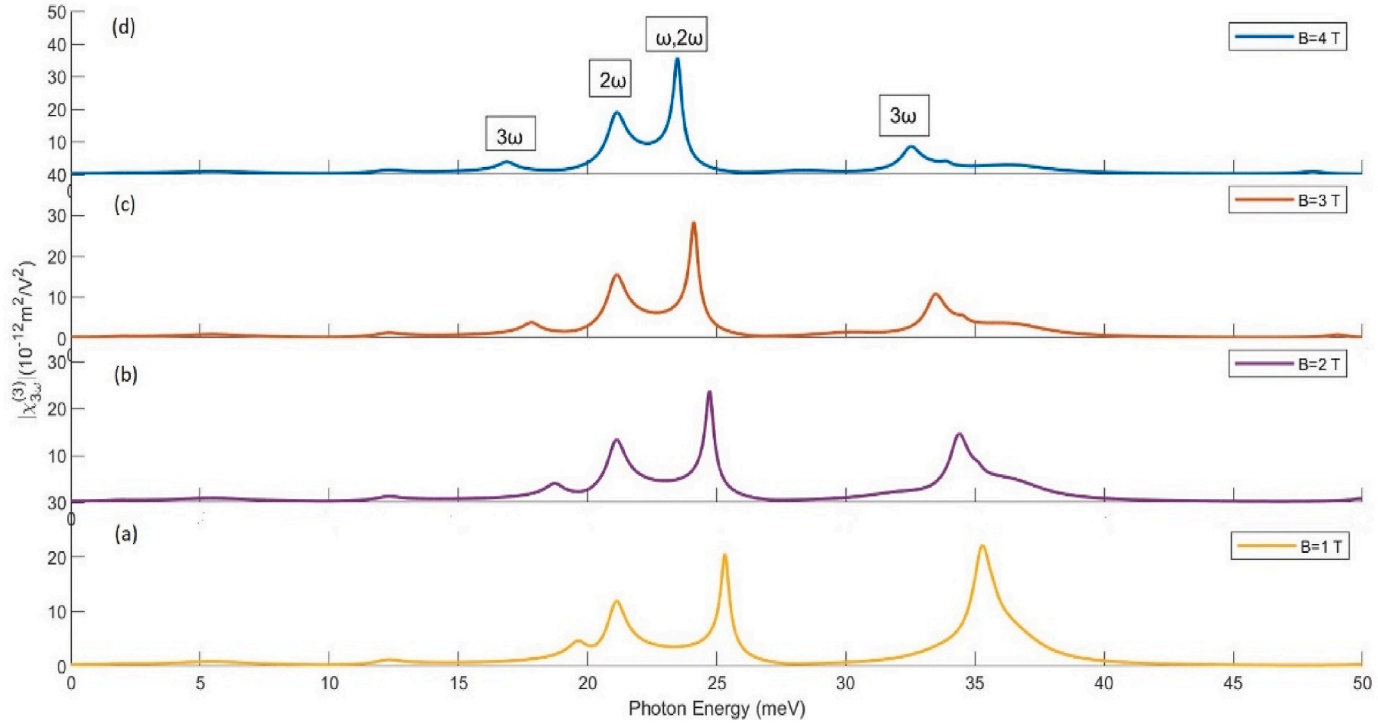

Fig. 4. Coefficient of THG vs incident photon energy at diverse Magnetic field values keeping α = 10 meV nm, P = 10 kbar, T = 10 K and confining potential $\hbar\omega$ = **10 meV.**

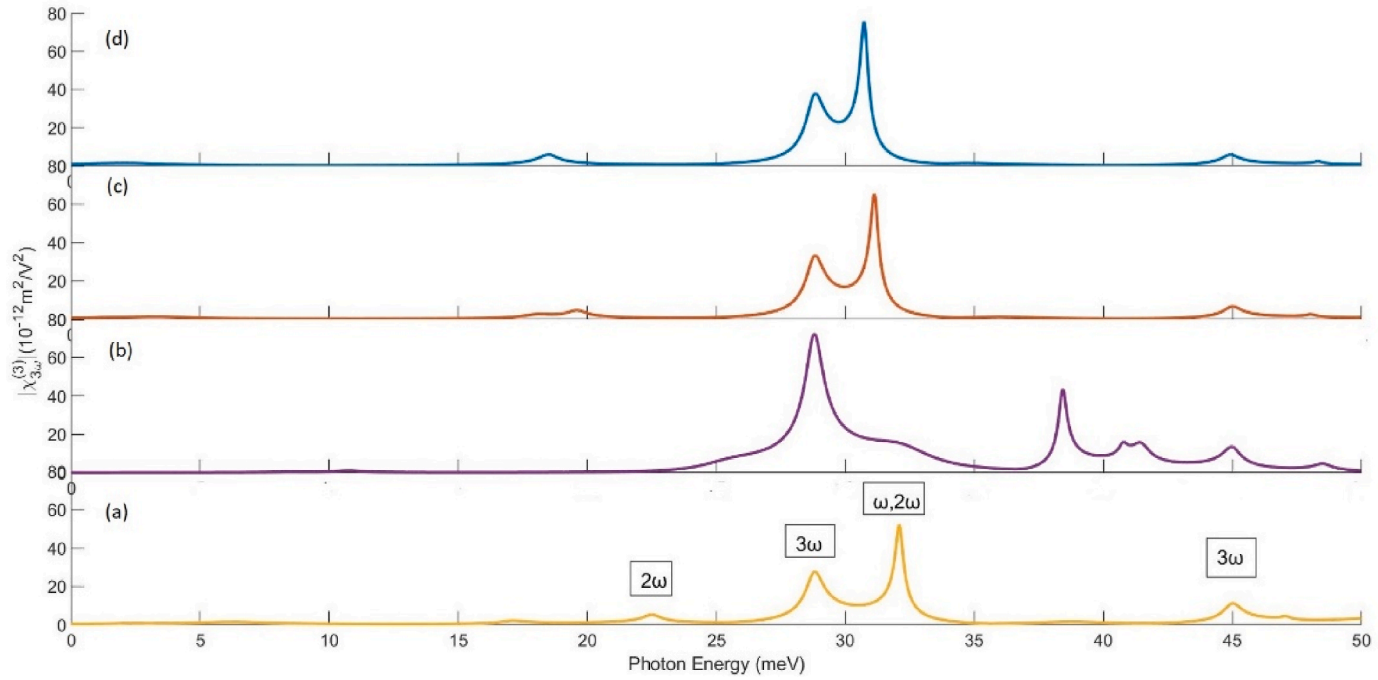

Fig. 5. Coefficient of THG vs incident photon energy for the diverse value of confining potential keeping B = 1T, P = 10 kbar, T = 10 K and α = 10 meV nm.

with an increase in the temperature as the resonant peaks are moving towards higher energy region with a significant increase in the peak height. As one can see from Fig. 8(b) that the dipole matrix element M01 gets enhanced with increase in temperature, consequently the peak height corresponding to (ω, 2ω) gets enhance along with its blueshift. The dipole matrix element M01's value increases with temperature as the effective radius changes with an increment in temperature. However, the peak corresponding to 3ω at higher energy gets suppressed at higher temperature. This can be attributed to the fact that as temperature increases, the sharp resonances get fuzzy due to the thermal energy of the electrons.

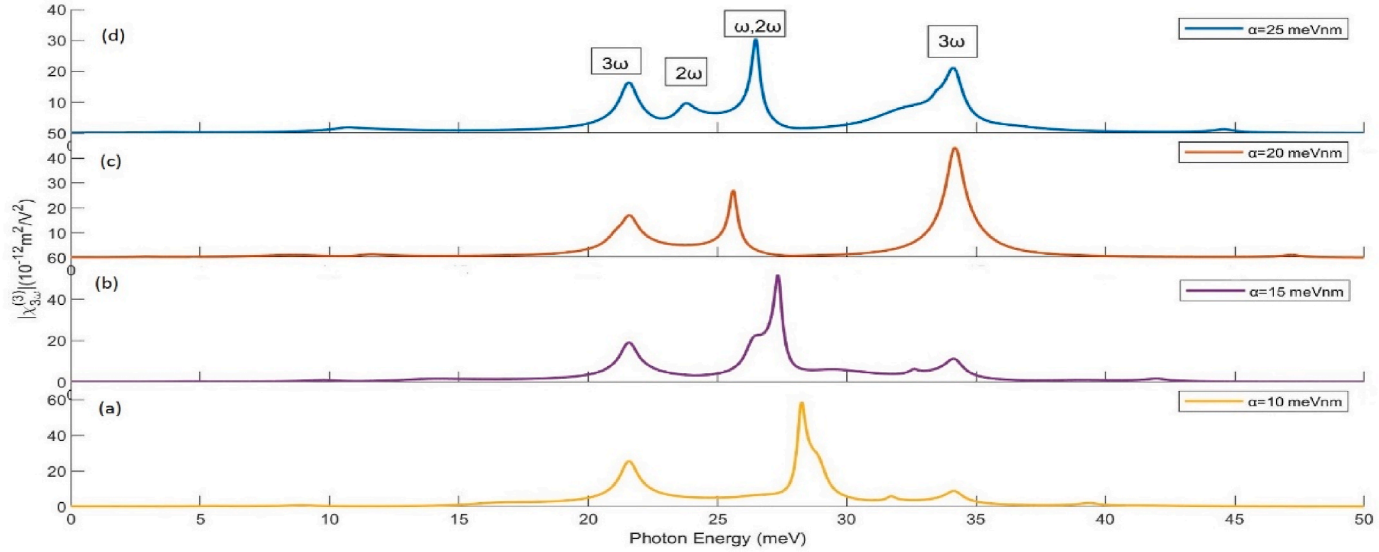

Fig. 6. Coefficient of THG vs incident photon energy for the diverse value of Rashba SOI coupling factor keeping confining potential $\hbar\,\omega = 10$ meV, P = 10 kbar, T = 10 K and B = 1 T.

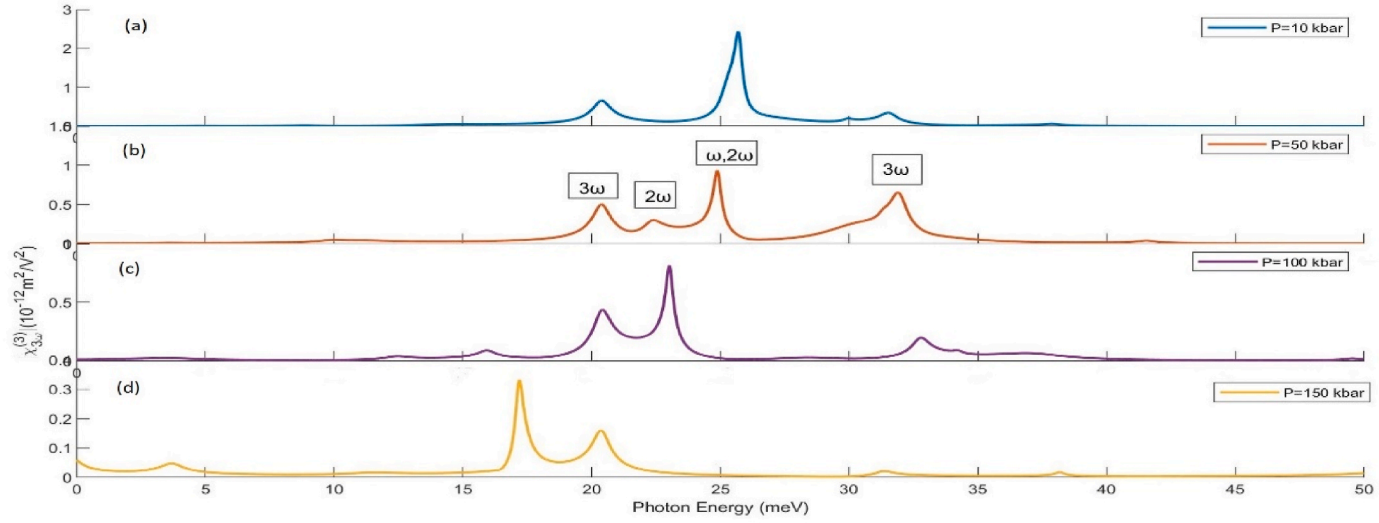

(a)

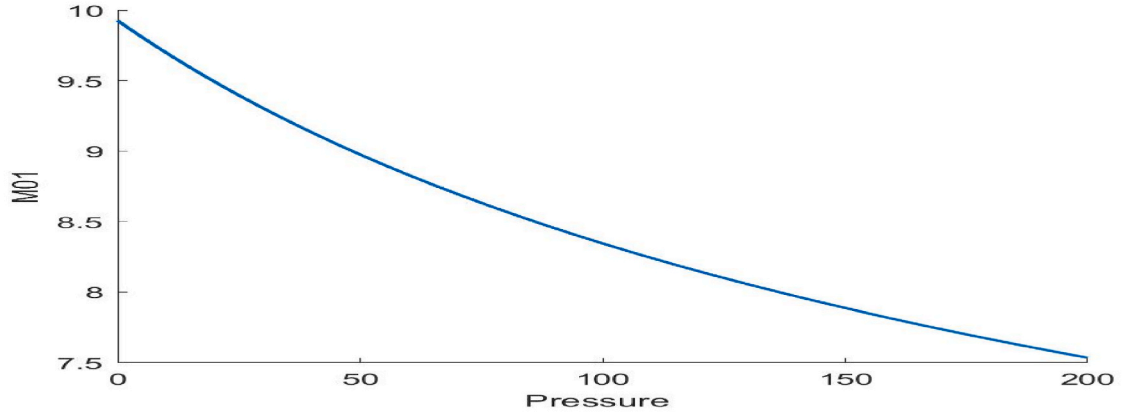

(b)

Fig. 7(a). Coefficient of THG vs incident photon energy for diverse value of pressure fixing confining potential $\hbar\,\omega = 10$ meV, T = 10 K, α = 10 meV nm and B = 1 T.

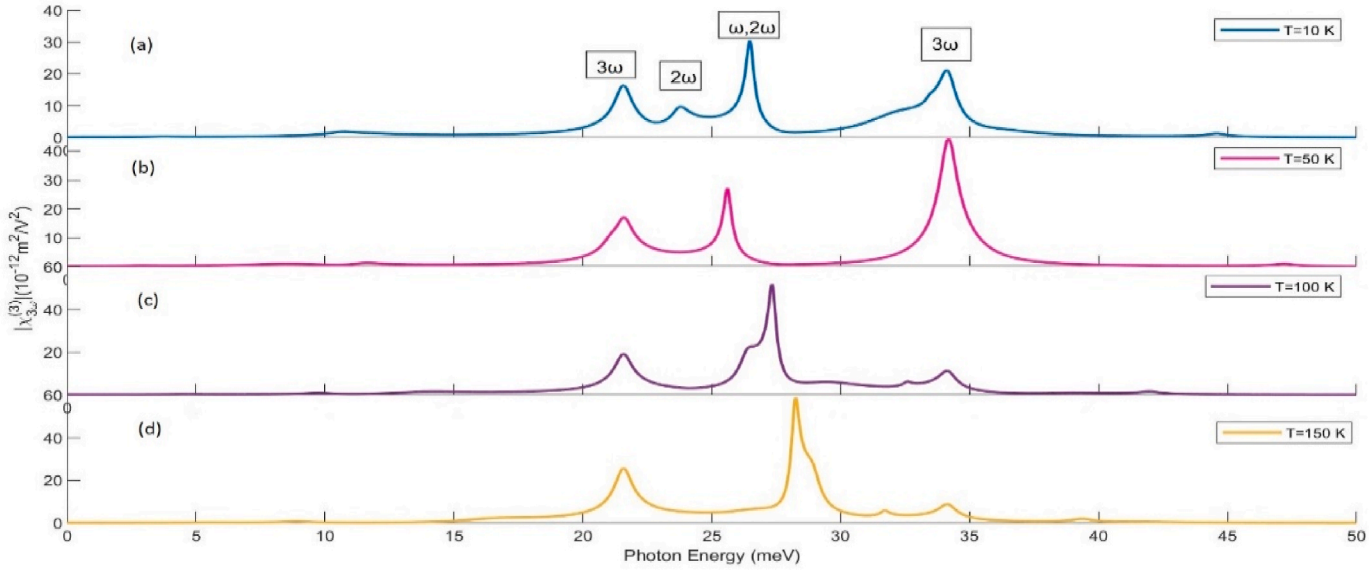

(a)

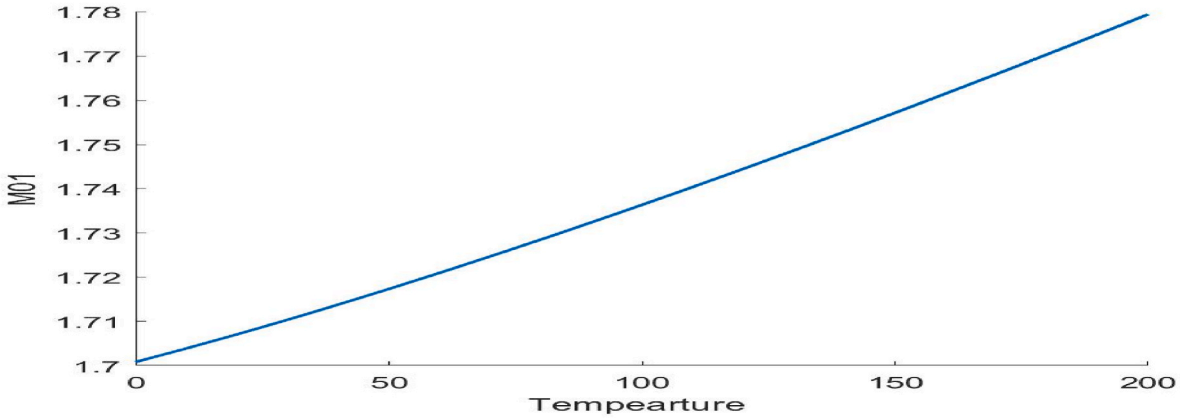

(b)

Fig. 8(a). Coefficient of THG vs incident photon energy for diverse value of Temperature fixing confining potential $\hbar\,\omega = 10$ meV, P = 10 kbar, $\alpha = 10$ meV nm and B = 1 T.

3. Conclusion

A detailed investigation for the THG coefficients for an $In_xGa_{1-x}As$ QD in THz laser field with Rashba SOI with the impact of the magnetic field in the vertical direction is carried out in the present study. To carry out the detailed investigation, energy levels with respective wave functions within the effect. mass approx. is being determined using the variational technique. The variation of THG coefficients vs incident photon energy is explored for various external parameters such as temperature, hydrostatic pressure, confining potential, the magnetic field in the presence of Rashba SOI strength. Results are signifying that with an upsurge in the Rashba SOI coefficient, a strong effect on the THG peak positions is observed. It can also be observed that the two-photon resonance peaks are stronger than three-photon resonance peaks due to an increase in the coupling of levels as the peak height corresponds to the strength of the dipole matrix element. The outcomes are displaying that for the detailed engineering of optical devices based on the QD's, consideration of SOI is a must and optical properties of the optoelectronic devices are controllable using the tunable strength parameter.

Declaration of competing interest

The authors declare that they have no known competing financial interests or personal relationships that could have appeared to influence the work reported in this paper.

Data availability

No data was used for the research described in the article.

Acknowledgement

We acknowledge sincere gratitude to Delhi Technological University to appreciate their help and enhance our services and facilities.

References

[1] S.J. Liang, W. Xie, Eur. Phys. J. B 81 (2011) 79.
[2] H. Hartmann &R. Schuck, Int. J. Quant. Chem. 18 (1980) 125.
[3] I. Zutic, J. Fabian, S. Das Sarma, Rev. Mod. Phys. 76 (2004) 323.

[4] J. Jayabalan, M.P. Singh, K.C. Rustagi, Phys. Rev. B 68 (2003), 075319.
[5] R. Khordad, Opt. Quant. Electron. 46 (2014) 283.
[6] R. Khordad, H. Bahramiyan, Pramana - J. Phys. 88 (2017) 50.
[7] S.A. Wolf, et al., Science 294 (2001) 148.
[8] W. Xie, S. Liang, Physica B 406 (2011) 4657.
[9] R. Khordad, S.K. Khaneghah, M. Masoumi, Superlattice. Microst. 47 (2010) 538.
[10] R. Khordad, Superlattice. Microst. 47 (2010) 422.
[11] G. Rezaei, S. S, Superlattice. Microst. 53 (2013) 99.
[12] B. Gil, P. Lefebvre, P. Boring, Phys. Rev. B 44 (1991) 1942.
[13] R. Khordad, J. Lumin. 134 (2013) 201.
[14] R. Khordad, Int. J. Mod. Phys. B 3 (2017), 1750055.
[15] S. Liang, W. Xie, X. Li, et al., Superlattice. Microst. 49 (2011) 623.
[16] P. Lefebvre, B. Gil, H. Mathieu, Phys. Rev. B 35 (1987) 5630.
[17] R. Khordad, Opt Commun. 391 (2017) 121.
[18] İ. Karabulut, H. Şafak, Physica B 82 (2005) 368.
[19] C.M. Duque, M.E. Mora-Ramos, C.A. Duque, J Nano part Res 13 (2011) 6103.
[20] S. Baskoutas, E. Paspalakis, A.F. Terzis, Phys. Rev. B 74 (2006), 153306.
[21] W. Xie, J. Lumin. 131 (5) (2011) 943.
[22] M. Bass, P.A. Franken, J.F. Ward, G. Weinreich, Phys. Rev. Lett. 9 (11) (1962) 446.
[23] P.A. Franken, A.E. Hill, C.W. Peters, G. Weinreich, Phys. Rev. Lett. 7 (4) (1961) 118.
[24] S. Baskoutas, E. Paspalakis, A.F. Terzis, Phys. Rev. B 74 (2006) 15.
[25] F. Ungan, M.K. Bahar, J.C. Martinez-Orozcoc, M.E. Mora-Ramos, Photonics and Nanostructures - Fundamentals and Applications 41 (2020), 100833.
[26] Xuechao Li, Chaojin Zhang, Superlattice. Microst. 60 (2013) 40.
[27] Manoj Kumar, Sukirti Gumber, Siddhartha Lahon, Pradip Kumar Jha, Man Mohan, Eur. Phys. J. B 87 (2014) 71.
[28] L. Jacak, P. Hawrylak, A. Wojs, Quantum Dots, Springer, Berlin, 1997.
[29] R. Khordad, B. Vaseghi, Chin. J. Phys. 59 (2019) 473.
[30] R. Khordad, H. Bahramiyan, Commun. Theor. Phys. 62 (2014) 283.
[31] Y. Khoshbakht, R. Khordad, Rastegar Sedehi, J. Low Temp. Phys. 202 (2021) 59.
[32] S. Dahiya, S. Lahon, R. Sharma, Physica E 118 (2020), 113918.
[33] R. Khordad, Opt. Quant. Electron. 46 (2014) 283.
[34] S. Dahiya, M. Verma, S. Lahon, R. Sharma, Journal of Atomic, Molecular, Condensed Matter and Nano Physics 5 (1) (2018) 41–53.
[35] R.F. Kopf, M.H. Herman, Lamont Schnoes, M. Perley, A.P. Livescu, G. Ohring, J. Appl. Phys. 71 (1992) 5004–5011.
[36] R. Chaurasiya, S. Dahiya, R. Sharma, IEEE International Conference on Nanoelectronics, Nanophotonics, Nanomaterials, Nanobioscience & Nanotechnology (5NANO), 2022, pp. 1–3.
[37] Zhi-Hai Zhang, Kang-Xian Guo, Bin Chen, Rui-Zhen Wang, Min-Wu Kang, Superlattice. Microst. 46 (2009) 672.
[38] L. Zhang, H.J. Xie, Phys. E 22 (2004) 791.
[39] G.H. Wang, Phys. Rev. B 72 (2005), 155329.
[40] Shuai Shao, Kang Xian Guo, Zhi Hai Zhang, Li Ning, Chao Pen, Solid State Commun. 151 (2011) 589.
[41] Junsaku Nitta, Tatsushi Akazaki, Hideaki Takayanagi, Takatomo Enoki, Phys. Rev. Lett. 78 (1997) 1335.
[42] M. Solaimani, L. Lavaei, S.M.A. Aleomraninejad, 1989, J. Opt. Soc. Am. B 9 (2017) 34.

NANOSYSTEMS:
PHYSICS, CHEMISTRY, MATHEMATICS

Dahiya S., et al. *Nanosystems: Phys. Chem. Math.*, 2024, **15** (5), 1–11.
http://nanojournal.ifmo.ru
DOI 10.17586/2220-8054-2024-15-5-1-11

Original article

Tuning the nonlinear optical properties of a 1D excitonic GaAs quantum dot system under a semi-parabolic potential with a detailed comparison with the experimental results: interplay of hydrostatic pressure and temperature

Suman Dahiya[1], Siddhartha Lahon[2,a], Rinku Sharma[1,b]

[1]Department of Applied Physics, Delhi Technological University, Delhi 110042, India
[2]Physics Department, KMC, University of Delhi, Delhi 110007, India

[a]sid.lahon@gmail.com, [b]rinkusharma@dtu.ac.in

Corresponding author: Siddhartha Lahon, sid.lahon@gmail.com

ABSTRACT The present study is dedicated to study the effect of Temperature and Hydrostatic Pressure on the absorption coefficient and refractive index of one-dimensional semi-parabolic excitonic GaAs QD's by applying the compact density matrix formalism. Calculations are performed to obtain the excitonic state wave functions and energies in the strong confinement regime using the effective mass approximation. A significant dependence of nonlinear optical refractive index and absorption coefficient on hydrostatic pressure and temperature can be observed for excitonic and without excitonic case. Our investigations show that the peaks blue/red shifts are substantial when the excitonic interactions are taken into account. The opposite effects caused by temperature and pressure have substantial practical importance as they extend an alternative approach to tune and control the optical frequencies resulting from the transitions. The comparative analysis of the analytical optical properties of excitonic system facilitates the experimental identification of these transitions which are often close. We have attempted a comparison of the absorption coefficient obtained in the present work with experimental data at $T \cong 10$ and 100 K and found that the theoretical prediction is in agreement for $T \cong 10$ K and it is in slight deviation from the experimental data for higher temperatures. The whole of these conclusions may have broad implications in future designing of Optoelectronic devices.

KEYWORDS nanostructures, quantum dot, exciton, nonlinear effects, hydrostatic pressure, temperature

ACKNOWLEDGEMENTS We acknowledge sincere gratitude to Delhi Technological University to appreciate their help and enhance our services and facilities.

FOR CITATION Dahiya S., Lahon S., Sharma R. Tuning the nonlinear optical properties of a 1D excitonic GaAs quantum dot system under a semi-parabolic potential with a detailed comparison with the experimental results: interplay of hydrostatic pressure and temperature. *Nanosystems: Phys. Chem. Math.*, 2024, **15** (5), 1–11.

1. Introduction

The semiconductor nanomaterials such as quantum dots (QD), quantum wires and quantum wells have many applications in the generation of optoelectronic devices such as lasers, infrared and THz photodetectors, solar cells, biological imaging devices, photovoltaics, LEDs, etc., owing to their enchanting physical properties due to the quantum confinement effects in all spatial directions [1–5]. Out of all these nanostructures, quantum dots of various shapes, sizes and strong confinement of electron and holes have been given special attention as they possess interesting physics in terms of the unique electronic and optical properties. Quasi-zero-dimensional quantum dots can be considered as nano crystalline structures that can provide limitless utility in the implementation of many semiconductors' optoelectronic devices such as quantum dot solar cells, spintronics and ultrafast quantum computers. Accordingly, unprecedented attention has been given to the semiconductor nanomaterials in the last few decades [6–13].

The parabolic and semi parabolic confinement potential can allow various resonances, due to the constant spacing of the discrete energy levels which accounts for the enormous enhancement of the nonlinear optical susceptibilities, optical transitions within the valence and conduction band, and absorption properties [14–17]. Furthermore, the parabolic and semi parabolic potential confinement is more relevant when the zero-dimensional quantum dots are fabricated by using an etching process, ion implantation or electrostatic gates. We have found considerable investigations on the nonlinear optical and electronic properties such as Refractive Index (RI), Absorption Coefficient (AC) and Rectification Coefficient (RC) with photon energy and external factors such as temperature, hydrostatic pressure and dot size [18–20]. For photons having energies equal to that of inter-subband transition energies, host material finds a significant change in dielectric constant, thereby inducing changes in the nonlinear excitonic optical properties [21–24].

Numerous investigations and interesting studies are done on the nonlinear optical properties of nanostructures especially Quantum dots under the influence of external factors such as electric field, magnetic field etc. [21–30]. Many

authors studied the effect of excitons in one dimensional semi parabolic quantum dots [31–34]. Duque et al. studied the effect of external factors such as electric field, magnetic field, hydrostatic pressure, laser field and temperature on nonlinear properties in excitonic system [35–38]. Bejan et al. demonstrated the effect of electric field on the optical properties of a semi parabolic quantum dot in an excitonic system [39]. Kumar et al. further investigated the effect of hydrostatic pressure, temperature and spin on the optical and electronic properties of nanostructures [40,41]. To summarize, the interesting results of the ramifications of external factors such as hydrostatic pressure, temperature, electric field and magnetic field on the nanostructures bring out plethora of novel and exciting physical properties.

The main objective of the present work is to investigate the effect of external factors such as temperature and hydrostatic pressure on the RI and AC of excitonic system in 1D semi parabolic quantum dot. An excitonic system is a bound electron-hole pair with more closely matched effective masses that is formed by the electrostatic interaction between the electron and hole. Theoretically, this system can be related to the hydrogenic system and it possess discrete energies. A 1D QD is principally a nanostructure which can be assumed as a small portion of a 1D QW which is bordered by a two-wall potential. The charge carriers are free to move along the wire in 1-D QW, whereas they are restricted to move along the spatial length in 1D QD [27, 42–45]. The core study undertaken in this research paper focuses on a one-dimensional semi parabolic quantum dot, which is strongly confined in the x and y direction and electrons and holes are confined by a semi parabolic potential along the z direction. We know that the hydrostatic pressure and temperature can alter the nonlinear properties such as the refractive index and absorption coefficient for excitonic effects (EE) as well as without excitonic effect (WEE). In order to keep the study concise and in line with the experimentally available results, we have restricted our studies to the two extreme limits of a temperature range 10 – 100 K where it is observed that the sharpest absorption peaks or transmittance dips are observed at low temperatures in the mentioned range or even lower than that. Furthermore, it is observed that as temperature increases above 100K, the value of the thermal excitation energy of the charge carriers, namely $kT/2$, attains significant values.

In our recent work, we have reported the effect of temperature and hydrostatic pressure on the optical rectification associated with the excitonic system in a semi-parabolic quantum dot [46]. It is highlighted that most available literature reports are primarily based on the nonlinear optical properties due to impurities or due to different shape of quantum structures. To our sincere understanding, there are no studies available where the hydrostatic pressure and temperature effects on the nonlinear optical properties of excitonic system in one dimensional semi parabolic quantum dots have been studied and explained. The present paper is structured as follows: In the next section, theoretical analytical framework is presented to calculate the eigen energies, eigen functions and optical properties for the excitonic system. In the Results and Discussion section, we have presented our numerical results and discussion. In the last section of conclusion, we have summarized our results.

2. Theory and model

A theoretical model of the system taken is presented in Fig. 1. Here, the gate voltage in the model is used to control Rashba spin-orbit interaction (SOI) where the effects of SOI are studied. In our case, we have kept the gate voltage to be Zero. The x-direction is kept to be very small i.e., about 2nm so that the charge carriers behave as a 2D charge carrier gas. The y-length of the wire is in μm-range, so the charge carrier exhibit e^{-ky} wave function. The z-directions breadth is determined by the potential strength and in our case, the effective z-length turns out to be 5 nm. Now, moving towards the mathematical calculations related to the system.

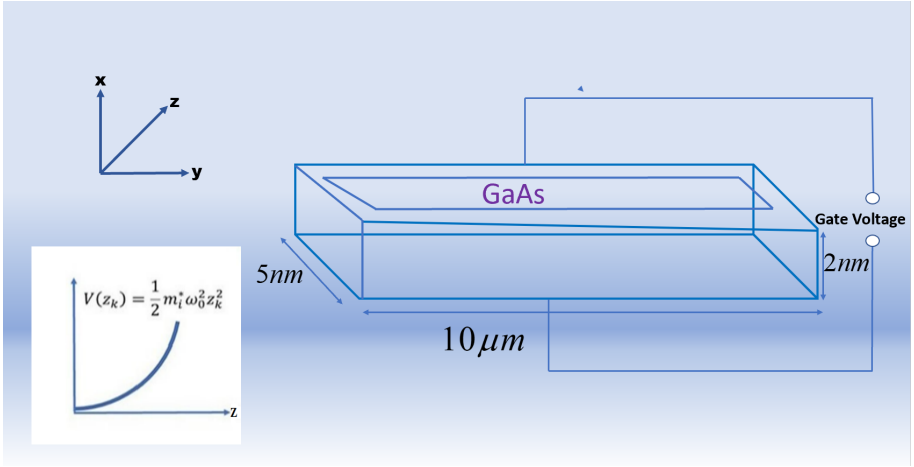

FIG. 1. Schematic diagram of GaAs Quantum Dot

Hamiltonian for a 1D excitonic QD having semi-parabolic confining potential within the framework of effective mass approximation can be written as [25, 27, 31, 42]:

$$H_e = \frac{p_h^2}{2m_h^*(P,T)} + \frac{p_e^2}{2m_e^*(P,T)} + V(z_e) + V(z_h) - \frac{e^2}{\varepsilon\,|z_e - z_h|}, \tag{1}$$

where $z_e, z_h > 0$.

Here m_h^* and m_e^* represents the effective mass of hole and electron, respectively, ε represents the background dielectric constant and the last term represents the electrostatic Coulomb interaction term between the electron and the hole. The semi-parabolic confinement potential $V(z_k)$ is written as:

$$V(z_k) = \begin{cases} \frac{1}{2} m_i^* \omega_0^2 z_k^2, & z_k \geq 0; \\ \infty, & z_k \leq 0 \quad (k = e, h). \end{cases} \tag{2}$$

The temperature and hydrostatic pressure dependent effective mass of the electron for GaAs is given as [38, 40, 41]:

$$m_e^*(P,T) = m_o \left[1 + \frac{7510}{E_g(P,T) + 341} + \frac{15020}{E_g(P,T)}\right]^{-1}, \tag{3a}$$

$$m_h^*(P,T) = \left(0.09 - 0.20 \cdot 10^{-3} P - 3.55 \cdot 10^{-5} T\right) m_0, \tag{3b}$$

with

$$E_g(P,T) = \left[1519 - \frac{0.5405 T^2}{T + 204} + 10.7P\right]. \tag{4}$$

Here temperature and hydrostatic pressure dependent energy gap GaAs, E_g is in meV, P is in "kbar" and T is in "Kelvin". The pressure dependent oscillator frequency is expressed as

$$\omega(P) = \omega_0 / \left[1 - 2P(1.16 \cdot 10^{-3} - 7.4 \cdot 10^{-4})\right]. \tag{5}$$

The Hamiltonian is segmented into two terms taking the relative motion and the center of mass into consideration and is given by:

$$H_{e1} = H_{r1} + H_{c1}, \tag{6}$$

$$H_{r1} = \frac{p^2}{2\mu} + \frac{1}{2}\mu\omega_0^2 z_{r1}^2 - \frac{e^2}{\varepsilon(P,T)\,|z_{r1}|}, \tag{7}$$

$$H_{c1} = \frac{P^2}{2M_{T1}} + \frac{1}{2} M_{T1} \omega_0^2 Z_{T1}^2. \tag{8}$$

For $T < 200$, the dielectric constant of GaAs is [38–40]:

$$\varepsilon(P,T) = 12.74 e^{(9.4 \cdot 10^{-5})(T - 75.6) + 1.73 \cdot 10^{-3} P}. \tag{9}$$

The coordinate of the centre of mass is written as:

$$Z_{T1} = \frac{m_h^*(P,T) z_h + m_e^*(P,T) z_e}{M_{T1}}. \tag{10}$$

Here, total mass is $M_{T1}(P,T) = m_h^*(P,T) + m_e^*(P,T)$; the relative coordinate is $z_{r1} = z_e - z_h$, the momentum operator is $p_{Z_{T1}} = \frac{\hbar}{i}\nabla_{Z_{T1}}$, and the reduced mass is

$$\mu_{r1} = m_h^*(P,T) m_e^*(P,T) / M_{T1}(P,T). \tag{11}$$

The excitonic wave function and energy levels are written as

$$\psi_{f1}(z_h, z_e) = \phi(z_{r1}) \varphi(Z_{T1}), \tag{12}$$

$$E_{T1} = E_{z_{r1}} + E_{Z_{T1}}. \tag{13}$$

The term signifying the center of mass part is considered as the problem for 1D semi-parabolic oscillator where the Hamiltonian is H_{c1} and eigenfunction and eigenenergies are [42]:

$$\varphi_{k1}(Z_{T1}) = N_{k1} \exp\left(-\frac{1}{2}\alpha^2 Z_{T1}^2\right) H_{2k1+1}(\alpha Z_{T1}), \tag{14}$$

$$E_{k1} = \left(2k1 + \frac{3}{2}\right)\hbar\omega_0, \quad k1 = (0, 1, 2.....), \tag{15}$$

where H_{2k1+1} is the Hermite polynomial

$$N_{k1} = \left[\frac{1}{\alpha}\sqrt{\pi} 2^{2k1} (2k1 + 1)!\right]^{-1/2}, \tag{16}$$

$$\alpha = \sqrt{M_{T1}\omega(P)/\hbar_k}. \tag{17}$$

We analytically obtained the eigenvalues and wave function of the relative motion part in the strong and weak confinement regime. For the strong regime, H_{r1} reduces to:

$$H_{r1s} = \frac{p^2}{2\mu} + \frac{1}{2}\mu\omega_0^2 z_{r1}^2. \tag{18}$$

Neglecting the coulomb term as per the strong confinement regime, $\varphi(z_{r1})$ is determined as:

$$\phi(z_{r1}) = N_n \exp\left[-\frac{1}{2}\beta^2 z_{r1}^2\right] H_{2n+1}(\beta z_{r1}), \tag{19}$$

$$E_{y1} = \left(2n + \frac{3}{2}\right)\hbar\omega_0, \quad (y1 = 0, 1, 2, ...), \tag{20}$$

$$N_n = \left[\frac{1}{\beta}\sqrt{\pi}2^{2n1}(2n+1)!\right]^{-1/2}, \tag{21}$$

$$\beta = \sqrt{\mu\omega(P)/\hbar}. \tag{22}$$

Our quantum dot interacts with the electromagnetic field $E(t)$ having a frequency ω, such that [47–49]:

$$E(t) = Ee^{i\omega t} + E^* e^{-i\omega t}. \tag{23}$$

Upon such interactions, the time evolution equation for the matrix elements of one-electron density operator, ρ, is given by

$$\frac{\partial\rho}{\partial t} = \frac{1}{i\hbar}\left[H_0 - qxE(t)\rho\right] - \Gamma(\rho - \rho^{(0)}), \tag{24}$$

where H_0 represents the Hamiltonian of this system in the absence of the electromagnetic field $E(t)$, and electronic charge is given by q, unperturbed density matrix operator is ρ^0, and Γ is the phenomenological operator responsible for the damping due to the electron-phonon interaction, collisions among electrons, etc. It is assumed that Γ is a diagonal matrix and its elements are equal to the inverse of relaxation time τ_0.

For solving Eq. (19), standard iterative method is being used and hence ρ has been expanded as $\rho(t) = \sum_n \rho^{(n)}(t)$. Now, using this expansion in Eq. (19), the density matrix elements can be obtained as shown below:

$$\frac{\partial\rho_{ij}^{(n+1)}}{\partial t} = \left[\frac{1}{i\hbar}[H_0, \rho^{(n+1)}]_{ij} - \Gamma_{ij}\rho_{ij}^{(n+1)} - \frac{1}{i\hbar}[qx, \rho^{(n)}]_{ij}E(t)\right]. \tag{25}$$

As the density matrix ρ has been obtained, the electronic polarization $P(t)$ and susceptibility $\chi(t)$ can be calculated as:

$$P(t) = \varepsilon_o\chi(\omega)Ee^{-i\omega t} + \varepsilon_o\chi(-\omega)Ee^{-i\omega t} = \frac{1}{V}\,\mathrm{Tr}(\rho M), \tag{26}$$

where ρ is the density matrix for one electron and V is the volume of the system, ε_0 represents permittivity of free space, and the symbol Tr (trace) denotes the summation over the diagonal elements of the matrix.

Now, using the real part of the susceptibility, refractive index changes can be determined as:

$$\frac{\Delta n(\omega)}{n_r} = \mathrm{Re}\left[\frac{\chi(\omega)}{2n_r^2}\right]. \tag{27}$$

Within a two-level system approach, the linear and the third order nonlinear optical absorption coefficient are obtained from the imaginary part of the susceptibility [25, 34, 45–51] as:

$$\alpha^{(1)}(\omega) = \omega\sqrt{\frac{\mu}{\varepsilon_r}}\frac{|M_{01}|^2 N\hbar\Gamma_0}{[(E_{10} - \hbar\omega)^2 + (\hbar\Gamma_0)]^2}, \tag{28}$$

$$\alpha^{(3,I)}(\omega) = -2\omega\sqrt{\frac{\mu}{\varepsilon_r}}\left(\frac{I}{\varepsilon_0\eta_r c}\right)\frac{|M_{01}|^4 N\hbar\Gamma_0}{\left[(E_{10} - \hbar\omega)^2 + (\hbar\Gamma_0)\right]^2} \times\left(1 - \frac{|M_{11} - M_{00}|^2}{4\,|M_{01}|^2}\left\{\frac{(E_{10} - \hbar\omega)^2 - (\hbar\Gamma_0)^2 + 2E_{10}(E_{10} - \hbar\omega)}{(E_{10})^2 + (\hbar\Gamma_0)^2}\right\}\right). \tag{29}$$

Total absorption coefficient $\alpha(\omega, I)$ is given as:

$$\alpha(\omega, I) = \alpha^{(1)}(\omega) + \alpha^{(3,I)}(\omega). \tag{30}$$

The linear and nonlinear changes in the refractive index are written as [25, 30, 46–54]:

$$\frac{\Delta\eta^{(1)}(\omega)}{\eta_r} = \frac{1}{2\eta_r^2\varepsilon_{\partial 0}}\,|M_{01}|^2\left[\frac{E_{10} - \hbar\omega}{(E_{10} - \hbar\omega)^2 + (\hbar\Gamma_0)^2}\right], \tag{31}$$

$$\frac{\Delta\eta^{(3,I)}(\omega,I)}{\eta_r} = -\frac{\mu c}{4\eta_r^3\varepsilon_{\partial 0}}\left|M_{01}\right|^2\left[\frac{NI}{[(E_{10}-\hbar\omega)^2+(\hbar\Gamma_0)^2]^2}\right] \times\left[4(E_{10}-\hbar\omega)\left|M_{01}\right|^2-\frac{\left|M_{11}-M_{00}\right|^2}{(E_{10})^2+(\hbar\Gamma_0)^2}\left\{E_{10}(E_{10}-\hbar\omega)\times-(\hbar\Gamma_0)^2(2E_{10}-\hbar\omega)\right\}\right]. \quad (32)$$

The total refractive index change is

$$\frac{\Delta\eta(\omega,I)}{\eta_r} = \frac{\Delta\eta^{(1)}(\omega)}{\eta_r} + \frac{\Delta\eta^{(3,I)}(\omega,I)}{\eta_r}, \quad (33)$$

where $\mu_{ij} = |\langle\psi_i|z_{T1}|\psi_j\rangle|$, $(i,j=0,1)$ are the matrix elements of the dipole moment, $\psi_i(\psi_j)$ are the eigenfunctions, $\omega_{01} = \dfrac{E_1-E_0}{\hbar}$ is the difference between two energy levels, is the frequency of the electromagnetic field, τ_0 is the relaxation time.

3. Results and discussions

We have considered the GaAs semiconductor material constants for our numerical results. We used the numerical parameters such as [38, 40–44] $m_e^* = 0.067m_0$, $m_h^* = 0.09m_0$ (m_0 is the mass of a free electron), $N = 3\cdot10^{22}$ m^{-3}, $\varepsilon = 12.53$, $\tau_0 = 0.2$ ps^{-1}, $I = 2000$ MW/m^2.

To understand the effect of change in hydrostatic pressure and temperature on the Linear Absorption Coefficient (LAC) and third order (Nonlinear) Absorption coefficient (NAC), we present the same in Fig. 2(a) and 2(b). Here we also have shown the effects of inclusion of Excitonic Effects (EE) on the LAC and NAC. One can observe that for the cases where (2(a) and 2(b)) the EE is not included, the NAC and LAC peaks occurred at photon energies much lower than the cases of inclusion of EE in the study. This is attributed to the energy associated with the excitonic interactions between the electron and holes. Moreover, the peak heights, for both LAC and Total Absorption Coefficient (TAC), increased when excitonic effects are taken into account. This is a consequence of enhancement of the dipole moment due to the positive-negative charge separation of the electron-hole pair, which otherwise is not there in the case of Without Excitonic Effects (WEE). In Fig. 2(a), shift from 60.28 to 56.70 meV when pressure is increased from 10 to 100 kbar in case of WEE. Whereas for identical change in pressure, the LAC and NAC peaks are shifted from 91.78 to 88.58 meV for the case of EE. This shifting is accompanied by decrease in absorption LAC peak height from $0.35\cdot10^5$ to $0.32\cdot10^5$ m^{-1} in case of WEE and from $0.80\cdot10^5$ to $0.72\cdot10^5$ m^{-1} for the EE case. Similar effects are also observed for the NAC. The LAC and NAC shift towards the lower energy end of the spectrum as the pressure increases. This shifting is accompanied by a diminishing absorption peak height for both EE and WEE case. These effects are due to the counter affecting action of pressure on the confinement potential and energy band gap. The pressure increases the confinement strength but it also strongly alters the energy band gap. For GaAs, in the pressure range of 10 kbar to 100 bar, these two opposing effects results in a net red shift of the peaks as the pressure increases. Whereas, in Fig. 2(b), one can see that the absorption peaks, LAC and NAC, moves from 60.28 to 62.40 meV and peak heights of LAC increase from $0.35\cdot10^5$ to $0.39\cdot10^5$ m^{-1} and NAC changes from $-0.062\cdot10^5$ to $-0.066\cdot10^5$ m^{-1} when the temperature increases from 10 to 100 K, keeping $P = 10$ kbar. For the case of EE, the blue shift in peaks happen from 91.7 to 94.39 meV and the LAC peak heights change from $0.80\cdot10^5$ to $0.85\cdot10^5$ m^{-1} and the NAC peak enhances from $-0.13\cdot10^5$ to $-0.17\cdot10^5$ m^{-1} as the temperature increases from 10 to 100 K. These effects, similar in nature for both EE and WEE, result from the interplay complex second term of Eq. (5) and the direct dependence of on the temperature. Physically, the change in the entropy of the charge carriers induces a change in the energy of the states. In Fig. 3(a,b), we present the TAC as a function of incoming photon energy. Here, we observe similar effects of change in pressure and temperature on the TAC peaks as in the case of LAC and NAC. However, in TAC, the effects of LAC dominate the NAC for the light intensity of 2000 MW/m^2. Furthermore, owing to the diametrically opposed behavior of the first and the third-order nonlinear ACs, a decrease in the total ACs is observed due to the reduction in the effective mass of the electron with the intensification of the temperature. A close relationship between the peak values of the total ACs, the transition dipole element and the difference between energy levels E_{10} can be disclosed from the figure. Total ACs is influenced in opposite by the dipole matrix element $|M_{10}|^2$ to that of the energy difference E_{10}. Hence, a blue shift is observed as a result of increase in the temperature and the red shift is observed when the pressure increases. This happens due to increase/decrease in the transition energy E_{10} on a significant increase in temperature/pressure. Upon increasing temperature/pressure, a drop/enhancement in the electron effective mass with an expansion/compression of the transition energy is observed due to the dependence of the electron-photon interaction of the temperature/pressure. Hence, the blue/red shift is observed. Same can be observed from Fig. 2(c,d) that how matrix elements get vary with pressure and temperature.

To compare our results in Fig. 3(b), we plotted the total absorption coefficient and compared with experimental data [55, 56] at $T \cong 10$ and 100 K. As it can be observed from the graph, a similar pattern is observed in both the experimental results as well as theoretical results but deviation can be observed in the theoretical prediction from the experimental data [55, 56]. At $T = 10$ K, the quantitative value is similar to the experimental value but this is not the same for the $T = 100$ K. Although, it can be observed from both experimental values as well as theoretical values that a

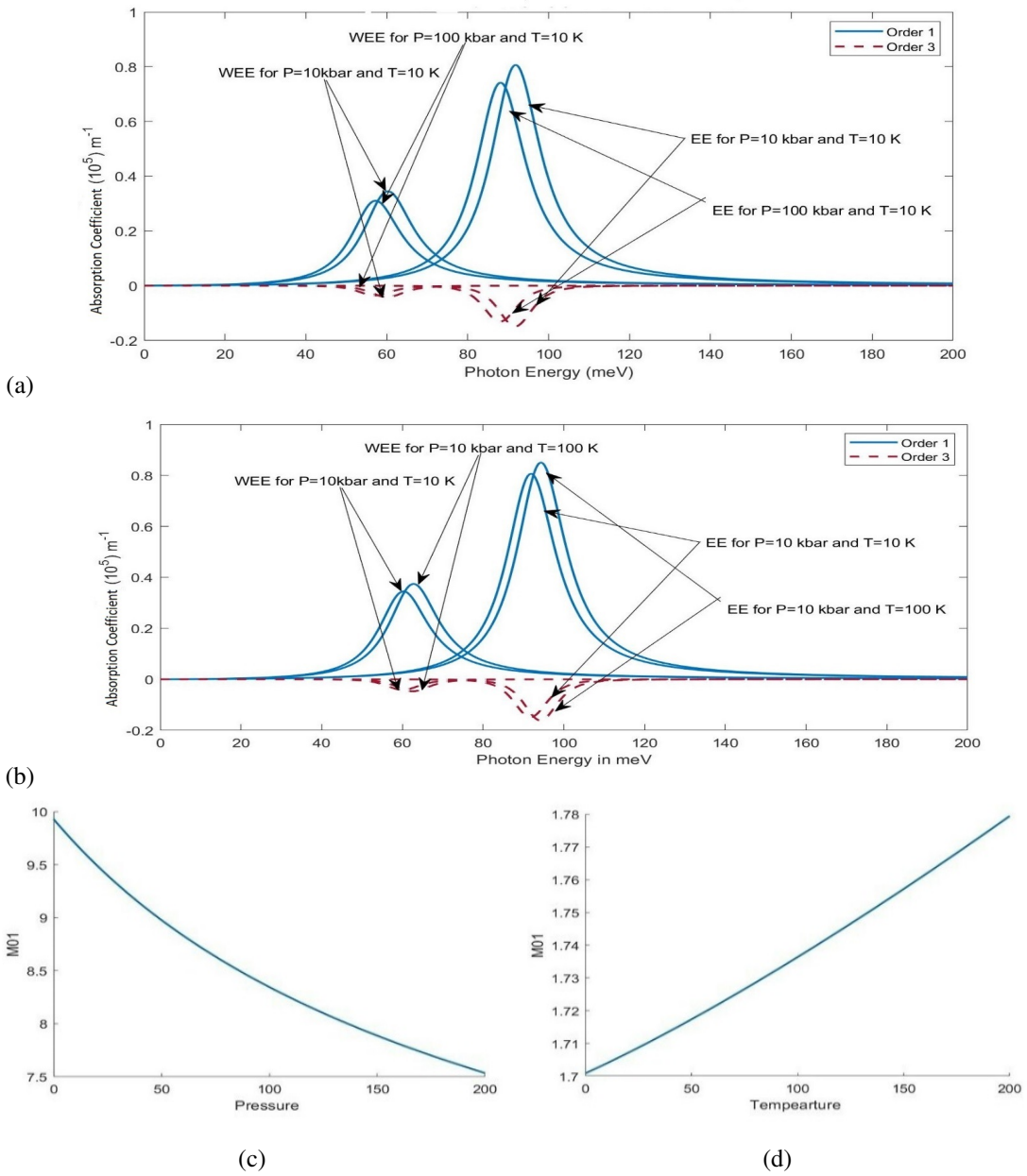

FIG. 2. (a,b) – the linear and nonlinear absorption coefficients with and without considering excitonic (EE and WEE) effects for $T = 10$ and 100 K and $P = 10$ kbar and $P = 100$ kbar and $I = 2000$ MWm^2; (c,d) – behavior of matrix element with pressure and temperature

blue shift is happening in the absorption coefficient on increasing the temperature. For example, for temperature between 0 – 20 and 40 – 100 K peaks shift towards higher energy values for the both cases, i.e., theoretical and experimental. But as there was no significant difference between the peaks ranging from 21 – 90 K, hence, only values for 20 and 100 K have been presented in the theoretical graphs. Several points can be thought of as a cause for this deviation in the quantitative value. Some of these points are: (i) electronic transitions are not perfectly exact for the two-level system, (ii) several parameters such as dot size, intensity, σ, υ are temperature dependent but are here considered as temperature independent, (iii) calculations have been performed theoretically using numerical methods and these methods have some limitations, (iv) approximation have been taken into account for solving the Eqs. (23–27).

As the interacting light changes the physical nature of the quantum dot material, it, therefore induces drastic changes in the refractive index of the QDs near the resonance energy. The same can be observed from the dispersion curves presented in Fig. 4(a,b) and 4(c,d). In 4(a), for WEE and hydrostatic pressure of 10 kbar, the dispersion curve of Linear Refractive Index change (LRI) rises to a maximum value 0.062 at photon energy 60.28 meV and crosses over to the negative polarity region to reach -0.063 at photon energy 74.40 meV. When the pressure increases to 100 kbar, this dispersion area shifts to 56.70 meV (maxima of 0.059) and 64.86 meV (minima of -0.059). Further, in 4(a), for pressure of 10 kbar, when EE is taken into account the area of polarity change of the LRI shifts to higher photon energy, viz. reaches

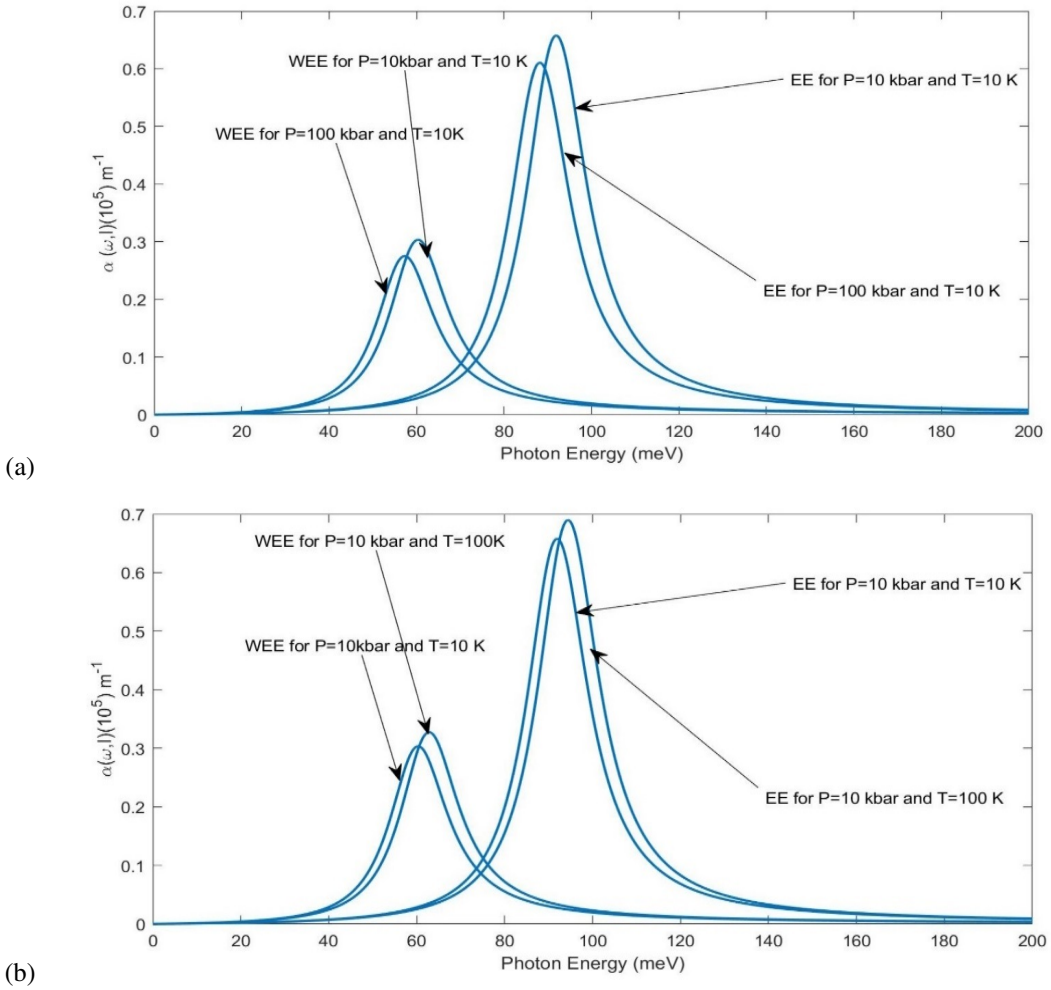

FIG. 3. Total absorption coefficients with and without considering excitonic (EE & WEE) effects for $T = 10$ & 100 K and $P = 10$ & $P = 100$ kbar and $I = 2000$ MWm^{-2}

maximum at photon energy 91.7 meV (maxima of 0.088) and crosses over to the negative values to reach the minimum value at 106.33 meV (minima of -0.088). Again, for EE case, when pressure increases to 100 kbar, the dispersion area red shifts to 88.58 meV (maxima 0.085) and 103.48 meV (minima -0.086). Similar effects are observed (Fig. 4(b)) for Nonlinear Refractive Index change (NRI) at the identical photon energies as in the case of LRI. However, in case of NRI, the polarity of the refractive index change first reaches a negative valued minima and then crosses over to a positive valued maximum. Opposite nature of shifting of the dispersion is observed when the temperature is changed from 10 to 100 K keeping $P = 10$ kbar (Fig. 4(c,d)). In Fig. 4(c), it is obtained that the maximum value of the LRI (minimum value of NRI in Fig. 4(d)) occurs at photon energy 60.28 meV (maxima of 0.062) when the temperature is kept at 10 K for the case of WEE. When the temperature increases to 100 K, in case of WEE, the maximum value of the LRI (minimum of NRI, Fig. 4(d)) shifts to a higher photon energy value of 62.40 meV. Whereas for the case of EE, the LRI (and NRI) maximum value (minima for NRI) shifts from 91.7 to 94.39 meV when the temperature increases to 100 from 10 K. These two-opposite natures of influences on the RI change of hydrostatic pressure and temperature are attributed to the fact that the increase in pressure strengthens the confinement whereas the temperature acts the other way.

In Fig. 5(a,b), the total refractive index change is presented at two values of applied hydrostatic pressure (5a) keeping $T = 10$ K and in (5b), the temperature is varied from 10 to 100 K keeping $P = 10$ kbar. It can be observed that the magnitude of the change in refractive index with variation in hydrostatic pressure and temperature are different on the two scenarios, i.e., one with the excitonic effect and the other without excitonic effects. This is the consequence of the fact that in case of WEE, the properties are determined by the effective mass of the electron whereas in case of EE, the properties are manifested from the reduced mass of the electron-hole pair. This is one of the major factors for variation in the optical properties in between EE and WEE, in addition to the fact of opposite polarity charges being involved in the case of EE.

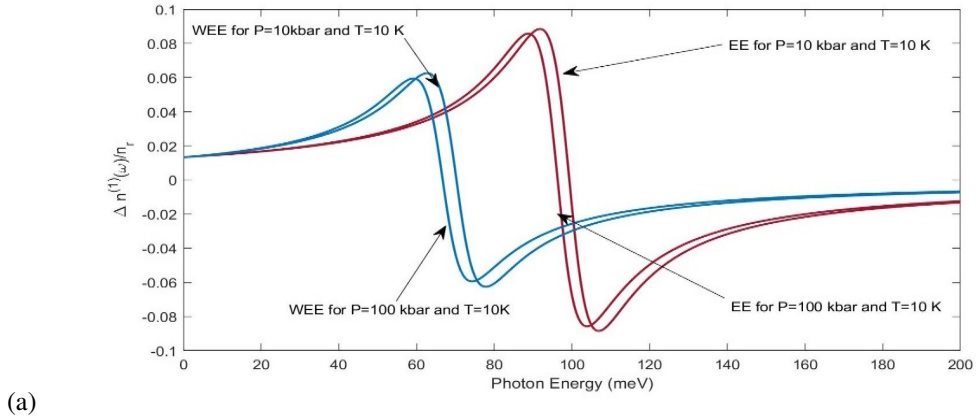

(a)

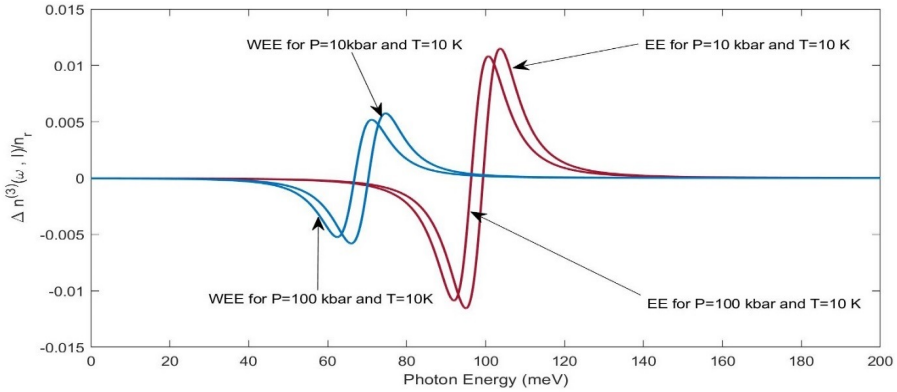

(b)

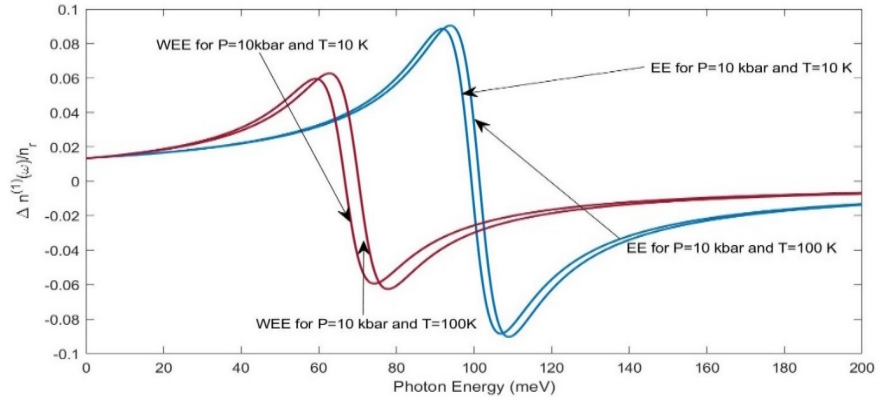

(c)

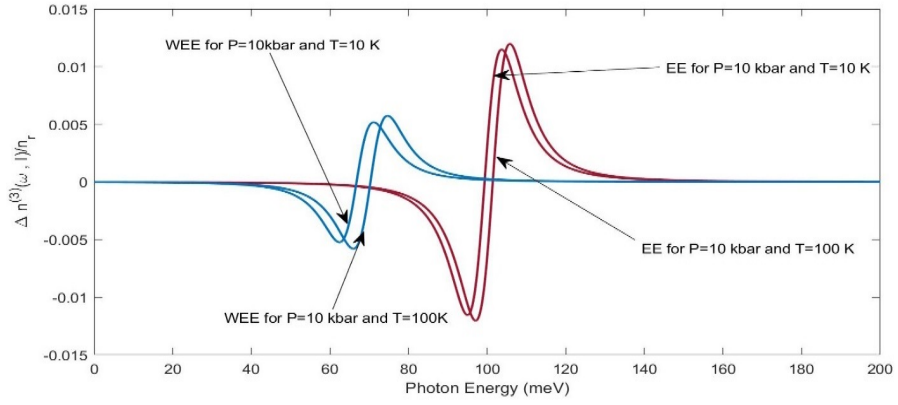

(d)

FIG. 4. Schematic diagram of GaAs Quantum Dot.The linear and nonlinear refractive index for with and without considering excitonic (EE & WEE) effects for $T = 10$ and 100 K and $P = 10$ kbar and $P = 100$ kbar and $I = 2000$ MWm^{-2}

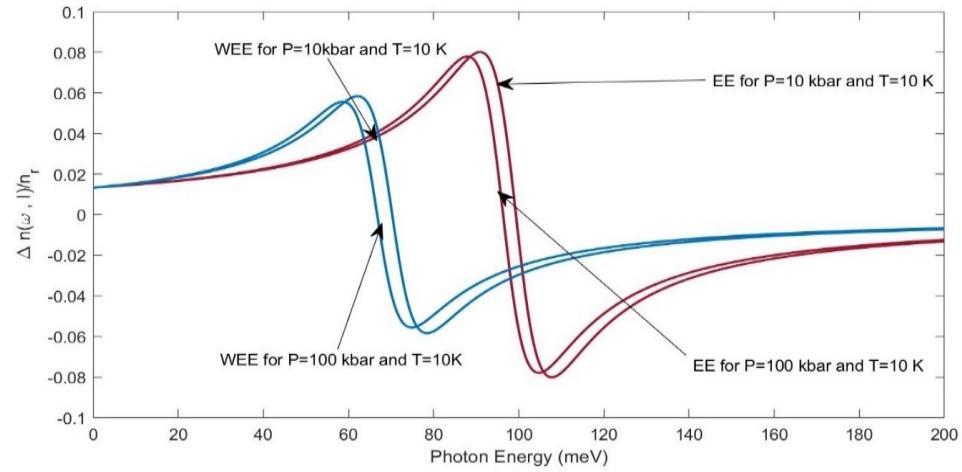

(a)

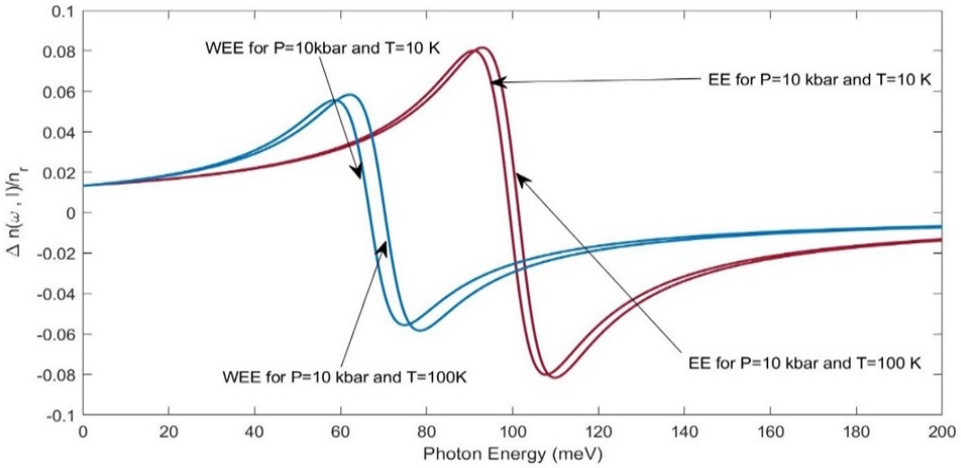

(b)

FIG. 5. The total refractive index for with and without considering excitonic (EE and WEE) effects for $T = 10$ and 100 K and $P = 10$ kbar and $P = 100$ kbar and $I = 2000$ MWm^{-2}

4. Conclusion

We have reported the linear and nonlinear optical properties, viz. absorption coefficient and refractive index of a GaAs semi-parabolic QD by employing the compact density matrix formalism. We have demonstrated that the absorption coefficient peaks and refractive index dispersion variation is blue shifted with the inclusion of excitonic effects. The increase in the pressure alters the optical properties of the QD by controlling the effective mass of electron, energy band gap and the dielectric constant. This intricate counter-balancing act results in a red shift in the nonlinear optical properties' resonance position when the applied hydrostatic pressure is incremented, while augmenting the ambient temperature results in blue shifts of the LAC, NAC and TAC and refractive index change. Further, it is observed that the enhancing the pressure lowers the peak height of the absorption coefficient and the refractive index dispersions curves. This is due to the diminishing of dipole moments of the QD by the reinforcing the confinement by the hydrostatic pressure which results in shrinking of the orbital wave functions. To our best knowledge no such research work illustrating the effects of Hydrostatic Pressure and Temperature on the RI and AC (Linear and third order) of GaAs QD for a semi-parabolic system (excitonic as well as non-excitonic cases) has been carried out earlier. According to our consideration, the obtained results can have important practical applications in fabricating optoelectronic devices and hence have a sound share in progressive product technology. The shifting of absorption peaks can specially be used in devices where optical switches can be turned on and off depending on absorption of incident radiation. Hydrostatic pressure and temperature can act as external parameters. Further, the same property may also be used to detect changes in temperature and pressure by observing the refractive index change and absorption of photons at particular wavelength. Analysis of the experimental results [55, 56] and comparing with the theoretical results obtained, some disagreement is observed in the absorption coefficients. This variation with the experimental results is explained in the previous section.

References

[1] Jamieson T., Bakhshi R., Petrova D., Pocock R., Imani M., Seifalian A.M. Biological applications of quantum dots. *Biomaterials*, 2007, **28** (31), P. 4717–4732.

[2] Salata O. Applications of nanoparticles in biology and medicine. *J. Nanobiotechnol.*, 2004 **2** (1), 3.

[3] Mocatta D., Cohen G., Schattner J., Millo O., Rabani E., Banin U. Heavily doped semiconductor nanocrystal quantum dots. *Science*, 2011, **332** (6025), P. 77–81.

[4] Koenraad P.M, Flatté M.E. Single dopants in semiconductors. *Nat. Mater.*, 2011, **10**, P. 91–100.

[5] Aghoutane N., Pérez L.M., Tiutiunnyk A., Laroze D., Baskoutas S., Dujardin F., Fatimy A.E., El-Yadri M., Feddi E.M. Adjustment of Terahertz Properties Assigned to the First Lowest Transition of (D+, X) Excitonic Complex in a Single Spherical Quantum Dot Using Temperature and Pressure. *Applied Sciences*, 2021, **11** (13), 5969.

[6] Schneider H., Fuchs F., Dischler B., Ralston J.D., Koidl P. Intersubband absorption and infrared photodetection at 3.5 and 4.2 μm in GaAs quantum wells. *Appl. Phys. Lett.*, 1991, **58**, P. 2234–2236.

[7] Ferry D.K., Goodnick S.M. *Transport in Nanostructures*. Cambridge University Press, Cambridge, 1997.

[8] Sarkisyan H.A. Direct optical absorption in cylindrical quantum dot. *Mod. Phys. Lett. B*, 2004, **18** (10), P. 443–452.

[9] Saravanamoorthy S.N., John Peter A., Lee C.W. Optical peak gain in a PbSe/CdSe core-shell quantum dot in the presence of magnetic field for mid-infrared laser applications. *Chem. Phys.*, 2017, **483–484**, P. 1–6.

[10] Bera A., Ghosh M. Dipole moment and polarizability of impurity doped quantum dots driven by noise: Influence of hydrostatic pressure and temperature. *Physica B*, 2017, **515**, P. 18–22.

[11] Schaller R.D., Klimov V.I. High Efficiency Carrier Multiplication in PbSe Nanocrystals: Implications for Solar Energy Conversion. *Phys. Rev. Lett.*, 2004, **92** (18), 186601.

[12] Huynh W.U., Dittmer J.J., Alivisatos A.P. Hybrid nanorod-polymer solar cells. *Science*, 2002, **295** (5564), P. 2425–2427.

[13] Zhong X., Xie R., Basche Y., Zhang T., Knoll W. High-Quality Violet- to Red-Emitting ZnSe/CdSe Core/Shell Nanocrystals. *Chem. Mater., Chem. Mater.*, 2005, **17** (16), P. 4038–4042.

[14] Ungan F., Mart´ınez-Orozco J.C., Restrepo R.L., Mora-Ramos M.E., Kasapoglu E., Duque C.A. Nonlinear optical rectification and second-harmonic generation in a semi-parabolic quantum well under intense laser field: Effects of electric and magnetic fields. *Superlattice Microstruct.*, 2015, **81**, 26.

[15] Karimi M.J., Rezaei G. Effects of external electric and magnetic fields on the linear and nonlinear intersubband optical properties of finite semi-parabolic quantum dots. *Physica B*, 2011, **406**, 4423.

[16] Fl´orez J., Camacho A. Excitonic effects on the second-order nonlinear optical properties of semi-spherical quantum dots. *Nanoscale Res. Lett.*, 2011, **6**, 268.

[17] Cristea M. Comparative study of the exciton states in CdSe/ZnS core-shell quantum dots under applied electric fields with and without permanent electric dipole moment. *Eur. Phys. J. Plus*, 2016, **131**, 86.

[18] Chaurasiya R., Dahiya S., Sharma R. A study of confined Stark effect, hydrostatic pressure and temperature on nonlinear optical properties in 1D GaxAl1-xAs/GaAs/GaxAl1-xAs quantum dots under a finite square well potential. *Nanosystems: Phys. Chem. Math.*, 2023, **14** (1), P. 44–53.

[19] Eseanu N. Simultaneous effects of laser field and hydrostatic pressure on the intersubband transitions in square and parabolic quantum wells. *Phys. Lett. A*, 2010, **374**, 1278.

[20] Rezaei G., Karimi M.J., Keshavarz A. Excitonic effects on the nonlinear intersubband optical properties of a semi-parabolic one-dimensional quantum dot. *Physica E*, 2010, **43**, 475.

[21] Yuan H.J., Zhang Y., Mo H., Chen N., Zhang Z.-H. Electric field effect on the second-order nonlinear optical properties in semiparabolic quantum wells. *Physica E*, 2016, **77**, 102.

[22] Karabulut I., Safak H., Tomak M. Nonlinear optical rectification in asymmetrical semiparabolic quantum wells. *Solid State Commun.*, 2005, **135**, 735.

[23] Bautista J.E., Lyra M.L., Lima R.P.A. Screening effect on the exciton mediated nonlinear optical susceptibility of semiconductor quantum dots. *Photon. Nanostruct.*, 2013, **11**, 8.

[24] Paspalakis E., Boviatsis J., Baskoutas S. Effects of probe field intensity in nonlinear optical processes in asymmetric semiconductor quantum dots. *J. Appl. Phys.*, 2013, **114**, 153107.

[25] Karabulut I., Safak H., Tomak M. Excitonic effects on the nonlinear optical properties of small quantum dots. *J. Phys. D: Appl. Phys.*, 2008, **41**, 155104.

[26] Baghramyan H.M., Barseghyan M.G., Kirakosyan A.A., Restrepo R.L., Duque C.A. Linear and nonlinear optical absorption coefficients in GaAs/$Ga_{1-x}Al_x$As concentric double quantum rings: Effects of hydrostatic pressure and aluminum concentration. *J. Lumin.*, 2013, **134**, P. 594–599.

[27] Gambhir M., Varsha, Prasad V. Pressure- and temperature-dependent EIT studies in a parabolic quantum dot coupled with excitonic effects in a static magnetic field. *Pramana – J. Phys.*, 2022, **96**, 81.

[28] Gambhir M., Kumar P., Kumar T. Investigation of linear and third-order nonlinear optical properties in a laser-dressed parabolic quantum dot with a hydrogenic donor impurity in the presence of a static electric field. *Indian J. Phys.*, 2023, **97**, P. 2169–2178.

[29] Zhang L., Li X., Zhao Z. The influence of optical absorption under the external electric field and magnetic field of parabolic quantum dots. *Indian J. Phys.*, 2022, **96**, P. 3645–3650.

[30] Duan Y., Li X., Chang C. Effects of Magnetic Field on Nonlinear Optical Absorption in Quantum Dots Under Parabolic-Inverse Squared Plus Modified Gaussian Potential. *Braz. J. Phys.*, 2022, **52**, 123.

[31] Yu Y.-B., Zhu S.-N., Guo K.-X. Exciton effects on the nonlinear optical rectification in one-dimensional quantum dots. *Phys. Lett. A*, 2005, **175**, 335.

[32] Karabulut İ., Şafak H. Nonlinear optical rectification in semiparabolic quantum wells with an applied electric field. *Physica B*, 2005, **82**, 368.

[33] Duque C.M., Mora-Ramos M.E., Duque C.A. Simultaneous effects of electron-hole correlation, hydrostatic pressure, and temperature on the third harmonic generation in parabolic GaAs quantum dots. *J. Nanopart. Res.*, 2013, **13**, P. 6103–6112.

[34] Baskoutas S., Paspalakis E., Terzis A.F. Effects of excitons in nonlinear optical rectification in semiparabolic quantum dots. *Phys. Rev. B*, 2006, **74**, 153306.

[35] Duque C.A., Porras-Montenegro N., Barticevic Z., Pacheco M., Oliveira L.E. Effects of applied magnetic fields and hydrostatic pressure on the optical transitions in self-assembled InAs/GaAs quantum dots. *J. Phys.: Condens. Matter*, 2006, **18**, P. 1877–1884.

[36] Duque C.M., Morales A.L., Mora-Ramos M.E., Duque C.A. Optical nonlinearities associated to applied electric fields in parabolic two-dimensional quantum rings. *J. of Luminescence*, 2013, **143**, P. 81–88.

[37] Mughnetsyan V.N., Manaselyan Kh.A., Barseghyan M.G., Kirakosyan A.A. Simultaneous effects of hydrostatic pressure and spin-orbit coupling on linear and nonlinear intraband optical absorption coefficients in a GaAs quantum ring. *J. Lumin.*, 2013, **134**, P. 24–27.
[38] Duque C.M., Mora-Ramos M.E., Duque C.A. Hydrostatic pressure and electric field effects and nonlinear optical rectification of confined excitons in spherical quantum dots. *Superlattices and Microstructures*, 2011, **49**, P. 264–268.
[39] Bejan D. Exciton effects on the nonlinear optical properties of semiparabolic quantum dot under electric field. *Eur. Phys. J. Plus*, 2017, **132**, 102.
[40] Antil S., Kumar M., Lahon S., Dahiya S., Ohlan A., Punia R., Maan A.S. Influence of hydrostatic pressure and spin orbit interaction on optical properties in quantum wire. *Physica B: Condensed Matter*, 2019, **552**, P. 202–208.
[41] Antil S., Kumar M., Lahon S., Maan A.S. Pressure dependent optical properties of quantum dot with spin orbit interaction and magnetic field. *Optik – Int. J. for Light and Electron Optics*, 2019, **176**, P. 278–286.
[42] Dahiya S., Lahon S., Sharma R. Effects of temperature and hydrostatic pressure on the optical rectification associated with the excitonic system in a semi-parabolic quantum dot. *Physica E*, 2020, **118**, 113918.
[43] Braggio A., Grifoni M., Sassetti M., Napoli F. Plasmon and charge quantization effects in a double-barrier quantum wire. *Europhys. Lett.*, 2000, **50**, 236.
[44] Unlu S., Karabulut I., Safak H. Linear and nonlinear intersubband optical absorption coefficients and refractive index changes in a quantum box with finite confining potential. *Physica E*, 2006, **33**, 319.
[45] Fickenscher M., Shi T., Jackson Howard E., Smith Leigh M., Yarrison-Rice Jan M., Zheng C., Miller P., Etheridge J., Wong Bryan M., Gao Q., Deshpande S., Hoe Tan H., Jagadish C. Optical, Structural, and Numerical Investigations of GaAs/AlGaAs Core-Multishell Nanowire Quantum Well Tubes. *Nano Letters*, 2013, **13** (3), P. 1016–1022.
[46] Raigoza N., Morales A., Montes A., Porras-Montenegro N., C.A. Duque, Optical nonlinearities associated to applied electric fields in parabolic two-dimensional quantum rings. *Phys. Rev. B*, 2004, **69**, 045323.
[47] Oyoko H., Parras-Montenegro N., Lopez S., Duque C.A. Comparative study of the hydrostatic pressure and temperature effects on the impurity-related optical properties in single and double GaAs–$Ga_{1-x}Al_xAs$ quantum wells. *Phys. Status Solidi C*, 2007, **4**, 298.
[48] Herbert Li E. Material parameters of InGaAsP and InAlGaAs systems for use in quantum well structures at low and room temperatures. *Physica E*, 2000, **5**, 215.
[49] Haldane F.D.M. 'Luttinger liquid theory' of one-dimensional quantum fluids. I. Properties of the Luttinger model and their extension to the general 1D interacting spinless Fermi gas. *J. Phys. C*, 1981, **14**, 2585.
[50] Boyd R.W. *Nonlinear Optics*, Elsevier Science, 2020.
[51] Naghmaish Aishah AL., Dakhlaoui H., Ghrib T. Effects of magnetic, electric, and intense laser fields on the optical properties of AlGaAs/GaAs quantum wells for terahertz photodetectors. *Physica B: Condensed Matter*, 2022, **635**, 413838.
[52] Dahiya S., Lahon S., Sharma R. Study of third harmonic generation in $In_xGa_{1-x}As$ semi-parabolic 2-D quantum dot under the influence of Rashba spin-orbit interactions (SOI): Role of magnetic field, confining potential, temperature & hydrostatic pressure. *Physica E: Low-dimensional Systems and Nanostructures*, 2023, **147**, 115620.
[53] Kuhn K.J., Lyengar G.U., Yee S. Free carrier induced changes in the absorption and refractive index for interurban optical transitions in $Al_xGa_{1-x}As$/GaAs/$Al_xGa_{1-x}As$ quantum wells. *J. Appl. Phys.*, 1991, **70**, 5010.
[54] Kopf R.F., Herman M.H., Lamont Schnoes M., Perley A.P., Livescu G., Ohring M. Band offset determination in analog graded parabolic and triangular quantum wells of GaAs/AlGaAs and GaInAs/AlInAs. *J. Appl. Phys.*, 1992, **71** (10), P. 5004–5011.
[55] Gurmessa A., Melese G., Choudary V.L., Shewamare S. Photoluminescence from GaAs nanostructures. *Int. J. of Physical Sciences*, 2015, **10** (3), P. 106–111.
[56] Lourenc S.A., Dias I.F.L., Duart J.L., Laureto E., Aquino V.M., Harmand J.C. Temperature-Dependent Photoluminescence Spectra of GaAsSb/AlGaAs and GaAsSbN/GaAs Single Quantum Wells under Different Excitation Intensities. *Brazilian J. of Physics*, 2007, **37** (4), P. 1212–1217.

Submitted 29 July 2024; revised 26 August 2024; accepted 1 September 2024

Information about the authors:

Suman Dahiya – Department of Applied Physics, Delhi Technological University, Delhi 110042, India; ORCID 0000-0003-4815-5354

Siddhartha Lahon – Physics Department, KMC, University of Delhi, Delhi 110007, India; sid.lahon@gmail.com

Rinku Sharma – Department of Applied Physics, Delhi Technological University, Delhi 110042, India; ORCID 0000-0003-6812-4358; rinkusharma@dtu.ac.in

Conflict of interest: the authors declare no conflict of interest.

Chapter 58
Temperature and Hydrostatic Pressure Effect on the Optical Rectification in a Semi-Parabolic Quantum Dot Associated with the Excitonic System

Suman Dahiya, Siddhartha Lahon, and Rinku Sharma

Abstract Here, we theoretically studied the optical properties of 1-D GaAs in semi-parabolic quantum dot under the effect of temperature, effective radius and hydrostatic pressure for correlation of electron–hole in effective mass approximation using the method of density matrix. The dependence of opt. rec. Coefficient on the temperature, radius and hydrostatic pressure in the strong regime for excitonic as well as without excitonic effect has been observed. The results shows blue/red shift with decrease/increase of peak size also.

58.1 Introduction

In the past two decades, there have been speedy developments in the field of nanoscience and nanotechnology. Hence the detailed study of all the aspects of the low-dimensional semiconductor nanostructures becomes imperative. These nanostructures which includes quantum dots (QDs), quantum wires and quantum wells differ in size from the macroscopic structures and hence possess some interesting and unique properties [1–3]. Because of these standalone properties, scientists have shown great interest in the nanostructures, as they offer a wide area of research to understand them as well as the associated physics. Linear and nonlinear optical [3–5] properties such as the nonlinear Opt. Rect. Coefficient, optical absorption coefficient, and alteration in the refractive index have some wide potential applications in optoelectronic and photonic devices such as in photodetectors, far infrared laser amplifiers, and high-speed electro-optical modulators.

S. Dahiya · R. Sharma (✉)
Department of Applied Physics, Delhi Technological University, Delhi 110042, India
e-mail: rinkusharma@dtu.ac.in

S. Lahon
Physics Department, Kirori Mal College, University of Delhi, Delhi 110007, India

K. Singh et al. (eds.), *ICOL-2019*, Springer Proceedings in Physics 258,
https://doi.org/10.1007/978-981-15-9259-1_58

58.2 Theory and Model

In the framework of effective mass approximation, for a pair of electron–hole in 1D QDs, Hamiltonian with semi-parabolic confining potential is given by [6–8]:

$$H_{\mathrm{e}} = \frac{p_{\mathrm{h}}^2}{2m_{\mathrm{h}}^*} + \frac{p_{\mathrm{e}}^2}{2m_{\mathrm{e}}^*} + V(z_{\mathrm{e}}) + V(z_{\mathrm{h}}) - \frac{e^2}{\varepsilon|z_{\mathrm{e}} - z_{\mathrm{h}}|} \tag{58.1}$$

and the semi-parabolic potential $V(z_l)$ is given by which is written as:

$$V(z_l) = \begin{cases} \frac{1}{2}m_i^*\omega_0^2 z_l^2, & z_l \geq 0, \\ \infty, & z_l \leq 0 \quad (l = e, h) \end{cases} \tag{58.2}$$

The nonlinear Opt. Rect. Coefficient for our 2-level system in 1D semi-parabolic QDs is arrived at by applying a density matrix approach wherein perturbation expansion are used. It is given as

$$\chi_0^{(2)} = 4\frac{e^3\sigma_s}{\varepsilon_0\hbar^2}\mu_{01}^2\delta_{01} \times \frac{\omega_{01}^2(1+\frac{T_1}{T_2}) + (\omega^2 + \frac{1}{T_2^2})(\frac{T_1}{T_2} - 1)}{[(\omega_{01}-\omega)^2 + \frac{1}{T_2^2}][(\omega_{01}+\omega)^2 + \frac{1}{T_2^2}]}$$

58.3 Results

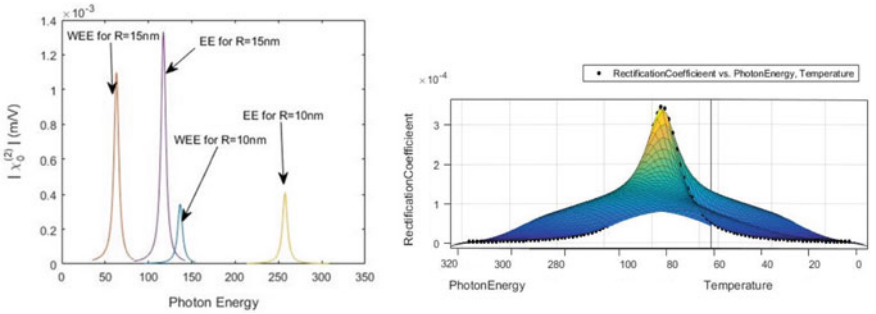

Figure shows the variation of optical rectification by the nanostructure for two values of radii of the semi-parabolic QD at $P = 100$ kbar and $T = 50$ K. It can be observed that the peaks are blue shifted when the radius of the QD is reduced to 10 nm from 15 nm. The consideration of excitonic effect for both the radii takes the peak position to higher values, viz. from 60 to 100 meV where $R = 15$ nm and from 140 to 255 meV for $R = 10$ nm. The peak height is reduced when the radius is lowered to 10 nm from 15 nm. This occurs due to the diminishing of the dipole

matrix element as the radius is decreased. Further, the inclusion of EE enhances the optical rectification peaks by enhancing the matrix element.

58.4 Conclusion

We found that the opt. Rect. Peak positions are affected by both temperature and pressure where the blue shift and red shift are induced when T and P are changed. Moreover, the OR strength is also found to be strongly affected by R, T and P. It is observed that the interplay of the variation of effective mass and induces varied alteration of the opt. rect.

References

1. Y.Y. Lin, J. Singh, J. Appl. Phys. **92**, 6205 (2002)
2. S.T. Perez-Merchancano, R. Franco, J. Silva-Valencia, Microelectron J. **39**, 383 (2008)
3. G. Almogy, A. Yariv, J. Nonlinear Opt. Phys. Mater. **4**, 401 (1995)
4. E. Rosencher, B. Vinter, *Optoelectronics* (Cambridge University Press, Cambridge, 2003)
5. C.-J. Zang, K.-X. Guo, Z.-E. Lu, Physica E **36**, 92 (2007)
6. Y.-B. Yu, S.-N. Zhu, K.-X. Guo, Phys Lett A **175**,335 (2005)
7. İ. Karabulut, H. Şafak, M. Tomak, J Phys D: Appl Phys **41**, 155104 (2008)
8. İ. Karabulut, H. Şafak, Physica B, **82**, 368 (2005)

Chapter 11
To Study Temperature and Hydrostatic Pressure Effect on ORC for a Semi-parabolic 1-D InAs Excitonic System

Suman Dahiya, Siddhartha Lahon, and Rinku Sharma

Abstract In the present paper, we studied the combined effect of hydrostatic pressure and temperature on ORC for a semi-parabolic 1-D InAs excitonic system is investigated under effective mass approximation and density matrix formalism is used to solve the Eigen function and Eigen energies. Effect of hydrostatic pressure and temperature on the OR has been studied for excitonic as well as without excitonic in the regime of strong confinement. The results showed a blue/red shift with application of hydrostatic pressure/temperature.

11.1 Introduction

As semiconductor nanomaterials have many potential applications in the field of electronics, photonics, and biological etc., hence they are provided with an exceptional consideration from the last few decades [1–4]. These nanostructures, especially quantum dots have been treated with special attention as they possess rare and unique electronic & optical properties. Quantum dots are considered as nano crystalline structures that are grown by using various physical & chemical methods.

Numerous investigations have been carried out to study the nonlinear optical properties of nanostructures under the effect of external factors such as lasers, spin, electric field, temperature etc. [5–8]. Effect of electron–hole correlation in quantum dots is also studied by many authors [3, 9, 10]. But in our sincere belief, there are no studies available on the effect of external factors in InAs semiconductor quantum dots.

In the present paper we carried out an investigation for the study of effect of tempt. and hydrost. pressure on the ORC of a 1-D InAs excitonic system in a semi-parabolic quantum dot. In the first section we present the theory including Hamiltonian, Eigen

S. Dahiya · R. Sharma (✉)
Department of Applied Physics, Delhi Technological University, New Delhi, Delhi 110042, India
e-mail: rinkusharma@dtu.ac.in

S. Lahon
Physics Department, Kirori Mal College, University of Delhi, New Delhi, Delhi 110007, India

V. Singh et al. (eds.), *Proceedings of the International Conference on Atomic, Molecular, Optical & Nano Physics with Applications*, Springer Proceedings in Physics 271,
https://doi.org/10.1007/978-981-16-7691-8_11

functions, Eigen energies etc. In the next section we presented our results. In the final section we concluded our results.

11.2 Theory

Hamiltonian for an excitonic system with semi-parabolic confining potential with effective mass approximation in 1D QDs is given by [3, 8–10]:

$$H_{e1} = \frac{p_h^2}{2m_h^*(P,T)} + \frac{p_e^2}{2m_e^*(P,T)} + V(z_e) + V(z_h) - \frac{e^2}{\varepsilon|z_e - z_h|} \tag{11.1}$$

where $(z_e, z_h > 0)$.

The semi-parabolic potential is:

$$V(z_k) = \begin{cases} \frac{1}{2}m_i^*\omega_0^2 z_k^2, & z_k \geq 0, \\ \infty, & z_k \leq 0 \quad (k = e, h) \end{cases} \tag{11.2}$$

Effective mass of the electron–hole dependent on temperature and pressure for InAs semiconductor is given by [11–13]:

$$m_e^*(P,T) = m_o\left[1 + \frac{7510}{E_g(P,T) + 341} + \frac{15020}{E_g(P,T)}\right]^{-1} \tag{11.3}$$

$$m_h^*(P,T) = \left(0.09 - 0.20 \times 10^{-3}P - 3.55 \times 10^{-5}T\right)m_0 \tag{11.4}$$

$$\text{With } E_g(P,T) = \left[1519 - \frac{0.5405T^2}{T + 204} + 10.7\,P\right] \tag{11.5}$$

Here E_g is in meV, P is in "kbar" and $_T$ is in "Kelvin".

The Hamiltonian is segmented into two terms:

$$H_{e1} = H_{r1} + H_{c1} \tag{11.6}$$

$$H_{r1} = \frac{p^2}{2\mu} + \frac{1}{2}\mu\omega_0^2 z_{r1}^2 - \frac{e^2}{\varepsilon(P,T)|z_{r1}|} \tag{11.7}$$

$$and \quad H_{c1} = \frac{P^2}{2M_{T1}} + \frac{1}{2}M_{T1}\omega_0^2 Z_{T1}^2 \tag{11.8}$$

Eigen wavefunction and eigen energies are:

$$\phi_{k1}(Z_{T1}) = N_{k1} \exp\left(-\frac{1}{2}\alpha^2 Z_{T1}^2\right) H_{2k1+1}(\alpha Z_{T1}) \tag{11.9}$$

$$E_{k1} = \left(2k1 + \frac{3}{2}\right)\hbar\omega_{0,} \quad (k1 = 0, 1, 2, \ldots), \tag{11.10}$$

The nonlinear ORC in 1D semi-parabolic QD given for 2-level system is given as

$$\chi_0^{(2)} = 4\frac{\sigma_s}{\varepsilon_0\hbar^2} M_{01}^2 \delta_{01} \times \frac{\omega_{01}^2\left(1 + \frac{\sigma_s}{T_2}\right) + \left(\omega^2 + \frac{1}{T_2^2}\right)\left(\frac{T_1}{T_2} - 1\right)}{\left[(\omega_{01} - \omega)^2 + \frac{1}{T_2^2}\right]\left[(\omega_{01} + \omega)^2 + \frac{1}{T_2^2}\right]} \tag{11.11}$$

11.3 Result

IaAs semiconductor material constants have been considered in our calculations where $T_1 = 1ps$ and $T_2 = 0.2ps$, and $m_e^* = 0.042m_0$, $m_h^* = 0.023m_0$ where m_0 is the mass of a free electron. σ_s is taken as $5 \times 10^{22}\,\mathrm{m}^{-3}$, $\varepsilon_r = 12.53$, and $\mathrm{I} = 10^9\,\mathrm{W/m}^2$ [8, 13].

In Fig. 11.1, results are presented for both of the cases by considering EE as well as WEE on the SHG peaks when the temperature is varied from 10 to 100 K keeping pressure constant at 50 kbar. As we can observe a blue shift in the peaks after increasing the temperature in both the cases but it is more significant in the case of excitonic effect. Also, we can observe peak height is also increasing as temperature is affecting energy band gap.

In Fig. 11.2, we presented the results for EE as well as WEE on the SHG peaks when pressure is varied from 10 to 100 kbar keeping temperature constant at 50 K. A

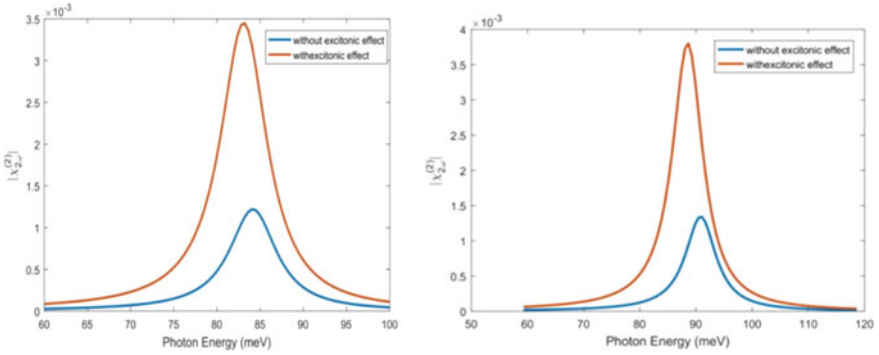

Fig. 11.1 ORC as a function of incident photon energy for T = 10 and 100 K keeping P constant at P = 50 kbar

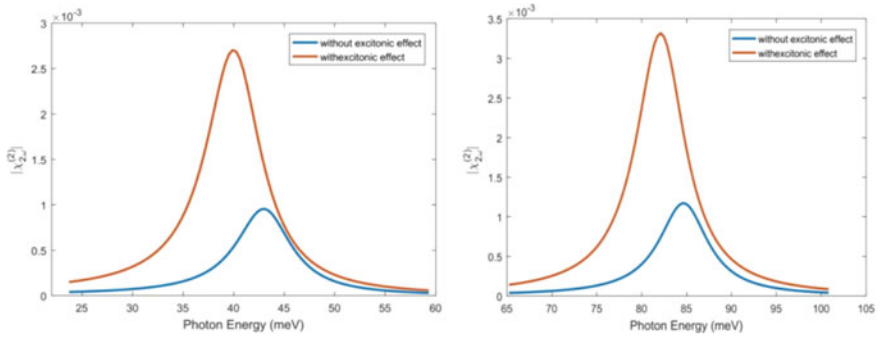

Fig. 11.2 ORC as a function of incident photon energy for P = 10 and 100 kbar keeping T constant at T = 50 K

red shift can be observed with decrease in size of the peaks with increase in pressure as effective is depending on pressure.

11.4 Conclusion

Combined effect of correlation of electron–hole pair with external factors such as temperature, and hydrostatic pressure on ORC in a 1-D semi-parabolic InAs QDs has been studied under effective mass approximation and by using density matrix approach eigen energies and eigenfunction in the regime of strong confinement has been calculated. The results are showing that the ORC is extensively enlarged when electron hole pair correlation has been considered in the QDs. It is also noticed that inclusion of hydrostatic pressure and temperature affected the ORC peak positions in a very significant way as changing the value of temperature and hydrostatic pressure induced a blue shift/red shift.

References

1. O. Salata, J. Nanobiotechnol. **2**, 1–6 (2004)
2. D. Mocatta, G. Cohen, J. Schattner, O. Millo, E. Rabani, U. Banin, Science **332**, 77–81 (2011)
3. D. Bejan, Eur. Phys. J. Plus **132**, 102 (2017)
4. I. Karabulut, H. Safak, M. Tomak, Solid State Commun. **135**, 735 (2005)
5. J.-H. Yuan, Y. Zhang, H. Mo, N. Chen, Z.-H. Zhang, Phys. E **77**, 102 (2016)
6. C.M. Duque, M.E. Mora-Ramos, C.A. Duque, J Nanopart Res. **13**, 6103–6112 (2011)
7. N. Eseanu, Phys. Lett. A **374**, 1278 (2010)
8. Y.-B. Yu, S.-N. Zhu, K.-X. Guo, Phys. Lett. A **175**, 335 (2005)
9. S. Antil, M. Kumar, S. Lahon, A.S. Maan, Opt.—Int. J. Light Electron Opt. **176**, 278–286 (2019)
10. S. Dahiya, S. Lahon, R. Sharma, Phys. E **118** 113918 (2020)

11. C.A. Duque, N. Porras-Montenegro, Z. Barticevic, M. Pacheco, L.E. Oliveira, J. Phys.: Condens. Matter **18**, 1877–1884 (2006)
12. J. Wu et al., Small band gap bowing in In1-xGaxN alloys. Appl. Phys. Lett. **80**, 4741 (2002)
13. I. Vurgaftman, J.R. Meyer, Band parameters for nitrogen-containing semiconductors. J. Appl. Phys. **94**, 3675–3696 (2003)